ITERATIVE AND VARIATIONAL HOMOGENIZATION METHODS FOR FILLED ELASTOMERS

BY

TAHA GOUDARZI

DISSERTATION

Submitted in partial fulfillment of the requirements
for the degree of Doctor of Philosophy in Civil Engineering
in the Graduate College of the
University of Illinois at Urbana-Champaign, 2014

Urbana, Illinois

Doctoral Committee:

Assistant Professor Oscar Lopez-Pamies, Chair
Professor Ioannis Chasiotis
Professor Harley T. Johnson
Professor Arif Masud
Professor Glaucio H. Paulino

ABSTRACT

Elastomeric composites have increasingly proved invaluable in commercial technological applications due to their unique mechanical properties, especially their ability to undergo large reversible deformation in response to a variety of stimuli (e.g., mechanical forces, electric and magnetic fields, changes in temperature). Modern advances in organic materials science have revealed that elastomeric composites hold also tremendous potential to enable new high-end technologies, especially as the next generation of sensors and actuators featured by their low cost together with their biocompatibility, and processability into arbitrary shapes. This potential calls for an in-depth investigation of the macroscopic mechanical/physical behavior of elastomeric composites directly in terms of their microscopic behavior with the objective of creating the knowledge base needed to guide their bottom-up design.

The purpose of this thesis is to generate a mathematical framework to describe, explain, and predict the macroscopic nonlinear elastic behavior of filled elastomers, arguably the most prominent class of elastomeric composites, directly in terms of the behavior of their constituents i.e., the elastomeric matrix and the filler particles and their microstructure i.e., the content, size, shape, and spatial distribution of the filler particles. This will be accomplished via a combination of novel iterative and variational homogenization techniques capable of accounting for interphasial phenomena and finite deformations.

Exact and approximate analytical solutions for the fundamental nonlinear elastic response of dilute suspensions of rigid spherical particles (either firmly bonded or bonded through finite size interphases) in Gaussian rubber are first generated. These results are in turn utilized to construct approximate so-

lutions for the nonlinear elastic response of non-Gaussian elastomers filled with a random distribution of rigid particles (again, either firmly bonded or bonded through finite size interphases) at finite concentrations. Three-dimensional finite element simulations are also carried out to gain further insight into the proposed theoretical solutions. Inter alia, we make use of these solutions to examine the effects of particle concentration, mono- and poly-dispersity of the filler particle size, and the presence of finite size interphases on the macroscopic response of filled elastomers. The solutions are found able to explain and describe experimental results that to date have been understood only in part. More generally, the solutions provide a robust tool to efficiently guide the design of filled elastomers with desired macroscopic properties.

The homogenization techniques developed in this work are not limited to nonlinear elasticity, but can be readily utilized to study multi-functional properties as well. For demonstration purposes, we work out a novel exact solution for the macroscopic dielectric response of filled elastomers with interphasial space charges.

To my Parents,
for their unconditional love and endless support

ACKNOWLEDGEMENTS

I would like to record my particular gratitude to my Ph.D. adviser, professor Lopez-Pamies. He shared with me his vast-precious knowledge of homogenization which formed mostly my understanding of this field and, broadly, guided me to grow in mechanics. Professor Lopez-Pamies has been an extraordinary person to work with during the entire span of this research.

I gratefully thank professor Glaucio Paulino, professor Ionnis Chasiotis, professor Arif Masud and professor Harley Johnson, who, in the midst of their activity, accepted to be members of my dissertation committee.

Special thanks go to professor Paulino for his expert advice, guidance and energetic support. Many thanks go to professor Chasiotis for his professional and technical guidance.

Many thanks go to Dr. Kostas Danas and professor Toshio Nakamura for their expert advice in the numerical parts of the research.

Special thanks go to my fellow Ph.D. students and close friends Amir Arbabi, Reza Avazmohammadi and Mahmud Etedadi for our great scientific and philosophical discussions.

I would also like to record my gratitude to my fellow colleagues Stephen Spinelli, Victor Lefévre, Chen Zhang and Daniel Spring.

Financial support for this research was provided by NSF CAREER Grant CMMI–1219336.

TABLE OF CONTENTS

LIST OF FIGURES

CHAPTER 1

INTRODUCTION

Elastomeric composites have pervasively been used in commercial technological applications due to their unique mechanical properties, especially their ability to undergo large reversible deformations in response to a variety of stimuli (e.g., mechanical forces, electric and magnetic fields, changes in temperature) (see, e.g., Zhang et al., 2002; Bar-Cohen, 2004; Wallace et al., 2008). Advances in organic materials science have revealed the tremendous potential of elastomeric composites to enable new high-end technologies, especially as the next generation of sensors and actuators featured by their low cost together with their biocompatibility, and processability into arbitrary shapes (see, e.g., Wang et al., 2002; Ma, 2008). This potential calls for an in-depth investigation of the macroscopic mechanical/physical behavior of elastomeric composites directly in terms of their microscopic behavior with the objective of creating the knowledge base needed to guide their bottom-up design.

It is well known that adding filler particles — such as carbon black and silica — to elastomers greatly improves the stiffness[1] (see, e.g., Gent and Park, 1984; Gent and Pulford, 1983; Leblanc, 2010). Moreover, the presence of fillers has also been shown to play a crucial role in providing elastomers with enhanced multifunctional properties (see, e.g., Zhang et al., 2002; Danas et al., 2012) of this increasingly pervasive class of materials. The precise nature of such a strong stiffening remains unresolved, but a number of dominant microscopic mechanisms have been identified including the so-called "hydrodynamic" effect and the presence of interphases and occluded rubber (see,

[1]The addition of fillers, even in small amounts, is known to significantly influence other mechanical properties including fracture, abrasion, and rheological properties

e.g., Heinrich et al., 2002; Fukahori, 2007; Ramier, 2004; Leblanc, 2010; Qu et al., 2011).

In this work we shall focus on investigating the "hydrodynamic" and "interphasial" reinforcing effects within the context of nonlinear elastic deformations. We view filled elastomers as particulate composites — comprising a continuous elastomeric matrix reinforced by a statistically uniform distribution of inclusions bonded through interphases (as schematically shown in Fig. 1.1) — and study their macroscopic (or overall) elastic response, which, roughly speaking, is expected to be some weighted average of the elastic response of the elastomer, the interphases, and the comparatively rigid response of the fillers.

The so-called hydrodynamic effect refers to the fact that the addition of fillers to an elastomer results in a composite material whose macroscopic (overall or homogenized) mechanical properties are, by construction, some weighted average of the properties of the soft elastomer and the *comparatively rigid* fillers. The interphasial effect refers to the fact that the "anchoring" of the polymer chains of the elastomer onto the stiff filler particles forces the chains into conformations that are very different from those in the bulk, hence resulting in "interphases" (often referred to as bound rubber) of possibly several tens of nanometers in thickness that are substantially *stiffer* than the elastomer in the bulk. Here, it is relevant to remark that the reinforcement of materials (not just elastomers) via the addition of inclusions bonded through finite-size interphases is a subject that has received considerable attention over the last three decades, but almost exclusively within the limited context of linear elasticity (see, e.g., Walpole, 1978; Mikata and Taya, 1985; Qiu and Weng, 1991; Herve and Zaoui, 1993; Duan et al., 2006).

Following the approach of Einstein (1906) and exploiting the mathematical analogy between Stokes flow and *small-strain* linear elastostatics, Smallwood (1944) generated a first rigorous result for the overall *linear* elastic response of isotropic incompressible rubber reinforced by a dilute distribution of rigid spherical particles. Yet within the restricted setting of small-strain linear theory, significant efforts were thereafter devoted to account for non-spherical particles and non-dilute distributions (see Guth 1945; see also Eshelby 1957; Batchelor and Green 1972; Chen and Acrivos 1978; Willis 1977).

It was not until the early 1970's that a formal framework for describing the overall *nonlinear* elastic response of filled elastomers undergoing *finite*

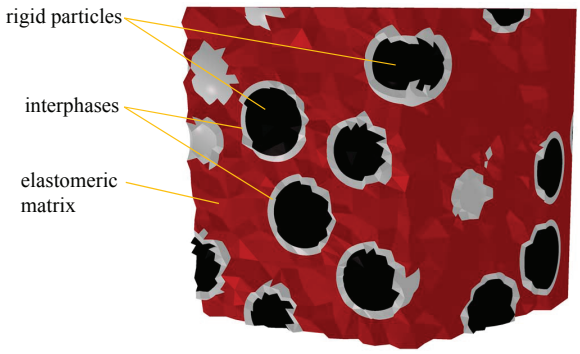

Figure 1.1: A schematic of the microstructure of filled elastomers under study in this work. Isotropic distribution of rigid spherical particles firmly bonded to the matrix through generally heterogeneous finite size interphases.

deformations was first made available by Hill (1972). Before then, however, Mullins and Tobin (1965) had proposed an empirical approach based on the notion of "strain-amplification" factor also within the context of finite elasticity. Their idea was to describe the behavior of filled elastomers as the behavior of the underlying matrix material evaluated at an amplified measure of strain. As pursued by various authors (see, e.g., Govindjee and Simo, 1991; Govindjee, 1997; Bergström and Boyce, 1999), different results can be generated depending on the choice of strain measure that is amplified.

In spite of the fact that the framework of Hill (1972) has been available for several decades, relatively little progress has been made in its application to generate rigorous results. This is because the *constitutive non-convexity* and *nonlinear incompressibility constraint* inherent of elastomers render the relevant equations formidably complex to solve (see, e.g., Braides, 1985; Müller, 1987). Such a degree of complexity is perhaps best highlighted by the fact that (upper or lower) bounds for the response of filled elastomers are still nonexistent[2]. In terms of analytical estimates, progress has recently been made via linear comparison methods (see Lopez-Pamies and Castañeda, 2006a, and references therein). Yet while these methods have desirable features — such as the ability to incorporate information on particle concentration, shape, and spatial distribution (Lopez-Pamies and Castañeda, 2006b) — and in addition have proved fairly accurate when compared with full-

[2]The only two rigorous bounds currently available in finite elasticity, the Voigt-type upper bound of Ogden (1978) and the Reuss-type lower bound of Ponte Castañeda (1989), become unbounded (plus and minus infinity, respectively) when the fillers are taken to be rigid.

field simulations (Moraleda et al., 2009; Michel et al., 2010), they are unable to rigorously recover the overall incompressibility constraint typical of filled elastomers beyond 2D problems (Lahellec et al., 2004; Lopez-Pamies et al., 2008). In terms of computational estimates, a variety of techniques and results have been successfully worked out in the context of *small-strain linear* elasticity (see, e.g., Gusev, 1997; Michel et al., 1999; Segurado and Llorca, 2002; Lusti et al., 2002; Galli et al., 2008). However, with the exception of a few finite-element (FE) simulations Bergström and Boyce (1999), no 3D full-field simulations of filled elastomers undergoing *finite deformations* have been reported to date in the literature.

The main objective of this research — to generate exact and approximated closed form solution for the overall responses of filled elastomers under arbitrarily finite deformations — is accomplished in three successive steps. In the first step, closed form solutions for dilute suspension of particles in Neo-Hookean rubber are generated (see e.g., Lopez-Pamies et al., 2013b; Goudarzi et al.). In the second step, the dilute solution is extended to finite-concentration suspensions of particles in Neo-Hookean rubber via an iterated dilute homogenization technique (see Lopez-Pamies et al., 2013a; Lopez-Pamies, 2014). In the third step, a nonlinear comparison medium technique is utilized to construct in turn an approximate solution for finite-concentration suspensions of particles in non-Gaussian rubber (Lopez-Pamies et al., 2013a; Goudarzi et al.).

Iterated dilute homogenization methods — also referred to as differential schemes — are a class of iterative techniques that make use of results for the overall properties of dilute composites in order to generate corresponding results for composites with finite concentration of constituents. The basic form of these techniques was introduced in the 1930's by Bruggeman (1935) to determine the linear dielectric constant and conductivity of a certain class of two-phase composites. The idea was later generalized by various authors to determine the *linear* mechanical/physical properties of multiphase composites with an admittedly broad range of microstructures; see, e.g., Norris (1985), Avellaneda (1987), Braides and Lukkassen (2000), and Chapter 10.7 in the monograph by Milton (2002). To be useful, these techniques require knowledge of a dilute solution from which to start the iterative construction process. It is because of this requirement that this approach has been utilized by and large in the restricted context of linear problems where — as opposed

to nonlinear problems — there is a wide variety of dilute solutions available. Nevertheless, the central idea of these techniques is geometrical in nature and can therefore be applied to any constitutively *nonlinear* problem of choice, provided, again, the availability of a relevant dilute solution. In the context of finite elasticity of interest in this chapter, Lopez-Pamies (2010a) has recently put forward an iterated dilute homogenization technique for the special case of two-phase composites. In this chapter, we utilize this technique together with the dilute solution of Chapter 2 in order to construct a solution for the nonlinear elastic response of Neo-Hookean rubber reinforced by an isotropic distribution of polydisperse rigid particles at finite concentration.

Comparison medium methods are variational techniques that allow to generate approximations for the overall properties of composites in terms of the properties of "simpler" comparison media. The idea behind these techniques was formalized for *linear* problems by Hashin and Shtrikman (1962) and later recognized by Willis (1983) to be apposite to deal with *nonlinear* problems as well. In a seminal contribution, Talbot and Willis (1985) provided a fairly general framework for constructing approximations for the overall nonlinear mechanical/physical properties of composites in terms of the overall properties of any comparison medium of choice, possibly nonlinear and heterogeneous. To render useful approximations, however, this framework requires the selection of an "optimal" comparison medium complex enough to mimic the behavior of the actual nonlinear composite yet simple enough that its overall properties can be computed. In the context of finite elasticity, such a selection process has proved particularly challenging because of the *constitutive non-convexity* and *nonlinear incompressibility constraint* typical of nonlinear elastic solids. Among the various attempts that have been pursued (Ponte Castañeda, 1989; Ponte Castañeda and Tiberio, 2000), the latest choice of a comparison medium that is a *linear composite* as prescribed by Lopez-Pamies and Castañeda (2006a) has led to the more physically consistent results thus far. Yet, a critical limitation of this approach is that it cannot rigorously recover the overall incompressibility constraint typical of filled elastomers beyond 2D problems (Lahellec et al., 2004; Lopez-Pamies et al., 2008). In this chapter, we work out an extension of the framework of Talbot and Willis (1985) that is free of the limitations of previous formulations at the expense of employing a *nonlinear composite* as the comparison medium. With the filled Neo-Hookean rubber constructed from the

above-described iterated dilute homogenization technique as the choice for the comparison medium, we then employ this new formulation to generate an explicit approximate solution for the nonlinear elastic response of isotropic suspensions of rigid particles of polydisperse sizes and finite concentration in non-Gaussian rubber.

The presentation of this document is organized as follows. In Chapter 2, a fundamental solution is constructed — via a novel iterative homogenization technique — for the nonlinear elastic response of dilute suspensions of rigid inclusions in Gaussian rubber.

In Chapter 3, the dilute solution of Chapter 2 is employed within the context of a new variational technique to construct in turn a solution for the response of suspensions of rigid inclusions in non-Gaussian rubber at finite concentrations. Via use of an iterated homogenization technique first a solution for the response of suspensions of rigid inclusions in Gaussian rubber is constructed. This solution later is used as a nonlinear comparison medium in a variational technique called "nonlinear comparison medium method" to generate approximate solutions for the response of isotropic suspension of rigid inclusions in non-Gaussian rubber at finite concentrations.

Enriching the solutions of Chapter 3 to account for "interphasial" reinforcing effects as well as hydrodynamic effect, a fundamental solution for the nonlinear response of isotropic dilute suspension of rigid spheres in Gaussian rubber — where the particles are bonded to the Gaussian matrix through dilute Gaussian interphases — is constructed in Chapter 4. Then, the variational machinery developed in Chapter 3 is extended for nonlinear multiphase systems to incorporate the dilute solution developed in Chapter 4, and generate non-dilute version of the solution for non-Gaussian filled elastomers accounting for hydrodynamic and interphasial effects.

Chapter 5 is devoted to devising a variational framework — based on the idea of composite-sphere assemblages — which allows to generate efficient numerical solutions for the response of filled elastomers under arbitrarily large deformations.

In Chapter 6, a new exact solution to the linear dielectric response of filled elastomers accounting for space charges is presented via use of the composite assemblages idea.

Finally in last chapter, Concluding Remarks, some open fields of research following the developed ideas in this document are portrayed.

List of publications resulted from this research

Goudarzi, T., Spring, D.W., Paulino, G.H., Lopez-Pamies, O., 2014. Filled elastomers: A theory of filler reinforcement based on hydrodynamic and interphasial effects. Submitted.

Lopez-Pamies, O., Goudarzi, T., Amira B. Meddeb, Zoubeida Ounaies. Extreme enhancement and reduction of the dielectric response of polymer nanoparticulate composites via interphasial charges. *Applied Physics Letter.* 104, 242904.

Goudarzi, T., Lopez-Pamies, O., 2013. Numerical modeling of the nonlinear elastic response of filled elastomers via composite-sphere assemblages. *J. Appl. Mech.* 80, 051021.

Lopez-Pamies, O., Goudarzi, T., Danas, K., 2013. The nonlinear elastic response of suspensions of rigid inclusions in rubber: II — A simple explicit approximation for finite-concentration suspensions. J. Mech. Phys. Solids 61, 19–37.

Lopez-Pamies, O., Goudarzi, T., Nakamura, T., 2013. The nonlinear elastic response of suspensions of rigid inclusions in rubber: I — An exact result for dilute suspensions. J. Mech. Phys. Solids 61, 1–18.

CHAPTER 2

THE NONLINEAR ELASTIC RESPONSE OF SUSPENSIONS OF RIGID INCLUSIONS IN RUBBER: AN EXACT RESULT FOR DILUTE SUSPENSIONS

The objective of this chapter is to generate a rigorous analytical result for the fundamental problem of the overall elastic response of rubber reinforced by a dilute distribution of rigid particles under arbitrarily large 3D deformations. The focus is on the basic case of ideal (Gaussian or, equivalently, Neo-Hookean) rubber and isotropic distributions of particles. This is accomplished here by making use of a novel iterated homogenization technique that allows to construct exact solutions for the homogenization problem of two-phase nonlinear elastic composites with particulate microstructures. This technique has been recently developed and utilized to generate solutions for the related fundamental problem of elastomers containing a dilute distribution of cavities — as opposed to rigid inclusions — within the analysis of cavitation instabilities (Lopez-Pamies et al., 2011a,b).

In addition to the analytical result, we also generate full 3D FE results for the large-deformation response of a block of Neo-Hookean rubber that contains a single rigid spherical inclusion of infinitesimal size located at its center.

2.1 The problem

Consider a filled elastomer, made up of a continuous matrix containing a random distribution of firmly bonded rigid particles, that occupies a domain Ω with boundary $\partial\Omega$ in its undeformed stress-free configuration. The regions occupied individually by the matrix and particles are collectively denoted by Ω_m and Ω_p so that $\Omega = \Omega_m \cup \Omega_p$. It is assumed that the random distribution is statistically uniform and that the characteristic length scale of the particles

(e.g., their average diameter) is much smaller than the size of Ω.

Material points are identified by their initial position vector $\mathbf{X}$ in the undeformed configuration Ω, while the current position vector of the same point in the deformed configuration Ω' is given by $\mathbf{x} = \boldsymbol{\chi}(\mathbf{X})$. Motivated by physical arguments, the mapping $\boldsymbol{\chi}$ is required to be one-to-one on Ω and twice continuously differentiable, except possibly on the particles/matrix boundaries where is only required to be continuous. The deformation gradient $\mathbf{F}$ at $\mathbf{X}$ is defined by

$$\mathbf{F} = \operatorname{Grad} \boldsymbol{\chi} \quad \text{in} \quad \Omega \tag{2.1}$$

and satisfies the local material impenetrability constraint $J \doteq \det \mathbf{F} > 0$.

The matrix is taken to be a nonlinear elastic solid characterized by a quasiconvex stored-energy function W of $\mathbf{F}$. For convenience, the rigid particles are also described as nonlinear elastic solids with stored-energy function

$$W_p(\mathbf{F}) = \begin{cases} 0 & \text{if} \quad \mathbf{F} = \mathbf{Q} \in Orth^+ \\ +\infty & \text{otherwise} \end{cases} . \tag{2.2}$$

Here, $Orth^+$ stands for the set of all proper orthogonal second-order tensors. At each material point $\mathbf{X}$ in the undeformed configuration, the first Piola-Kirchhoff stress $\mathbf{S}$ is formally given in terms of the deformation gradient $\mathbf{F}$ by

$$\mathbf{S} = \frac{\partial W}{\partial \mathbf{F}}(\mathbf{X}, \mathbf{F}), \quad W(\mathbf{X}, \mathbf{F}) = (1 - \theta(\mathbf{X}))\ W(\mathbf{F}) + \theta(\mathbf{X})\ W_p(\mathbf{F}), \tag{2.3}$$

where the indicator function θ takes the value 1 if the position vector $\mathbf{X}$ is in a particle, and 0 otherwise, and serves therefore to describe the microstructure (here, the size, shape, and spatial location of the particles) in the undeformed configuration Ω.

Granted the hypotheses of separation of length scales and statistical uniformity of the microstructure together with the constitutive quasiconvexity of W, the overall or macroscopic response of the filled elastomer can be defined as the relation between the volume averages of the first Piola-Kirchoff stress $\mathbf{S}$ and the deformation gradient $\mathbf{F}$ over Ω when the material is subjected to the affine boundary condition

$$\mathbf{x} = \overline{\mathbf{F}}\mathbf{X} \quad \text{on } \partial\Omega, \tag{2.4}$$

where the second-order tensor $\overline{\mathbf{F}}$ is a prescribed quantity (Hill, 1972). In this case, it directly follows from the divergence theorem that the average deformation gradient over Ω is given by $|\Omega|^{-1}\int_\Omega \mathbf{F}(\mathbf{X})\,\mathrm{d}\mathbf{X} = \overline{\mathbf{F}}$, and hence the derivation of the macroscopic response reduces to finding the average stress $\overline{\mathbf{S}} \doteq |\Omega|^{-1}\int_\Omega \mathbf{S}(\mathbf{X})\,\mathrm{d}\mathbf{X}$ for a given $\overline{\mathbf{F}}$. The result reads formally as

$$\overline{\mathbf{S}} = \frac{\partial \overline{W}}{\partial \overline{\mathbf{F}}}(\overline{\mathbf{F}}, c) \tag{2.5}$$

with

$$\overline{W}(\overline{\mathbf{F}}, c) = (1-c)\ \min_{\mathbf{F}\in\mathcal{K}} \frac{1}{|\Omega_m|}\int_{\Omega_m} W(\mathbf{F})\ \mathrm{d}\mathbf{X}. \tag{2.6}$$

In this last expression, $c \doteq |\Omega|^{-1}\int_\Omega \theta(\mathbf{X})\mathrm{d}\mathbf{X}$ is the initial volume fraction or concentration of particles, $\overline{W}$ is the so-called effective stored-energy function, which physically corresponds to the total elastic energy (per unit undeformed volume) stored in the material, and $\mathcal{K}$ denotes the set of kinematically admissible deformation gradient fields:

$$\begin{aligned}\mathcal{K} = \{\mathbf{F} : \exists\ \mathbf{x} = \boldsymbol{\chi}(\mathbf{X}) \text{with } \mathbf{F} = \mathrm{Grad}\,\boldsymbol{\chi}, J > 0 \text{ in } \Omega,\\ \mathbf{F} = \mathbf{Q} \in Orth^+ \text{ in } \Omega_p,\ \ \mathbf{x} = \overline{\mathbf{F}}\mathbf{X} \text{ on } \partial\Omega\}\,.\end{aligned} \tag{2.7}$$

The foregoing formulation for the overall finite-deformation response of filled elastomers is valid for any physically admissible value of concentration of particles c. The interest here is in the asymptotic limit as $c \to 0+$, when the above-defined material reduces to a nonlinear elastic solid with stored-energy function W that contains a random distribution of rigid particles, with shapes and spatial locations characterized by θ, at dilute concentration. Assuming a polynomial asymptotic behavior[1], the effective stored-energy function (2.6) in this limiting case takes the form

$$\overline{W}(\overline{\mathbf{F}}, c) = W(\overline{\mathbf{F}}) + \mathcal{G}\left\{W; \overline{\mathbf{F}}\right\} c + O(c^2), \tag{2.8}$$

where $\mathcal{G}$ is a functional[2] with respect to its first argument W and a function with respect to its second argument $\overline{\mathbf{F}}$.

[1]For the problem of filled Neo-Hookean rubber considered in this chapter the asymptotic behavior is indeed of the polynomial form (2.8).

[2]That is, $\mathcal{G}$ is an operator with respect to the stored-energy function W of the elastomeric matrix.

2.1.1 The case of dilute isotropic suspensions in Neo-Hookean rubber

The main objective of this chapter is to determine the functional $\mathcal{G}$ in (2.8) for the basic case when the distribution of particles is isotropic and the elastomeric matrix is Neo-Hookean rubber with stored-energy function

$$W(\mathbf{F}) = \begin{cases} \dfrac{\mu}{2}\left[I_1 - 3\right] = \dfrac{\mu}{2}\left[\lambda_1^2 + \lambda_2^2 + \lambda_3^2 - 3\right] & \text{if} \quad J = \lambda_1\lambda_2\lambda_3 = 1 \\ +\infty & \text{otherwise} \end{cases} . \tag{2.9}$$

Here, it is recalled that the parameter μ denotes the initial shear modulus of the Neo-Hookean matrix, $I_1 = \mathbf{F}\cdot\mathbf{F}$, and $\lambda_1, \lambda_2, \lambda_3$ have been introduced to denote the singular values of the deformation gradient $\mathbf{F}$.

Owing to the assumed isotropy of the microstructure and the constitutive isotropy and incompressibility of the matrix material (2.9) and rigid particles (2.2), the resulting overall elastic response is isotropic and incompressible. This implies that the effective stored-energy function $\overline{W}$ in this case depends on the macroscopic deformation gradient $\overline{\mathbf{F}}$ only through its singular values $\overline{\lambda}_1, \overline{\lambda}_2, \overline{\lambda}_3$ and becomes unbounded for non-isochoric deformations when $\overline{J} \doteq \det\overline{\mathbf{F}} = \overline{\lambda}_1\overline{\lambda}_2\overline{\lambda}_3 \neq 1$. More explicitly, the result (2.8) specializes to

$$\overline{W} = \begin{cases} \dfrac{\mu}{2}\left[\overline{\lambda}_1^2 + \overline{\lambda}_2^2 + \overline{\lambda}_3^2 - 3\right] + \mu\, G(\overline{\lambda}_1, \overline{\lambda}_2, \overline{\lambda}_3)\, c + O(c^2) \text{ if } \overline{J} = \overline{\lambda}_1\overline{\lambda}_2\overline{\lambda}_3 = 1 \\ +\infty \qquad\qquad \text{otherwise} \end{cases} , \tag{2.10}$$

where $G(\overline{\lambda}_1, \overline{\lambda}_2, \overline{\lambda}_3)$ is a symmetric function.

In order to assist the presentation of the results, the unbounded branch of the energy (2.10) is omitted in most of the sequel. For this purpose and without loss of generality we restrict attention to isochoric pure stretch loadings of the form

$$\overline{\mathbf{F}} = \operatorname{diag}(\overline{\lambda}_1, \overline{\lambda}_2, \overline{\lambda}_3) \quad \text{with} \quad \overline{\lambda}_3 = \frac{1}{\overline{\lambda}_1\overline{\lambda}_2} \tag{2.11}$$

and, with a slight abuse of notation, rewrite the effective stored-energy function (2.10) of the filled Neo-Hookean rubber as

$$\overline{W} = \frac{\mu}{2}\left[\overline{\lambda}_1^2 + \overline{\lambda}_2^2 + \frac{1}{\overline{\lambda}_1^2\overline{\lambda}_2^2} - 3\right] + \mu\, G(\overline{\lambda}_1, \overline{\lambda}_2)\, c \tag{2.12}$$

to first order in the concentration of particles c.

2.2 An exact solution via a novel iterated homogenization method

In this section, we derive a precise form of the effective stored-energy function (2.12) for isotropic dilute suspensions of rigid particles in Neo-Hookean rubber. This amounts to solving asymptotically the relevant minimization problem (2.6) with (2.9) in the limit as $c \to 0+$. Our strategy involves two main steps. In the first step (Section 2.2.1), we make use of the new iterated homogenization technique of Lopez-Pamies et al. (2011a) to work out an exact result for the overall response of a Neo-Hookean solid containing a particular class of isotropic distributions of rigid particles with *finite* concentration c. The second step (Section 2.2.2) deals with the asymptotic analysis of this result in the limit as the concentration of the particles is taken to zero.

2.2.1 Iterated homogenization solution for finite concentration of particles

By means of a combination of iterative processes (Idiart, 2008; Lopez-Pamies, 2010a; Lopez-Pamies et al., 2011a) have recently generated an exact solution for the effective stored-energy function of a two-phase composite made up of a nonlinear elastic matrix containing a specific — but fairly general — class of distributions (i.e., a specific class of indicator functions θ) of nonlinear elastic particles. For the special case of isotropic distributions of interest in this chapter, their result for $\overline{W}(\overline{\mathbf{F}}, c)$ in the present notation is implicitly given by the following first-order nonlinear partial differential equation (pde)

$$c\frac{\partial \overline{W}}{\partial c} - \overline{W} - \frac{1}{4\pi}\int_{|\boldsymbol{\xi}|=1} \max_{\boldsymbol{\omega}} \left[\boldsymbol{\omega}\cdot\frac{\partial \overline{W}}{\partial \overline{\mathbf{F}}}\,\boldsymbol{\xi} - W\left(\overline{\mathbf{F}} + \boldsymbol{\omega}\otimes\boldsymbol{\xi}\right)\right] \mathrm{d}\boldsymbol{\xi} = 0 \quad (2.13)$$

subject to the initial condition

$$\overline{W}(\overline{\mathbf{F}}, 1) = W_p(\overline{\mathbf{F}}). \quad (2.14)$$

The interested reader is referred to Section 3 of Lopez-Pamies et al. (2011a) for the derivation and thorough discussion of the above result, but at this stage it is appropriate to record a few of its properties:

- *Constitutive behavior and concentration of the matrix and particles.* The result (2.13)–(2.14) is valid for any choice of (including compressible and anisotropic) stored-energy functions W and W_p for the elastomeric matrix and particles, provided that these satisfy usual physically based mathematical requirements. The result also holds applicable for any value of concentration of particles in the physical range $c \in [0, 1]$.

- *Interaction among particles.* By construction, the underlying microstructure associated with the stored-energy function (2.13)–(2.14) corresponds to an isotropic distribution of disconnected particles of polydisperse sizes that interact in such a manner that they deform *uniformly*[3], irrespectively of the applied macroscopic deformation $\overline{\mathbf{F}}$ or the value of particle concentration c. Such a special type of deformation is usually associated with the softest possible response of stiff materials. Thus, (2.13)–(2.14) is generally expected to bound from below the effective stored-energy functions of nonlinear elastic solids reinforced by any type of isotropic distribution of particles (whether (2.13)–(2.14) is a rigorous lower bound remains yet to be proved or disproved).

- *Connection with the classical result of Eshelby.* A direct implication of the fact that the particles deform uniformly is that in the limit of small deformations and small particle concentration as $\overline{\mathbf{F}} \to \mathbf{I}$ and $c \to 0+$, expressions (2.13)–(2.14) recover identically the classical result of Eshelby for the overall response of a dilute distribution of linearly elastic spherical particles embedded in a linearly elastic matrix. The formulation (2.13)–(2.14) can thus be thought of as a direct extension of the classical result of Eshelby to deal with finite deformations. Further comments on this key aspect are deferred to the end of this section and to Section 5.

[3]That is, the deformation gradient field $\mathbf{F}(\mathbf{X})$ — and hence the stress field $\mathbf{S}(\mathbf{X})$ — within each particle is uniform and the same for all particles.

Now, for a Neo-Hookean matrix characterized by (2.9) it is not difficult to show that the maximizing vector $\boldsymbol{\omega}$ in (2.13) specializes to

$$\boldsymbol{\omega} = \frac{1}{\mu}\frac{\partial \overline{W}}{\partial \overline{\mathbf{F}}}\boldsymbol{\xi} - \overline{\mathbf{F}}\boldsymbol{\xi} + \frac{1}{\overline{J}\,\overline{\mathbf{F}}^{-T}\boldsymbol{\xi}\cdot\overline{\mathbf{F}}^{-T}\boldsymbol{\xi}}\,\overline{\mathbf{F}}^{-T}\boldsymbol{\xi} - \frac{\dfrac{\partial \overline{W}}{\partial \overline{\mathbf{F}}}\boldsymbol{\xi}\cdot\overline{\mathbf{F}}^{-T}\boldsymbol{\xi}}{\mu\overline{\mathbf{F}}^{-T}\boldsymbol{\xi}\cdot\overline{\mathbf{F}}^{-T}\boldsymbol{\xi}}\,\overline{\mathbf{F}}^{-T}\boldsymbol{\xi} \quad (2.15)$$

and hence that the effective stored-energy function in this case can be conveniently written as

$$\overline{W}(\overline{\mathbf{F}}, c) = 2\mu\,\overline{U}(\overline{\mathbf{F}}, c) + \frac{\mu}{2}\left[\,\overline{\mathbf{F}}\cdot\overline{\mathbf{F}} - 3\right], \quad (2.16)$$

where the function $\overline{U}$ is solution of the initial-value problem

$$\begin{aligned} c\frac{\partial \overline{U}}{\partial c} - \overline{U} - \int_{|\boldsymbol{\xi}|=1} \frac{1}{4\pi}\frac{\partial \overline{U}}{\partial \overline{\mathbf{F}}}\boldsymbol{\xi}\cdot\frac{\partial \overline{U}}{\partial \overline{\mathbf{F}}}\boldsymbol{\xi} - \frac{\left(\dfrac{\partial \overline{U}}{\partial \overline{\mathbf{F}}}\boldsymbol{\xi}\cdot\overline{\mathbf{F}}^{-T}\boldsymbol{\xi}\right)^2}{\overline{\mathbf{F}}^{-T}\boldsymbol{\xi}\cdot\overline{\mathbf{F}}^{-T}\boldsymbol{\xi}}\mathrm{d}\boldsymbol{\xi} \\ + \int_{|\boldsymbol{\xi}|=1} \frac{(1-\overline{J})\left(\overline{J} - 1 + 4\overline{J}\,\dfrac{\partial \overline{U}}{\partial \overline{\mathbf{F}}}\boldsymbol{\xi}\cdot\overline{\mathbf{F}}^{-T}\boldsymbol{\xi}\right)}{4\overline{J}^{\,2}\overline{\mathbf{F}}^{-T}\boldsymbol{\xi}\cdot\overline{\mathbf{F}}^{-T}\boldsymbol{\xi}}\mathrm{d}\boldsymbol{\xi} = 0, \\ \overline{U}(\overline{\mathbf{F}}, 1) = \frac{1}{2\,\mu}W_p(\overline{\mathbf{F}}) - \frac{1}{4}\left[\,\overline{\mathbf{F}}\cdot\overline{\mathbf{F}} - 3\right], \end{aligned} \quad (2.17)$$

and where it is reemphasized that (2.17) holds applicable for any choice of W_p.

In order to account for the perfectly rigid behavior (2.2) within the context of the formulation (2.13)–(2.14), it proves expedient not to work with (2.2) directly but to consider instead the regularized and hence more general case of *elastic isotropic incompressible* particles with stored-energy function

$$W_p(\mathbf{F}) = \begin{cases} \dfrac{4(\mu_p - \mu)}{5}\,H(\mathbf{F}) + \dfrac{\mu}{2}\left[\,\mathbf{F}\cdot\mathbf{F} - 3\right] & \text{if} \quad J = 1 \\ +\infty & \text{otherwise} \end{cases}. \quad (2.18)$$

In this last expression, the parameter μ_p denotes the shear modulus of the particles in their undeformed state and H is an objective and isotropic function of $\mathbf{F}$, satisfying the conditions $H(\mathbf{Q}) = 0$ for all $\mathbf{Q} \in Orth^+$ and $H(\mathbf{F}) > 0$ for $\mathbf{F} \notin Orth^+$, to be specified subsequently. The perfectly rigid behavior (2.2) can then be readily recovered as a special case of (2.18) by

taking the limit of $\mu_p \to +\infty$.

Given the incompressible stored-energy function (2.18) for the particles, it follows that the effective stored-energy function (2.16) for the filled Neo-Hookean rubber reduces to

$$\overline{W}(\overline{\mathbf{F}}, c) = \begin{cases} 2\mu\, \overline{U}(\overline{\mathbf{F}}, c) + \dfrac{\mu}{2}\left[\, \overline{\mathbf{F}} \cdot \overline{\mathbf{F}} - 3\right] & \text{if} \quad \overline{J} = 1 \\ +\infty & \text{otherwise} \end{cases} \tag{2.19}$$

with $\overline{U}$ now being defined by equations

$$\begin{aligned} &c\frac{\partial \overline{U}}{\partial c} - \overline{U} - \int_{|\boldsymbol{\xi}|=1} \frac{1}{4\pi} \left[\frac{\partial \overline{U}}{\partial \overline{\mathbf{F}}}\boldsymbol{\xi} \cdot \frac{\partial \overline{U}}{\partial \overline{\mathbf{F}}}\boldsymbol{\xi} - \frac{\left(\dfrac{\partial \overline{U}}{\partial \overline{\mathbf{F}}}\boldsymbol{\xi} \cdot \overline{\mathbf{F}}^{-T}\boldsymbol{\xi}\right)^2}{\overline{\mathbf{F}}^{-T}\boldsymbol{\xi} \cdot \overline{\mathbf{F}}^{-T}\boldsymbol{\xi}} \right] \mathrm{d}\boldsymbol{\xi} = 0, \\ &\overline{U}(\overline{\mathbf{F}}, 1) = \frac{2(\mu_p - \mu)}{5\mu}\, H(\overline{\mathbf{F}}), \end{aligned} \tag{2.20}$$

subject to the constraint $\overline{J} = 1$. To make further progress, it is helpful to exploit the overall isotropy and incompressibility of the problem. Thus, after restricting attention to isochoric pure stretch loadings of the form (2.11), carrying out the required integrals in (2.20), and with a little abuse of notation[4], the (finite branch of the) effective stored-energy function (2.19) for the filled Neo-Hookean rubber can be compactly rewritten as

$$\overline{W}(\overline{\lambda}_1, \overline{\lambda}_2, c) = 2\mu\, \overline{U}(\overline{\lambda}_1, \overline{\lambda}_2, c) + \frac{\mu}{2}\left[\overline{\lambda}_1^2 + \overline{\lambda}_2^2 + \frac{1}{\overline{\lambda}_1^2 \overline{\lambda}_2^2} - 3 \right] \tag{2.21}$$

where the function $\overline{U}$ is implicitly defined by the pde

$$c\frac{\partial \overline{U}}{\partial c} - \overline{U} + \alpha_1(\overline{\lambda}_1, \overline{\lambda}_2) \left(\frac{\partial \overline{U}}{\partial \overline{\lambda}_1} \right)^2 + \alpha_2(\overline{\lambda}_1, \overline{\lambda}_2) \left(\frac{\partial \overline{U}}{\partial \overline{\lambda}_2} \right)^2 + \alpha_3(\overline{\lambda}_1, \overline{\lambda}_2) \frac{\partial \overline{U}}{\partial \overline{\lambda}_1} \frac{\partial \overline{U}}{\partial \overline{\lambda}_2} = 0 \tag{2.22}$$

subject to the initial condition

$$\overline{U}(\overline{\lambda}_1, \overline{\lambda}_2, 1) = \frac{2(\mu_p - \mu)}{5\mu}\, H(\overline{\lambda}_1, \overline{\lambda}_2). \tag{2.23}$$

[4]The fact that the same symbols $\overline{W}$, $\overline{U}$, and H are utilized to denote the corresponding functions in terms of the stretches $\overline{\lambda}_1$ and $\overline{\lambda}_2$ should not lead to confusion.

The coefficients α_1, α_2, α_3 above are functions of their arguments given in explicit form by expressions (A.1) in Appendix A. In view of the definition (2.18), it is also appropriate to record here for later reference that the function $H : \{(a,b) \in \mathbb{R}^2 : a,b > 0\} \to \mathbb{R}$ in (2.23) must satisfy the following properties:

$$\begin{aligned}
&H(1,1) = 0,\\
&H(\overline{\lambda}_1,\overline{\lambda}_2) > 0 \qquad \forall\, \overline{\lambda}_1,\overline{\lambda}_2 \neq 1,\\
&H(\overline{\lambda}_1,\overline{\lambda}_2) = H(\overline{\lambda}_2,\overline{\lambda}_1) = H\left(\overline{\lambda}_1,(\overline{\lambda}_1\overline{\lambda}_2)^{-1}\right) = H\left((\overline{\lambda}_1\overline{\lambda}_2)^{-1},\overline{\lambda}_1\right)\\
&= H\left(\overline{\lambda}_2,(\overline{\lambda}_1\overline{\lambda}_2)^{-1}\right) = H\left((\overline{\lambda}_1\overline{\lambda}_2)^{-1},\overline{\lambda}_2\right) \qquad \forall\, \overline{\lambda}_1,\overline{\lambda}_2.
\end{aligned} \tag{2.24}$$

The final step in this first part of the derivation is to solve the initial-value problem (2.22)–(2.23) for the function $\overline{U}$ and then take the limit of rigid particles $\mu_p \to +\infty$. To this end, it is gainful to recognize two key aspects of equations (2.22)–(2.23). First, the particular form of the function H in (2.23) is immaterial, provided that the choice satisfies conditions (2.24). Second, as a result of the overall isotropy of the problem, the function $\overline{U}$ defined by (2.22)–(2.23) is symmetric with respect to its first two arguments, namely, $\overline{U}(\overline{\lambda}_1,\overline{\lambda}_2,c) = \overline{U}(\overline{\lambda}_2,\overline{\lambda}_1,c)$. In the sequel, we exploit the flexibility in the choice of H and the symmetry of $\overline{U}$ in order to construct a solution of (2.22)–(2.23). The idea is to utilize a particular choice of the function H that simplifies the calculations involved. And to make use of the symmetry of $\overline{U}$ in order to rewrite the initial condition (2.23) in terms of the more convenient deformation variables $\overline{\lambda}_1,\overline{\lambda}_2$, instead of in terms of the concentration of particles c. As elaborated next, the proposed strategy requires the successive analyses of axisymmetric ($\overline{\lambda}_1 = \overline{\lambda}_2 = \overline{\lambda}$) and general loading conditions.

I) Axisymmetric loading conditions. We begin by analyzing the special case of axisymmetric loading with

$$\overline{\lambda}_2 = \overline{\lambda}_1 = \overline{\lambda}. \tag{2.25}$$

By introducing the notation

$$\overline{U}_A(\overline{\lambda},c) \doteq \overline{U}(\overline{\lambda},\overline{\lambda},c) \tag{2.26}$$

and recognizing the identities

$$\frac{\partial \overline{U}}{\partial \overline{\lambda}_1}(\overline{\lambda},\overline{\lambda},c) = \frac{\partial \overline{U}}{\partial \overline{\lambda}_2}(\overline{\lambda},\overline{\lambda},c) = \frac{1}{2}\frac{\partial \overline{U}_A}{\partial \overline{\lambda}}(\overline{\lambda},c) \tag{2.27}$$

due to the symmetry of $\overline{U}$, it is straightforward to show (see relations (A.6) and (A.7) in Appendix A) that the initial-value problem (2.22)–(2.23) reduces to the simpler initial-value problem

$$\begin{aligned} &c\frac{\partial \overline{U}_A}{\partial c} - \overline{U}_A \\ &-\frac{\overline{\lambda}^6}{12(\overline{\lambda}^6-1)^2}\left[1+2\overline{\lambda}^6 - \frac{3\overline{\lambda}^6}{\sqrt{1-\overline{\lambda}^6}}\ln\left[\frac{\sqrt{1-\overline{\lambda}^6}+1}{\overline{\lambda}^3}\right]\right]\left(\frac{\partial \overline{U}_A}{\partial \overline{\lambda}}\right)^2 = 0 \end{aligned} \tag{2.28}$$

with

$$\overline{U}_A(\overline{\lambda},1) = \frac{2(\mu_p-\mu)}{5\mu}\,H(\overline{\lambda},\overline{\lambda}) \tag{2.29}$$

for the function $\overline{U}_A$. In spite of the fact that the pde (2.28) is nonlinear, the suitable choice

$$H(\overline{\lambda},\overline{\lambda}) = 3\left[\int_1^{\overline{\lambda}} \frac{\sqrt{(\,z^6-1)^2}}{z^3\sqrt{1+2z^6-\frac{3z^6}{\sqrt{1-z^6}}\ln\left[\frac{1+\sqrt{1-z^6}}{z^3}\right]}}\,\mathrm{d}z\right]^2 \tag{2.30}$$

makes it possible to solve (2.28)–(2.29) in *closed form*. The result reads as follows:

$$\begin{aligned} &\overline{U}_A(\overline{\lambda},c) = \\ &3\frac{2c(\mu_p-\mu)}{2(1-c)\mu_p+(3+2c)\mu}\left[\int_1^{\overline{\lambda}} \frac{\sqrt{(\,z^6-1)^2}}{z^3\sqrt{1+2z^6-\frac{3z^6}{\sqrt{1-z^6}}\ln\left[\frac{1+\sqrt{1-z^6}}{z^3}\right]}}\,\mathrm{d}z\right]^2. \end{aligned} \tag{2.31}$$

Here, we remark that the choice (2.30) for H is such that $H(1,1) = 0$ and $H(\overline{\lambda},\overline{\lambda}) > 0$ if $\overline{\lambda} \neq 1$, as required by conditions (2.24). Given the quadratic nonlinearity of the pde (2.28), it is also worth mentioning that equations

(2.28)–(2.29) with (2.30) have two solutions, but that both are identical and given by (2.31) in this case.

II) General loading conditions. Having determined the axisymmetric solution (2.31) for *any value of particle concentration* $c \in [0,1]$, the initial-value problem (2.22)–(2.23) can now be rewritten as

$$c\frac{\partial \overline{U}}{\partial c} - \overline{U} + \alpha_1(\overline{\lambda}_1,\overline{\lambda}_2)\left(\frac{\partial \overline{U}}{\partial \overline{\lambda}_1}\right)^2 + \alpha_2(\overline{\lambda}_1,\overline{\lambda}_2)\left(\frac{\partial \overline{U}}{\partial \overline{\lambda}_2}\right)^2 + \alpha_3(\overline{\lambda}_1,\overline{\lambda}_2)\frac{\partial \overline{U}}{\partial \overline{\lambda}_1}\frac{\partial \overline{U}}{\partial \overline{\lambda}_2} = 0 \tag{2.32}$$

subject to the alternative *deformation-based* initial condition

$$\overline{U}(\overline{\lambda},\overline{\lambda},c) = \\ 3\frac{2c(\mu_p-\mu)}{2(1-c)\mu_p+(3+2c)\mu}\left[\int_1^{\overline{\lambda}} \frac{\sqrt{(\,z^6-1)^2}}{z^3\sqrt{1+2z^6-\frac{3z^6}{\sqrt{1-z^6}}\ln\left[\frac{1+\sqrt{1-z^6}}{z^3}\right]}}\,\mathrm{d}z\right]^2 \tag{2.33}$$

as opposed to the original concentration-based condition (2.23), where it is recalled that the coefficients α_1, α_2, α_3 in (2.32) are given in explicit form by expressions (A.1) in Appendix A.

In view of the separable structure of the alternative initial condition (2.33), it is not difficult to deduce from the governing pde (2.32) that the solution for $\overline{U}$ is given by

$$\overline{U}(\overline{\lambda}_1,\overline{\lambda}_2,c) = \frac{2c(\mu_p-\mu)}{2(1-c)\mu_p+(3+2c)\mu}\,H(\overline{\lambda}_1,\overline{\lambda}_2), \tag{2.34}$$

where the function H is implicitly defined by the initial-value problem

$$H+\alpha_1(\overline{\lambda}_1,\overline{\lambda}_2)\left(\frac{\partial H}{\partial \overline{\lambda}_1}\right)^2+\alpha_2(\overline{\lambda}_1,\overline{\lambda}_2)\left(\frac{\partial H}{\partial \overline{\lambda}_2}\right)^2+\alpha_3(\overline{\lambda}_1,\overline{\lambda}_2)\frac{\partial H}{\partial \overline{\lambda}_1}\frac{\partial H}{\partial \overline{\lambda}_2} = 0 \tag{2.35}$$

with

$$H(\overline{\lambda},\overline{\lambda}) = 3\left[\int_1^{\overline{\lambda}} \frac{\sqrt{(\,z^6-1)^2}}{z^3\sqrt{1+2z^6-\frac{3z^6}{\sqrt{1-z^6}}\ln\left[\frac{1+\sqrt{1-z^6}}{z^3}\right]}}\,\mathrm{d}z\right]^2. \tag{2.36}$$

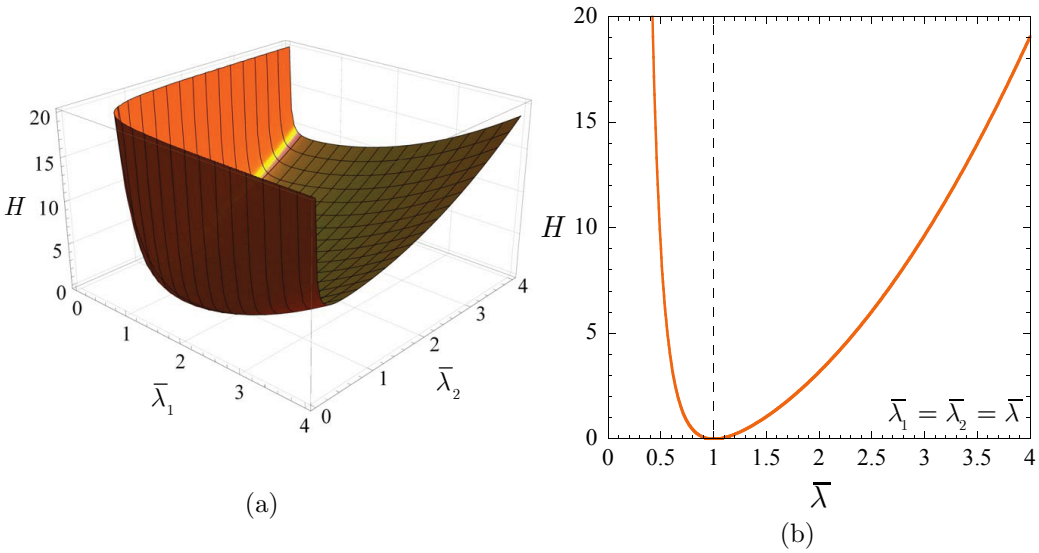

Figure 2.1: (a) Plot of the function H defined by equations (2.35)–(2.36) for a large range of stretches $\overline{\lambda}_1$ and $\overline{\lambda}_2$. Part (b) shows the cross section of the function along axisymmetric deformations with $\overline{\lambda}_1 = \overline{\lambda}_2 = \overline{\lambda}$, that is, $H(\overline{\lambda}, \overline{\lambda})$, as given explicitly by expression (2.36).

Rather interestingly, the first-order nonlinear pde (2.35) subject to (2.36) is an Eikonal equation[5]. This class of equations has appeared pervasively in a wide variety of problems concerning geometrical optics and other wave-propagation phenomena (see, e.g., Born and Wolf, 1999). Unfortunately, the specific type of Eikonal equation (2.35)–(2.36) does not appear to be solvable in closed form, but it can be solved numerically by available techniques. Fig. 1 shows plots of such a solution over a large range of stretches $\overline{\lambda}_1$ and $\overline{\lambda}_2$.

In addition to the required properties (2.24), two further features of the function H defined by (2.35)–(2.36) worth recording for later use are that in the limit of small deformation as $\overline{\varepsilon}_1 \doteq \overline{\lambda}_1 - 1 \to 0$ and $\overline{\varepsilon}_2 \doteq \overline{\lambda}_2 - 1 \to 0$ it takes the polynomial asymptotic form

$$H(\overline{\lambda}_1, \overline{\lambda}_2) = \frac{5}{4}\left[\overline{\varepsilon}_1^2 + \overline{\varepsilon}_2^2 + (\overline{\varepsilon}_1 + \overline{\varepsilon}_2)^2\right] - \frac{5}{2}(\overline{\varepsilon}_1^3 + \overline{\varepsilon}_2^3) - \frac{55}{14}(\overline{\varepsilon}_1^2\overline{\varepsilon}_2 + \overline{\varepsilon}_1\overline{\varepsilon}_2^2) + O(\overline{\varepsilon}_1^4) + O(\overline{\varepsilon}_2^4) \quad (2.37)$$

[5]With the change of variables $H = \widehat{H}^2$ and the notation $\alpha_1 = -(M_{11}^2 + M_{12}^2)/4$, $\alpha_2 = -(M_{22}^2 + M_{12}^2)/4$, $\alpha_3 = -M_{12}(M_{11} + M_{22})/2$, the Eikonal equation (2.35) takes the more standard invariant form $\left|\mathbf{M}\nabla\widehat{H}\right| = 1$.

while in the opposite limit of infinitely large deformations as $\overline{\lambda}_1 \to 0, +\infty$ and/or $\overline{\lambda}_2 \to 0, +\infty$ it reduces asymptotically to

$$H(\overline{\lambda}_1, \overline{\lambda}_2) = \frac{3}{4}\left[\overline{\lambda}_1^2 + \overline{\lambda}_2^2 + \frac{1}{\overline{\lambda}_1^2 \overline{\lambda}_2^2}\right] \tag{2.38}$$

to leading order, hence becoming unbounded. The proof of relations (2.24), (2.37), and (2.38) together with relevant comments on the numerical computation of H are given in Appendix B.

At this stage, it is a trivial matter to take the limit of rigid particles $\mu_p \to +\infty$ in expression (2.34) to conclude that the effective stored-energy function for Neo-Hookean rubber reinforced by the class of isotropic distributions of rigid particles specified by the formulation (2.13)–(2.14) is given by

$$\overline{W}(\overline{\lambda}_1, \overline{\lambda}_2, c) = \frac{2\mu\, c}{1-c}\, H(\overline{\lambda}_1, \overline{\lambda}_2) + \frac{\mu}{2}\left[\overline{\lambda}_1^2 + \overline{\lambda}_2^2 + \frac{1}{\overline{\lambda}_1^2 \overline{\lambda}_2^2} - 3\right] \tag{2.39}$$

with H being defined by equations (2.35)–(2.36). Again, this result is valid[6] for any value of concentration of particles in the range $c \in [0, 1]$. The analysis of its asymptotic behavior in the limit as $c \to 0+$ is the final step of the derivation and the subject of the next subsection.

2.2.2 Asymptotic solution in the dilute limit of particles as $c \to 0+$

We are now in a position to readily take the limit $c \to 0+$ in the result (2.39) to finally establish that the overall elastic response of Neo-Hookean rubber reinforced by a dilute isotropic distribution of rigid particles is characterized by the effective stored-energy function

$$\overline{W}(\overline{\lambda}_1, \overline{\lambda}_2, c) = \frac{\mu}{2}\left[\overline{\lambda}_1^2 + \overline{\lambda}_2^2 + \frac{1}{\overline{\lambda}_1^2 \overline{\lambda}_2^2} - 3\right] + 2\mu\, H(\overline{\lambda}_1, \overline{\lambda}_2)\, c \tag{2.40}$$

[6] As indicated above, the result (2.39) is exact for a specific type of isotropic distribution of rigid particles and expected to be a lower bound for the response of Neo-Hookean rubber rigidly reinforced by any other type of isotropic distribution. This expectation is supported by the results presented in the next chapter, where a variety of finite-concentration suspensions of rigid particles in rubber are studied.

to first order in the concentration of particles c. As derived in the foregoing development, the function H is implicitly defined by the Eikonal pde (2.35) subject to the initial condition (2.36). In general, again, these equations must be solved numerically. For the special case of axisymmetric loading, however, they admit a closed-form solution and expression (2.40) reduces to

$$\overline{W}(\overline{\lambda},\overline{\lambda},c) = \\ \frac{\mu}{2}\left[2\overline{\lambda}^2+\frac{1}{\overline{\lambda}^4}-3\right]+6\mu\left[\int_1^{\overline{\lambda}}\frac{\sqrt{(z^6-1)^2}}{z^3\sqrt{1+2z^6-\frac{3z^6}{\sqrt{1-z^6}}\ln\left[\frac{1+\sqrt{1-z^6}}{z^3}\right]}}\,\mathrm{d}z\right]^2 c. \tag{2.41}$$

Comparing (2.12) with (2.40), it is seen that the asymptotic form of the solution is indeed polynomial and that $G(\overline{\lambda}_1,\overline{\lambda}_2)=2H(\overline{\lambda}_1,\overline{\lambda}_2)$. The following remarks are in order:

i. Owing to the properties (2.24) of the function H, the effective stored-energy function (2.40) is such that

$$\begin{aligned}
&\overline{W}(1,1,c)=0,\\
&\overline{W}(\overline{\lambda}_1,\overline{\lambda}_2,c)>0 \quad \forall\,\overline{\lambda}_1,\overline{\lambda}_2\neq 1,\\
&\overline{W}(\overline{\lambda}_1,\overline{\lambda}_2,c)=\overline{W}(\overline{\lambda}_2,\overline{\lambda}_1,c)=\overline{W}\left(\overline{\lambda}_1,(\overline{\lambda}_1\overline{\lambda}_2)^{-1},c\right)\\
&=\overline{W}\left((\overline{\lambda}_1\overline{\lambda}_2)^{-1},\overline{\lambda}_1,c\right)=\overline{W}\left(\overline{\lambda}_2,(\overline{\lambda}_1\overline{\lambda}_2)^{-1},c\right)\\
&=\overline{W}\left((\overline{\lambda}_1\overline{\lambda}_2)^{-1},\overline{\lambda}_2,c\right) \quad \forall\,\overline{\lambda}_1,\overline{\lambda}_2,\\
&\overline{W}(\overline{\lambda}_1,\overline{\lambda}_2,c)>\overline{W}(\overline{\lambda}_1,\overline{\lambda}_2,0) \quad \forall\,\overline{\lambda}_1,\overline{\lambda}_2\neq 1,\ c>0.
\end{aligned} \tag{2.42}$$

The first three of these conditions are direct consequences of the fact that the filled Neo-Hookean rubber is stress-free in the undeformed configuration, isotropic, and incompressible. The last condition entails physically that the addition of rigid particles consistently leads to a stiffer material response irrespectively of the applied loading, in agreement with experience.

ii. In the limit of small deformations as $\overline{\varepsilon}_1=\overline{\lambda}_1-1\to 0$ and $\overline{\varepsilon}_2=\overline{\lambda}_2-1\to 0$, based on the asymptotic behavior (2.37) of H, the effective stored-

energy function (2.40) takes the explicit asymptotic form

$$\begin{aligned}&\overline{W}(\overline{\lambda}_1,\overline{\lambda}_2,c)=\\&\mu\left[\overline{\varepsilon}_1^2+\overline{\varepsilon}_2^2+(\overline{\varepsilon}_1+\overline{\varepsilon}_2)^2-2(\overline{\varepsilon}_1^3+\overline{\varepsilon}_2^3)-3(\overline{\varepsilon}_1^2\overline{\varepsilon}_2+\overline{\varepsilon}_1\overline{\varepsilon}_2^2)\right]+\\&\frac{5}{2}\mu\left[\overline{\varepsilon}_1^2+\overline{\varepsilon}_2^2+(\overline{\varepsilon}_1+\overline{\varepsilon}_2)^2-2(\overline{\varepsilon}_1^3+\overline{\varepsilon}_2^3)-\frac{110}{35}(\overline{\varepsilon}_1^2\overline{\varepsilon}_2+\overline{\varepsilon}_1\overline{\varepsilon}_2^2)\right]c\end{aligned}\tag{2.43}$$

to order three in the deformation measures $\overline{\varepsilon}_1$ and $\overline{\varepsilon}_2$. As anticipated in the description of the formulation (2.13)–(2.14), the leading order of expression (2.43) agrees identically with the Einstein-Smallwood (or, more generally, Eshelby) result for the overall elastic response of a dilute distribution of rigid spherical particles embedded in an isotropic incompressible linearly elastic matrix (cf. Eq. (12) in Smallwood (1944)).

iii. In terms of the principal invariants $\overline{I}_1=\overline{\mathbf{F}}\cdot\overline{\mathbf{F}}=\overline{\lambda}_1^2+\overline{\lambda}_2^2+\overline{\lambda}_1^{-2}\overline{\lambda}_2^{-2}$ and $\overline{I}_2=\overline{\mathbf{F}}^{-T}\cdot\overline{\mathbf{F}}^{-T}=\overline{\lambda}_1^{-2}+\overline{\lambda}_2^{-2}+\overline{\lambda}_1^2\overline{\lambda}_2^2$, the asymptotic result (2.43) can be rewritten as

$$\overline{W}(\overline{\lambda}_1,\overline{\lambda}_2,c)=\frac{\mu}{2}(\overline{I}_1-3)+2\mu\left[\frac{145}{224}(\overline{I}_1-3)-\frac{5}{224}(\overline{I}_2-3)\right]c\tag{2.44}$$

to order one in the deformation measures $(\overline{I}_1-3)$ and $(\overline{I}_2-3)$. This expression illustrates explicitly that the overall response of the filled Neo-Hookean rubber depends not only on the first invariant $\overline{I}_1$ but also on the second invariant $\overline{I}_2$ (in spite of the fact that the underlying Neo-Hookean matrix depends only on the first invariant). Given that the associated coefficient $5/224$ is significantly smaller than unity, however, the dependence on $\overline{I}_2$ is weak. Rather remarkably, as discussed below and in Section 5, the dependence on $\overline{I}_2$ remains weak for large deformations (of order $(\overline{I}_2-3)^2$ and higher) and it completely disappears in the limit of deformations that are infinitely large.

iv. In the limit when the deformation becomes unbounded as $\overline{\lambda}_1\to 0,+\infty$ and/or $\overline{\lambda}_2\to 0,+\infty$, the function H reduces to (2.38) and hence it is straightforward to deduce that the effective stored-energy function

(2.40) reduces in turn to the explicit form

$$\overline{W}(\overline{\lambda}_1, \overline{\lambda}_2, c) = \frac{\mu}{2}\left[\overline{\lambda}_1^2 + \overline{\lambda}_2^2 + \frac{1}{\overline{\lambda}_1^2\overline{\lambda}_2^2}\right] + \frac{3\mu}{2}\left[\overline{\lambda}_1^2 + \overline{\lambda}_2^2 + \frac{1}{\overline{\lambda}_1^2\overline{\lambda}_2^2}\right] c \tag{2.45}$$

or, equivalently,

$$\overline{W}(\overline{\lambda}_1, \overline{\lambda}_2, c) = \frac{\mu}{2}\,\overline{I}_1 + \frac{3\mu}{2}\,\overline{I}_1\, c \tag{2.46}$$

to leading order. That is, for large enough deformations, the overall energy of the filled Neo-Hookean rubber grows *linearly* in the first invariant $\overline{I}_1$ and *independently* of $\overline{I}_2$.

v. Consistent with recent bifurcation analyses (Triantafyllidis et al., 2006; Michel et al., 2010), the effective stored-energy function (2.40) is strongly elliptic. In the present context of isotropic incompressible elasticity, it is possible to write down explicit necessary and sufficient conditions for strong ellipticity in the form of 9 scalar inequalities involving first and second derivatives of (2.40) with respect to $\overline{\lambda}_1$ and $\overline{\lambda}_2$, as detailed in Appendix **??**. While difficult by analytical means, it is a simple matter to verify numerically that all such 9 scalar inequalities are satisfied by (2.40). Interestingly, despite being strongly elliptic, (2.40) is *not* polyconvex. To see this, as also elaborated in Appendix **??**, it suffices to recognize that (2.44) is not convex in $\overline{I}_2 (= \overline{\mathbf{F}}^{-T} \cdot \overline{\mathbf{F}}^{-T})$ to leading order in the limit of small deformations, and hence that (2.40) is not convex in $\overline{\mathbf{F}}^{-T}$.

vi. By construction, the microstructure associated with the result (2.40) corresponds to a dilute isotropic distribution of rigid particles that interact in such a manner that the stress within each particle is uniform and the same in all particles, irrespectively of the value of the applied macroscopic stretches $\overline{\lambda}_1$ and $\overline{\lambda}_2$. For small enough deformations, such a special stress field is in precise agreement with that of a dilute distribution of rigid spheres (Eshelby, 1957). This is the key reason why the result (2.40) recovers the classical Einstein-Smallwood result in the limit of small deformations. For finite deformations, on the other hand, the intraparticle stress field in a dilute distribution of spherical particles does *not* remain uniform. Yet, the large-deformation response of a dilute distribution of rigid spherical particles is expected to be very

similar to that characterized by (2.40). This expectation is based on the argument that the effect of particle interactions on the overall response of *dilute* suspensions should be small (even at large deformations), and hence that different interactions associated with different dilute isotropic distributions of particles should lead to similar overall responses. This argument is supported by comparisons with the FE simulations presented next.

2.3 FE solutions for a rigid spherical inclusion in a block of rubber under large deformations

In the sequel, we work out a 3D FE solution for the overall large-deformation response of a block of Neo-Hookean rubber that contains a single rigid spherical inclusion of infinitesimal size at its center. The comparison between this solution for an *isolated spherical particle* with the above-derived analytical solution for an *isotropic distribution of particles* shall shed light on the importance of particle interactions in the overall elastic response of dilute suspensions of rigid particles in rubber.

2.3.1 The FE model

For convenience and without loss of generality, we consider the block of Neo-Hookean rubber to be a cube of side L in its undeformed stress-free configuration. Given that the radius of the spherical inclusion, a say, in the FE model must be necessarily *finite*, we need to identify how small its concentration $c = 4\pi a^3/3L^3$ ought to be in order to accurately approximate an actual infinitesimal particle with $c \to 0+$. To this end, we carried out a parametric study with decreasing values of c ranging from 10^{-6} to 10^{-11}. For the kind of deformations of interest in this chapter, the results indicate that concentrations $c \leq 10^{-8}$ are sufficiently small to be representative of an infinitesimal particle. Accordingly, in this chapter we set the particle concentration at

$$c = \frac{125\pi}{48} \times 10^{-9} \tag{2.47}$$

corresponding to a spherical inclusion of radius $a = 1$ in a cube of side $L = 800$.

Having identified the geometry of the block and of the particle, we now turn to their discretization. We first note that there is no need to mesh the particle in order to model exactly its rigid behavior, but that instead it suffices to spatially fix the particle/matrix interface in its undeformed configuration. We further note that the geometric and constitutive symmetry of the problem allows to perform the calculations in just one octant of the cube. A mesh generator code is utilized to construct the 3D geometry for such an octant, as depicted in Fig. 2.2. Small elements are placed near the rigid particle at uniform angular intervals of 3°, while the radial length is gradually increased toward the outer boundary. In all, the mesh consists of 18,900 brick elements with 675 elements on a radial plane and 28 layers along the radial direction. This discretization was selected after various mesh refinements were tried to assess sufficient mesh convergence. In selecting an appropriate type of finite element, we tested 8-node linear and 20-node quadratic hybrid elements, where the pressure is treated as a further degree of freedom in order to be able to handle the incompressibility of the Neo-Hookean rubber exactly (in a numerical sense). Although both elements generated similar results, a close inspection revealed that more consistent behaviors with the known Einstein-Smallwood solution at very small loads were obtained with the 20-node element model. We thus make use here of higher-order 20-node elements for the analysis. Since the computations are carried out using the FE package ABAQUS, we make use in particular of the C3D20H hybrid elements available in this code (see Abaqus version 6.11 documentation).

2.3.2 Computation of the overall elastic response

As already discussed within the more general context of Section 2, the overall elastic response of the above-defined reinforced block of Neo-Hookean rubber amounts to computing the total elastic energy per unit undeformed volume when the outer boundary of the block is subjected to the affine displacement boundary condition (2.4). Similar to the analytical approach presented above, here it also proves convenient to restrict attention — without loss of generality — to isochoric pure stretch loadings of the form (2.11). In terms

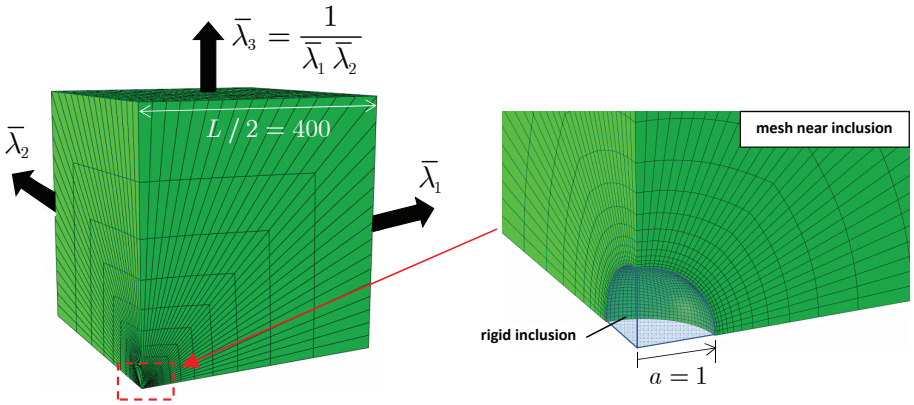

Figure 2.2: Finite element model — in the undeformed configuration — of a small rigid spherical particle of radius $a = 1$ located at the center of a cubic block of side $L = 800$. The outer boundary of the cube is subjected to the isochoric affine stretches $\overline{\lambda}_1$, $\overline{\lambda}_2$, $\overline{\lambda}_3 = (\overline{\lambda}_1\overline{\lambda}_2)^{-1}$ aligned with the three principal axes of the cube.

of these stretch variables and based on the parametric study performed for decreasing values of particle concentration $c \in [10^{-6}, 10^{-11}]$, the effective stored-energy function computed from the FE model turns out to be of the expected asymptotic form

$$\overline{W}^{FE}(\overline{\lambda}_1, \overline{\lambda}_2, c) = \frac{\mu}{2}\left[\overline{\lambda}_1^2 + \overline{\lambda}_2^2 + \frac{1}{\overline{\lambda}_1^2\overline{\lambda}_2^2} - 3\right] + 2\mu\, H^{FE}(\overline{\lambda}_1, \overline{\lambda}_2)\, c + O(c^2), \tag{2.48}$$

where it is worth remarking that this asymptotic behavior in the limit as $c \to 0+$ is of identical polynomial form as that of the analytical solution (2.40). It is also important to emphasize that the correction term in (2.48) is in the order of 10^{-9} (i.e., in the order of the particle concentration (2.47)), and hence that the computation of $\overline{W}^{FE}$ must be carefully carried out in double precision in order to be able to accurately determine the correcting function H^{FE}.

A convenient manner to numerically implement the affine boundary conditions (2.4) with (2.11) is to follow radial straining paths in principal-logarithmic-strain space $(\ln \overline{\lambda}_i)$. Specifically, we set

$$\overline{\lambda}_1 = \lambda \quad \text{and} \quad \overline{\lambda}_2 = \lambda^m \tag{2.49}$$

(and hence $\overline{\lambda}_3 = (\overline{\lambda}_1\overline{\lambda}_2)^{-1} = \lambda^{-(1+m)}$), where λ is a positive load parameter that takes the value of 1 in the undeformed configuration and $m \in \mathbb{R}$. Any de-

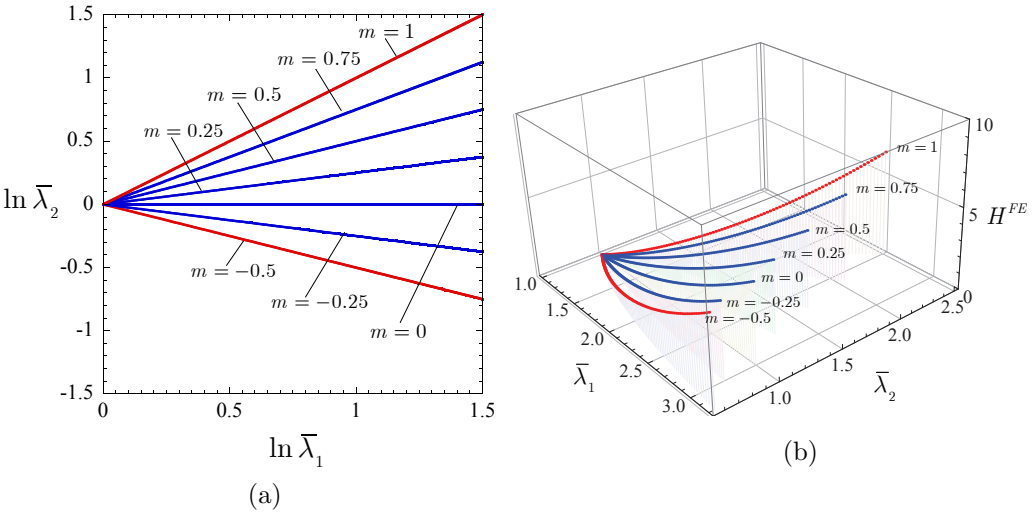

Figure 2.3: (a) A set of seven evenly distributed radial loading paths (2.49) in principal-logarithmic-strain space $\ln \overline{\lambda}_1$–$\ln \overline{\lambda}_2$ for values of the parameters $\lambda \geq 1$ and $m \in [-0.5, 1]$. (b) The corresponding correcting function (2.50) computed from the FE model in terms of the applied stretches $\overline{\lambda}_1$ and $\overline{\lambda}_2$.

sired macroscopic deformation state $(\overline{\lambda}_1, \overline{\lambda}_2, \overline{\lambda}_3 = (\overline{\lambda}_1 \overline{\lambda}_2)^{-1})$ can be accessed by marching along (starting at $\lambda = 1$) radial paths (4.19) with appropriate fixed values of m. Because of the overall isotropy and incompressibility of the response it actually suffices to consider $\overline{\lambda} \geq 1$ and $m \in [-0.5, 1]$, where $m = -0.5$ and $m = 1$ correspond to axisymmetric tension (or, equivalently, biaxial compression) and axisymmetric compression (or, equivalently, biaxial tension), respectively. Figure 2.3 shows FE results for seven different loading paths with $\lambda \geq 1$ and values of $m = -0.5, -025, 0, 0.25, 0.50, 0.75$ and 1.0. Results are shown for the radial loading paths in principal-logarithmic-strain space in part (a), and for the correcting function

$$H^{FE}(\overline{\lambda}_1, \overline{\lambda}_2) = \frac{1}{c}\left[\frac{1}{2\mu}\overline{W}^{FE}(\overline{\lambda}_1, \overline{\lambda}_2, c) - \frac{1}{4}\left[\overline{\lambda}_1^2 + \overline{\lambda}_2^2 + \frac{1}{\overline{\lambda}_1^2 \overline{\lambda}_2^2} - 3\right]\right] \tag{2.50}$$

in stretch space in part (b). The entire correcting function H^{FE} can be constructed by carrying out further computations with $\overline{\lambda} \geq 1$ and $m \in [-0.5, 1]$, and by exploiting the inherent symmetries

$$\begin{aligned} &H^{FE}(\overline{\lambda}_1, \overline{\lambda}_2) = H^{FE}(\overline{\lambda}_2, \overline{\lambda}_1) = H^{FE}\left(\overline{\lambda}_1, (\overline{\lambda}_1 \overline{\lambda}_2)^{-1}\right) \\ &= H^{FE}\left((\overline{\lambda}_1 \overline{\lambda}_2)^{-1}, \overline{\lambda}_1\right) = H^{FE}\left(\overline{\lambda}_2, (\overline{\lambda}_1 \overline{\lambda}_2)^{-1}\right) = H^{FE}\left((\overline{\lambda}_1 \overline{\lambda}_2)^{-1}, \overline{\lambda}_2\right). \end{aligned} \tag{2.51}$$

2.4 Results and discussion

Figures 2.5 and 2.4 present results for the overall response of Neo-Hookean rubber reinforced by a dilute isotropic distribution of rigid particles, as characterized by the analytical solution (2.40), and the FE simulations of the preceding section for the overall response of a Neo-Hookean block of rubber reinforced by a single rigid spherical particle. For clarity of presentation, results are shown for the correcting functions H and H^{FE} instead of the stored-energy functions $\overline{W}$ and $\overline{W}^{FE}$ themselves.

Figures 2.5(a) and 2.5(b) provide a full 3D comparison between the analytical and FE solutions in $\overline{\lambda}_1$–$\overline{\lambda}_2$-space. To aid the visualization of the quantitative differences, parts (c) through (f) of the figure also provide 2D views of both solutions along various fixed deformation paths: parts (c) and (d) display results for axisymmetric tension ($\overline{\lambda}_1 = \overline{\lambda}_2 = \overline{\lambda} \leq 1$) and compression ($\overline{\lambda}_1 = \overline{\lambda}_2 = \overline{\lambda} \geq 1$), whereas parts (e) and (f) display results for pure shear ($\overline{\lambda}_1 = \overline{\lambda}, \overline{\lambda}_2 = 1$) and a further intermediate deformation path ($\overline{\lambda}_1 = \overline{\lambda}, \overline{\lambda}_2 = \overline{\lambda}^{0.5}$). In all these plots, the solid line corresponds to the analytical solution, while the dashed line denotes the FE results.

An immediate observation from Fig. 2.5 is that the FE results are in good qualitative and quantitative agreement with the analytical solution (2.40) for all loading conditions. More specifically, the FE results are practically identical to the analytical solution up to sufficiently large deformations after which they start to exhibit a consistently stiffer behavior. The largest discrepancy between the two results occurs along axisymmetric compression (shown in Fig. 2.5(d)), but even in this case the quantitative difference is less than 7% at the maximum stretch of $\overline{\lambda}_1 = \overline{\lambda}_2 = \overline{\lambda} = 2.5$ reached with the FE model.

To further explore the connections between the analytical and FE solutions, Fig. 2.4 provides plots for H and H^{FE} as functions of the principal invariants $\overline{I}_1 = \overline{\lambda}_1^2 + \overline{\lambda}_2^2 + \overline{\lambda}_1^{-2}\overline{\lambda}_2^{-2}$ and $\overline{I}_2 = \overline{\lambda}_1^{-2} + \overline{\lambda}_2^{-2} + \overline{\lambda}_1^2\overline{\lambda}_2^2$. Part (a) of the figure shows H and H^{FE} for fixed values of the second invariant $\overline{I}_2 = 4$ and 6 as functions of $\overline{I}_1$, while part (b) shows corresponding results for fixed values of the first invariant $\overline{I}_1 = 4, 6, 8$, and 10 as functions of $\overline{I}_2$. Here, it is appropriate to recall that the constraint of incompressibility imposes a restriction on the physically allowable values of $\overline{I}_1$ and $\overline{I}_2$. Thus, for fixed $\overline{I}_2 = 4$ and 6 the first invariant is restricted to take values in the ranges $\overline{I}_1 \in [3.71, 4.52]$

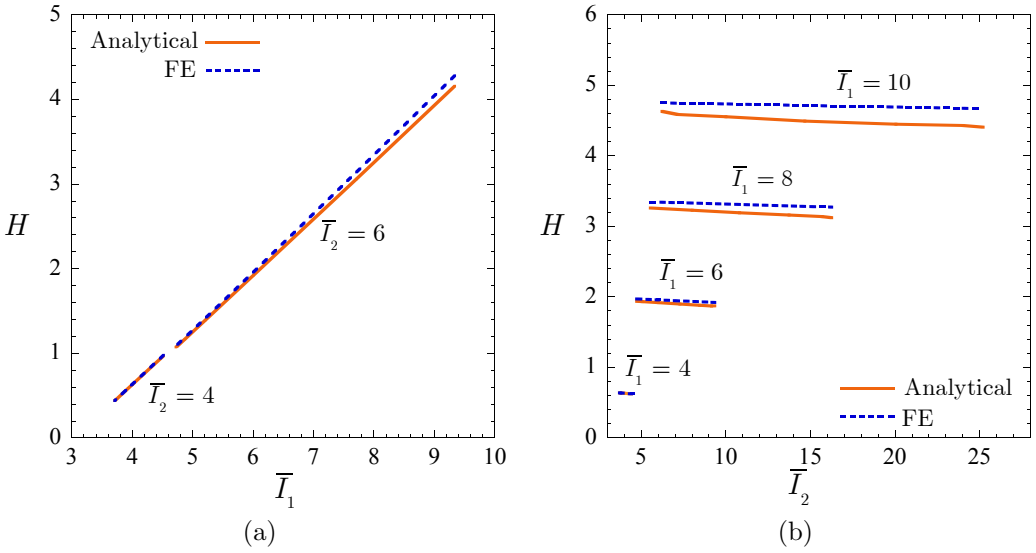

Figure 2.4: Comparison of the analytical solution (2.40) for the overall response of Neo-Hookean rubber reinforced by a dilute isotropic distribution of rigid particles with the FE solution (2.48) for the overall response of a Neo-Hookean block of rubber reinforced by a single rigid spherical particle. The results are shown for the correcting functions H and H^{FE} in terms of the principal invariants $\overline{I}_1 = \overline{\lambda}_1^2 + \overline{\lambda}_2^2 + \overline{\lambda}_1^{-2}\overline{\lambda}_2^{-2}$ and $\overline{I}_2 = \overline{\lambda}_1^{-2} + \overline{\lambda}_2^{-2} + \overline{\lambda}_1^2\overline{\lambda}_2^2$. Part (a) shows results for various fixed values of $\overline{I}_2$ as a function of $\overline{I}_1$, while part (b) shows results for various fixed values of $\overline{I}_1$ as a function of $\overline{I}_2$.

and $\overline{I}_1 \in [4.72, 9.34]$, respectively. For fixed $\overline{I}_1 = 4, 6, 8$, and 10, the corresponding allowable values of the second invariant are $\overline{I}_2 \in [3.71, 4.52]$, $\overline{I}_2 \in [4.72, 9.34]$, $\overline{I}_2 \in [5.53, 16.25]$, and $\overline{I}_2 \in [6.22, 25.20]$. These are the ranges of values utilized in the figure.

Similar to Fig. 2.5, Fig. 2.4 shows that indeed the FE results are in good agreement with the analytical solution, being slightly stiffer at large deformations. More importantly, Fig. 2.4 serves to illustrate that both solutions are approximately *linear* in the first invariant $\overline{I}_1$ and *independent* of second invariant $\overline{I}_2$. That is, in addition to being similar quantitatively, the analytical and FE solutions are essentially identical in their functional character.

The agreement between the FE and analytical solutions revealed by the above results is somewhat remarkable, given that they correspond to different microstructures: while the FE results correspond to the overall response of a block of rubber reinforced by a *single rigid spherical particle*, the analytical solution corresponds to the overall response of rubber reinforced by a specific

class of *isotropic distribution of rigid particles*.

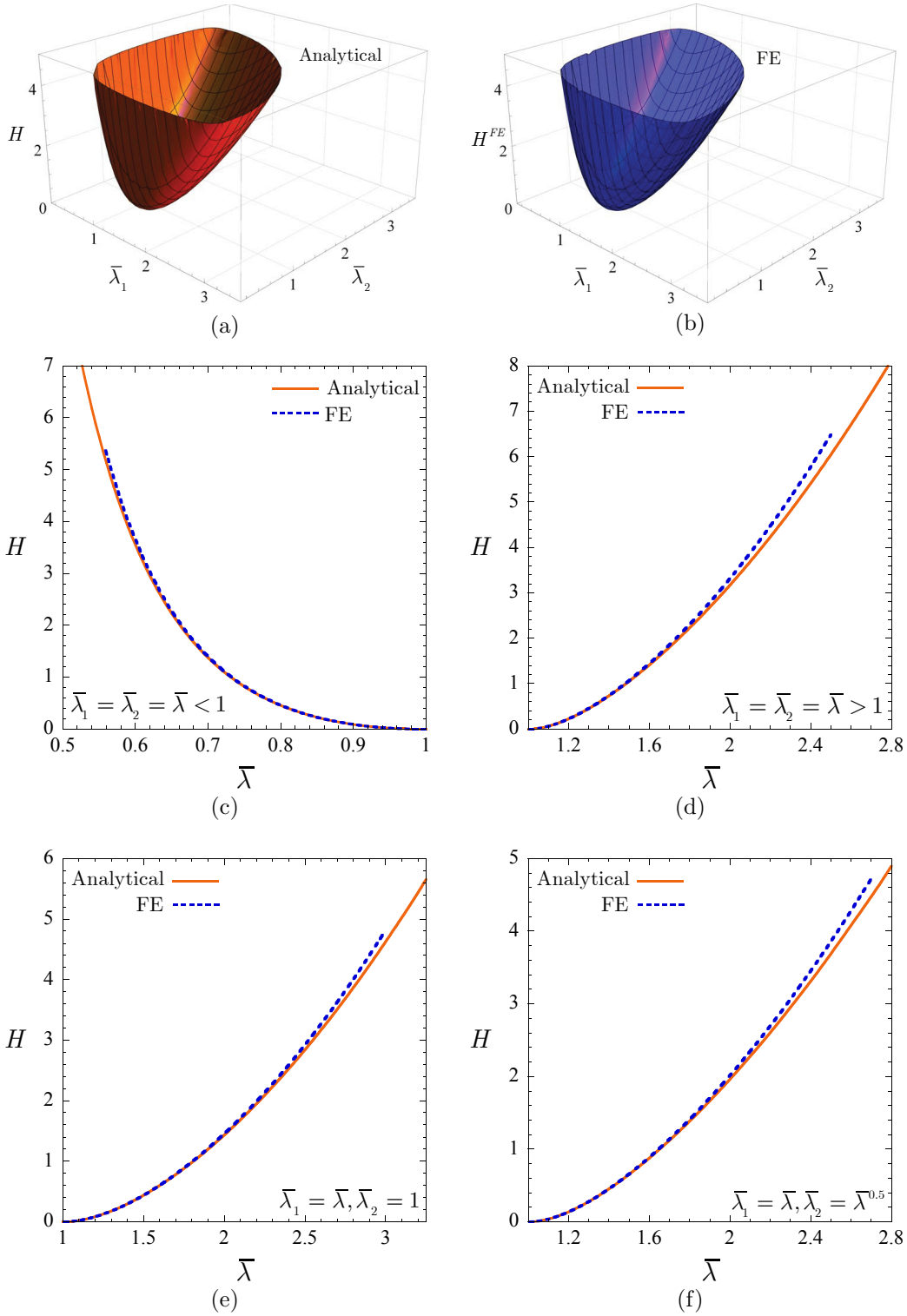

Figure 2.5: Comparison of the analytical solution (2.40) for the overall response of Neo-Hookean rubber reinforced by a dilute isotropic distribution of rigid particles with the FE solution (2.48). The results are shown for the correcting functions H (part(a)) and H^{FE} (part (b)) in terms of the stretches $\overline{\lambda}_1$ and $\overline{\lambda}_2$ in $\overline{\lambda}_1$–$\overline{\lambda}_2$–space, as well as along various fixed deformation paths: (c) $\overline{\lambda}_1 = \overline{\lambda}_2 = \overline{\lambda} < 1$, (d) $\overline{\lambda}_1 = \overline{\lambda}_2 = \overline{\lambda} > 1$, (e) $\overline{\lambda}_1 = \overline{\lambda}, \overline{\lambda}_2 = 1$, and (f) $\overline{\lambda}_1 = \overline{\lambda}$, $\overline{\lambda}_2 = \overline{\lambda}^{0.5}$.

Again, while in the case of the FE result the particle is isolated and hence *does not* interact with other particles, in the case of the analytical solution the underlying particles *do* interact with each other in such a manner that their stress is uniform. The close functional and quantitative agreement between the two results thus suggests that the interaction among particles does not play an important role in the overall nonlinear elastic response of dilute suspensions of rigid particles in rubber, even at large deformations. In turn, this suggests that different dilute isotropic distributions of particles exhibiting different particle interactions lead to similar overall responses.

2.5 An approximate *closed-form* solution for dilute suspensions

The evaluation of the effective stored-energy function (2.40) requires knowledge of the function H, which ultimately amounts to solving numerically the Eikonal pde (2.35) subject to the initial condition (2.36). In this section, we propose an approximate closed-form solution for (2.35)–(2.36), very close to the exact solution, which allows in turn to generate a closed-form approximation for (2.40).

The approximation is based on the observation that the function H is *linear* in the invariant $\overline{I}_1$ and *independent* of $\overline{I}_2$ in the limiting regimes of small and large deformations; see remarks *iii* and *iv* in Section 2.2.2. For intermediate deformations, H *does* depend nonlinearly on $\overline{I}_1$ and on the second invariant $\overline{I}_2$, but both these dependencies are exceptionally weak, as illustrated in Fig. 2.4. Thus, we can readily generate an approximate solution that agrees identically with the exact solution (2.37) of (2.35)–(2.36) in the limit of small deformations — and hence linearizes properly — by simply taking

$$H(\overline{\lambda}_1, \overline{\lambda}_2) = \frac{5}{8}\left[\overline{\lambda}_1^2 + \overline{\lambda}_2^2 + \frac{1}{\overline{\lambda}_1^2\overline{\lambda}_2^2} - 3\right]. \tag{2.52}$$

In the limit of large deformations, the approximation (2.52) also agrees identically with the exact solution (2.38) of (2.35)–(2.36) but only in a functional form, as their coefficients are different. Note in particular that the 5/8 coefficient in (2.52) is smaller that the 3/4 coefficient in (2.38), indicating that the

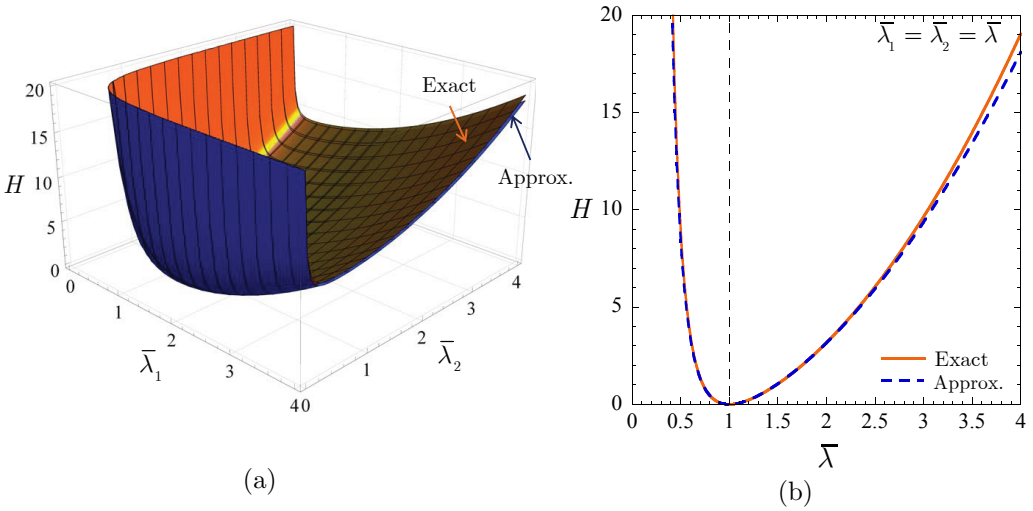

(a) (b)

Figure 2.6: Comparison between the function H defined by equations (2.35)–(2.36) and its closed-form approximation (2.52). Part (a) shows the comparison for a wide range of stretches $\overline{\lambda}_1$ and $\overline{\lambda}_2$, while part (b) shows the comparison for the case of axisymmetric deformations with $\overline{\lambda}_1 = \overline{\lambda}_2 = \overline{\lambda}$.

approximate solution (2.52) bounds from below the exact solution of (2.35)–(2.36) for large enough deformations. For intermediate deformations, the proposed closed-form approximation (2.52) is remarkably close to the exact function H. This is shown by Fig. 2.6(a) in $\overline{\lambda}_1$–$\overline{\lambda}_2$-space and by Fig. 2.6(b) for the special case of axisymmetric deformations with $\overline{\lambda}_1 = \overline{\lambda}_2 = \overline{\lambda}$.

In view of the approximation (2.52) for H, it readily follows from (2.40) that the resulting closed-form approximate solution for $\overline{W}$ is given by

$$\overline{W}(\overline{\lambda}_1, \overline{\lambda}_2, c) = \frac{\mu}{2}\left[\overline{\lambda}_1^2 + \overline{\lambda}_2^2 + \frac{1}{\overline{\lambda}_1^2\overline{\lambda}_2^2} - 3\right] + \frac{5\mu}{4}\left[\overline{\lambda}_1^2 + \overline{\lambda}_2^2 + \frac{1}{\overline{\lambda}_1^2\overline{\lambda}_2^2} - 3\right] c \tag{2.53}$$

or, equivalently,

$$\overline{W}(\overline{\lambda}_1, \overline{\lambda}_2, c) = \frac{\mu}{2}\left[\overline{I}_1 - 3\right] + \frac{5\mu}{4}\left[\overline{I}_1 - 3\right] c. \tag{2.54}$$

Because of the properties of (2.52), the approximate solution (2.53) is identical to the exact solution (2.40) in the limit of small deformations — and hence recovers the classical Einstein-Smallwood result — and quantitatively very close to (2.40) for arbitrarily large deformations. In addition, the result (2.53) is functionally very similar to (2.40) in that it is linear in $\overline{I}_1$, indepen-

dent of $\overline{I}_2$, and strongly elliptic (see Appendix C). The approximate solution (2.53) provides then a mathematically simple, quantitatively accurate, and functionally sound result — which can be utilized in lieu of (2.40) for all practical purposes — for the overall elastic response of Neo-Hookean solids reinforced by a dilute isotropic distribution of rigid particles under arbitrarily large deformations.

CHAPTER 3

THE NONLINEAR ELASTIC RESPONSE OF SUSPENSIONS OF RIGID INCLUSIONS IN RUBBER: AN EXPLICIT APPROXIMATION FOR FINITE-CONCENTRATION SUSPENSIONS

In the preceding chapter we determined an exact solution for the overall (or macroscopic) nonlinear elastic response of Gaussian (or Neo-Hookean) rubber reinforced by a dilute isotropic distribution of rigid particles. The objective of this Chapter is to make use of this fundamental result to construct an approximate solution for the corresponding response of *non-Gaussian* rubber reinforced by an isotropic distribution of rigid particles at *finite concentration*. Given that standard reinforcing fillers (e.g., carbon black and silica) typically agglomerate into "particles" of many different sizes (see, e.g., Chapter 4 in Leblanc, 2010, and references therein), the focus is in particular on isotropic distributions of particles of polydisperse sizes. This is accomplished here with the help of two different techniques in two successive steps. In the first step of the derivation, the dilute solution ofLopez-Pamies et al. (2013b) elaborated in Chapter 2 is extended to finite-concentration suspensions of particles in Neo-Hookean rubber via an iterated dilute homogenization technique. In the second step, a nonlinear comparison medium technique is utilized to construct in turn an approximate solution for finite-concentration suspensions of particles in non-Gaussian rubber.

For purposes of gaining further insight and of assessing the accuracy of the proposed analytical approximation, in this chapter we also generate full 3D FE (finite-element) results for the large-deformation response of Neo-Hookean and non-Gaussian rubber reinforced by isotropic distributions of rigid spherical particles. Specifically, we consider the cases of infinite periodic media where the repeated unit cells contain a large number of monodisperse and polydisperse spherical particles that are randomly distributed as dictated by a sequential adsorption algorithm. Full 3D computations of this sort

have been previously considered in the context of infinitesimal elasticity by a number of authors (see, e.g. Gusev, 1997; Michel et al., 1999; Segurado and Llorca, 2002; Galli et al., 2008), but the finite elasticity simulations performed in this chapter appear to be the first of their kind in the literature.

3.1 The problem

The general problem to be addressed is that of determining the overall (or macroscopic) elastic response of an elastomer reinforced by a random distribution of rigid particles firmly bonded across interfaces that is subjected to arbitrarily large deformations. The spatial distribution of the particles is taken to be statistically uniform and their sizes to be much smaller than the macroscopic size. The constitutive behavior of the elastomer is characterized by a quasi-convex stored-energy function W of the deformation gradient $\mathbf{F}$. The rigid particles are also described as nonlinear elastic solids with stored-energy function

$$W_p(\mathbf{F}) = \begin{cases} 0 & \text{if} \quad \mathbf{F} = \mathbf{Q} \in Orth^+ \\ +\infty & \text{otherwise} \end{cases}, \tag{3.1}$$

where $Orth^+$ stands for the set of all proper orthogonal second-order tensors. The Lagrangian pointwise constitutive relation for the material is thus formally given by

$$\mathbf{S} = \frac{\partial W}{\partial \mathbf{F}}(\mathbf{X}, \mathbf{F}), \quad W(\mathbf{X}, \mathbf{F}) = (1 - \theta(\mathbf{X}))\ W(\mathbf{F}) + \theta(\mathbf{X})\ W_p(\mathbf{F}), \tag{3.2}$$

where $\mathbf{S}$ denotes the first Piola-Kirchhoff stress tensor and θ is the indicator function of the spatial regions occupied collectively by the particles, taking the value of 1 if the position vector $\mathbf{X}$ lies in a particle and zero otherwise.

The filled elastomer is considered to occupy a domain Ω, with boundary $\partial\Omega$, in its undeformed stress-free configuration and, for convenience, units of length are chosen so that Ω has unit volume. The regions occupied by the elastomer and particles are respectively denoted by Ω_m and Ω_p so that $\Omega = \Omega_m \cup \Omega_p$. The macroscopic response of the material can then be defined as the relation between the averages of the first Piola-Kirchhoff stress $\mathbf{S}$ and the deformation gradient $\mathbf{F}$ over the volume Ω under the affine displacement

boundary condition $\mathbf{x} = \overline{\mathbf{F}}\mathbf{X}$ on $\partial\Omega$, where the second-order tensor $\overline{\mathbf{F}}$ is a prescribed quantity (Hill, 1972). In this case, it follows from the divergence theorem that $\int_\Omega \mathbf{F}(\mathbf{X})\,\mathrm{d}\mathbf{X} = \overline{\mathbf{F}}$, and hence the derivation of the macroscopic response reduces to finding the average stress $\overline{\mathbf{S}} \doteq \int_\Omega \mathbf{S}(\mathbf{X})\,\mathrm{d}\mathbf{X}$ for a given $\overline{\mathbf{F}}$. The result reads formally as

$$\overline{\mathbf{S}} = \frac{\partial \overline{W}}{\partial \overline{\mathbf{F}}}(\overline{\mathbf{F}}, c) \tag{3.3}$$

with

$$\overline{W}(\overline{\mathbf{F}}, c) = (1-c)\ \min_{\mathbf{F}\in\mathcal{K}} \frac{1}{|\Omega_m|} \int_{\Omega_m} W(\mathbf{F})\ \mathrm{d}\mathbf{X}. \tag{3.4}$$

In these last expressions, $\overline{W}$ is the so-called effective stored-energy function (which physically corresponds to the total elastic energy per unit undeformed volume stored in the material), $c \doteq \int_\Omega \theta(\mathbf{X})\mathrm{d}\mathbf{X}$ is the initial volume fraction or concentration of particles, and $\mathcal{K}$ denotes a suitable set of kinematically admissible deformation gradient fields with prescribed volume average $\overline{\mathbf{F}}$.

3.1.1 The case of isotropic suspensions in non-Gaussian rubber

The main objective of this chapter is to determine the effective stored-energy function (3.4) for the practically relevant case when the particles are polydisperse in size and isotropically distributed in space, and the elastomeric matrix is isotropic and incompressible. The focus is on elastomers characterized by I_1-based stored-energy functions

$$W(\mathbf{F}) = \begin{cases} \Psi(I_1) & \text{if} \quad J \doteq \lambda_1\lambda_2\lambda_3 = 1 \\ +\infty & \text{otherwise} \end{cases}, \tag{3.5}$$

where $I_1 = \mathbf{F}\cdot\mathbf{F} = \lambda_1^2 + \lambda_2^2 + \lambda_3^2$, $\lambda_1, \lambda_2, \lambda_3$ have been introduced to denote the singular values of the deformation gradient $\mathbf{F}$, and Ψ is any non-negative function of choice satisfying the linearization conditions

$$\Psi(3) = 0 \qquad \text{and} \qquad \frac{\mathrm{d}\Psi}{\mathrm{d}I_1}(3) = \frac{\mu}{2}, \tag{3.6}$$

with μ denoting the initial shear modulus of the elastomeric matrix, and the physically-based strong ellipticity conditions (Zee and Sternberg, 1983)

$$\begin{aligned}&\frac{\mathrm{d}\Psi}{\mathrm{d}I_1}(I_1) > 0 \qquad \text{and}\\ &\frac{\mathrm{d}\Psi}{\mathrm{d}I_1}(I_1) + 2[I_1 - \lambda_k^2 - 2\lambda_k^{-1}]\frac{\mathrm{d}^2\Psi}{\mathrm{d}I_1^2}(I_1) > 0 \quad (k=1,2,3) \qquad \forall\, I_1 \geq 3. \end{aligned} \tag{3.7}$$

Stored-energy functions of the functional form (3.5) with (3.6)–(3.7) are generalizations of the classical Neo-Hookean energy $\Psi(I_1) = \mu/2\,[I_1 - 3]$ that have been shown to describe reasonably well the response of a wide variety of elastomers over large ranges of deformations (see, e.g. Arruda and Boyce, 1993; Gent, 1996; Lopez-Pamies, 2010b). These types of constitutive models have the further merit that they are derivable from microscopic considerations based on realistic non-Gaussian statistical distributions of the underlying polymeric chains (see, e.g. Beatty, 2003).

Owing to the assumed isotropy of the microstructure and the constitutive isotropy and incompressibility of the matrix material (3.5) and rigid particles (3.1), the resulting overall elastic response is isotropic and incompressible. This implies that the effective stored-energy function $\overline{W}$ in this case depends on the macroscopic deformation gradient $\overline{\mathbf{F}}$ only through its singular values $\overline{\lambda}_1, \overline{\lambda}_2, \overline{\lambda}_3$ and becomes unbounded for non-isochoric deformations when $\overline{J} \doteq \det \overline{\mathbf{F}} = \overline{\lambda}_1\overline{\lambda}_2\overline{\lambda}_3 \neq 1$. Accordingly, the result (3.4) can be simply written as a symmetric function of $\overline{\lambda}_1, \overline{\lambda}_2, \overline{\lambda}_3$ subject to the constraint $\overline{\lambda}_1\overline{\lambda}_2\overline{\lambda}_3 = 1$. Alternatively, in this chapter we shall find it more convenient to write (3.4) as a function solely of the two principal invariants $\overline{I}_1 = \overline{\mathbf{F}} \cdot \overline{\mathbf{F}} = \overline{\lambda}_1^2 + \overline{\lambda}_2^2 + \overline{\lambda}_3^2$ and $\overline{I}_2 = \overline{\mathbf{F}}^{-T} \cdot \overline{\mathbf{F}}^{-T} = \overline{\lambda}_1^2\overline{\lambda}_2^2 + \overline{\lambda}_1^2\overline{\lambda}_3^2 + \overline{\lambda}_2^2\overline{\lambda}_3^2$ in the form

$$\overline{W}(\overline{\mathbf{F}}, c) = \begin{cases} \overline{\Psi}(\overline{I}_1, \overline{I}_2, c) & \text{if} \quad \overline{J} = \overline{\lambda}_1\overline{\lambda}_2\overline{\lambda}_3 = 1 \\ +\infty & \text{otherwise} \end{cases}. \tag{3.8}$$

As outlined above, our strategy to generate a solution for (3.8) involves two main steps and makes use of two different techniques. In the first step, presented in Section 3.2, we work out a solution for the special case of filled Neo-Hookean rubber by means of an iterated dilute homogenization technique. This Neo-Hookean solution is then utilized in the second step, presented in Section 3.3, to work out in turn a solution for filled non-Gaussian

rubber via a nonlinear comparison medium method. In order to assist the presentation of the results, the unbounded branch of the energies (3.5) and (3.8) is omitted in most of the remainder of the analysis.

3.2 A solution for filled Neo-Hookean rubber via iterated dilute homogenization

In this section, we construct a solution for the effective stored-energy function (3.8) for the special case when the elastomeric matrix is Neo-Hookean rubber. This amounts to solving the relevant minimization problem (3.4) with (3.5) and

$$\Psi(I_1) = \frac{\mu}{2}[I_1 - 3]. \tag{3.9}$$

To this end, we make use of the iterated dilute homogenization procedure of Lopez-Pamies (2010a) together with the result derived in Chapter 2 as the required dilute solution from which we start the iterative construction process. For clarity of exposition, we first present the iterated dilute homogenization technique in its general form (Section 3.2.1) and then work out its application to filled Neo-Hookean rubber (Section 3.2.2).

3.2.1 An iterated dilute homogenization method in finite elasticity

Following Lopez-Pamies (2010a), we begin by considering that the unit-volume domain Ω is occupied by matrix material 0, a homogeneous elastomer with stored-energy function W (possibly compressible and anisotropic at this stage). We then embed a *dilute* distribution of rigid particles (of possibly any shape and orientation) with infinitesimal concentration ϕ_1 in material 0 in such a way that the total volume of the composite remains unaltered at $|\Omega| = 1$; that is, we remove a total volume ϕ_1 of material 0 and replace it with rigid particles. Assuming a polynomial asymptotic behavior in ϕ_1, the resulting reinforced material has an effective stored-energy function $\overline{W}_1$ of the form

$$\overline{W}_1(\overline{\mathbf{F}}, \phi_1) = W(\overline{\mathbf{F}}) + \mathcal{G}\left\{W(\overline{\mathbf{F}}); \overline{\mathbf{F}}\right\}\phi_1 + O\left(\phi_1^2\right), \tag{3.10}$$

where $\mathcal{G}$ is a functional with respect to its first argument W and a function with respect to its second argument $\overline{\mathbf{F}}$.

Considering next $\overline{W}_1$ as the stored-energy function of a "homogeneous" matrix material 1, we repeat the same process of removal and replacing while keeping the volume fixed at $|\Omega| = 1$. This second iteration requires utilizing rigid particles that are much larger in size than those used in the first iteration, since the matrix material 1 with stored-energy function (3.10) is being considered as homogeneous. Specifically, we remove an infinitesimal volume ϕ_2 of matrix material 1 and replace it with rigid particles. The composite has now an effective stored-energy function

$$\overline{W}_2(\overline{\mathbf{F}}, c_2) = \overline{W}_1(\overline{\mathbf{F}}, \phi_1) + \mathcal{G}\left\{\overline{W}_1(\overline{\mathbf{F}}, \phi_1); \overline{\mathbf{F}}\right\} \phi_2, \tag{3.11}$$

where the order of the asymptotic correction term has been omitted for notational simplicity. We remark that the functional $\mathcal{G}$ in (3.11) is the same as in (3.10) because we are considering *exactly the same* dilute distribution as in (3.10). More elaborate construction processes are possible (corresponding, for instance, to using different particle shapes and orientations at each iteration), but such a degree of generality is not needed for our purposes here. We further remark that the total concentration of rigid particles at this stage is given by $c_2 = \phi_2 + \phi_1(1 - \phi_2) = 1 - \prod_{j=1}^{2}(1 - \phi_j)$, and hence that the increment in total concentration of rigid particles in this second iteration is given by $c_2 - \phi_1 = \phi_2(1 - \phi_1)$.

It is apparent now that repeating the same above process $i+1$ times, where i is an arbitrarily large integer, generates a particle-reinforced nonlinear elastic solid with effective stored-energy function

$$\overline{W}_{i+1}(\overline{\mathbf{F}}, c_{i+1}) = \overline{W}_i(\overline{\mathbf{F}}, c_i) + \mathcal{G}\left\{\overline{W}_i(\overline{\mathbf{F}}, c_i); \overline{\mathbf{F}}\right\} \phi_{i+1}, \tag{3.12}$$

which contains a *total* concentration of rigid particles given by

$$c_{i+1} = 1 - \prod_{j=1}^{i+1}(1 - \phi_j)\,. \tag{3.13}$$

For unbounded i the right-hand side of expression (3.13) is, roughly speaking, the sum of infinitely many concentrations of infinitesimal value, which can amount to a total concentration c_{i+1} of *finite* value. The increment in total

concentration of rigid particles in this iteration (i.e., in passing from i to $i+1$) reads as

$$c_{i+1} - c_i = \prod_{j=1}^{i} (1 - \phi_j) - \prod_{j=1}^{i+1} (1 - \phi_j) = \phi_{i+1}(1 - c_i), \tag{3.14}$$

from which it is a trivial matter to establish the following identity

$$\phi_{i+1} = \frac{c_{i+1} - c_i}{1 - c_i}\,. \tag{3.15}$$

Substituting expression (3.15) in (3.12) renders

$$(1 - c_i)\frac{\overline{W}_{i+1}(\overline{\mathbf{F}}, c_{i+1}) - \overline{W}_i(\overline{\mathbf{F}}, c_i)}{c_{i+1} - c_i} - \mathcal{G}\left\{\overline{W}_i(\overline{\mathbf{F}}, c_i); \overline{\mathbf{F}}\right\} = 0. \tag{3.16}$$

This difference equation can be finally recast — upon using the facts that the increment $c_{i+1} - c_i$ is infinitesimally small and that i is arbitrarily large — as the following initial value problem

$$(1 - c)\frac{\partial \overline{W}}{\partial c}(\overline{\mathbf{F}}, c) - \mathcal{G}\left\{\overline{W}(\overline{\mathbf{F}}, c); \overline{\mathbf{F}}\right\} = 0, \quad \overline{W}(\overline{\mathbf{F}}, 0) = W(\overline{\mathbf{F}}). \tag{3.17}$$

The differential equation $(3.17)_1$, subject to the initial condition $(3.17)_2$, provides an implicit framework for constructing solutions for the effective stored-energy function $\overline{W}$ of elastomers reinforced by *finite concentrations* c of rigid particles directly in terms of corresponding solutions — as characterized by the functional $\mathcal{G}$ — when the particles are present in dilute concentration. It is worthwhile to emphasize that the formulation (3.17) is applicable to any choice of the stored-energy function W (including compressible and anisotropic) describing the behavior of the underlying elastomeric matrix. By construction, the results generated from (3.17) correspond to polydisperse microstructures where the particles have infinitely many diverse sizes. Again, this feature is of practical relevance here because standard reinforcing fillers (e.g., carbon black and silica) typically agglomerate, resulting effectively in polydisperse microstructures with "particles" of many different sizes. By the same token, the results generated from (3.17) are *realizable* in the sense that they are exact for a given class of microstructures. This implies that the generated effective stored-energy functions $\overline{W}$ are theoretically and

physically sound. They are then guaranteed, for instance, to be objective in $\overline{\mathbf{F}}$, to linearize properly, and to comply with any macroscopic constraints imposed by microscopic constraints, such as the strongly nonlinear constraint of incompressibility. To be useful, however, the formulation (3.17) requires having knowledge of the functional $\mathcal{G}$ describing the relevant dilute response of the filled elastomer of interest, which is in general a notable challenge.

3.2.2 Application to filled Neo-Hookean rubber

In Chapter 2, with help of the realizable homogenization theory developed in (Lopez-Pamies et al., 2011a), we derived a solution for the overall nonlinear elastic response of Neo-Hookean rubber reinforced by a dilute isotropic distribution of rigid particles. Below, we make direct use of this result in the framework (3.17) to construct in turn a corresponding solution for Neo-Hookean rubber reinforced by an isotropic distribution of rigid particles with polydisperse sizes at *finite concentration*.

The exact form of the solution derived in Chapter 2 is given implicitly in terms of an Eikonal partial differential equation in two variables which ultimately needs to be solved numerically (see equations (2.40) and (2.35)–(2.36)). To make analytical progress, we do not utilize here the exact form of the solution but instead invoke its closed-form approximation, as devised in Section 2.5. In terms of the notation introduced in (3.8), (3.9), and (3.10), this approximate dilute solution takes the form

$$\overline{\Psi}(\overline{I}_1,\overline{I}_2,c)=\Psi(\overline{I}_1)+\mathcal{G}\left\{\Psi(\overline{I}_1);\overline{I}_1,\overline{I}_2\right\}c, \tag{3.18}$$

where c is the infinitesimal concentration of particles, $\Psi(\overline{I}_1)=\mu/2[\,\overline{I}_1-3]$, and the functional $\mathcal{G}$ is given explicitly by

$$\mathcal{G}\left\{\Psi(\overline{I}_1);\overline{I}_1,\overline{I}_2\right\}=\frac{5}{2}\,\Psi(\overline{I}_1). \tag{3.19}$$

Substitution of (3.19) in the general formulation (3.17) leads to the initial-value problem

$$(1-c)\frac{\partial\overline{\Psi}}{\partial c}(\overline{I}_1,\overline{I}_2,c)-\frac{5}{2}\overline{\Psi}(\overline{I}_1,\overline{I}_2,c)=0,\qquad \overline{\Psi}(\overline{I}_1,\overline{I}_2,0)=\Psi(\overline{I}_1)=\frac{\mu}{2}\left[\,\overline{I}_1-3\right], \tag{3.20}$$

which defines the effective stored-energy function $\overline{\Psi}$ of Neo-Hookean rubber filled with an isotropic distribution of rigid particles of polydisperse sizes and finite concentration c. Remarkably, this first-order partial differential equation admits the explicit solution

$$\overline{\Psi}(\overline{I}_1, \overline{I}_2, c) = \frac{\mu}{2(1-c)^{5/2}} \left[\overline{I}_1 - 3 \right]. \tag{3.21}$$

Thorough comments on the theoretical and practical merits of this result are deferred to Section 3.3.2, where the more general case of filled non-Gaussian rubber is addressed. At this stage it is important to emphasize, however, that the effective stored-energy function (3.21) is not in general an exact realizable result. This is because use has been made of the approximate functional (3.19) — and *not* the exact functional — in the formulation (3.17) in order to favor analytical tractability. Nevertheless, in view of the high functional and quantitative accuracy of the approximation (3.19) for the dilute response (see Section 2.5), the stored-energy function (3.21) is expected to be very close to an exact realizable result[1].

3.3 A solution for filled non-Gaussian rubber via a nonlinear comparison medium method

The general case of isotropic suspensions of rigid particles in non-Gaussian rubber could be addressed by means of the same iterated dilute homogenization technique utilized in the foregoing section for Neo-Hookean rubber. That route would require explicit knowledge of the appropriate functional $\mathcal{G}$ in (3.17), which in principle could be computed by means of the same procedure followed in Chapter 2 but now specialized to energies of the form (3.5) as opposed to just the Neo-Hookean energy (3.9). While plausible, preliminary calculations indicate that this approach is not likely to provide explicit results and hence we do not pursue it here.

In the sequel, stimulated by the works of Willis (1994), Talbot and Willis (1994) and deBotton and Shmuel (2010), we pursue instead a nonlinear com-

[1]In this regard, it is interesting to recall that the analogous solution $\overline{\Psi} = \frac{\mu}{2(1-c)^2} \left[\overline{I}_1 - 2 \right]$ for the corresponding 2D problem is an exact realizable result (Lopez-Pamies, 2010a).

parison medium approach. Roughly speaking, the idea is to make use of the formalism of Talbot and Willis (1985) to devise a variational framework that allows to construct an explicit approximate solution for the effective stored-energy function (3.8) for filled non-Gaussian rubber directly in terms of the "simpler" effective stored-energy function (3.21) for filled Neo-Hookean rubber. We begin in Section 3.3.1 by presenting the comparison medium framework in its general form and then work out its application to filled non-Gaussian rubber in Section 3.3.2.

3.3.1 A nonlinear comparison medium method in finite elasticity

In order to account for the perfectly rigid behavior (3.1) of the particles in the analysis that follows, it is expedient not to work with (3.1) directly but to consider instead the regularized case of *compressible non-rigid* particles with stored-energy function

$$W_p(\mathbf{F}) = f_p(\mathbf{F}, J) = \frac{\mu_p}{2}\left[\mathbf{F}\cdot\mathbf{F} - 3\right] + \mu_p\left[\frac{1}{2}(J-1)^2 - (J-1)\right], \qquad (3.22)$$

where the material parameter μ_p denotes the initial shear modulus of the particles and the notation $W_p(\mathbf{F}) = f_p(\mathbf{F}, J)$ has been introduced for subsequent use; the special case of rigid behavior (3.1) can then be readily recovered from (3.22) by taking the limit $\mu_p \to +\infty$. Also for subsequent use, the stored-energy function for the elastomeric matrix material is rewritten here in the form

$$W(\mathbf{F}) = f_m(\mathbf{F}, J). \qquad (3.23)$$

Consistent with the notation introduced in (3.22) and (3.23), we henceforth rewrite the pointwise energy (3.2) for the filled elastomer as

$$W(\mathbf{X}, \mathbf{F}) = f(\mathbf{X}, \mathbf{F}, J) = (1 - \theta(\mathbf{X}))f_m(\mathbf{F}, J) + \theta(\mathbf{X})f_p(\mathbf{F}, J). \qquad (3.24)$$

Now, borrowing ideas from Talbot and Willis (1985), it proves fruitful to introduce a comparison medium with pointwise energy

$$W_0(\mathbf{X}, \mathbf{F}) = f_0(\mathbf{X}, \mathbf{F}, J), \qquad (3.25)$$

where f_0 is at this stage an arbitrary function, and to define the Legendre transformation[2]

$$(f - f_0)^*(\mathbf{X}, \mathbf{P}, Q) \doteq \sup_{\mathbf{F},J} \left[\mathbf{P} \cdot \mathbf{F} + QJ - f(\mathbf{X}, \mathbf{F}, J) + f_0(\mathbf{X}, \mathbf{F}, J)\right]. \quad (3.26)$$

Note that while the function $(f - f_0)$ may not be convex in $\mathbf{F}$ and J, the function $(f - f_0)^*$ is convex in $\mathbf{P}$ and Q by definition.

A direct consequence from (3.26) is that, for any $\mathbf{P}$, Q, $\mathbf{F}$, and J,

$$W(\mathbf{X}, \mathbf{F}) = f(\mathbf{X}, \mathbf{F}, J) \geq f_0(\mathbf{X}, \mathbf{F}, J) + \mathbf{P} \cdot \mathbf{F} + QJ - (f - f_0)^*(\mathbf{X}, \mathbf{P}, Q), \quad (3.27)$$

and hence that

$$\overline{W}(\overline{\mathbf{F}}, c) \geq \min_{\mathbf{F} \in \mathcal{K}} \int_\Omega \left[f_0(\mathbf{X}, \mathbf{F}, J) + \mathbf{P} \cdot \mathbf{F} + QJ\right] \mathrm{d}\mathbf{X} - \int_\Omega (f - f_0)^*(\mathbf{X}, \mathbf{P}, Q) \mathrm{d}\mathbf{X}, \quad (3.28)$$

the minimum being evaluated over a suitable set $\mathcal{K}$ of kinematically admissible deformation gradient fields with prescribed volume average $\overline{\mathbf{F}}$ as for (3.4). The further inequality

$$\begin{aligned} \overline{W}(\overline{\mathbf{F}}, c) \geq \min_{\mathbf{F} \in \mathcal{K}} \int_\Omega f_0(\mathbf{X}, \mathbf{F}, J) \mathrm{d}\mathbf{X} + \min_{\mathbf{F} \in \mathcal{K}} \int_\Omega \mathbf{P} \cdot \mathbf{F} \mathrm{d}\mathbf{X} \\ + \min_{\mathbf{F} \in \mathcal{K}} \int_\Omega QJ \mathrm{d}\mathbf{X} - \int_\Omega (f - f_0)^*(\mathbf{X}, \mathbf{P}, Q) \mathrm{d}\mathbf{X} \end{aligned} \quad (3.29)$$

follows from a well-known property of the minimum of sums. The first term in (3.29) is nothing more than the effective stored-energy function of the comparison medium with local energy (3.25). We denote it by

$$\overline{W}_0(\overline{\mathbf{F}}) \doteq \min_{\mathbf{F} \in \mathcal{K}} \int_\Omega W_0(\mathbf{X}, \mathbf{F}) \mathrm{d}\mathbf{X}. \quad (3.30)$$

The second and third terms in (3.29) are bounded from below only so long as $\mathbf{P}$ is divergence-free and Q is a constant (and hence also divergence-free). For simplicity, we choose both these fields to be constant and denote them

[2]It is possible to invoke Legendre transformations that are more general and efficient than (3.26) (see, e.g., Chapter 6 in Dacorogna, 2007), but the choice (3.26) proves general enough for the isotropic material systems of interest in this chapter.

by $\mathbf{P} = \overline{\mathbf{P}}$ and $Q = \overline{Q}$. This gives

$$\overline{W}(\overline{\mathbf{F}}, c) \geq \overline{W}_0(\overline{\mathbf{F}}) + \overline{\mathbf{P}} \cdot \overline{\mathbf{F}} + \overline{Q}\,\overline{J} - \int_\Omega (f - f_0)^*(\mathbf{X}, \overline{\mathbf{P}}, \overline{Q}) \mathrm{d}\mathbf{X}. \tag{3.31}$$

Relation (3.31) provides a lower bound for the effective stored-energy function $\overline{W}$ for the filled elastomer with local energy (3.24) in terms of the effective stored-energy function $\overline{W}_0$ for a comparison medium with local energy (3.25). It is valid for any choice of constants $\overline{\mathbf{P}}$ and $\overline{Q}$, and any choice of the function f_0 describing the local constitutive behavior and microstructure of the comparison medium. Optimization of (3.31) with respect to $\overline{\mathbf{P}}$ and $\overline{Q}$ leads to

$$\begin{aligned} \overline{W}(\overline{\mathbf{F}}, c) &\geq \overline{W}_0(\overline{\mathbf{F}}) + \sup_{\overline{\mathbf{P}}, \overline{Q}} \left[\overline{\mathbf{P}} \cdot \overline{\mathbf{F}} + \overline{Q}\,\overline{J} - \int_\Omega (f - f_0)^*(\mathbf{X}, \overline{\mathbf{P}}, \overline{Q}) \mathrm{d}\mathbf{X} \right] \\ &= \overline{W}_0(\overline{\mathbf{F}}) + \left(\int_\Omega (f - f_0)^* \mathrm{d}\mathbf{X} \right)^* (\overline{\mathbf{F}}, \overline{J}). \end{aligned} \tag{3.32}$$

Optimizing this result in turn with respect to f_0 leads formally to

$$\overline{W}(\overline{\mathbf{F}}, c) \geq \sup_{f_0} \left\{ \overline{W}_0(\overline{\mathbf{F}}) + \left(\int_\Omega (f - f_0)^* \mathrm{d}\mathbf{X} \right)^* (\overline{\mathbf{F}}, \overline{J}) \right\}. \tag{3.33}$$

A partially optimized explicit formulation. The computation of the "optimal" bound (3.33) involves two technical difficulties. First, the polar function $(f - f_0)^*$ may have corners, and hence the computation of the Legendre transform of its average in (3.33) may require the use of subgradients as opposed to standard differentiation; see, e.g., Willis (1991) for similar difficulties in the classical context of convex energies. Second, the supremum operation in (3.33) involves optimization with respect to the local constitutive behavior of the comparison medium as well as with respect to its microstructure, which may require the computation of complicated integrals in the second term of (3.33). A detailed analysis of these two issues is a substantial task more appropriate for presentation elsewhere. In this chapter, we shall be content with employing a partially optimized version of the result (3.31) — and *not* the fully optimized bound (3.33) — which avoids the above-mentioned technical difficulties altogether.

A natural prescription to avoid the computation of subgradients in the above development is to set $\overline{\mathbf{P}} = \mathbf{0}$ and $\overline{Q} = 0$. Then, after recognizing from

(3.26) that

$$\begin{aligned}(f-f_0)^*(\mathbf{X},\mathbf{0},0) &= \sup_{\mathbf{A},\,a}\left[-f(\mathbf{X},\mathbf{A},a)+f_0(\mathbf{X},\mathbf{A},a)\right]\\ &= -\min_{\mathbf{A},\,a}\left[f(\mathbf{X},\mathbf{A},a)-f_0(\mathbf{X},\mathbf{A},a)\right],\end{aligned}\tag{3.34}$$

it follows from (3.31) that

$$\overline{W}(\overline{\mathbf{F}},c)\geq\overline{W}_0(\overline{\mathbf{F}})+\int_\Omega\min_{\mathbf{A},\,a}\left[f(\mathbf{X},\mathbf{A},a)-f_0(\mathbf{X},\mathbf{A},a)\right]\mathrm{d}\mathbf{X}.\tag{3.35}$$

To avoid the computation of complicated integrals in the second term of (3.35), it is reasonable to restrict attention to a comparison medium in the form of a filled elastomer with the same microstructure as the actual filled elastomer, namely,

$$W_0(\mathbf{X},\mathbf{F})=f_0(\mathbf{X},\mathbf{F},J)=(1-\theta(\mathbf{X}))f_{0_m}(\mathbf{F},J)+\theta(\mathbf{X})f_{0_p}(\mathbf{F},J),\tag{3.36}$$

where the indicator function θ is the same as in (3.24). Since the interest here is in elastomers reinforced by rigid particles, it suffices in fact to restrict attention to a comparison filled elastomer of the form (3.36) in which the particles are also rigid. Without loss of generality, this can be easily accomplished by setting

$$f_{0_p}(\mathbf{F},J)=f_p(\mathbf{F},J)=\frac{\mu_p}{2}\left[\mathbf{F}\cdot\mathbf{F}-3\right]+\mu_p\left[\frac{1}{2}(J-1)^2-(J-1)\right].\tag{3.37}$$

Substituting (3.24) and (3.36) with (3.37) in (3.35) and then taking the limit of rigid particles $\mu_p\to+\infty$ renders[3], with a slight change in notation,

$$\overline{W}(\overline{\mathbf{F}},c)\geq\overline{W}_0(\overline{\mathbf{F}},c)+(1-c)\min_{\mathbf{A},a}\left[f_m(\mathbf{A},a)-f_{0_m}(\mathbf{A},a)\right].\tag{3.38}$$

This lower bound is non-trivial only so long as f_m grows faster than the choice of stored-energy function f_{0_m} for the comparison matrix material in the limit as $||\mathbf{F}||,|J|\to+\infty$. For the opposite case[4] when f_{0_m} grows faster

[3]An alternative direct derivation of the formula (3.38) follows *mutatis mutandis* from a derivation of Willis (see, e.g., equation (3.3) in Willis, 1991; equation (8.17) in Willis, 2002; see also deBotton and Shmuel, 2010) of Ponte Castañeda's bound (1991) in the context of convex energies: $\overline{W}=\min_{\mathbf{F}\in\mathcal{K}}\int_\Omega\left[W_0+(W-W_0)\right]\mathrm{d}\mathbf{X}\geq\overline{W}_0+\int_\Omega\min(W-W_0)\mathrm{d}\mathbf{X}$.

[4]For the isotropic matrix materials of interest in this chapter, mixed cases in which

than f_m as $||\mathbf{F}||, |J| \to +\infty$, the symmetry of (3.38) in the pairs $(\overline{W}, f_m)$ and $(\overline{W}_0, f_{0_m})$ implies the following non-trivial upper bound

$$\overline{W}(\overline{\mathbf{F}}, c) \leq \overline{W}_0(\overline{\mathbf{F}}, c) + (1-c) \max_{\mathbf{A},a} \left[f_m(\mathbf{A}, a) - f_{0_m}(\mathbf{A}, a) \right]. \tag{3.39}$$

At this stage, it is a simple matter to combine the inequalities (3.38) and (3.39) to finally establish the main result of this section:

$$\overline{W}(\overline{\mathbf{F}}, c) = \begin{cases} \overline{W}_0(\overline{\mathbf{F}}, c) + (1-c) \min\limits_{\mathbf{A},a} \left[f_m(\mathbf{A}, a) - f_{0_m}(\mathbf{A}, a) \right] \\ \qquad\qquad\qquad\qquad\qquad\qquad \text{if } f_m - f_{0_m} > -\infty \\ \\ \overline{W}_0(\overline{\mathbf{F}}, c) + (1-c) \max\limits_{\mathbf{A},a} \left[f_m(\mathbf{A}, a) - f_{0_m}(\mathbf{A}, a) \right] \\ \qquad\qquad\qquad\qquad\qquad\qquad \text{if } f_m - f_{0_m} < \infty \end{cases}, \tag{3.40}$$

where the equality has been used in the sense of a variational approximation. Expression (3.40) provides an explicit framework for constructing approximate solutions for the effective stored-energy function $\overline{W}$ of elastomers with (possibly compressible and anisotropic) stored-energy function $W(\mathbf{F}) = f_m(\mathbf{F}, J)$ reinforced by a finite concentration c of rigid particles directly in terms of the effective stored-energy function $\overline{W}_0$ of different elastomers with stored-energy function $W_0(\mathbf{F}) = f_{0_m}(\mathbf{F}, J)$ reinforced by exactly the same distribution of rigid particles (i.e., exactly the same indicator function θ). The framework is valid for any choice of the function f_{0_m}, which prompts the following optimization

$$\overline{W}(\overline{\mathbf{F}}, c) = \begin{cases} \sup\limits_{f_{0_m}} \left\{ \overline{W}_0(\overline{\mathbf{F}}, c) + (1-c) \min\limits_{\mathbf{A},a} \left[f_m(\mathbf{A}, a) - f_{0_m}(\mathbf{A}, a) \right] \right\} \\ \qquad\qquad\qquad\qquad\qquad\qquad \text{if } f_m - f_{0_m} > -\infty \\ \\ \inf\limits_{f_{0_m}} \left\{ \overline{W}_0(\overline{\mathbf{F}}, c) + (1-c) \max\limits_{\mathbf{A},a} \left[f_m(\mathbf{A}, a) - f_{0_m}(\mathbf{A}, a) \right] \right\} \\ \qquad\qquad\qquad\qquad\qquad\qquad \text{if } f_m - f_{0_m} < \infty \end{cases}. \tag{3.41}$$

The usefulness of the formulation (3.41) — or more generally (3.40) — hinges upon having knowledge of the effective stored-energy function $\overline{W}_0$ for the

f_{0_m} grows faster (slower) in $\mathbf{F}$ but slower (faster) in J than f_m need not be considered.

comparison filled elastomer. While there have been no prior results available for such classes of materials (other than a few strictly in 2D), we now have at our disposal the results for filled Neo-Hookean rubber worked out in the preceding section.

3.3.2 Application to filled non-Gaussian rubber

Below, we make use of the filled Neo-Hookean rubber considered in Section 3.2.2 as the choice for the comparison medium in the formulation (3.41) in order to construct an approximate solution for the effective stored-energy function (3.8) for filled non-Gaussian rubber. To this end, we set

$$\begin{aligned} f_m(\mathbf{F},J) &= \Psi(I_1) + \frac{\mu+\mu'}{2}(J-1)^2 - \mu(J-1); \quad \text{and} \\ f_{0_m}(\mathbf{F},J) &= \frac{\mu_0}{2}[I_1-3] + \frac{\mu_0+\mu'}{2}(J-1)^2 - \mu_0(J-1), \end{aligned} \tag{3.42}$$

where μ' and μ_0 are positive material parameters, and note that in the limit as $\mu' \to +\infty$ these regularized compressible energies reduce identically to the incompressible non-Gaussian and Neo-Hookean stored-energy functions

$$f_m(\mathbf{F},J) = \begin{cases} \Psi(I_1) & \text{if} \quad J=1 \\ +\infty & \text{otherwise} \end{cases} \quad \text{and} \quad f_{0_m}(\mathbf{F},J) = \begin{cases} \dfrac{\mu_0}{2}[I_1-3] & \text{if} \quad J=1 \\ +\infty & \text{otherwise} \end{cases} \tag{3.43}$$

of interest here.

Upon substitution of (3.42) in the general formulation (3.41), it is straight-

forward to show that

$$\overline{W}(\overline{\mathbf{F}},c) = \begin{cases} \begin{cases} \max\limits_{\mu_0}\left\{\overline{W}_0(\overline{\mathbf{F}},c)+(1-c)\min\limits_{\mathcal{I}_1}\left[\Psi(\mathcal{I}_1)-\dfrac{\mu_0}{2}[\mathcal{I}_1-3]\right]\right\} & \\ \qquad\qquad\qquad\qquad\qquad\qquad\qquad\qquad \text{if } \ \Psi(\mathcal{I}_1)-\mathcal{I}_1>-\infty & \\ \qquad\qquad\qquad\qquad\qquad\qquad\qquad\qquad \text{if } \ \overline{J}=1 & \\ \min\limits_{\mu_0}\left\{\overline{W}_0(\overline{\mathbf{F}},c)+(1-c)\max\limits_{\mathcal{I}_1}\left[\Psi(\mathcal{I}_1)-\dfrac{\mu_0}{2}[\mathcal{I}_1-3]\right]\right\} & \\ \qquad\qquad\qquad\qquad\qquad\qquad\qquad\qquad \text{if } \ \Psi(\mathcal{I}_1)-\mathcal{I}_1<\infty & \end{cases} \\ +\infty \qquad\qquad\qquad\qquad\qquad\qquad\qquad\qquad \text{otherwise} \end{cases} \tag{3.44}$$

in the limit as $\mu' \to +\infty$, where the macroscopic incompressibility constraint $\overline{J} = 1$ in (3.44) ensuing from the microscopic incompressibility constraint $J = 1$ in (3.43) and the rigid behavior (3.1) of the particles is the expected exact constraint. The result (3.44) is applicable to any distribution of rigid particles (i.e., any indicator function θ). By restricting attention to the isotropic distributions of rigid particles of polydisperse sizes of interest here and invoking the notation introduced in (3.8) together with the result (3.21) for filled Neo-Hookean rubber, the finite branch of the energy (3.44) specializes to

$$\overline{\Psi}(\overline{I}_1,\overline{I}_2,c) = \begin{cases} \max\limits_{\mu_0}\left\{\dfrac{\mu_0}{2(1-c)^{5/2}}\left[\,\overline{I}_1-3\right]+(1-c)\min\limits_{\mathcal{I}_1}\left[\Psi(\mathcal{I}_1)-\dfrac{\mu_0}{2}\left[\mathcal{I}_1-3\right]\right]\right\} & \\ \qquad\qquad\qquad\qquad\qquad\qquad\qquad\qquad \text{if } \ \Psi(\mathcal{I}_1)-\mathcal{I}_1>-\infty & \\ \min\limits_{\mu_0}\left\{\dfrac{\mu_0}{2(1-c)^{5/2}}\left[\,\overline{I}_1-3\right]+(1-c)\max\limits_{\mathcal{I}_1}\left[\Psi(\mathcal{I}_1)-\dfrac{\mu_0}{2}\left[\mathcal{I}_1-3\right]\right]\right\} & \\ \qquad\qquad\qquad\qquad\qquad\qquad\qquad\qquad \text{if } \ \Psi(\mathcal{I}_1)-\mathcal{I}_1<\infty & \end{cases} \tag{3.45}$$

.

In view of the property $(3.7)_1$ of the function Ψ, it is not difficult to deduce that the max-min and the min-max problems in (3.45) are solved by exactly

the same stationarity conditions[5]

$$\frac{\partial \Psi}{\partial \mathcal{I}_1}(\mathcal{I}_1) = \frac{\mu_0}{2} \qquad \text{and} \qquad \mathcal{I}_1 = \frac{\overline{I}_1 - 3}{(1-c)^{7/2}} + 3 \tag{3.46}$$

irrespectively of the growth conditions of Ψ, and hence that the energy (3.45) can be compactly written as

$$\overline{\Psi}(\overline{I}_1, \overline{I}_2, c) = (1-c)\Psi\left(\frac{\overline{I}_1 - 3}{(1-c)^{7/2}} + 3\right). \tag{3.47}$$

The simple explicit effective stored-energy function (3.47) constitutes the main result of this chapter. It characterizes the overall nonlinear elastic response of non-Gaussian rubber with stored-energy function $\Psi(I_1)$ filled with an isotropic distribution of rigid particles of polydisperse sizes and finite concentration c. The following theoretical and practical remarks are in order:

i. Owing to the properties (3.6) and $(3.7)_1$ of the function Ψ, the effective stored-energy function (3.47) is such that

$$\begin{aligned} &\overline{\Psi}(3,3,c) = 0, \\ &\overline{\Psi}(\overline{I}_1, \overline{I}_2, c) > 0 \quad \forall\, \overline{I}_1, \overline{I}_2 > 3, \\ &\overline{\Psi}(\overline{I}_1, \overline{I}_2, c_2) > \overline{\Psi}(\overline{I}_1, \overline{I}_2, c_1) \quad \forall\, \overline{I}_1, \overline{I}_2 > 3,\ c_2 > c_1 \geq 0. \end{aligned} \tag{3.48}$$

The first two of these conditions are direct consequences of the fact that the filled non-Gaussian rubber is stress-free in the undeformed configuration, isotropic, and incompressible. The last condition entails physically that the addition of rigid particles consistently leads to a stiffer material response irrespectively of the applied loading, in agreement with experience.

ii. Remarkably, the effective stored-energy function (3.47) is independent of the second principal invariant $\overline{I}_2 = \overline{\mathbf{F}}^{-T} \cdot \overline{\mathbf{F}}^{-T}$. The origin of this independence can be traced back to the first step of the derivation, when the weak but existent dependence on $\overline{I}_2$ of the dilute response of filled Neo-Hookean rubber (see Sections 3.2.2 and 2.4) was neglected in order to favor analytical tractability. Neither the iterated dilute

[5]It is of practical relevance to note here that the optimal values of the variables μ_0 and $\mathcal{I}_1$ dictated by (3.46) are physically consistent in the sense that $\mu_0 \geq 0$ and $\mathcal{I}_1 \geq 3$.

homogenization procedure to account for finite concentration of particles (Section 3.2.1), nor the comparison medium procedure to account for non-Gaussian behavior (Section 3.3.1) introduced dependence on $\overline{I}_2$ thereafter. This suggests — given the different nature and generality of these two procedures — that the response of any filled I_1-based non-Gaussian elastomer is in all likelihood practically insensitive to $\overline{I}_2$. The FE simulations presented in the next section provide further support that this is indeed the case.

iii. For the common case when the stored-energy function Ψ for the underlying non-Gaussian matrix material is convex in I_1,

$$\frac{\mathrm{d}\Psi}{\mathrm{d}I_1}(I_1) > 0 \qquad \text{and} \qquad \frac{\mathrm{d}^2\Psi}{\mathrm{d}I_1^2}(I_1) \geq 0, \tag{3.49}$$

it is a simple matter to deduce that

$$\begin{aligned}
&\frac{\partial\overline{\Psi}}{\partial\overline{I}_1}(\overline{I}_1,\overline{I}_2,c) > 0,\\
&\frac{\partial\overline{\Psi}}{\partial\overline{I}_1}(\overline{I}_1,\overline{I}_2,c) + 2\left[\overline{I}_1 - \overline{\lambda}_k^2 - 2\overline{\lambda}_k^{-1}\right]\frac{\partial^2\overline{\Psi}}{\partial\overline{I}_1^2}(\overline{I}_1,\overline{I}_2,c) > 0 \quad (k=1,2,3),\\
&\forall\ \overline{I}_1,\overline{I}_2 \geq 3,\ c \geq 0,
\end{aligned} \tag{3.50}$$

and hence that the effective stored-energy function (3.47) is strongly elliptic (see, e.g., Section 4 in Zee and Sternberg, 1983). This stability property is consistent with recent 2D bifurcation analyses (Triantafyllidis et al., 2006; Michel et al., 2010) which have shown that isotropic filled elastomers that are microscopically (i.e., pointwise) convex in I_1 are macroscopically strongly elliptic. For the case when Ψ is merely strongly elliptic (i.e., it satisfies the weaker conditions (3.7)) but not convex in I_1, the effective stored-energy function (3.47) can still be shown to be strongly elliptic for small enough deformations, but it may lose strong ellipticity at sufficiently large values of $\overline{I}_1 > 3$.

iv. In the limit of small deformations ($\overline{I}_1, \overline{I}_2 \to 3$), the stored-energy function (3.47) reduces asymptotically to

$$\overline{\Psi}(\overline{I}_1,\overline{I}_2,c) = \overline{\mu}\left[\overline{\varepsilon}_1^2 + \overline{\varepsilon}_2^2 + \overline{\varepsilon}_3^2\right] \qquad \text{with} \qquad \overline{\varepsilon}_1 + \overline{\varepsilon}_2 + \overline{\varepsilon}_3 = 0 \tag{3.51}$$

to leading order in the deformation measures $\overline{\varepsilon}_k = \overline{\lambda}_k - 1$ $(k = 1, 2, 3)$, where it is recalled that $\overline{\lambda}_k$ denote the singular values of the macroscopic deformation gradient $\overline{\mathbf{F}}$ and

$$\overline{\mu} = \frac{\mu}{(1-c)^{5/2}} \tag{3.52}$$

stands for the initial effective shear modulus of the filled rubber. Expression (3.52) agrees identically with the exact Brinkman-Roscoe result (cf. equation (12) in Roscoe, 1973) for the effective shear modulus of an isotropic incompressible linearly elastic solid reinforced by an isotropic distribution of rigid spherical particles of infinitely many diverse sizes. In the further limit of small concentration of particles as $c \to 0$, the effective shear modulus (3.52) reduces to

$$\overline{\mu} = \mu + \frac{5}{2}\mu\, c + O(c^2), \tag{3.53}$$

which agrees in turn with the classical Einstein-Smallwood result (cf. equation (12) in Smallwood, 1944) for the effective shear modulus of an isotropic incompressible linearly elastic solid reinforced by a dilute distribution of rigid spherical particles.

v. The connection with the effective shear modulus (3.52) for isotropic distributions of spherical particles is not restricted to small deformations. Indeed, for the special case when the elastomeric matrix is Neo-Hookean rubber, $\Psi = \mu/2[I_1 - 3]$ and the effective stored-energy function (3.47) reduces to

$$\overline{\Psi}(\overline{I}_1, \overline{I}_2, c) = \frac{\mu}{2(1-c)^{5/2}} \left[\, \overline{I}_1 - 3 \right], \tag{3.54}$$

which is seen to have the same functional form as the Neo-Hookean matrix material, with the effective shear modulus given by (3.52). While the effective stored-energy function (3.54) is not an exact realizable result for Neo-Hookean rubber filled with an isotropic distribution of rigid spherical particles of polydisperse sizes, owing to its iterative construction process (see Section 3.2.1), it is expected to provide a very accurate approximation for this class of material systems. By the same token, the approximate effective stored-energy function (3.47) is expected to describe very accurately the response of any non-Gaussian

rubber filled with an isotropic distribution of rigid spherical particles of polydisperse sizes in the small and moderate deformation regimes. For large deformations, the result (3.47) is likely to be relatively less accurate for this class of material systems, as its variational construction process (see Section 3.3.1) entails that it corresponds to some sort of lower (upper) bound when the underlying matrix material has stronger (weaker) growth conditions than Neo-Hookean rubber. These expectations are supported by comparisons with the FE simulations presented in the next section.

vi. Rather interestingly, the result (3.47) indicates that the nonlinear elastic response of filled non-Gaussian rubber corresponds in essence to the response of the underlying non-Gaussian rubber — as characterized by its stored-energy function Ψ — evaluated at the "amplified" measure of strain

$$\overline{I}_1^{Amp} = \frac{\overline{I}_1 - 3}{(1-c)^{7/2}} + 3. \tag{3.55}$$

The idea of modeling the behavior of filled elastomers as the behavior of the underlying matrix material evaluated at some amplified measure of strain was originally proposed by Mullins and Tobin (1965) on heuristic grounds. The homogenization result (3.47) derived in this chapter suggests that this empirical idea is roughly correct, at least for filled I_1-based non-Gaussian rubber, and that the strain measure that is amplified is the first principal invariant I_1.

3.4 FE simulations of suspensions of rigid spherical particles in rubber under large deformations

In order to compare the above theoretical results with a separate solution, in this section we work out full 3D finite-element (FE) simulations of the large-deformation response of Neo-Hookean and non-Gaussian rubber reinforced by random isotropic distributions of rigid spherical particles. To simulate the randomness and isotropy of the microstructure, we consider infinite periodic media made up of the repetition of cubic unit cells of unit volume $L^3 = 1$ containing a random distribution of a large number of particles. With the aim of gaining insight into the effect of the size dispersion of the filler particles,

we examine distributions with particles of the same (monodisperse) and of different (polydisperse) sizes.

3.4.1 Monodisperse microstructures

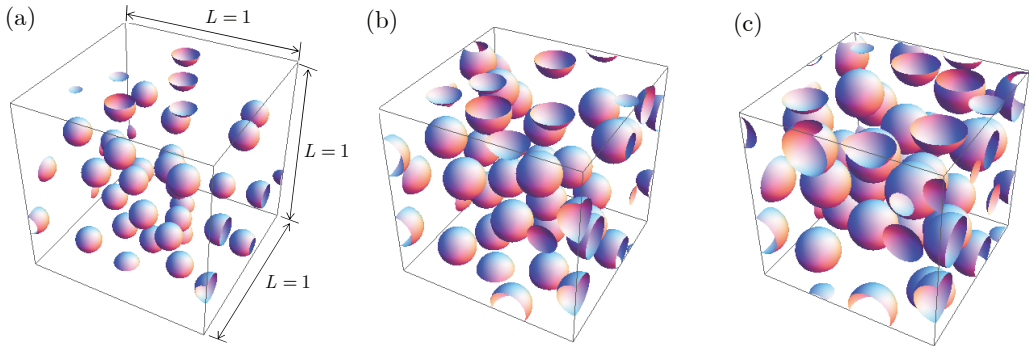

Figure 3.1: Representative unit cells of unit volume $L^3 = 1$ containing $N = 30$ randomly distributed spherical particles of monodisperse sizes with three different concentrations: (a) $c = 0.05$, (b) $c = 0.15$ and (c) $c = 0.25$.

The monodisperse microstructures are constructed by means of a random sequential adsorption algorithm (see, e.g., Chapter 3 in Torquato, 2002, and references therein) in which the sequential addition of particles is constrained so that the distance between the particles with other particles and with the boundaries of the cubic unit cell take a minimum value that guaranties adequate spatial discretization (see, e.g., Segurado and Llorca, 2002; Fritzen et al., 2012), namely:

- The center-to-center distance between a new particle i in the sequential algorithm and any previously accepted particle $j = 1, 2, ..., i-1$ has to exceed the minimum value $s_1 = 2R_m(1 + d_1)$, where the offset distance d_1 is fixed here at $d_1 = 0.02$. This condition can be compactly written in the form

$$||\mathbf{X}^i - \mathbf{X}^j - \mathbf{h}|| \geq s_1, \tag{3.56}$$

  where $\mathbf{X}^i$ ($\mathbf{X}^j$) denotes the location of the center of particle i (j) and $\mathbf{h}$ is a vector with entries 0, L, or $-L$ for each of its three Cartesian components with respect to the principal axes of the cubic unit cell[6].

[6]Note that condition (3.56) accounts for the fact that the excess of particles exceeding the spatial domain of the unit cell are appropriately relocated within the unit cell as dictated by the periodicity of the microstructure (see Fig. 3.1).

- The particles should be sufficiently distant from the boundaries of the unit cell as enforced by the inequalities

$$|X_k^i - R_m| \geq s_2 \qquad \text{and} \qquad |X_k^i + R_m - L| \geq s_2 \qquad (k = 1, 2, 3), \quad (3.57)$$

  where $s_2 = d_2\, R_m$ with d_2 being fixed here at $d_2 = 0.05$.

In the above expressions,

$$R_m = L \left(\frac{3\, c}{4\pi N} \right)^{1/3} \quad (3.58)$$

stands for the radius of the particles, where N has been introduced to denote the number of particles in the unit cell. For the material systems of interest in this chapter, a parametric study varying the number of particles in the range $N \in [5, 35]$ indicates that $N = 30$ is a sufficiently large number to approximate overall isotropy; more specific comments on the degree of isotropy resulting by the use of $N = 30$ are deferred to Section 3.4.4. Figure 3.1 shows representative unit cells generated by the above-described algorithm for $N = 30$ with three different particle concentrations: (a) $c = 0.05$, (b) $c = 0.15$, and (c) $c = 0.25$.

3.4.2 Polydisperse microstructures

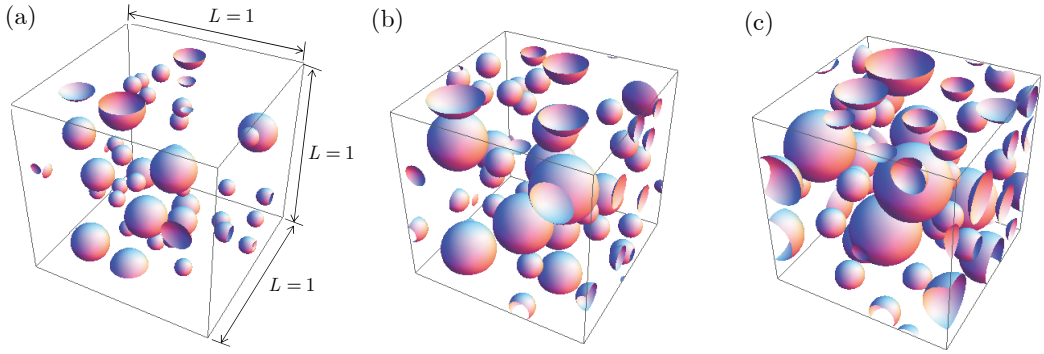

Figure 3.2: Representative unit cells of unit volume $L^3 = 1$ containing $N = 36$ randomly distributed spherical particles of three different sizes with three different concentrations: (a) $c \simeq 0.05$, (b) $c \simeq 0.15$ and (c) $c \simeq 0.25$.

The polydisperse microstructures are constructed by means of a similar constrained adsorption algorithm. The focus is on polydisperse microstruc-

tures with three different families of particle sizes. While there is no distinct rule for the creation of such microstructures and the possibilities are many, we consider for definiteness the following procedure:

- Three different families of particles with radii $R_p^{(I)}$ and concentrations $c^{(I)}$ $(I = 1, 2, 3)$ are utilized such that

$$\left\{R_p^{(1)}, R_p^{(2)}, R_p^{(3)}\right\} = \left\{R_p, \frac{7}{9}R_p, \frac{4}{9}R_p\right\} \qquad \text{with} \qquad R_p = L\left(\frac{3\,c^{(1)}}{4\pi N_p}\right)^{1/3}, \tag{3.59}$$

and

$$\left\{c^{(1)}, c^{(2)}, c^{(3)}\right\} = \{0.5\,c, 0.25\,c, 0.25\,c\} \qquad \text{with} \qquad c^{(1)} + c^{(2)} + c^{(3)} = c, \tag{3.60}$$

where N_p stands for the number of particles with the largest radius $R_p^{(1)} = R_p$ in the unit cell.

- The microstructures are generated sequentially by first adding particles with the largest radius $R_p^{(1)}$ until the concentration reaches the value $c^{(1)} = 0.5c$, subsequently adding particles with radius $R_p^{(2)}$ until $c^{(1)} + c^{(2)} \simeq 0.75c$, and finally adding particles with the smallest radius $R_p^{(3)}$ until $c^{(1)} + c^{(2)} + c^{(3)} \simeq c$. In following this construction process, we note that a target concentration c can only be achieved approximately (up to a small error that depends on the various choices of the parameters). To guarantee adequate spatial discretization, similar to conditions (3.56)–(3.57), the randomly generated placements of the centers of the particles are enforced to satisfy the following constraints

$$||\mathbf{X}^i - \mathbf{X}^j - \mathbf{h}|| \geq s_1, \quad s_1 = \left(R_p^{(m_i)} + R_p^{(m_j)}\right)(1 + d_1), \tag{3.61}$$

$$|X_k^i - R_p^{(m_i)}| \geq s_2, \quad |X_k^i + R_p^{(m_i)} - 1| \geq s_2,\ s_2 = d_2\, R_p^{(m_i)}\ (k = 1, 2, 3), \tag{3.62}$$

for $i, j = 1, 2, ..., N$ with N again denoting the total number of particles in the unit cell. Here, the offset parameters are set at $d_1 = 0.02$ and $d_2 = 0.05$ as in the monodisperse case, and the superscript $m_i = 1, 2, 3$ has been introduced to denote the size of the sphere that should be added at step i in the sequential construction process, namely, $m_i = 1$ if $c^{(m_i)} \leq c^{(1)}$, $m_i = 2$ if $c^{(1)} < c^{(m_i)} \leq c^{(1)} + c^{(2)}$, and $m_i = 3$ if

$c^{(1)} + c^{(2)} < c^{(m_i)}$.

Guided by a parametric study, in this chapter we utilize $N_p = 10$ which results into unit cells containing a total of $N = 36$ particles. As discussed in Section 3.4.4, such unit cells are sufficiently large to be representative of isotropic microstructures. Figure 3.2 displays sample unit cells generated by the above-described algorithm for $N = 36$ with three different particle concentrations: (a) $c \simeq 0.05$, (b) $c \simeq 0.15$ and (c) $c \simeq 0.25$.

3.4.3 Meshing, material properties, and computation of the overall nonlinear elastic response

Having identified the monodisperse and polydisperse microstructures of interest, we now turn to their discretization. We make use of the mesh generator code Netgen (Schöberl, 1997), which has the capability to create periodic meshes as required here. Ten-node tetrahedral hybrid elements are utilized in order to handle exactly (in a numerical sense) the incompressible behavior of the elastomeric matrix and of the rigid particles. Since the computations are carried out using the FE package ABAQUS, we make use in particular of the C3D10H hybrid elements available in this code (see Abaqus version 6.11 documentation). Figure 3.3 shows three meshes of increasing refinement for a distribution of monodisperse particles with concentration $c = 0.25$. Mesh sensitivity studies reveal that meshes with approximately $75,000$ elements (such as the fine mesh shown in Fig. 3.3(b)) produce sufficiently accurate results.

Within the present formulation, the behavior of the matrix phase can be modeled exactly by any incompressible stored-energy function (3.5) of choice. On the other hand, the perfectly rigid behavior (3.1) of the particles can only be modeled approximately by means of a very (but not infinitely) stiff material. Here, for definiteness, we model the particles as incompressible Neo-Hookean solids with stored-energy function

$$W_p^{FE}(\mathbf{F}) = \begin{cases} \dfrac{\mu_p^{FE}}{2}\,[I_1 - 3] & \text{if} \quad J = 1 \\ +\infty & \text{otherwise} \end{cases}, \tag{3.63}$$

where the parameter μ_p^{FE} is set to be three orders of magnitude larger than

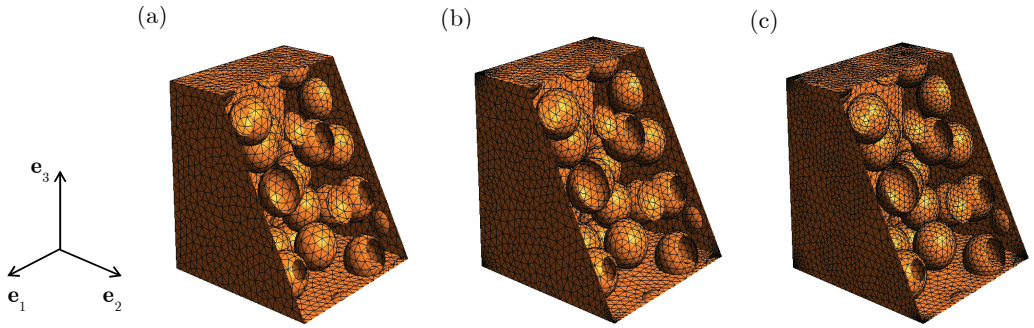

Figure 3.3: Three representative meshes in the undeformed configuration for a distribution of monodisperse particles with concentration $c = 0.25$: (a) coarse mesh with 34629, (b) fine mesh with 69556, and (c) very fine mesh with 170203 elements.

the initial shear modulus of the underlying matrix material, i.e., $\mu_p^{FE} = 10^3 \times \mu$.

By virtue of their periodicity, the overall nonlinear elastic response of any of the above-defined classes of filled elastomers amounts to subjecting their defining cubic unit cells to the periodic boundary conditions

$$\begin{aligned} u_k(L, X_2, X_3) - u_k(0, X_2, X_3) &= (\overline{F}_{k1} - \delta_{k1})L, \\ u_k(X_1, L, X_3) - u_k(X_1, 0, X_3) &= (\overline{F}_{k2} - \delta_{k2})L, \\ u_k(X_1, X_2, L) - u_k(X_1, X_2, 0) &= (\overline{F}_{k3} - \delta_{k3})L \end{aligned} \tag{3.64}$$

$(k = 1, 2, 3)$, and computing the resulting total elastic energy $\overline{W}$, from which the macroscopic first Piola-Kirchhoff stress $\overline{\mathbf{S}}$ can then be determined; alternatively, $\overline{\mathbf{S}}$ can be computed directly by averaging the resulting local stresses $\mathbf{S}(\mathbf{X})$ over the undeformed unit cell. In expression (4.67), the components u_k and X_k $(k = 1, 2, 3)$ refer to a Cartesian frame of reference with origin placed at a corner of the cubic unit cell whose axes $\{\mathbf{e}_k\}$ are aligned with the principal axes of the cubic unit cell (see Fig. 3.3), δ_{kl} denotes the Kronecker delta, and $\overline{\mathbf{F}}$ is the prescribed average deformation gradient. As a practical remark, we note that the periodic boundary conditions (4.67) can be expediently implemented in ABAQUS by using the "Equation" option to couple the nodes of opposite sides of the cubic unit cells.

3.4.4 Assessment of the simulated microstructures

Because of the finite number of particles — $N = 30$ for the monodisperse and $N = 36$ for the polydisperse microstructures — included per unit cell, the microstructures simulated here are (not exactly but) only approximately isotropic. In order to assess their isotropy, we have constructed and compared three different realizations for each concentration of particles that is simulated. For all matrix materials, loading conditions, and particle concentrations considered, the maximum difference in the total elastic energy between any two corresponding realizations has been computed to be less than 0.5%.

Further, for each realization, we have examined the co-axiallity between the average Cauchy stress tensor $\overline{\mathbf{T}} \doteq \overline{\mathbf{S}}\,\overline{\mathbf{F}}^{T}$ and the average left Green-Cauchy strain tensor $\overline{\mathbf{B}} \doteq \overline{\mathbf{F}}\,\overline{\mathbf{F}}^{T}$ under three types of loading conditions: (i) axisymmetric tension where $\overline{\mathbf{F}} = \overline{\lambda}\,\mathbf{e}_1 \otimes \mathbf{e}_1 + \overline{\lambda}^{-1/2}(\mathbf{e}_2 \otimes \mathbf{e}_2 + \mathbf{e}_3 \otimes \mathbf{e}_3)$ with $\overline{\lambda} \geq 1$, (ii) axisymmetric compression where $\overline{\mathbf{F}} = \overline{\lambda}\,\mathbf{e}_1 \otimes \mathbf{e}_1 + \overline{\lambda}^{-1/2}(\mathbf{e}_2 \otimes \mathbf{e}_2 + \mathbf{e}_3 \otimes \mathbf{e}_3)$ with $\overline{\lambda} \leq 1$, and (iii) simple shear where $\overline{\mathbf{F}} = \mathbf{I} + \overline{\gamma}\,\mathbf{e}_1 \otimes \mathbf{e}_2$ with $\overline{\gamma} \geq 0$. For all matrix materials, loading conditions, and particle concentrations considered, the maximum difference between any two corresponding principal axes of $\overline{\mathbf{T}}$ and $\overline{\mathbf{B}}$ has been computed to be less than 0.05 radians.

The above two sets of checks indicate that the monodisperse (polydisperse) microstructures with $N = 30$ ($N = 36$) particles per unit cell utilized in this chapter are indeed good approximations of isotropic distributions of spherical particles.

In the comparisons with the analytical solution (3.47) that follow in the next section, all presented FE results correspond to the average of three realizations. Moreover, all FE results are computed by following an incremental loading path, at each step of which the incremental equilibrium equations are solved directly in ABAQUS. We utilize the default dual convergence criterion in this code (Abaqus version 6.11 documentation), namely, the permissible ratio of the largest solution correction to the largest corresponding incremental solution is set at $|\Delta\mathbf{u}|/|\mathbf{u}_{max}| = 10^{-2}$, while the permissible ratio of the largest residual to the corresponding average force norm is set at $R_{tol} = 5 \times 10^{-3}$. Whenever one of these criteria is not satisfied the computations are stopped. This typically happens whenever the elements in between two particles become exceedingly distorted because of the locally

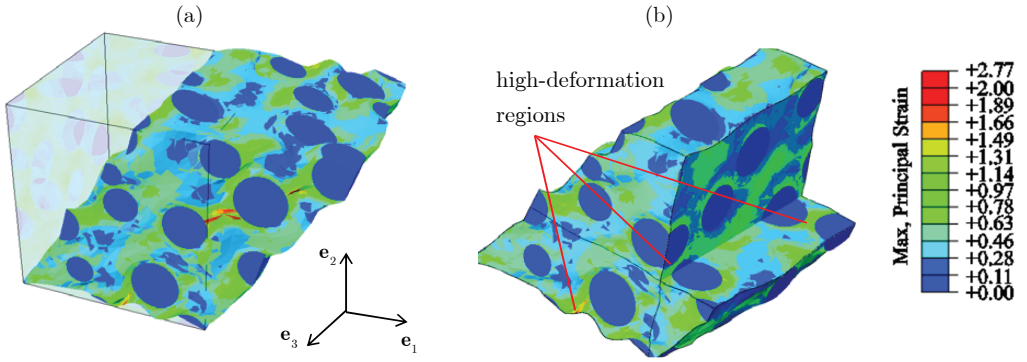

Figure 3.4: (a) Contour plots of the maximum principal logarithmic strain for a monodisperse realization with $c = 0.25$ and Neo-Hookean matrix subjected to an overall simple shear strain of $\overline{\gamma} = 0.64$; the undeformed configuration is also depicted for comparison purposes. Part (b) shows an inside view of three pairs of particles in between which the matrix material is highly deformed.

large deformations involved.

Figure 3.4 presents an example of large local deformations in between particles for the case of a monodisperse realization with $c = 0.25$ and Neo-Hookean matrix under simple shear. Part (a) shows contour plots of the maximum principal logarithmic strain at an overall shear strain level of $\overline{\gamma} = 0.64$; the initial undeformed geometry is also depicted for comparison purposes. The deformation contours are seen to be highly heterogeneous with principal logarithmic strains as large as 2.77 within regions between particles. In part (b), an inside view is shown of three regions of strong particle interaction and high local strains that lead to significant mesh distortion and therefore problems with the numerical convergence of the FE calculations. In principle, re-meshing of these regions should allow to reach further overall deformations (see, e.g., Moraleda et al., 2009, for the analogous problem), but this is beyond the scope of this chapter and hence not pursued here.

3.5 Sample results and discussion

A range of specific results are presented next for the overall nonlinear elastic response of filled rubber as described by the analytical approximation (3.47) and the FE simulations of Section 3.4. Results for the linear elastic response in the small-deformation regime are presented first followed by results for

the large-deformation response of filled Neo-Hookean rubber under various loading conditions. The third set of results pertains to the response of a filled rubber wherein the underlying elastomeric matrix is characterized by the non-Gaussian stored-energy function (Lopez-Pamies, 2010b)

$$\Psi(I_1) = \frac{3^{1-\alpha_1}}{2\alpha_1}\mu_1\left[I_1^{\alpha_1} - 3^{\alpha_1}\right] + \frac{3^{1-\alpha_2}}{2\alpha_2}\mu_2\left[I_1^{\alpha_2} - 3^{\alpha_2}\right] \tag{3.65}$$

with $\mu_1 = 0.032$ MPa, $\mu_2 = 0.3$ MPa, $\alpha_1 = 3.837$, $\alpha_2 = 0.559$, corresponding to a model that has been shown to accurately describe the nonlinear elastic response of typical silicone rubber over large ranges of deformations (see Section 2.3 in Lopez-Pamies, 2010b).

The selection of results presented here aims at providing further insight into the constructed analytical solution (3.47) and at assessing its accuracy for a wide range of particle concentrations, elastomeric matrix materials, and loading conditions. The results also aim at shedding light on the effect of the size dispersion of fillers in the overall nonlinear elastic response of filled elastomers.

3.5.1 Linear elastic results

In the limit of small deformations (see remark *iv* in Section 3.3.2), the analytical approximation (3.47) reduces to the exact effective stored-energy function (3.51) with (3.52) for an isotropic incompressible linearly elastic solid reinforced by an isotropic distribution of rigid spherical particles of infinitely many diverse sizes. Figure 3.5 presents plots for the initial effective shear modulus (3.52), normalized by the initial shear modulus μ of the underlying elastomeric matrix, as a function of the concentration of particles c. Results are also presented for the FE simulations of Section 3.4 for isotropic distributions of spherical particles with the same size (monodisperse) and with three different sizes (polydisperse). To gain further insight, the corresponding Hashin-Shtrikman lower bound for the effective shear modulus of rigidly reinforced, isotropic, incompressible, linearly elastic materials (Hashin and Shtrikman, 1961) is included in the figure. As expected, all four results stiffen monotonically with increasing values of c. Although exact for infinitely polydisperse particles, the analytical response is seen to be in good agreement with the FE results for polydisperse particles with only three families

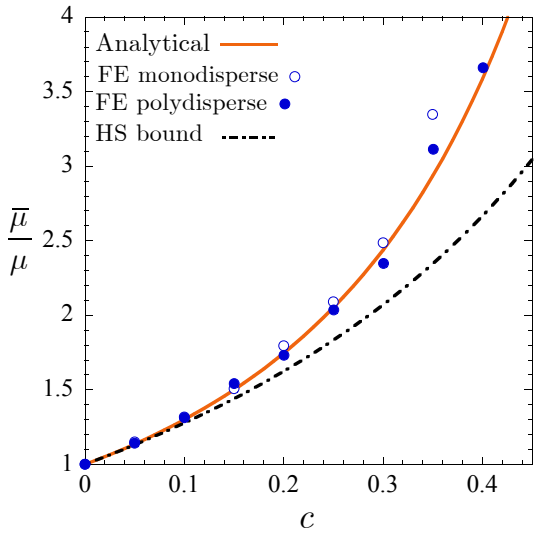

Figure 3.5: The normalized initial effective shear modulus $\overline{\mu}/\mu$ of isotropic incompressible elastomers filled with random isotropic distributions of rigid particles. Plots are shown for: (i) the analytical result (3.52), (ii) FE simulations for distributions of spherical particles with the same (monodisperse) and with three different (polydisperse) sizes, and (iii) the corresponding Hashin-Shtrikman lower bound $\overline{\mu}/\mu = (2+3c)/(2-2c)$, as functions of the concentration of particles c.

of particle sizes for the entire range of concentrations considered $c \in [0, 0.4]$. More remarkably, the analytical solution exhibits good agreement with the FE results for monodisperse particles up to the relatively high concentration of $c = 0.3$. These favorable comparisons are consistent with earlier 2D results (Moraleda et al., 2009; Lopez-Pamies, 2010a) suggesting that polydispersity does *not* play a role in the response of particle-reinforced materials for particle concentrations sufficiently below the percolation limit. A further relevant observation from Fig. 3.5 is that all three particulate results (analytical, FE monodisperse, FE polydisperse) are very close to the Hashin-Shtrikman lower bound up to a concentration of particles of about $c = 0.1$, after which they become significantly stiffer.

3.5.2 Results for filled Neo-Hookean rubber

For the case when the underlying matrix material is Neo-Hookean rubber (see remark v in Section 3.3.2), the analytical approximation (3.47) takes the form (3.54). Figure 3.6 presents results for the large-deformation response of filled Neo-Hookean rubber, as characterized by the effective stored-energy

function (3.54), for three values of particle concentration $c = 0.05, 0.15$, and 0.25 under: (a) uniaxial compression, (b) uniaxial tension, (c) pure shear, and (d) simple shear. The constitutive stress-deformation relations for these loading conditions read explicitly as

- *Uniaxial loading* ($\overline{\lambda}_1 = \overline{\lambda}$, $\overline{\lambda}_2 = \overline{\lambda}_3 = \overline{\lambda}^{-1/2}$ with $\bar{t}_2 = \bar{t}_3 = 0$):

$$\overline{S}_{un} = \overline{\lambda}^{-1}\bar{t}_1 = \frac{\mathrm{d}\overline{\Psi}}{\mathrm{d}\overline{\lambda}} = \frac{\mu}{(1-c)^{5/2}}\left[\overline{\lambda} - \overline{\lambda}^{-2}\right] \tag{3.66}$$

- *Pure shear* ($\overline{\lambda}_1 = \overline{\lambda}$, $\overline{\lambda}_2 = \overline{\lambda}^{-1}$, $\overline{\lambda}_3 = 1$ with $\bar{t}_2 = 0$):

$$\overline{S}_{ps} = \overline{\lambda}^{-1}\bar{t}_1 = \frac{\mathrm{d}\overline{\Psi}}{\mathrm{d}\overline{\lambda}} = \frac{\mu}{(1-c)^{5/2}}\left[\overline{\lambda} - \overline{\lambda}^{-3}\right] \tag{3.67}$$

- *Simple shear* ($\overline{\lambda}_1 = (\overline{\gamma} + \sqrt{\overline{\gamma}^{\,2} + 4})/2$, $\overline{\lambda}_2 = \overline{\lambda}_1^{-1}$, $\overline{\lambda}_3 = 1$):

$$\overline{S}_{ss} = \frac{\mathrm{d}\overline{\Psi}}{\mathrm{d}\overline{\gamma}} = \frac{\mu}{(1-c)^{5/2}}\,\overline{\gamma} \tag{3.68}$$

where $\overline{S}_{un}$, $\overline{S}_{ps}$, $\overline{S}_{ss}$ denote first Piola-Kirchhoff stress measures, while $\bar{t}_1$, $\bar{t}_2$, $\bar{t}_3$ have been introduced to denote the macroscopic principal Cauchy stresses. Figure 3.6 includes corresponding FE results for isotropic distributions of rigid spherical particles. No distinction is made here of whether the particles are of the same or of different sizes since, somewhat remarkably, both classes of microstructures exhibit essentially the same large-deformation response. This is consistent with the linear elastic results of Fig. 3.5, where the monodisperse and polydisperse FE simulations render practically identical effective shear moduli for concentrations below $c = 0.3$.

As anticipated by remark *i* in Section 3.3.2, Fig. 3.6 shows that the overall stiffness of filled Neo-Hookean rubber increases monotonically with increasing concentration of particles for all loading conditions. Another immediate observation is that the analytical and FE results are in good qualitative and quantitative agreement, with the FE results exhibiting a slightly stiffer behavior at large deformations. This trend appears to be independent of the concentration of particles.

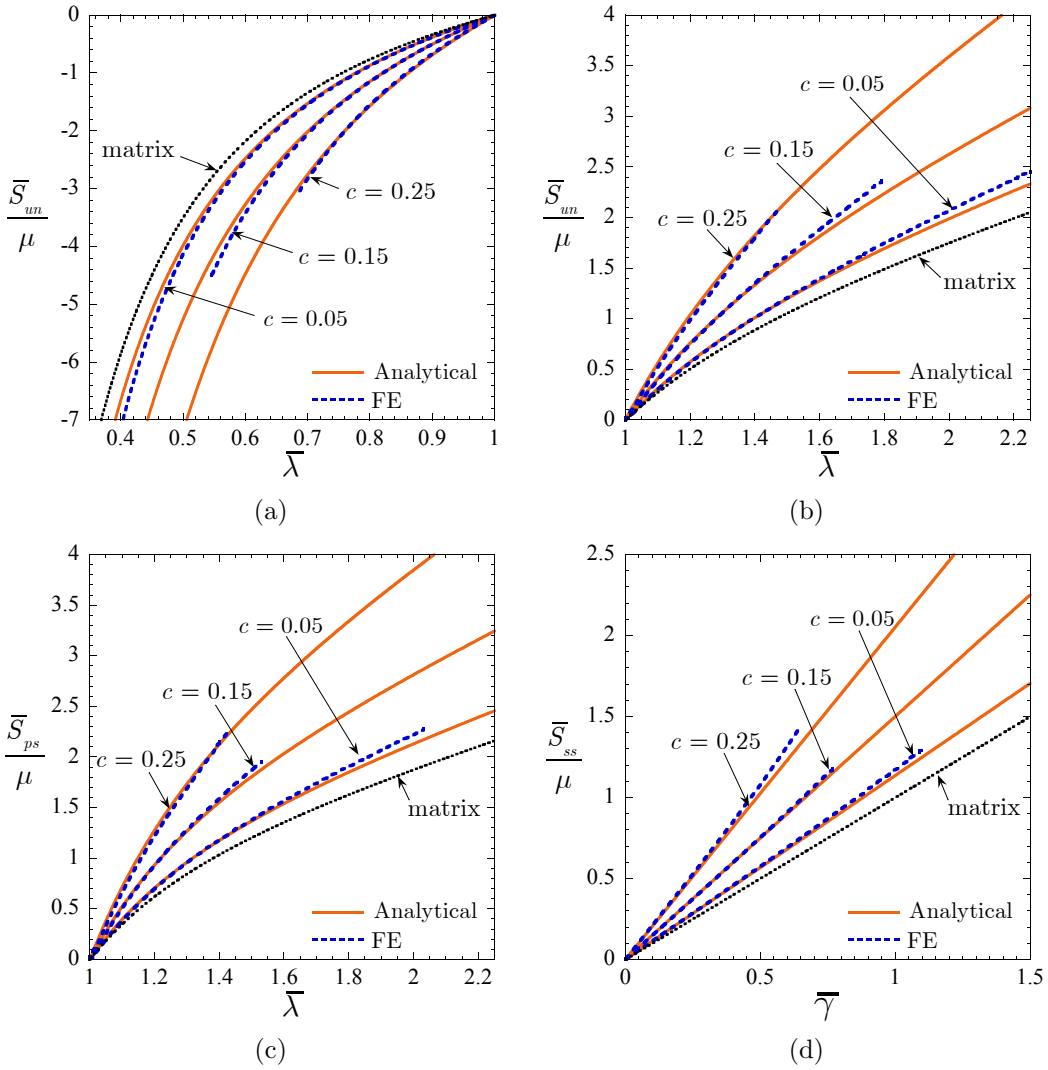

Figure 3.6: Macroscopic response of filled Neo-Hookean rubber with various values of concentration of particles c under: (a) uniaxial compressive, (b) uniaxial tensile, (c) pure shear, and (d) simple shear loading conditions. Plots are shown for the analytical stress-deformation results (3.66), (3.67), (3.68), and corresponding FE simulations for isotropic distributions of spherical particles.

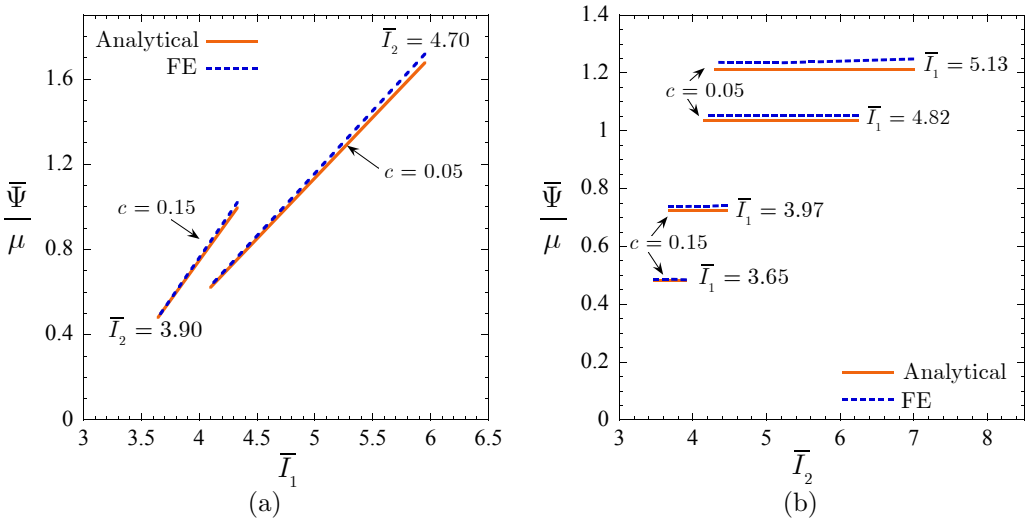

Figure 3.7: Comparison of the analytical stored-energy function (3.54) for filled Neo-Hookean rubber with corresponding FE simulations for isotropic distributions of spherical particles. The results are shown in terms of the principal invariants $\overline{I}_1$ and $\overline{I}_2$ for two values of concentration of particles. Part (a) shows results for fixed values of $\overline{I}_2$ as functions of $\overline{I}_1$, while part (b) shows results for fixed values of $\overline{I}_1$ as functions of $\overline{I}_2$.

To further probe the connections between the analytical approximation and the FE simulations, Fig. 3.7 compares their elastic energies $\overline{\Psi}/\mu$, normalized by the initial shear modulus μ of the underlying Neo-Hookean matrix, as functions of the principal invariants $\overline{I}_1$ and $\overline{I}_2$. Part (a) of the figure shows $\overline{\Psi}/\mu$ for fixed values of the second invariant $\overline{I}_2 = 3.90$ for $c = 0.15$ and $\overline{I}_2 = 4.70$ for $c = 0.05$ as functions of $\overline{I}_1$, while part (b) shows results for fixed values of the first invariant $\overline{I}_1 = 3.65, 3.97$ for $c = 0.15$ and $\overline{I}_1 = 4.82, 5.13$ for $c = 0.05$ as functions of $\overline{I}_2$. It is recalled that the constraint of incompressibility $\overline{J} = 1$ imposes a restriction on the physically allowable values of $\overline{I}_1$ and $\overline{I}_2$. Thus, for fixed $\overline{I}_2 = 3.90$ and 4.70 the first invariant is restricted to take values in the ranges $\overline{I}_1 \in [3.65, 4.34]$ and $\overline{I}_1 \in [4.10, 5.96]$, respectively. For fixed $\overline{I}_1 = 3.65, 3.97, 4.82$, and 5.13, the corresponding allowable values of the second invariant are $\overline{I}_2 \in [3.49, 3.91]$, $\overline{I}_2 \in [3.69, 4.46]$, $\overline{I}_2 \in [4.16, 6.23]$, and $\overline{I}_2 \in [4.31, 6.98]$. These are the ranges of values utilized in the figure.

The main observation from Fig. 3.7 is that the FE results are approximately linear in the first invariant $\overline{I}_1$ and independent of the second invariant $\overline{I}_2$. This behavior is in accordance with that of the analytical approximation, corroborating that both results are very much identical in their functional form. The fact that the macroscopic behavior of filled Neo-Hookean rubber

is functionally the same — i.e., linear in $\overline{I}_1$ and independent of $\overline{I}_2$ — as that of its underlying Neo-Hookean matrix is of note. Indeed, the functional character of the average behavior of nonlinear material systems is in general substantially different from that of its constituents, but that is not the case here.

3.5.3 Results for a filled silicone rubber

Finally, Fig. 3.8 presents various results for the large-deformation response of a filled non-Gaussian rubber, wherein the underlying matrix material is a typical silicone rubber characterized here by the stored-energy function (3.65) with material parameters $\mu_1 = 0.032$ MPa, $\mu_2 = 0.3$ MPa, $\alpha_1 = 3.837$, $\alpha_2 = 0.559$. The analytical approximation (3.47) specializes in this case to

$$\overline{\Psi}(\overline{I}_1, \overline{I}_2, c) = (1-c)\sum_{r=1}^{2} \frac{3^{1-\alpha_r}}{2\alpha_r}\mu_r \left[\left(\frac{\overline{I}_1 - 3}{(1-c)^{7/2}} + 3\right)^{\alpha_r} - 3^{\alpha_r}\right]. \tag{3.69}$$

Parts (a), (b), and (c) of the figure show stress-deformation results for uniaxial compression, uniaxial tension, and simple shear for particle concentrations $c = 0.05, 0.15$, and 0.25. The constitutive stress-deformation relations for these loading conditions are given explicitly by

- *Uniaxial loading* ($\overline{\lambda}_1 = \overline{\lambda}$, $\overline{\lambda}_2 = \overline{\lambda}_3 = \overline{\lambda}^{-1/2}$ with $\overline{t}_2 = \overline{t}_3 = 0$):

$$\overline{S}_{un} = \overline{\lambda}^{-1}\overline{t}_1 = \frac{\mathrm{d}\overline{\Psi}}{\mathrm{d}\overline{\lambda}} = \frac{\overline{\lambda} - \overline{\lambda}^{-2}}{(1-c)^{5/2}} \sum_{r=1}^{2} 3^{1-\alpha_r}\mu_r \left[\frac{\overline{\lambda}^2 + 2\overline{\lambda}^{-1} - 3}{(1-c)^{7/2}} + 3\right]^{\alpha_r - 1} \tag{3.70}$$

- *Simple shear* ($\overline{\lambda}_1 = (\overline{\gamma} + \sqrt{\overline{\gamma}^2 + 4})/2$, $\overline{\lambda}_2 = \overline{\lambda}_1^{-1}$, $\overline{\lambda}_3 = 1$):

$$\overline{S}_{ss} = \frac{\mathrm{d}\overline{\Psi}}{\mathrm{d}\overline{\gamma}} = \frac{\overline{\gamma}}{(1-c)^{5/2}} \sum_{r=1}^{2} 3^{1-\alpha_r}\mu_r \left[\frac{\overline{\gamma}^2}{(1-c)^{7/2}} + 3\right]^{\alpha_r - 1} \tag{3.71}$$

where, again, $\overline{S}_{un}$, $\overline{S}_{ss}$ denote first Piola-Kirchhoff stress measures and $\overline{t}_1$, $\overline{t}_2$, $\overline{t}_3$ stand for the macroscopic principal Cauchy stresses. Part (d) displays results for the effective stored-energy function (3.69) for fixed values of the first principal invariant $\overline{I}_1 = 3.76$ for $c = 0.15$ and $\overline{I}_1 = 4.75$ for $c = 0.05$,

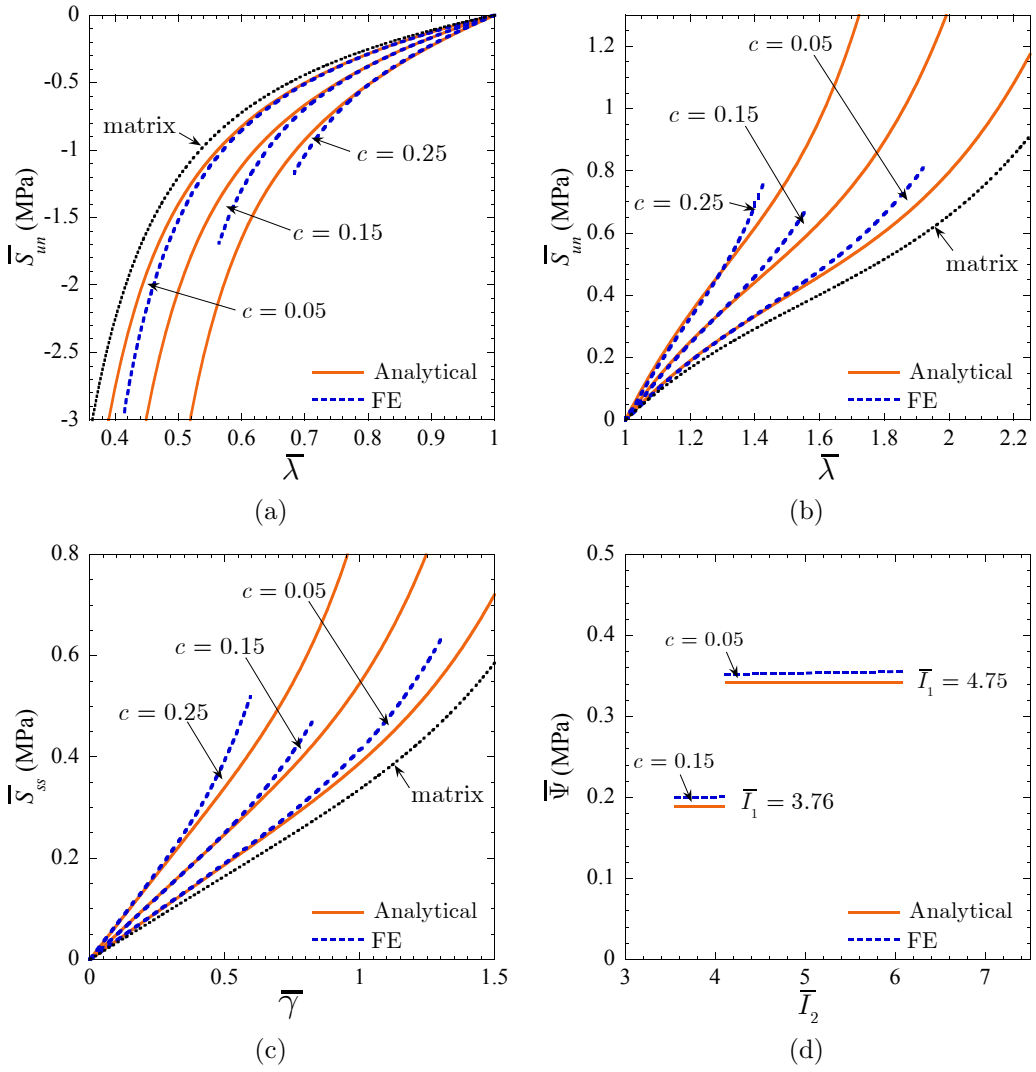

Figure 3.8: Macroscopic response of filled silicone rubber with various values of concentration of particles c under: (a) uniaxial compressive, (b) uniaxial tensile, and (c) simple shear loading conditions. Plots are shown for the analytical stress-deformation results (3.70), (3.71), and corresponding FE simulations for isotropic distributions of spherical particles. Part (d) of the figure shows comparisons between the analytical stored-energy function (3.69) and corresponding FE results for two fixed values of the first principal invariant $\overline{I}_1$ and c, in terms of the second invariant $\overline{I}_2$.

in terms of the second invariant $\overline{I}_2$. All four parts of the figure include corresponding FE results for isotropic distributions of spherical particles. Akin to the preceding Neo-Hookean case, we make no distinction here of whether the particles are of the same or of different sizes since, again, the simulated monodisperse and polydisperse microstructures turn out to exhibit practically the same response for particle concentrations below $c = 0.3$.

In addition to the monotonic stiffening of the response for increasing values of particle concentration, it is immediate from parts (a) through (c) of Fig. 3.8 that the analytical and FE results are in fairly good qualitative and quantitative agreement for all loading conditions, especially for small and moderate deformations. For large enough deformations at which the limiting chain extensibility of the silicone rubber comes into effect, the analytical results are consistently softer — as expected from their variational construction process (see remark v in Section 3.3.2) — than their FE counterparts. Part (d) of the figure shows that the FE results for filled silicone rubber, much like those for filled Neo-Hookean rubber, are approximately independent of the second macroscopic invariant $\overline{I}_2$, in functional accord with the analytical approximation (3.69).

The above three sets of sample results indicate that the analytical approximation (3.47) provides a mathematically simple, functionally sound, and quantitatively fairly accurate result for the overall nonlinear elastic response of non-Gaussian elastomers reinforced by isotropic distributions of rigid spherical particles of polydisperse sizes. The results have also served to reveal that size dispersion of the underlying reinforcing particles is inconsequential, in that it does not affect the overall response of the material, for particle concentrations up to the relatively high value of about $c = 0.3$. Accordingly, the analytical approximation (3.47) can additionally be utilized to describe the response of non-Gaussian elastomers filled with isotropic distributions of spherical particles of the same size with small-to-moderate concentrations.

CHAPTER 4

FILLED ELASTOMERS: A THEORY OF FILLER REINFORCEMENT BASED ON HYDRODYNAMIC AND INTERPHASIAL EFFECTS

The object of this chapter is to build upon the work of Lopez-Pamies et al. (2013a) to develop a microscopic theory of filler reinforcement, accounting directly for both the hydrodynamic and the interphasial reinforcement effects, with the capability to describe, explain, and predict the nonlinear elastic response of filled elastomers under arbitrarily large deformations. Specifically, the focus is on the industrially prominent case of isotropic incompressible elastomers filled with a random and isotropic distribution of rigid particles of polydisperse sizes. Paralleling the work of Lopez-Pamies et al. (2013b,a), this is accomplished here by way of a twofold strategy. Roughly speaking, a solution is first constructed for the homogenized nonlinear elastic response of Gaussian elastomers filled with a dilute isotropic distribution of rigid particles and interphases. By means of a combination of iterative and variational techniques, this fundamental dilute result is then utilized to generate in turn a solution for the homogenized nonlinear elastic response of non-Gaussian elastomers filled with an isotropic distribution of rigid particles and interphases at finite concentrations.

In this chapter, for purposes of gaining further insight and of assessing the accuracy of the proposed theory, full 3D FE (finite-element) results are also generated for the large-deformation response of Gaussian and non-Gaussian elastomers reinforced by isotropic distributions of rigid spherical particles bonded through interphases of constant thickness. While this numerical approach for such a practically relevant problem seems simple enough, its presentation in the literature is not known to the authors.

4.1 The problem

4.1.1 Microscopic description of filled elastomers

A filled elastomer is taken here to consist of a random distribution of rigid particles bonded to an elastomeric matrix through interphases of finite sizes; Fig. 4.1 shows a schematic illustration of this microscopic view. The domain occupied by the entire composite in its ground state is denoted by Ω and its boundary by $\partial\Omega$. Similarly, Ω_m, Ω_p, and Ω_i denote the domains occupied collectively by the matrix, the particles, and the interphases so that $\Omega = \Omega_m \cup \Omega_p \cup \Omega_i$ and their respective initial volume fractions (or concentrations) are given by $c_m \doteq |\Omega_m|/|\Omega|$, $c_p \doteq |\Omega_p|/|\Omega|$, and $c_i \doteq |\Omega_i|/|\Omega|$. We assume that the distribution of the particles is statistically uniform (i.e., translation invariant) and that their sizes and those of their surrounding interphases are much smaller that the size of Ω.

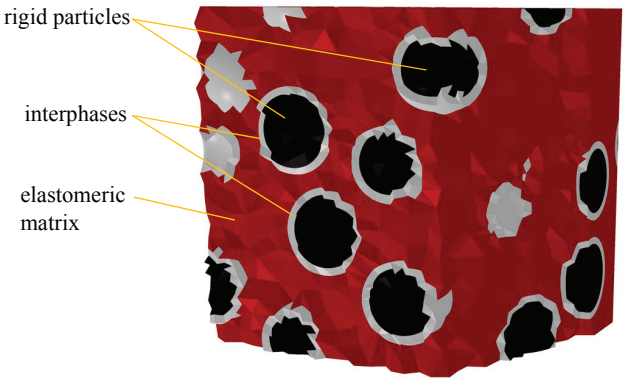

Figure 4.1: Schematic microscopic view of a filled elastomer.

Upon the application of mechanical loads, the initial position vector $\mathbf{X}$ of a material point in Ω moves to a new position specified by $\mathbf{x} = \boldsymbol{\chi}(\mathbf{X})$, where $\boldsymbol{\chi}$ is a one-to-one mapping from Ω to the deformed configuration Ω'. We assume that $\boldsymbol{\chi}$ is twice continuously differentiable, expect possibly on the matrix/interphase and interphase/particles boundaries, where is only required to be continuous. The associated deformation gradient is denoted by

$$\mathbf{F} = \mathrm{Grad}\boldsymbol{\chi} \tag{4.1}$$

and its determinant by $J = \det \mathbf{F}$. The elastomeric matrix is considered to be a homogeneous nonlinear elastic solid with stored-energy function $W_m =$

$W_m(\mathbf{F})$. Similarly, the rigid particles are homogeneous nonlinear elastic solids characterized by the stored-energy function

$$W_p(\mathbf{F}) = \begin{cases} 0 & \text{if} \quad \mathbf{F} = \mathbf{Q} \in Orth^+ \\ +\infty & \text{otherwise} \end{cases} , \tag{4.2}$$

where $Orth^+$ stands for the set of all proper orthogonal second-order tensors. The interphases are taken to be nonlinear elastic solids as well, but need *not* be homogeneous. We write their stored-energy function as $W_i = W_i(\mathbf{X}, \mathbf{F})$. Given the above local constitutive descriptions, it follows that at each material point $\mathbf{X}$ in the undeformed configuration Ω, the first Piola-Kirchhoff stress tensor $\mathbf{S}$ is given in terms of $\mathbf{F}$ simply by

$$\mathbf{S} = \frac{\partial W}{\partial \mathbf{F}}(\mathbf{X}, \mathbf{F}), \tag{4.3}$$

where

$$W(\mathbf{X}, \mathbf{F}) = [1 - \theta_p(\mathbf{X}) - \theta_i(\mathbf{X})] \; W_m(\mathbf{F}) + \theta_p(\mathbf{X}) W_p(\mathbf{F}) + \theta_i(\mathbf{X}) W_i(\mathbf{X}, \mathbf{F}) \tag{4.4}$$

with θ_p and θ_i denoting the characteristic functions of the spatial regions occupied by the particles and interphases: $\theta_p(\mathbf{X})$=1 if $\mathbf{X} \in \Omega_p$ and zero otherwise, and, likewise, $\theta_i(\mathbf{X})$=1 if $\mathbf{X} \in \Omega_i$ and zero otherwise.

4.1.2 The macroscopic response

In view of the assumed separation of length scales and statistical uniformity of the microstructure, the above-defined filled elastomer behaves macroscopically as a "homogenous" material. Its macroscopic or overall response is defined as the relation between the volume average of the first Piola-Kirchhoff stress $\mathbf{S}$ and the volume average of the deformation gradient $\mathbf{F}$ over the undeformed configuration Ω when the composite is subjected to affine boundary conditions (Hill, 1972). Consistent with our choice of $\mathbf{F}$ as the independent variable of the problem, we consider boundary conditions that are affine in the deformation, namely,

$$\mathbf{x} = \overline{\mathbf{F}}\mathbf{X} \quad \text{on} \quad \partial\Omega, \tag{4.5}$$

where the second-order tensor $\overline{\mathbf{F}}$ stands for a prescribed quantity. Granted the boundary data (4.5), the divergence theorem warrants that the average of deformation gradient over the undeformed configuration $|\Omega|^{-1}\int_\Omega \mathbf{F}(\mathbf{X})\mathrm{d}\mathbf{X} = \overline{\mathbf{F}}$ and hence the derivation of the macroscopic response reduces to finding the average stress $\overline{\mathbf{S}} \doteq |\Omega|^{-1}\int_\Omega \mathbf{S}(\mathbf{X})\mathrm{d}\mathbf{X}$ for a given $\overline{\mathbf{F}}$. The result can be conveniently written in a variational form as (Ogden, 1978)

$$\overline{\mathbf{S}} = \frac{\partial \overline{W}}{\partial \overline{\mathbf{F}}}(\overline{\mathbf{F}}, c_p, c_i), \tag{4.6}$$

where

$$\overline{W}(\overline{\mathbf{F}}, c_p, c_i) = \min_{\mathbf{F}\in\mathcal{K}} \frac{1}{|\Omega|}\int_\Omega W(\mathbf{X}, \mathbf{F})\ \mathrm{d}\mathbf{X}, \tag{4.7}$$

the effective stored-energy function, corresponds physically to the total elastic energy per unit undeformed volume stored in the filled elastomer. In these expressions, the concentrations c_p and c_i are utilized as explicit variables for later convenience and $\mathcal{K}$ denotes a sufficiently large set of kinematically admissible deformation gradient fields with prescribed volume average $\overline{\mathbf{F}}$.

4.1.3 Filled elastomers with overall isotropic incompressible behavior: the basic case of spherical filler particles and constant-thickness Gaussian interphases

The foregoing formulation is valid for arbitrary stored-energy functions for the elastomeric matrix, $W_m(\mathbf{F})$, and interphases, $W_i(\mathbf{X}, \mathbf{F})$, as well as for general classes of microstructures as characterized by $\theta_p(\mathbf{X})$ and $\theta_i(\mathbf{X})$. The focus of this chapter is on the prominent case of elastomeric matrices that are constitutively *isotropic* and *incompressible* and microstructures that are *isotropic*. Within this class of materials, we further restrict attention to those wherein the particles are *spherical* and the interphases are of *constant thickness* and made up of a *Gaussian* elastomer[1]. Specifically, we consider

[1] As elaborated further below, these geometric and constitutive idealizations prove sufficiently general for most filled elastomers wherein the interphases are typically stiffer than the matrix.

I_1-based stored-energy functions of the form

$$W_m = \begin{cases} \Psi_m(I_1) & \text{if } J = \lambda_1\lambda_2\lambda_3 = 1 \\ +\infty & \text{otherwise} \end{cases} \qquad \text{and}$$
$$W_i = \begin{cases} \dfrac{\mu_i}{2}[I_1 - 3] & \text{if } J = \lambda_1\lambda_2\lambda_3 = 1 \\ +\infty & \text{otherwise} \end{cases} \tag{4.8}$$

for the elastomeric matrix and interphases. In these expressions, λ_1, λ_2, λ_3 stand for the singular values of the deformation gradient tensor $\mathbf{F}$, $I_1 = \mathbf{F}\cdot\mathbf{F}$, $\mu_i > 0$ denotes the initial shear modulus of the interphases, and Ψ_m is any non-negative function of choice satisfying the linearization conditions[2]

$$\Psi_m(3) = 0, \qquad \Psi'_m(3) = \frac{\mu_m}{2}, \tag{4.9}$$

where μ_m denotes the initial shear modulus of the elastomeric matrix, and the strong ellipticity conditions (Zee and Sternberg, 1983)

$$\Psi'_m(I_1) > 0, \quad \Psi'_m(I_1) + 2[I_1 - \lambda_\alpha^2 - 2\lambda_\alpha^{-1}]\Psi''_m(I_1) > 0 \quad (\alpha = 1, 2, 3) \quad \forall\, I_1 \geq 3. \tag{4.10}$$

Stored-energy functions of the form $(4.8)_1$ with (4.9)-(4.10) are generalization of the classical Gaussian or Neo-Hookean energy $\Psi_m(I_1) = \mu_m/2\,[I_1 - 3]$ that have been shown to describe reasonably well the response of a wide variety of elastomers over large ranges of deformations (see, e.g., Arruda and Boyce, 1993; Gent, 1996; Lopez-Pamies, 2010b). A further merit of these types of constitutive models is that they are derivable from microscopic considerations (see, e.g., Beatty, 2003).

Owing to assumed constitutive isotropy and incompressibility of the matrix material $(4.8)_1$, interphases $(4.8)_2$, and rigid particles (4.2), and the assumed isotropy of the microstructure, the resulting overall elastic response is isotropic and incompressible. This implies that the effective stored-energy function $\overline{W}$ in this case depends on the macroscopic deformation gradient $\overline{\mathbf{F}}$ only through its singular values $\overline{\lambda}_1$, $\overline{\lambda}_2$, $\overline{\lambda}_3$ and becomes unbounded for non-isochoric deformations when $\overline{J} = \det\overline{\mathbf{F}} = \overline{\lambda}_1\overline{\lambda}_2\overline{\lambda}_3 \neq 1$. Accordingly, the result (4.7) can be simply written as a symmetric function of $\overline{\lambda}_1$, $\overline{\lambda}_2$, $\overline{\lambda}_3$

[2]Throughout this Chapter, the notation $\Psi'_m(I_1) \doteq \mathrm{d}\Psi_m(I_1)/\mathrm{d}I_1$ and $\Psi''_m(I_1) \doteq \mathrm{d}^2\Psi_m(I_1)/\mathrm{d}I_1^2$ is used for convenience.

subject to the constraint $\overline{\lambda}_1\overline{\lambda}_2\overline{\lambda}_3 = 1$. Alternatively, in this chapter we shall find it more convenient to write the effective stored-energy function (4.7) as a function of the two principal invariants $\overline{I}_1 = \overline{\mathbf{F}} \cdot \overline{\mathbf{F}} = \overline{\lambda}_1^2 + \overline{\lambda}_2^2 + \overline{\lambda}_3^2$ and $\overline{I}_2 = \overline{\mathbf{F}}^{-T} \cdot \overline{\mathbf{F}}^{-T} = \overline{\lambda}_1^2\overline{\lambda}_2^2 + \overline{\lambda}_1^2\overline{\lambda}_3^2 + \overline{\lambda}_2^2\overline{\lambda}_3^2$ in the form

$$\overline{W}(\overline{\mathbf{F}}, c_p, c_i) = \begin{cases} \overline{\Psi}(\overline{I}_1, \overline{I}_2, c_p, c_i) & \text{if} \quad \overline{J} = 1 \\ +\infty & \text{otherwise} \end{cases} . \tag{4.11}$$

The object of this chapter reduces hence to generating a solution for the finite branch $\overline{\Psi}$ of the effective stored-energy function (4.11). Paralleling previous work on filled elastomers without interphases (Lopez-Pamies et al., 2013b,a), our strategy to generate such a solution involves two main steps. In the first step, presented in Section 4.2, we work out a solution for the fundamental limiting case of Gaussian (or Neo-Hookean) elastomers filled with a dilute concentration of particles and interphases. This dilute solution for Gaussian elastomers is then utilized in a second step, presented in Section 4.3, to work out in turn a solution for non-Gaussian elastomers filled with a finite concentration of particles and interphases. In order to assist the presentation of the results, the unbounded branch of the energies (4.8) and (4.11) is omitted in most of the remainder of the analysis.

4.2 Dilute concentration of particles and interphases in Gaussian elastomers

In this section, we derive an asymptotic solution for the effective stored-energy function $\overline{\Psi}$, as defined by (4.11) with (4.7), of filled elastomers in the limit when the filler particles and surrounding interphases are present in dilute concentrations, as $c_p \to 0+$ and $c_i \to 0+$, and the behavior of the matrix is characterized by the Gaussian stored-energy function

$$\Psi_m(I_1) = \frac{\mu_m}{2}[\, I_1 - 3], \tag{4.12}$$

where, again, μ_m stands for the shear modulus of the elastomeric matrix; recall that the interphase is also comprised of a Gaussian elastomer but with different shear modulus μ_i.

Assuming that the particles are "well separated" and thus do not interact

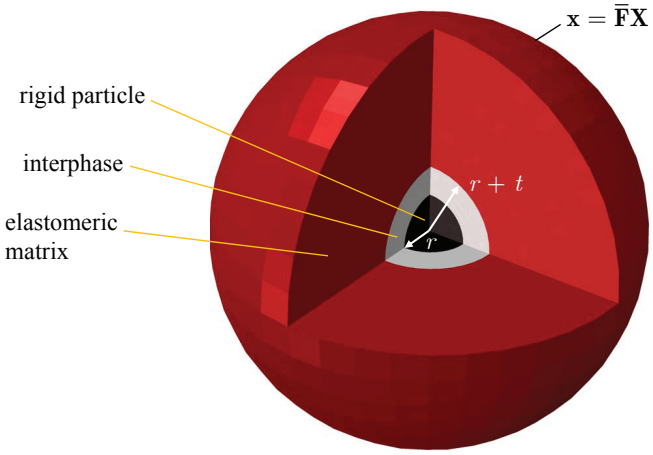

Figure 4.2: Schematic of the single-particle problem: a rigid spherical particle of radius r is bonded through an interphase of thickness t to a matrix of infinite extent that is subjected to the affine boundary condition $\mathbf{x} = \overline{\mathbf{F}}\mathbf{X}$. The matrix and interphase are both Gaussian elastomers with shear moduli μ_m and μ_i.

with one another in the limit as $c_p \to 0+$ and $c_i \to 0+$, the effective stored-energy function $\overline{\Psi}$ for a dilute suspension of particles is expected to agree identically with the total elastic energy per unit undeformed volume of an infinitely large matrix containing just a *single* spherical particle. This single-particle problem, schematically depicted in Fig. 4.2, is now taken up. In the calculations that follow, we shall denote the radius of the particle by r and the initial thickness of the interphase by t.

4.2.1 The exact solution in the small-deformation limit

It is instructive to begin by examining the small deformation limit as the applied macroscopic deformation $\overline{\mathbf{F}} \to \mathbf{I}$ with $\det \overline{\mathbf{F}} = 1$. In this limit, the elasticity problem (4.7) for the case of the single spherical particle admits an exact closed-form solution; for clarity of presentation, the relevant calculations are provided in Appendix D. The result for the finite branch $\overline{\Psi}$ of the effective stored-energy function reads as

$$\begin{aligned}\overline{\Psi}(\overline{I}_1, \overline{I}_2, c_p, c_i) &= \mu_m \,\mathrm{tr}\overline{\boldsymbol{\varepsilon}}^{\,2} + \frac{5\,\mu_m}{2}\, c_p \,\mathrm{tr}\overline{\boldsymbol{\varepsilon}}^{\,2} \\ &+ \frac{5(\mu_i - \mu_m)\,(q_1\mu_i + q_4\mu_m)\,\mu_m}{2(q_1\mu_i^2 + q_2\,\mu_i\mu_m + q_3\mu_m^2)}\, c_i \,\mathrm{tr}\overline{\boldsymbol{\varepsilon}}^{\,2} \\ &= \overline{\mu}^{\,\mathrm{dil}} \,\mathrm{tr}\overline{\boldsymbol{\varepsilon}}^{\,2} \end{aligned} \tag{4.13}$$

to leading order in the deformation measure $\overline{\boldsymbol{\varepsilon}} \doteq (\overline{\mathbf{F}} + \overline{\mathbf{F}}^T - 2\mathbf{I})/2$ and $O(1)$ in c_p and c_i, where the coefficient

$$\overline{\mu}^{\,\mathrm{dil}} \doteq \mu_m + \frac{5\,\mu_m}{2}\,c_p + \frac{5(\mu_i - \mu_m)\,(q_1\mu_i + q_4\mu_m)\,\mu_m}{2(q_1\mu_i^2 + q_2\,\mu_i\mu_m + q_3\mu_m^2)}\,c_i \tag{4.14}$$

has been introduced for later reference and

$$\begin{aligned} q_1 &= 38k^{10} + 225k^7 - 336k^5 + 200k^3 + 48, \\ q_2 &= 89k^{10} + 75k^7 - 168k^5 + 100k^3 - 96, \\ q_3 &= 48k^{10} - 300k^7 + 504k^5 - 300k^3 + 48, \\ q_4 &= \frac{4(k-1)^3\,(2k^3+3)\,(4k^6 + 16k^5 + 40k^4 + 55k^3 + 40k^2 + 16k + 4)}{k^2 + k + 1} \end{aligned} \tag{4.15}$$

with

$$k = 1 + \frac{t}{r} = \left(1 + \frac{c_i}{c_p}\right)^{1/3}. \tag{4.16}$$

Expression (4.14) corresponds to the effective shear modulus of an isotropic incompressible elastomer, with shear modulus μ_m, filled with a dilute distribution of rigid spherical particles that are bonded through isotropic incompressible interphases with shear modulus μ_i and thickness t. Three key points are worth remarking:

- The dependence of the effective shear modulus (4.14) on t enters through the interphase-thickness-to-particle-radius ratio t/r, or equivalently, through the ratio of concentration of interphases to concentration of particles c_i/c_p. A corollary of such a dimensionless dependence is that the result (4.14) applies not only to microstructures with monodisperse particles, but also to microstructures with polydisperse particles provided that all particles and surrounding interphases have the same interphase-thickness-to-particle-radius ratio t/r.

- The result (4.14) constitutes a generalization of the classical result of Einstein-Smallwood (Smallwood, 1944) for the effective shear modulus of a dilute suspension of rigid spherical particles in rubber with perfect bonding (i.e., without interphases) between the particles and the rubber. Indeed, in the absence of interphases when $c_i = 0$, the effec-

tive shear modulus (4.14) reduces identically to the well-known formula $\overline{\mu}^{\,\mathrm{dil}} = \mu_m + 5/2\,\mu_m\,c_p$. The choices $\mu_i = \mu_m$ and $\mu_i = +\infty$ also recover this classical result; in the latter, $\overline{\mu}^{\,\mathrm{dil}} = \mu_m + 5/2\,\mu_m\,(c_p + c_i)$ since the total concentration of particles is $c_p + c_i$ in that limiting case.

- A further salient feature of the solution (4.13)–(4.16) is that the stress fields inside the particles are *not* uniform; see Appendix A for details. Uniform intra-particle (stress and strain) fields are the hallmark of the classical solution of Einstein-Smallwood, and, more generally, that of Eshelby (1957), where no interphases are accounted for. The solution (4.13)–(4.16) reveals that the presence of interphases, however small, disrupts the uniformity of the fields inside the particles. The theoretical and practical implications of this feature are far reaching since many homogenization techniques (e.g., the Mori-Tanaka approximation and most techniques based on Hashin-Shtrikman-type variational principles) make critical use of the very fact that the fields in at least one of the underlying constituents are uniform. The employment of such techniques to study the behavior of particulate composites with interphases might hence lead to inaccurate results.

4.2.2 An approximate closed-form solution for arbitrarily large deformations

For arbitrarily large applied deformations $\overline{\mathbf{F}}$, the single-particle problem does not appear to admit an exact analytical solution. In the following two subsections, guided by earlier results for dilute suspensions of rigid particles without interphases (Lopez-Pamies et al., 2013b), we first construct a FE (finite-element) solution for the effective stored-energy function $\overline{\Psi}$ from which we are then able to devise a closed-form approximation for it.

Finite element solution

By virtue of the invariance of the equations of elastostatics under the transformation $(\mathbf{X}, \mathbf{x}) \to (\beta\mathbf{X}, \beta\mathbf{x})$, it is indifferent to consider the problem of an infinitely large elastomeric matrix containing a finite-size particle or that of a finite-size block of elastomer that contains a particle of infinitesimal size. In

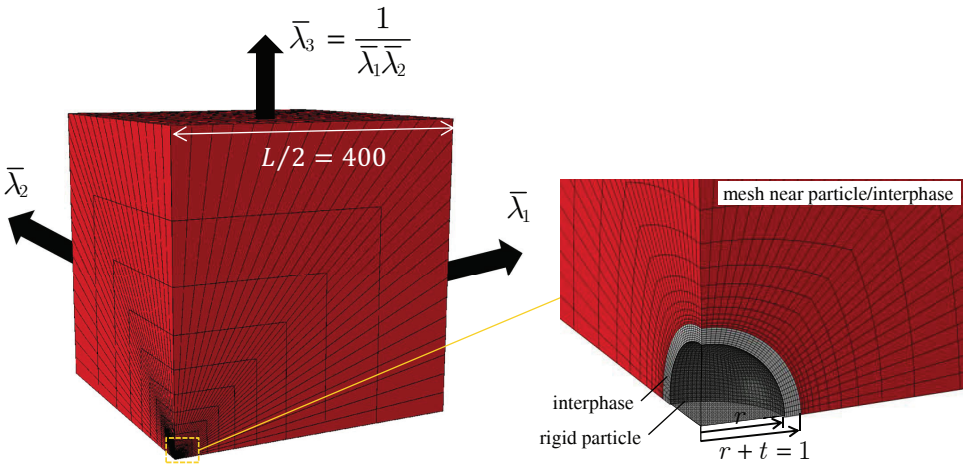

Figure 4.3: A representative finite element model — in the undeformed configuration — of a small rigid spherical particle of radius r bonded to the matrix through an interphase of thickness $t = 1 - r$ located at the center of a cubic block of side $L = 800$. The boundary of the cube is subjected to the stretches $\overline{\lambda}_1$, $\overline{\lambda}_2$, and $\overline{\lambda}_3 = (\overline{\lambda}_1\overline{\lambda}_2)^{-1}$ aligned with the three principal axes of the cube.

constructing a FE solution, we are compelled to consider the latter. Without loss of generality, we take the elastomer block to be a cube of side L. In this context, given that the radius r of the particle and the thickness t of its surrounding interphase must be necessarily finite, we need to identify how small their concentrations $c_p = 4\pi r^3/3L^3$ and $c_i = 4\pi[(r+t)^3 - r^3]/3L^3$ ought to be in order to accurately approximate an infinitesimally small particle and infinitesimally small interphase. To this end, we carried out a parametric study with decreasing concentrations of the particle c_p and interphase c_i. The results indicate that for combined values $c_p + c_i \leq 10^{-8}$, the particle and interphase behave effectively as infinitesimally small. Based on this analysis, all the calculations that follow are such that

$$c_p + c_i = \frac{125\pi}{48} \times 10^{-9}, \tag{4.17}$$

corresponding to a combined particle-interphase length of $r + t = 1$ in a cube of side $L = 800$.

The geometric and constitutive symmetries of the problem allow to perform the calculations in just one octant of the cube. A mesh generator code is utilized to construct the 3D geometry for such an octant. The particle needs not be meshed, instead, the nodes at the particle/interphase boundary are fixed in the undeformed configuration in order to model the rigid behavior of

the particle. For illustration purposes, Fig. 4.3 shows the mesh utilized for the case with $r = 5/6$ and $t = 0.2r = 1/6$, which correspond to $c_p \approx 4.73 \times 10^{-9}$ and $c_i \approx 3.45 \times 10^{-9}$. Small elements are placed near the rigid particle at uniform angular intervals of 3°, while the radial length is gradually increased toward the outer boundary. In all, the mesh consists of 18,900 brick elements with 675 elements on a radial plane and 28 layers along the radial direction. The interphase is comprised of 8 layers of elements in the radial direction. This discretization was selected after various mesh refinements were tried to assess sufficient mesh convergence. In selecting an appropriate type of element, we tested 8-node linear and 20-node quadratic hybrid elements, where the pressure is treated as a further degree of freedom in order to be able to handle the incompressibility of the Gaussian matrix and interphase exactly (in a numerical sense). The 20-node quadratic elements with linearly varying pressure proved to have a faster convergence and thus were selected.

Given the overall isotropy and incompressibility of the problem, it suffices to restrict attention to affine boundary conditions (4.5) with deformation gradients of the diagonal form

$$\overline{\mathbf{F}} = \operatorname{diag}\left(\overline{\lambda}_1, \overline{\lambda}_2, \overline{\lambda}_3 = \frac{1}{\overline{\lambda}_1 \overline{\lambda}_2}\right). \tag{4.18}$$

We find it convenient to implement this type of loading conditions by following radial straining paths in principal-logarithmic-strain space. Specifically, we set

$$\overline{\lambda}_1 = \lambda \quad \text{and} \quad \overline{\lambda}_2 = \lambda^a \tag{4.19}$$

(and hence $\overline{\lambda}_3 = (\overline{\lambda}_1 \overline{\lambda}_2)^{-1} = \lambda^{-(1+a)}$), where λ is a positive load parameter that takes the value of 1 in the undeformed configuration and $a \in \mathbb{R}$. Any desired macroscopic deformation state $(\overline{\lambda}_1, \overline{\lambda}_2, \overline{\lambda}_3 = (\overline{\lambda}_1 \overline{\lambda}_2)^{-1})$ can be accessed by marching along (starting at $\lambda = 1$) radial paths (4.19) with appropriate fixed values of a.

Under boundary conditions (4.5) with (4.18), the total elastic energy per unit undeformed volume computed from the FE model, denoted here by

$\overline{\Psi}^{FE}$, turns out to be of the expected asymptotic form

$$\overline{\Psi}^{FE}(\overline{\lambda}_1, \overline{\lambda}_2, c_p, c_i) = \frac{\mu_m}{2}\left[\overline{\lambda}_1^2 + \overline{\lambda}_2^2 + \frac{1}{\overline{\lambda}_1^2\overline{\lambda}_2^2} - 3\right] + \mu_m\, H(\overline{\lambda}_1, \overline{\lambda}_2)\, c_p + \mu_m\, G(\overline{\lambda}_1, \overline{\lambda}_2)\, c_i \qquad (4.20)$$

to $O(1)$ in c_p and c_i. In this expression, H and G are functions of the applied stretches $\overline{\lambda}_1$ and $\overline{\lambda}_2$ such that

$$\begin{aligned} H(\overline{\lambda}_1, \overline{\lambda}_2) &= H(\overline{\lambda}_2, \overline{\lambda}_1) = H(\overline{\lambda}_1, (\overline{\lambda}_1\overline{\lambda}_2)^{-1}) = H((\overline{\lambda}_1\overline{\lambda}_2)^{-1}, \overline{\lambda}_1) \\ &= H(\overline{\lambda}_2, (\overline{\lambda}_1\overline{\lambda}_2)^{-1}) = H((\overline{\lambda}_1\overline{\lambda}_2)^{-1}, \overline{\lambda}_2), \\ G(\overline{\lambda}_1, \overline{\lambda}_2) &= G(\overline{\lambda}_2, \overline{\lambda}_1) = G(\overline{\lambda}_1, (\overline{\lambda}_1\overline{\lambda}_2)^{-1}) = G((\overline{\lambda}_1\overline{\lambda}_2)^{-1}, \overline{\lambda}_1) \\ &= G(\overline{\lambda}_2, (\overline{\lambda}_1\overline{\lambda}_2)^{-1}) = G((\overline{\lambda}_1\overline{\lambda}_2)^{-1}, \overline{\lambda}_2), \end{aligned} \qquad (4.21)$$

as a result of the overall isotropy and incompressibility; in addition to the applied stretches, the function G depends also on the ratio μ_i/μ_m between the shear moduli of the Gaussian interphase and the matrix, as well as on the ratio t/r between the thickness of the interphase and the radius of the particle, but such a dependence is not stated explicitly here for notational simplicity. Now, in order to extract the correcting functions H and G from the computed values of $\overline{\Psi}^{FE}$, an expedient strategy is first to compute $\overline{\Psi}^{FE}$ in the absence of the interphase when $c_i = 0$ so that

$$H(\overline{\lambda}_1, \overline{\lambda}_2) = \frac{1}{c_p}\left\{\frac{1}{\mu_m}\overline{\Psi}^{FE}(\overline{\lambda}_1, \overline{\lambda}_2, c_p, 0) - \frac{1}{2}\left[\overline{\lambda}_1^2 + \overline{\lambda}_2^2 + \frac{1}{\overline{\lambda}_1^2\overline{\lambda}_2^2} - 3\right]\right\}. \qquad (4.22)$$

Having determined H from (4.22), the function G can then be readily extracted from the computed values of $\overline{\Psi}^{FE}$ for the case when the interphase is accounted for, namely,

$$G(\overline{\lambda}_1, \overline{\lambda}_2) = \frac{1}{c_i}\left\{\frac{1}{\mu_m}\overline{\Psi}^{FE}(\overline{\lambda}_1, \overline{\lambda}_2, c_p, c_i) - \frac{1}{2}\left[\overline{\lambda}_1^2 + \overline{\lambda}_2^2 + \frac{1}{\overline{\lambda}_1^2\overline{\lambda}_2^2} - 3\right] - H(\overline{\lambda}_1, \overline{\lambda}_2)\, c_p\right\}. \qquad (4.23)$$

Here, it is important to emphasize that the correction terms in (4.20) are in

the order of 10^{-9} or smaller, as dictated by the combined concentration of particle and interphase (4.17), and hence that the computation of $\overline{\Psi}^{FE}$ must be carefully carried out in double precision in order to be able to accurately determine the correcting functions H and G from (4.22) and (4.23). It is also important to emphasize that in the computation of the functions H and G, by virtue of their symmetries (4.21), it suffices to restrict attention to radial loadings (4.19) with $\lambda \geq 1$ and $a \in [-0.5, 1]$.

Results and discussion

Figure 4.4 shows the FE solution for the correcting function H. Part (a) of the figure shows the full 3D view of the function over a large range of stretches $\overline{\lambda}_1$ and $\overline{\lambda}_2$, while part (b) shows its 2D view along the axisymmetric shear loading with $\overline{\lambda}_1 = \overline{\lambda}_2 = \overline{\lambda}$.

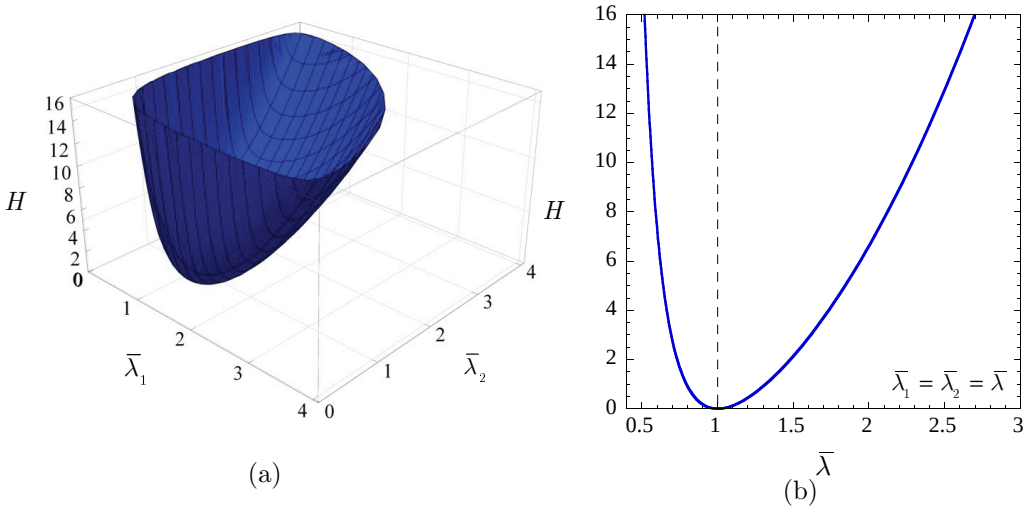

Figure 4.4: (a) Full 3D view of the FE solution for the correcting function H, defined in (4.20), over a large range of applied macroscopic stretches $\overline{\lambda}_1$ and $\overline{\lambda}_2$. (b) 2D view along the axisymmetric shear loading with $\overline{\lambda}_1 = \overline{\lambda}_2 = \overline{\lambda}$.

Similarly, Fig. 4.5 shows the FE solution for the correcting function G. Part (a) of the figure shows the full 3D view of the function over a large range of stretches $\overline{\lambda}_1$ and $\overline{\lambda}_2$, while part (b) shows its 2D view along the axisymmetric shear loading with $\overline{\lambda}_1 = \overline{\lambda}_2 = \overline{\lambda}$. As opposed to H, the function G *does* depend on the ratio μ_i/μ_m between the shear moduli of the interphase and the matrix, as well as on the ratio t/r between the thickness of the

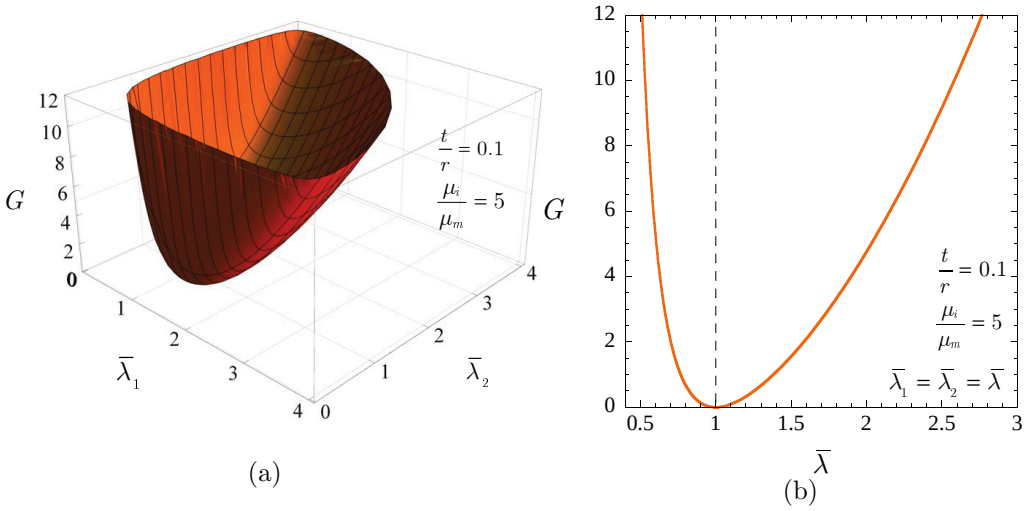

Figure 4.5: (a) Full 3D view of the FE solution for the correcting function G, defined in (4.20), over a large range of applied macroscopic stretches $\overline{\lambda}_1$ and $\overline{\lambda}_2$. (b) 2D view along the axisymmetric shear loading with $\overline{\lambda}_1 = \overline{\lambda}_2 = \overline{\lambda}$. The results correspond to an interphase that is five times stiffer than the matrix, $\mu_i/\mu_m = 5$, whose thickness is one tenth the particle radius, $t/r = 0.1$.

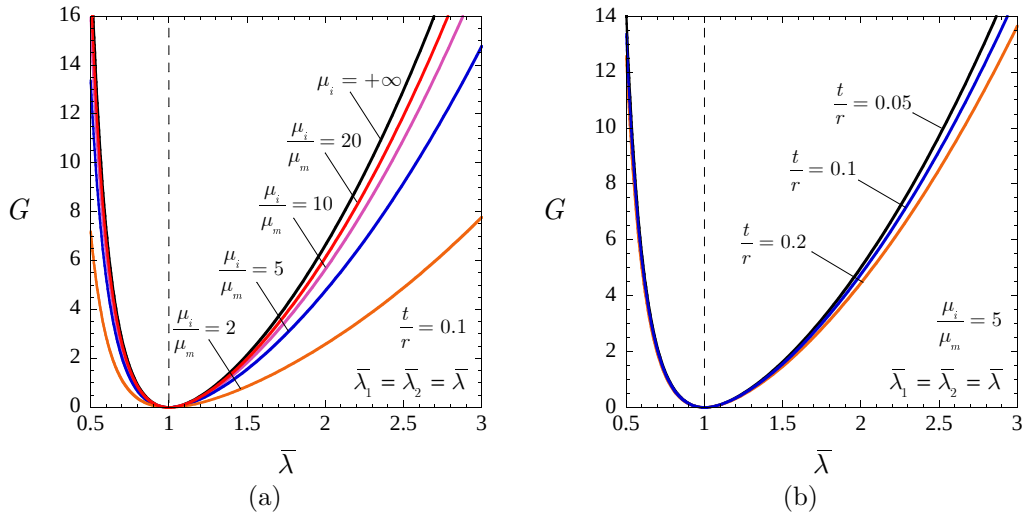

Figure 4.6: FE solutions for the correcting function G along the axisymmetric shear loading with $\overline{\lambda}_1 = \overline{\lambda}_2 = \overline{\lambda}$. Part (a) shows results for various ratios μ_i/μ_m between the interphase and matrix shear moduli at fixed $t/r = 0.1$, while part (b) shows results for various ratios t/r between the interphase thickness and particle radius at fixed $\mu_i/\mu_m = 5$.

interphase and the radius of the particle. The results displayed in Fig. 4.5 correspond to the values $\mu_i/\mu_m = 10$ and $t/r = 0.1$.

The dependence of G on μ_i/μ_m and t/r is illustrated in Fig. 4.6. For purposes of visualization, the results are presented only for the case of axisym-

metric shear loading when $\overline{\lambda}_1 = \overline{\lambda}_2 = \overline{\lambda}$. Specifically, Fig. 4.6(a) displays the function G for $\mu_i/\mu_m = 2, 5, 10, 20, +\infty$ and $t/r = 0.1$. On the other hand, Fig. 4.6(b) displays G for $t/r = 0.05, 0.1, 0.2$ and $\mu_i/\mu_m = 5$. An immediate observation from these plots is that G is a monotonically increasing function of the interphase stiffness μ_i/μ_m, but a decreasing function of its thickness t/r. With respect to the dependence on the interphase stiffness, it is worth remarking that G saturates quickly with increasing values of μ_i/μ_m. There is indeed little difference between the result for $\mu_i/\mu_m = 10$ and that for $\mu_i/\mu_m = +\infty$. It is also worth remarking that $G = H$ for $\mu_i/\mu_m = +\infty$, as expected, since in this limiting case there is actually no interphase but instead a rigid spherical particle of radius $r + t$ perfectly bonded to the matrix.

For further scrutiny of the correcting functions H and G, Fig. 4.7 shows results for H and G in terms of the first and second principal invariants of the applied macroscopic loading: $\overline{I}_1 = \overline{\mathbf{F}} \cdot \overline{\mathbf{F}} = \overline{\lambda}_1^2 + \overline{\lambda}_2^2 + \overline{\lambda}_1^{-2}\overline{\lambda}_2^{-2}$ and $\overline{I}_2 = \overline{\mathbf{F}}^{-T} \cdot \overline{\mathbf{F}}^{-T} = \overline{\lambda}_1^{-2} + \overline{\lambda}_2^{-2} + \overline{\lambda}_1^2\overline{\lambda}_2^2$. Parts (a) and (c) show H and G as functions of $\overline{I}_1$ for the two fixed values $\overline{I}_2 = 4, 6$. Parts (b) and (d), on the other hand, show H and G as functions of $\overline{I}_2$ for the four fixed values $\overline{I}_1 = 4, 7, 10, 13$. The results for G correspond to the case of an interphase with $\mu_i/\mu_m = 5$ and $t/r = 0.1$. In the context of these plots, it is appropriate to recall that the constraint of incompressibility imposes a restriction on the physically allowable values of $\overline{I}_1$ and $\overline{I}_2$. Thus, for fixed $\overline{I}_2 = 4, 6$, the first invariant is restricted to take values in the ranges $\overline{I}_1 \in [3.71, 4.52]$ and $\overline{I}_1 \in [4.72, 9.34]$, respectively. For fixed $\overline{I}_1 = 4, 7, 10, 13$, the allowable values of the second principal invariant are such that $\overline{I}_2 \in [3.71, 4.52]$, $\overline{I}_2 \in [5.14, 12.54]$, $\overline{I}_2 \in [6.22, 25.20]$, and $\overline{I}_2 \in [7.13, 42.40]$, respectively. These are the ranges of values utilized in the figure. The dominant observation from Fig. 4.7 is that both correcting functions H and G are approximately *linear* in $\overline{I}_1$ and *independent* of $\overline{I}_2$; while the results for G in this figure correspond to the particular case of interphase stiffness $\mu_i/\mu_m = 5$ and thickness $t/r = 0.1$, the approximately linear dependence on $\overline{I}_1$ and independence from $\overline{I}_2$ of this function has been checked (through a parametric study) to be insensitive to the choice of values for μ_i/μ_m and t/r. The fact that these macroscopic or average correcting functions are, in essence, functionally identical — namely, linear in $\overline{I}_1$ and independent of $\overline{I}_2$ — to the local stored-energy functions for the underlying Gaussian matrix and interphase is admittedly remarkable. Indeed, the functional character of the average behavior of nonlinear material

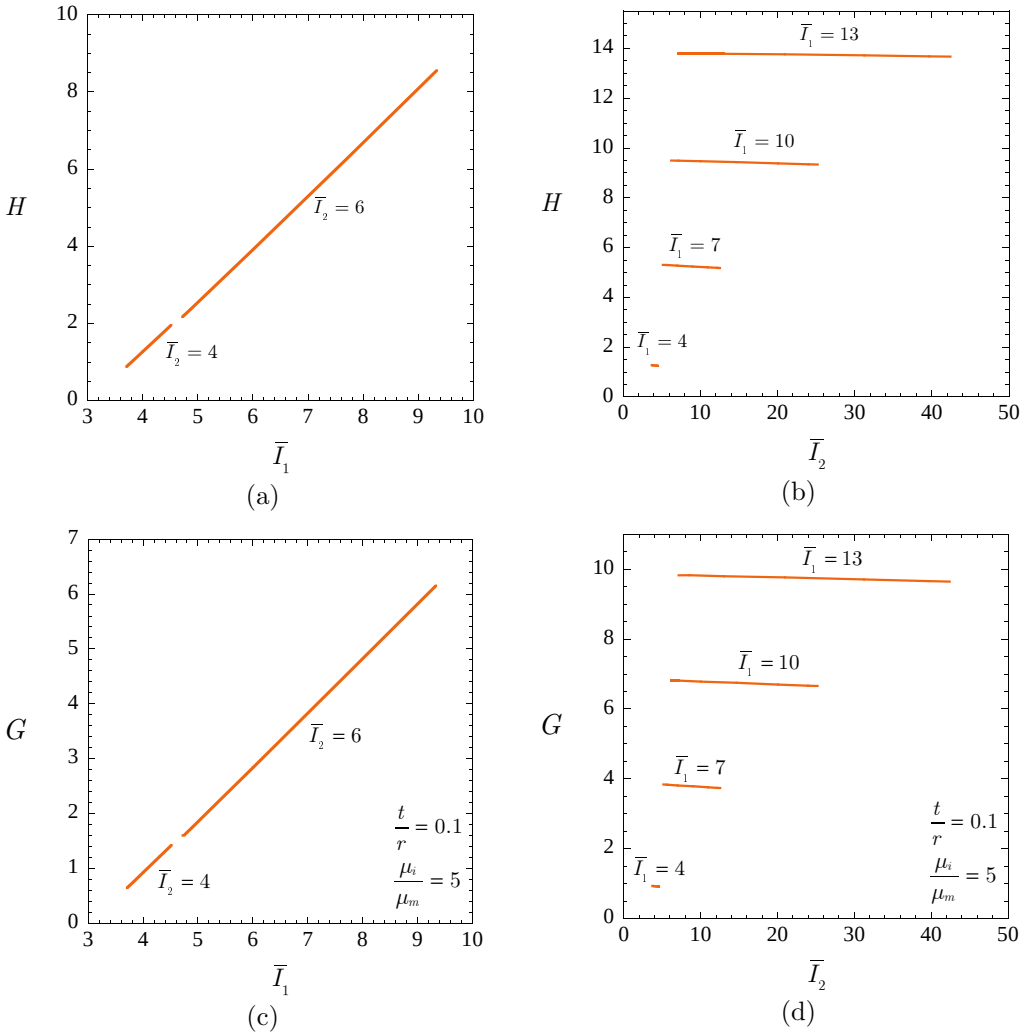

Figure 4.7: FE solutions for the correcting functions H and G plotted in terms of the principal invariants $\overline{I}_1 = \overline{\lambda}_1^2 + \overline{\lambda}_2^2 + \overline{\lambda}_1^{-2}\overline{\lambda}_2^{-2}$ and $\overline{I}_2 = \overline{\lambda}_1^{-2} + \overline{\lambda}_2^{-2} + \overline{\lambda}_1^2\overline{\lambda}_2^2$. Parts (a) and (c) show H and G as functions of $\overline{I}_1$ for different fixed values of $\overline{I}_2$, whereas parts (b) and (d) show corresponding plots as functions of $\overline{I}_2$ for different fixed values of $\overline{I}_1$. The results shown for the function G in (c) and (d) correspond to an interphase that is five times stiffer than the matrix, $\mu_i/\mu_m = 5$, whose thickness is one tenth the particle radius, $t/r = 0.1$.

systems is in general substantially different from that of its constituents, but that is not the case here. This is a most distinctive trait that we exploit next to generate a simple yet accurate closed-form approximation.

The proposed approximate closed-form solution

In view of the analytical asymptotic solution (4.13) in the small-deformation limit together with the foregoing numerical observations for finite deformations, we propose the following closed-form approximations

$$H(\overline{\lambda}_1, \overline{\lambda}_2) = \frac{5}{4}\left[\overline{\lambda}_1^2 + \overline{\lambda}_2^2 + \frac{1}{\overline{\lambda}_1^2\overline{\lambda}_2^2} - 3\right], \tag{4.24}$$

$$G(\overline{\lambda}_1, \overline{\lambda}_2) = \frac{5(\mu_i - \mu_m)\,(q_1\mu_i + q_4\mu_m)}{4(q_1\mu_i^2 + q_2\,\mu_i\mu_m + q_3\mu^2)}\left[\overline{\lambda}_1^2 + \overline{\lambda}_2^2 + \frac{1}{\overline{\lambda}_1^2\overline{\lambda}_2^2} - 3\right] \tag{4.25}$$

for the correcting functions H and G. By construction, the approximations (4.24)–(4.25) have the merit to be exact in the limit of small deformations, as $\overline{\lambda}_1,\ \overline{\lambda}_2 \to 1$. For arbitrarily large deformations, although not exact, the approximations (4.24)–(4.25) are practically identical to the exact solution in a functional sense: they are linear in $\overline{I}_1(= \overline{\lambda}_1^2+\overline{\lambda}_2^2+\overline{\lambda}_1^{-2}\overline{\lambda}_2^{-2})$ and independent of $\overline{I}_2(= \overline{\lambda}_1^{-2}+\overline{\lambda}_2^{-2}+\overline{\lambda}_1^2\overline{\lambda}_2^2)$. In addition, as illustrated by Figs. 4.8 and 4.9, the simple closed-form expressions (4.24)–(4.25) are remarkably accurate when compared with the corresponding FE solutions. Specifically, Fig. 4.8 shows comparisons between the proposed approximation (4.24) for the function H and its FE solution. Similarly, Fig. 4.9 shows comparisons between the proposed approximation (4.25) for G and its FE solution. Parts (a) and (b) of Fig. 4.9 correspond to the case of an interphase that is five times stiffer than the matrix, $\mu_i/\mu_m = 5$, whose thickness is one tenth the particle radius, $t/r = 0.1$, while parts (c) and (d) illustrate comparisons for various values of the ratios μ_i/μ_m and t/r.

Making use of the approximations (4.24)–(4.25) for H and G, it follows trivially that the resulting closed-form approximate solution for the effective stored-energy function $\overline{\Psi}$ of a Gaussian elastomer with shear modulus μ_m, filled with a dilute distribution of rigid spherical particles that are bonded through interphases of constant thickness t, made up of a different Gaussian

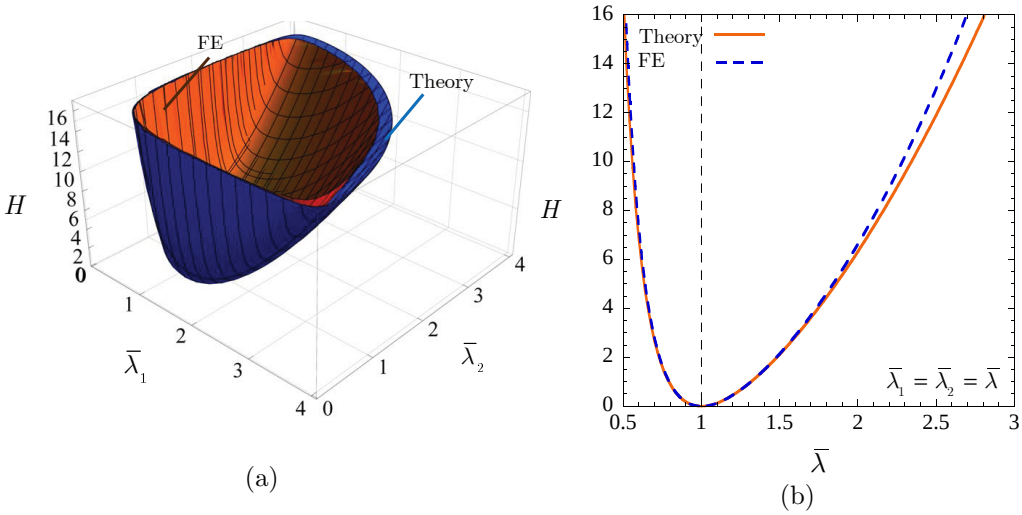

Figure 4.8: Comparison between the correcting function H computed from the FE simulations and its closed-form approximations (4.24). Part (a) shows the comparison for a wide range of stretches $\overline{\lambda}_1$ and $\overline{\lambda}_2$, while part (b) shows the comparison for the case of axisymmetric deformations with $\overline{\lambda}_1 = \overline{\lambda}_2 = \overline{\lambda}$.

elastomer with shear modulus μ_i, is given by

$$\begin{aligned}\overline{\Psi}(\overline{I}_1, \overline{I}_2, c_p, c_i) &= \frac{\mu_m}{2}\left[\overline{I}_1 - 3\right] \\ &\quad \frac{5\,\mu_m}{4}\left[\overline{I}_1 - 3\right] c_p + \frac{5(\mu_i - \mu_m)\,(q_1\mu_i + q_4\mu_m)\,\mu_m}{4(q_1\mu_i^2 + q_2\,\mu_i\mu_m + q_3\mu_m^2)}\left[\overline{I}_1 - 3\right] c_i \\ &= \frac{\overline{\mu}^{\,\mathrm{dil}}}{2}\left[\overline{I}_1 - 3\right] \qquad (4.26)\end{aligned}$$

to $O(1)$ in the concentration of particles c_p and interphases c_i. Here, it is recalled that the coefficients q_1, q_2, q_3, q_4 are given in terms of the concentration ratio c_i/c_p by expressions (4.15), whereas the effective shear modulus $\overline{\mu}^{\,\mathrm{dil}}$ is given by expression (4.14). Because of the above-discussed properties of the functions (4.24)–(4.25), the approximate solution (4.26) is identical to the exact solution (4.13) in the limit of small deformations and, while not exact, qualitatively and quantitatively very close to the FE solution for arbitrarily large deformations. We conclude by remarking that the dependence of the effective stored-energy function (4.26) on t enters via the effective shear modulus $\overline{\mu}^{\,\mathrm{dil}}$ through the *dimensionless* interphase-thickness-to-particle-radius ratio $t/r = (1 + c_i/c_p)^{1/3} - 1$. This implies that the result (4.26) applies not only to microstructures with monodisperse particles, but also to microstructures with polydisperse particles wherein all particles and surround-

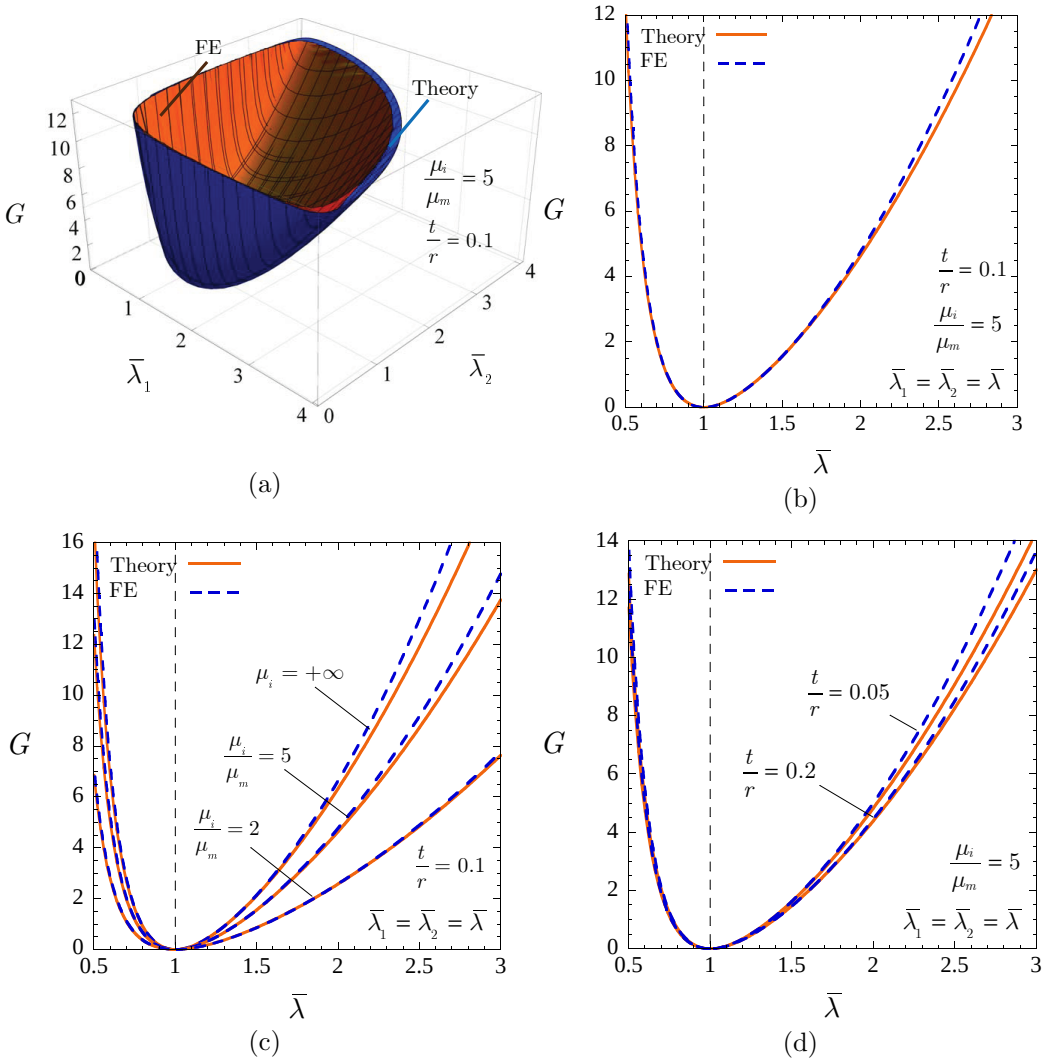

Figure 4.9: Comparison between the correcting function G computed from the FE simulations and its closed-form approximation (4.25). Parts (a) and (b) show the comparison for a wide range of stretches $\overline{\lambda}_1$ and $\overline{\lambda}_2$ for $\mu_i/\mu_m = 5$ and $t/r = 0.1$. Part (c) shows results for various ratios μ_i/μ_m between the interphase and the matrix shear moduli at fixed $t/r = 0.1$, while part (d) shows results for various ratios t/r between the interphase thickness and particle radius at fixed $\mu_i/\mu_m = 5$ along axisymmetric deformations with $\overline{\lambda}_1 = \overline{\lambda}_2 = \overline{\lambda}$.

ing interphases have the same interphase-thickness-to-particle-radius ratio $t/r = (1 + c_i/c_p)^{1/3} - 1$.

4.3 Finite concentration of particles and interphases in non-Gaussian elastomers

In this section, we construct a solution for the effective stored-energy function $\overline{\Psi}$, as defined by (4.11) with (4.7), of non-Gaussian elastomers filled with an isotropic distribution of rigid spherical particles of polydisperse sizes and finite concentration c_p that are bonded through constant-thickness Gaussian interphases of finite concentration c_i. This is accomplished by making use of two different techniques in two successive steps. First, as elaborated in Section 4.3.1, the fundamental dilute solution (4.26) is utilized within the context of an iterated homogenization method in finite elasticity (Lopez-Pamies, 2010a, 2014) to generate a finite-concentration solution for filled Gaussian elastomers. In Section 4.3.2, this finite-concentration result is then employed within the context of a variational nonlinear comparison medium method (Lopez-Pamies et al., 2013a) to generate in turn a corresponding solution for the more general case when the underlying elastomeric matrix is non-Gaussian, as characterized by any I_1-based stored-energy function $\Psi_m(I_1)$ of choice.

4.3.1 Filled elastomers with Gaussian matrix

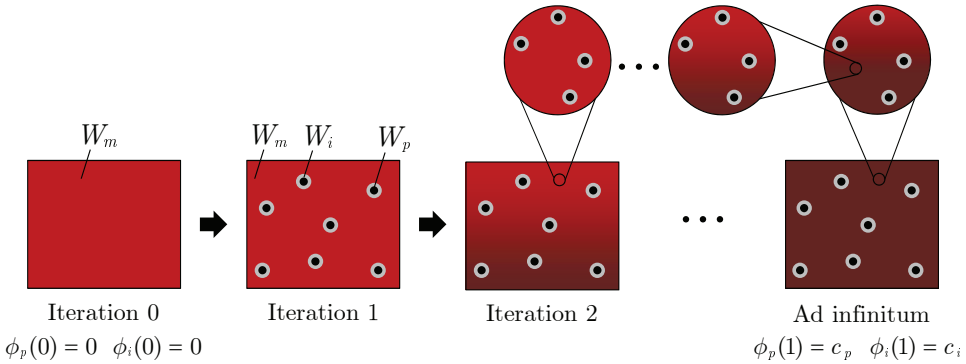

Figure 4.10: Schematic of the iterative dilute construction process of an elastomer (characterized by a stored-energy function W_m) filled with particles (characterized by a stored-energy function W_p) at finite concentration c_p bonded through interphases (characterized by a stored-energy function W_i) at finite concentration c_i.

Iterated dilute homogenization methods are a class of iterative techniques that make use of results for the overall properties of dilute composites in order

to generate corresponding results for composites with finite concentration of constituents. Within the non-convex realm of finite elasticity, extending the formulation of Lopez-Pamies (2010a) for two-phase composites, Lopez-Pamies (2014) has put forward an iterated dilute homogenization technique applicable to composite materials with any number of phases. For the generic three-phase problem outlined in Sections 4.1.1 and 4.1.2, assuming that the effective stored-energy function (4.7) is of the asymptotic form

$$\overline{W}(\overline{\mathbf{F}}, c_p, c_i) = W_m(\overline{\mathbf{F}}) + \mathcal{H}\left\{W_m, W_p, W_i; \overline{\mathbf{F}}\right\} c_p + \mathcal{G}\left\{W_m, W_p, W_i; \overline{\mathbf{F}}\right\} c_i \tag{4.27}$$

to $O(1)$ in the concentration of particles c_p and interphases c_i, the formulation states that the effective stored-energy function (4.7) of elastomers filled with particles bonded through interphases is given implicitly by the differential equation

$$\begin{aligned}(1-\phi_p-\phi_i)\frac{\partial \overline{W}}{\partial \tau} \;=\; & \left[(1-\phi_i)\frac{\mathrm{d}\phi_p}{\mathrm{d}\tau} + \phi_p \frac{\mathrm{d}\phi_i}{\mathrm{d}\tau}\right] \mathcal{H}\left\{\overline{W}, W_p, W_i; \overline{\mathbf{F}}\right\} + \\ & \left[(1-\phi_p)\frac{\mathrm{d}\phi_i}{\mathrm{d}\tau} + \phi_i \frac{\mathrm{d}\phi_p}{\mathrm{d}\tau}\right] \mathcal{G}\left\{\overline{W}, W_p, W_i; \overline{\mathbf{F}}\right\}\end{aligned} \tag{4.28}$$

subject to the initial condition

$$\overline{W}(\overline{\mathbf{F}}, c_p, c_i)\,|_{\tau=0} = W_m(\overline{\mathbf{F}}). \tag{4.29}$$

The functionals $\mathcal{H}$ and $\mathcal{G}$ in (4.28) are the same as in the asymptotic result (4.27), τ is a time-like variable taking values from 0 and 1, the range over which the differential equation (4.28) must be integrated, and $\phi_p(\tau)$ and $\phi_i(\tau)$ are non-negative, non-decreasing functions of choice that must satisfy the properties $\phi_p(\tau) + \phi_i(\tau) \leq 1$, $\phi_p(0) = \phi_i(0) = 0$, $\phi_p(1) = c_p$, $\phi_i(1) = c_i$. More specifically, the functions $\phi_p(\tau)$ and $\phi_i(\tau)$ characterize the manner in which the composite is constructed and thus contain microstructural information; see Fig. 4.10 for a schematic depiction of the iterative construction process. The interested reader is referred to Section 3.1 of Lopez-Pamies (2014) for the derivation and full description of the above results. Here, it suffices to remark that knowledge of an exact (approximate) dilute solution (4.27) allows to compute exact (approximate) non-dilute solutions via the initial-value problem (4.28)–(4.29). And that, by construction, such non-

dilute solutions correspond to polydisperse microstructures with particles of infinitely many sizes. This feature is of practical relevance here because standard reinforcing fillers (e.g., carbon black and silica) typically agglomerate, resulting effectively in polydisperse microstructures with "particles" of many different sizes.

When specialized to the class of isotropic incompressible filled elastomers described in Section 4.1.3, assuming that the matrix is Gaussian and employing the analytical approximation (4.26) as (the finite-branch of) the dilute solution (4.27), the formulation (4.28)–(4.29) generates the following result:

$$\overline{\Psi}(\overline{I}_1, \overline{I}_2, c_p, c_i) = \frac{\overline{\mu}}{2}[\overline{I}_1 - 3] \tag{4.30}$$

with the coefficient $\overline{\mu}$ being defined implicitly by the first-order nonlinear ode

$$\begin{aligned}(1-\phi_p-\phi_i)\frac{\mathrm{d}\overline{\mu}}{\mathrm{d}\tau} &= \left[(1-\phi_i)\frac{\mathrm{d}\phi_p}{\mathrm{d}\tau} + \phi_p\frac{\mathrm{d}\phi_i}{\mathrm{d}\tau}\right]\frac{5\overline{\mu}}{2} \\ &\quad + \left[(1-\phi_p)\frac{\mathrm{d}\phi_i}{\mathrm{d}\tau} + \phi_i\frac{\mathrm{d}\phi_p}{\mathrm{d}\tau}\right]\frac{5\overline{\mu}(\mu_i-\overline{\mu})\,(\widehat{q}_1\mu_i + \widehat{q}_4\overline{\mu})}{2(\widehat{q}_1\mu_i^2 + \widehat{q}_2\,\mu_i\overline{\mu} + \widehat{q}_3\overline{\mu}^2)},\end{aligned} \tag{4.31}$$

again, to be integrated from $\tau = 0$ to $\tau = 1$, subject to the initial condition

$$\overline{\mu}|_{\tau=0} = \mu_m, \tag{4.32}$$

where

$$\begin{aligned}\widehat{q}_1 &= 38\widehat{k}^{10} + 225\widehat{k}^7 - 336\widehat{k}^5 + 200\widehat{k}^3 + 48, \\ \widehat{q}_2 &= 89\widehat{k}^{10} + 75\widehat{k}^7 - 168\widehat{k}^5 + 100\widehat{k}^3 - 96, \\ \widehat{q}_3 &= 48\widehat{k}^{10} - 300\widehat{k}^7 + 504\widehat{k}^5 - 300\widehat{k}^3 + 48, \\ \widehat{q}_4 &= \frac{4(\widehat{k}-1)^3(2\widehat{k}^3+3)(4\widehat{k}^6 + 16\widehat{k}^5 + 40\widehat{k}^4 + 55\widehat{k}^3 + 40\widehat{k}^2 + 16\widehat{k} + 4)}{\widehat{k}^2 + \widehat{k} + 1}\end{aligned} \tag{4.33}$$

with

$$\widehat{k} = \left(1 + \frac{(1-\phi_p)\dfrac{\mathrm{d}\phi_i}{\mathrm{d}\tau} + \phi_i\dfrac{\mathrm{d}\phi_p}{\mathrm{d}\tau}}{(1-\phi_i)\dfrac{\mathrm{d}\phi_p}{\mathrm{d}\tau} + \phi_p\dfrac{\mathrm{d}\phi_i}{\mathrm{d}\tau}}\right)^{1/3}. \tag{4.34}$$

Expression (4.30) with (4.31)–(4.34) corresponds to the effective stored-energy

function of a Gaussian elastomer, with shear modulus μ_m, filled with an isotropic distribution of polydisperse rigid spherical particles at finite concentration c_p that are bonded through constant-thickness Gaussian interphases, with shear modulus μ_i and finite concentration c_i. Thorough comments on the theoretical and practical merits of this result are deferred to Section 4.3.2 4.2, where the more general case of filled elastomers with non-Gaussian matrix is addressed. At this stage it is important to emphasize, however, that in addition to its explicit dependence on the concentration of particles c_p and interphases c_i, the result (4.30) depends on the microstructure through the functions ϕ_p and ϕ_i, which, again, characterize the way in which the composite is constructed.

Microstructures with constant interphase-thickness-to-particle-radius ratio. In this chapter, for relative simplicity, we shall consider microstructures wherein all filler particles, irrespectively of their size, are surrounded by interphases with the same interphase-thickness-to-particle-radius ratio. This amounts to choosing

$$\phi_p = c_p\,\tau \qquad \text{and} \qquad \phi_i = c_i\,\tau, \tag{4.35}$$

in which case $\widehat{q}_1 = q_1$, $\widehat{q}_2 = q_2$, $\widehat{q}_3 = q_3$, $\widehat{q}_4 = q_4$, $\widehat{k} = k$, and the initial-value problem (4.31)–(4.32) for the coefficient $\overline{\mu}$ reduces to

$$[1-(c_p+c_i)\tau]\,\frac{\mathrm{d}\overline{\mu}}{\mathrm{d}\tau} = \frac{5c_p}{2}\overline{\mu} + \frac{5c_i(\mu_i-\overline{\mu})\,(q_1\mu_i+q_4\overline{\mu})}{2(q_1\mu_i^2+q_2\,\mu_i\overline{\mu}+q_3\overline{\mu}^2)}\overline{\mu} \quad \text{with} \quad \overline{\mu}|_{\tau=0} = \mu_m, \tag{4.36}$$

where, again, q_1, q_2, q_3, q_4, and k are given explicitly in terms of the concentration ratio c_i/c_p by expressions (4.15) and (4.16). Upon integration from $\tau = 0$ to $\tau = 1$, the ode $(4.36)_1$ takes the form

$$\int_{\mu_m}^{\overline{\mu}} \frac{\mathrm{d}z}{\dfrac{5c_p}{2}z + \dfrac{5c_i(\mu_i-z)\,(q_1\mu_i+q_4z)}{2(q_1\mu_i^2+q_2\,\mu_i z+q_3 z^2)}z} = -\frac{\ln\left[1-c_p-c_i\right]}{c_p+c_i}. \tag{4.37}$$

Further, upon recognizing that the integral in (4.37) can be carried out explicitly together with some algebraic manipulation, this last equation can be

rewritten as

$$\mathcal{F}_1\{\overline{\mu},\mu_m\} \doteq \left[\tanh^{-1}\left(\Gamma(\overline{\mu})\right) - \tanh^{-1}\left(\Gamma(\mu_m)\right)\right] \times$$
$$\frac{c_i\left[q_4^2 - q_4(q_1+2q_2+q_3) + q_1q_3\right] + c_p[q_3(2q_1+q_2) - q_4(q_2+2q_3)]}{\sqrt{c_i^2(q_1+q_4)^2 + 2c_ic_p[q_4(2q_1+q_2) - q_1(q_2+2q_3)] + c_p^2\left(q_2^2 - 4q_1q_3\right)}}$$
$$-\frac{1}{2}(q_3+q_4)\ln\left[\frac{c_i(\overline{\mu}-\mu_i)(\mu_iq_1+q_4\overline{\mu}) - c_p\left(\mu_i^2q_1+\mu_iq_2\overline{\mu}+q_3\overline{\mu}^2\right)}{c_i(\mu_m-\mu_i)(\mu_iq_1+q_4\mu_m) - c_p\left(\mu_i^2q_1+\mu_iq_2\mu_m+q_3\mu_m^2\right)}\right]$$
$$+\left(q_4 - \frac{c_p}{c_i}q_3\right)\ln\left[(1-c_i-c_p)^{5/2}\frac{\overline{\mu}}{\mu_m}\right] = 0, \tag{4.38}$$

where

$$\Gamma(x) = \frac{c_i(q_4-q_1) + c_pq_2 + 2(c_pq_3 - c_iq_4)\dfrac{x}{\mu_i}}{\sqrt{c_i^2(q_1+q_4)^2 + 2c_ic_p[q_4(2q_1+q_2) - q_1(q_2+2q_3)] + c_p^2\left(q_2^2-4q_1q_3\right)}} \tag{4.39}$$

and the function $\mathcal{F}_1$ has been introduced for later reference. In general, as discussed in more detail below, equation (4.38) does *not* admit an explicit solution for the coefficient $\overline{\mu}$. For given values of μ_m, μ_i, c_p, and c_i it is, however, straightforward to generate a numerical solution for it.

4.3.2 Filled elastomers with non-Gaussian matrix

Comparison medium methods are variational techniques that allow to generate approximations for the overall properties of composites in terms of the properties of "simpler" comparison media. Generalizing ideas from the works of Talbot and Willis (1985), Ponte Castañeda (1991), Willis (1994), deBotton and Shmuel (2010) and Lopez-Pamies et al. (2013a) have introduced a nonlinear comparison medium approach that is capable to deal with the general types of non-convex behaviors inherent to finite elasticity. For the problem of filled elastomers formulated in Sections 4.1.1 and 4.1.2, the method provides the following variational approximation for the effective stored-energy function (4.7):

$$\overline{W}(\overline{\mathbf{F}}, c_p, c_i) =$$
$$\begin{cases} \max\limits_{W_0} \left\{ \min\limits_{\mathbf{F}\in\mathcal{K}} \frac{1}{|\Omega|} \int_\Omega W_0(\mathbf{X},\mathbf{F})\mathrm{d}\mathbf{X} + \frac{1}{|\Omega|} \int_\Omega \min\limits_{\mathbf{A},a} [f(\mathbf{X},\mathbf{A},a) - f_0(\mathbf{X},\mathbf{A},a)]\mathrm{d}\mathbf{X} \right\} \\ \qquad\qquad\qquad\qquad\qquad\qquad\qquad\qquad \text{if } \; f - f_0 > -\infty \\ \\ \min\limits_{W_0} \left\{ \min\limits_{\mathbf{F}\in\mathcal{K}} \frac{1}{|\Omega|} \int_\Omega W_0(\mathbf{X},\mathbf{F})\mathrm{d}\mathbf{X} + \frac{1}{|\Omega|} \int_\Omega \max\limits_{\mathbf{A},a} [f(\mathbf{X},\mathbf{A},a) - f_0(\mathbf{X},\mathbf{A},a)]\mathrm{d}\mathbf{X} \right\} \\ \qquad\qquad\qquad\qquad\qquad\qquad\qquad\qquad \text{if } \; f - f_0 < +\infty, \end{cases} \tag{4.40}$$

In this expression, W_0 stands for the local stored-energy function of any comparison medium of choice, possibly heterogeneous, while the functions f and f_0 are defined such that $f(\mathbf{X},\mathbf{F},J) = W(\mathbf{X},\mathbf{F})$ and $f_0(\mathbf{X},\mathbf{F},J) = W_0(\mathbf{X},\mathbf{F})$ when $J = \det\mathbf{F}$. The interested reader is referred to Section 4.1 of Lopez-Pamies et al. (2013a) for the derivation and full description of the above result. Here, it suffices to remark that knowledge of the overall nonlinear elastic response of a medium with local energy W_0, as characterized by its effective stored-energy function $\min_{\mathbf{F}\in\mathcal{K}} |\Omega|^{-1} \int_\Omega W_0(\mathbf{X},\mathbf{F})\mathrm{d}\mathbf{X}$, allows to compute a solution (approximate in general, but possibly exact in some cases) for the effective stored-energy function $\overline{W}$ of the filled elastomer of interest via the variational relation (4.40).

When specialized to the class of isotropic incompressible filled elastomers described in Section 4.1.3, by taking the comparison medium to be a filled Gaussian elastomer with the *same microstructure* and the *same constitutive behaviors for the underlying rigid particles and Gaussian interphases* as the actual filled elastomer of interest,

$$W_0(\mathbf{X},\mathbf{F}) =$$
$$\begin{cases} [1 - \theta_p(\mathbf{X}) - \theta_i(\mathbf{X})]\,\dfrac{\mu_0}{2}[I_1 - 3] + \theta_p(\mathbf{X})\Psi_p(I_1) + \theta_i(\mathbf{X})\dfrac{\mu_i}{2}[I_1 - 3] & \text{if } J = 1 \\ +\infty & \text{otherwise} \end{cases} \tag{4.41}$$

with

$$\Psi_p(I_1) = \begin{cases} 0 & \text{if} \quad I_1 = 3 \\ +\infty & \text{otherwise} \end{cases}, \tag{4.42}$$

and employing the approximation (4.30) as (the finite-branch of) the effective stored-energy function of such a comparison medium, the formulation (4.40) generates the following result:

$$\overline{\Psi}(\overline{I}_1,\overline{I}_2,c_p,c_i) = \begin{cases} \max\limits_{\mu_0}\left\{\dfrac{\overline{\mu}_0}{2}\left[\,\overline{I}_1-3\right]+(1-c_p-c_i)\min\limits_{\mathcal{I}_1}\left[\Psi_m(\mathcal{I}_1)-\dfrac{\mu_0}{2}\left[\mathcal{I}_1-3\right]\right]\right\} \\ \qquad\qquad\qquad\qquad\qquad\qquad\qquad\qquad \text{if}\;\; \Psi_m(\mathcal{I}_1)-\mathcal{I}_1>-\infty \\ \\ \min\limits_{\mu_0}\left\{\dfrac{\overline{\mu}_0}{2}\left[\,\overline{I}_1-3\right]+(1-c_p-c_i)\max\limits_{\mathcal{I}_1}\left[\Psi_m(\mathcal{I}_1)-\dfrac{\mu_0}{2}\left[\mathcal{I}_1-3\right]\right]\right\} \\ \qquad\qquad\qquad\qquad\qquad\qquad\qquad\qquad \text{if}\;\; \Psi_m(\mathcal{I}_1)-\mathcal{I}_1<+\infty, \end{cases} \tag{4.43}$$

where the coefficient $\overline{\mu}_0$ is defined implicitly by the nonlinear algebraic equation $\mathcal{F}_1\{\overline{\mu}_0,\mu_0\}=0$, cf. equation (4.38). In view of the monotonicity $(4.9)_1$ of the function Ψ_m, the max-min and min-max problems in (4.43) are solved by exactly the same stationary conditions

$$\Psi_m'(\mathcal{I}_1)=\frac{\mu_0}{2} \qquad \text{and} \qquad \frac{\mathrm{d}\overline{\mu}_0}{\mathrm{d}\mu_0}\left[\,\overline{I}_1-3\right]-(1-c_p-c_i)\left[\mathcal{I}_1-3\right]=0, \tag{4.44}$$

irrespectively of the growth conditions of Ψ_m. Making use of these relations, the effective stored-energy function (4.43) can be written more explicitly as

$$\overline{\Psi}(\overline{I}_1,\overline{I}_2,c_p,c_i)=(1-c_p-c_i)\Psi_m\left(\mathcal{I}_1\right)+\frac{\overline{\mu}_0}{2}\left[\,\overline{I}_1-3\right]-(1-c_p-c_i)\frac{\mu_0}{2}\left[\mathcal{I}_1-3\right] \tag{4.45}$$

with

$$\mathcal{I}_1=\left(\frac{c_p\overline{\mu}_0+\dfrac{(\mu_i-\overline{\mu}_0)\,(q_1\mu_i+q_4\overline{\mu}_0)}{q_1\mu_i^2+q_2\,\mu_i\overline{\mu}_0+q_3\overline{\mu}_0^2}c_i\overline{\mu}_0}{c_p\mu_0+\dfrac{(\mu_i-\mu_0)\,(q_1\mu_i+q_4\mu_0)}{q_1\mu_i^2+q_2\,\mu_i\mu_0+q_3\mu_0^2}c_i\mu_0}\right)\frac{\left[\,\overline{I}_1-3\right]}{1-c_p-c_i}+3 \tag{4.46}$$

and the variables $\overline{\mu}_0$, μ_0 being defined implicitly by the system of two coupled nonlinear algebraic equations

$$\mathcal{F}_1\{\overline{\mu}_0,\mu_0\}=0, \qquad \mathcal{F}_2\{\overline{\mu}_0,\mu_0\}\doteq\Psi_m'\left(\mathcal{I}_1\right)-\frac{\mu_0}{2}=0, \tag{4.47}$$

where it is recalled that the coefficients q_1, q_2, q_3, q_4 are given explicitly in

terms of the concentration ratio c_i/c_p by expressions (4.15) and the function $\mathcal{F}_1$ is defined by expression (4.38).

The effective stored-energy function (4.45) with (4.46)–(4.47) constitutes the main result of this chapter. It characterizes the overall nonlinear elastic response of a non-Gaussian elastomer, with stored-energy function Ψ_m, filled with an isotropic distribution of rigid spherical particles, of polydisperse sizes and finite concentration c_p, that are bonded to the elastomer through Gaussian interphases with shear modulus μ_i, finite concentration c_i, and constant thickness-to-particle-radius ratio $(1 + c_i/c_p)^{1/3} - 1$. The following theoretical and practical remarks are in order:

i. In terms of the macroscopic first Piola-Kirchhoff stress tensor $\overline{\mathbf{S}}$ and macroscopic deformation gradient tensor $\overline{\mathbf{F}}$, the constitutive response implied by the effective stored-energy function (4.45) is given by

$$\begin{aligned} \overline{\mathbf{S}} &= 2\frac{\partial \overline{\Psi}}{\partial \overline{I}_1}\,\overline{\mathbf{F}} - \overline{p}\,\overline{\mathbf{F}}^{-T} \\ &= \overline{\mu}_0\,\overline{\mathbf{F}} - \overline{p}\,\overline{\mathbf{F}}^{-T} \end{aligned} \tag{4.48}$$

where $\overline{p}$ stands for the arbitrary hydrostatic pressure associated with the incompressibility constraint $\det \overline{\mathbf{F}} = 1$ and, again, the coefficient $\overline{\mu}_0$ is defined implicitly by the system of two coupled nonlinear algebraic equations (4.47), which ultimately depend on the concentration of the particles c_p, the concentration of the interphases c_i, the stored-energy function of the matrix Ψ_m, the stiffness of the interphases μ_i, and the applied loading via the first principal invariant $\overline{I}_1 = \overline{\mathbf{F}} \cdot \overline{\mathbf{F}}$.

ii. The effective stored-energy function (4.45) is independent of the second principal invariant $\overline{I}_2 = \overline{\mathbf{F}}^{-T} \cdot \overline{\mathbf{F}}^{-T}$. The origin of this independence can be traced back to the choice of approximation (4.26) for the dilute response of filled Gaussian elastomers, which neglects the weak but existent dependence on $\overline{I}_2$ of the exact solution in order to favor analytical tractability (see Section 4.2.2). Neither the iterated dilute homogenization procedure to account for finite concentrations of particles and interphases (Section 4.3.1), nor the comparison medium procedure to account for non-Gaussian behavior (Section 4.3.2) introduced dependence on $\overline{I}_2$ thereafter. This suggests that the response of any

filled I_1-based non-Gaussian elastomer is by and large independent of $\overline{I}_2$. The FE simulations presented below provide further support that this is indeed the case.

iii. For stored-energy functions Ψ_m that are convex in I_1,

$$\Psi'_m(I_1) > 0 \qquad \text{and} \qquad \Psi''_m(I_1) \geq 0, \tag{4.49}$$

it follows that

$$\begin{aligned}
&\frac{\partial\overline{\Psi}}{\partial\overline{I}_1}(\overline{I}_1,\overline{I}_2,c_p,c_i) > 0,\\
&\frac{\partial\overline{\Psi}}{\partial\overline{I}_1}(\overline{I}_1,\overline{I}_2,c_p,c_i) + 2\left[\overline{I}_1 - \overline{\lambda}_\alpha^2 - 2\overline{\lambda}_\alpha^{-1}\right]\frac{\partial^2\overline{\Psi}}{\partial\overline{I}_1^2}(\overline{I}_1,\overline{I}_2,c_p,c_i) > 0\\
&(\alpha = 1,2,3), \quad \forall\, \overline{I}_1,\overline{I}_2 \geq 3,
\end{aligned} \tag{4.50}$$

and hence that the effective stored-energy function (4.45) is strongly elliptic. For the case when Ψ_m is merely strongly elliptic (i.e., it satisfies the weaker conditions (4.10)) but not convex in I_1, the effective stored-energy function (4.45) can still be shown to be strongly elliptic for small enough deformations, but it may lose strong ellipticity at sufficiently large values of deformation.

iv. In the limit of small deformations ($\overline{I}_1,\overline{I}_2 \to 3$), $\mu_0 = 2\Psi'_m(3) = \mu_m$ to leading order in $\overline{I}_1$ and the stored-energy function (4.45) reduces asymptotically to

$$\overline{\Psi}(\overline{I}_1,\overline{I}_2,c_p,c_i) = \overline{\mu}\,\mathrm{tr}\overline{\boldsymbol{\varepsilon}}^2 \tag{4.51}$$

to leading order in the deformation measure $\overline{\boldsymbol{\varepsilon}} = (\overline{\mathbf{F}} + \overline{\mathbf{F}}^T - 2\mathbf{I})/2$, where the effective shear modulus $\overline{\mu} = \overline{\mu}_0$ in (5.29) is defined implicitly by the remaining equation

$$\mathcal{F}_1\{\overline{\mu},\mu_m\} = 0. \tag{4.52}$$

In general, equation (4.52) does not admit an explicit solution and thus $\overline{\mu}$ must be evaluated numerically. In this regard, it is useful to deduce

that $\overline{\mu}$ is strictly positive, bounded from below by

$$\overline{\mu} \geq \begin{cases} \mu_m + \dfrac{5[(3c_p - 2c_i)\mu_m + 2(c_p + c_i)\mu_i]\mu_m}{2[3(1-c_p) + 2c_i]\mu_m + 4(1 - c_p - c_i)\mu_i} & \text{if} \quad \mu_i \geq \mu_m \\ \mu_m + \dfrac{(2\mu_m + 3\mu_i)[5c_p\mu_i + 2c_i(\mu_i - \mu_m)]}{2[5(1-c_p) - 2c_i]\mu_i + 4c_i\mu_m} & \text{if} \quad \mu_i < \mu_m \end{cases}, \tag{4.53}$$

and from above by

$$\overline{\mu} \leq \frac{\mu_m}{(1 - c_p - c_i)^{5/2}} \tag{4.54}$$

for any choice of shear moduli μ_m, $\mu_i > 0$ and any choice of concentrations $c_p, c_i \geq 0$ with $c_p + c_i \leq 1$. Further, in the dilute limit as $c_p, c_i \to 0+$,

$$\overline{\mu} = \overline{\mu}^{\,\mathrm{dil}} = \mu_m + \frac{5\,\mu_m}{2}\,c_p + \frac{5(\mu_i - \mu_m)\,(q_1\mu_i + q_4\mu_m)\,\mu_m}{2(q_1\mu_i^2 + q_2\,\mu_i\mu_m + q_3\mu_m^2)}\,c_i \tag{4.55}$$

to $O(1)$ in the concentration of particles c_p and interphases c_i.

The result (4.52) for $\overline{\mu}$ constitutes a generalization of the classical result of Brinkman-Roscoe (Roscoe, 1973) for the effective shear modulus of a suspension of polydisperse rigid spherical particles in rubber with perfect bonding (i.e., without interphases) between the particles and the rubber. Indeed, in the absence of interphases when $c_i = 0$, equation (4.52) can be solved explicitly to render identically the well-known formula

$$\overline{\mu} = \frac{\mu_m}{(1 - c_p)^{5/2}}. \tag{4.56}$$

v. The connection with the effective shear modulus $\overline{\mu}$ for isotropic distributions of polydisperse rigid spherical particles bonded through interphases as defined by equation (4.52) is not restricted to small deformations. Indeed, for the special case when the underlying matrix material is a Gaussian elastomer, $\Psi_m = \mu_m/2[I_1 - 3]$, $\mu_0 = \mu_m$, and the effective stored-energy function (4.45) reduces to

$$\overline{\Psi}(\overline{I}_1, \overline{I}_2, c_p, c_i) = \frac{\overline{\mu}}{2}\left[\,\overline{I}_1 - 3\right], \tag{4.57}$$

which is seen to have the same functional form as the Gaussian matrix material, with the effective shear modulus $\overline{\mu}$ defined by (4.52).

While exact and realizable in the limit of small deformations, for arbitrarily large deformations the effective stored-energy function (4.57) is *not* an exact realizable result for Gaussian elastomers filled with an isotropic distribution of rigid spherical particles of polydisperse sizes bonded through Gaussian interphases. Owing to its iterative construction process (see Section 4.3.1), however, it is expected to provide a very accurate approximation for this class of material systems. By the same token, the approximate effective stored-energy function (4.45) is also expected to describe very accurately the response of any such type of filled elastomer when the underlying matrix is a non-Gaussian elastomer, especially in the small and moderate deformation regimes. For large deformations, the result (4.45) is likely to be relatively less accurate for this class of material systems, as its variational construction process (see Section 4.3.2) entails that it corresponds to some sort of lower (upper) bound when the underlying matrix material has stronger (weaker) growth conditions than a Gaussian elastomer. These expectations are supported by comparisons with the FE simulations presented in Section 4.5.

vi. In the absence of interphases when $c_i = 0$, equations (4.47) admit the explicit solution $\overline{\mu}_0 = \mu_0/(1-c_p)^{5/2}$, $\mu_0 = 2\Psi'_m\left([\overline{I}_1 - 3]/(1-c_p)^{7/2} + 3\right)$, and the effective stored-energy function (4.45) reduces to the result of Lopez-Pamies et al. (2013a) for the effective stored-energy function of a suspension of polydisperse rigid spherical particles in rubber with perfect bonding between the particles and the rubber, namely,

$$\overline{\Psi}(\overline{I}_1, \overline{I}_2, c_p, 0) = (1-c_p)\Psi_m\left(\frac{\overline{I}_1 - 3}{(1-c_p)^{7/2}} + 3\right). \tag{4.58}$$

vii. In the limit of rigid interphases when $\mu_i = +\infty$, equations (4.47) similarly admit the explicit solution $\overline{\mu}_0 = \mu_0/(1-c_p-c_i)^{5/2}$, $\mu_0 = 2\Psi'_m\left([\overline{I}_1 - 3]/(1-c_p-c_i)^{7/2} + 3\right)$, and the effective stored-energy function (4.45) reduces to

$$\overline{\Psi}(\overline{I}_1, \overline{I}_2, c_p, c_i) = (1-c_p-c_i)\Psi_m\left(\frac{\overline{I}_1 - 3}{(1-c_p-c_i)^{7/2}} + 3\right). \tag{4.59}$$

This result also agrees with the effective stored-energy function of Lopez-

Pamies et al. (2013a) for a suspension of polydisperse rigid spherical particles in rubber with perfect bonding between the particles and the rubber, since in this limiting case there are actually no interphases but instead a distribution of rigid particles with total concentration $c_p + c_i$.

4.4 FE simulations of filled elastomers undergoing large deformations

With the aim of gaining further insight, in Section 4.5 we confront the above-developed theoretical results to full 3D FE simulations of the large-deformation response of Gaussian and non-Gaussian elastomers filled by random isotropic distributions of rigid spherical particles that are bonded through constant-thickness interphases. In particular, following common practice (see, e.g., Gusev, 1997; Michel et al., 1999), we consider infinite periodic media made up of the repetition of unit cells that contain a random distribution of a large but *finite* number of particles, as dictated by a sequential adsorption algorithm. In order to probe the effect that particle polydispersity plays on the overall response of filled elastomers with interphases[3], we consider distributions with both, particles of the same (monodisperse) size and particles of different (polydisperse) sizes. The details of the simulations are as follows.

4.4.1 Monodisperse microstructures

The monodisperse microstructures are constructed using a random sequential adsorption algorithm in which the sequential addition of spherical particles, of the same radius r with surrounding interphases of the same constant thickness t, is constrained so that the distance between a given interphase with other interphases and with the boundaries of the unit cell — chosen here to be a cube of unit side $L = 1$ — take a minimum value that allows for an adequate spatial discretization (see, e.g., Segurado and Llorca, 2002; Lopez-Pamies et al., 2013a), namely:

[3]In the absence of interphases, Lopez-Pamies et al. (2013a) have shown that the effect of polydispersity, rather remarkably, is negligible up to relative large concentrations of particles in the order of $c_p = 0.3$.

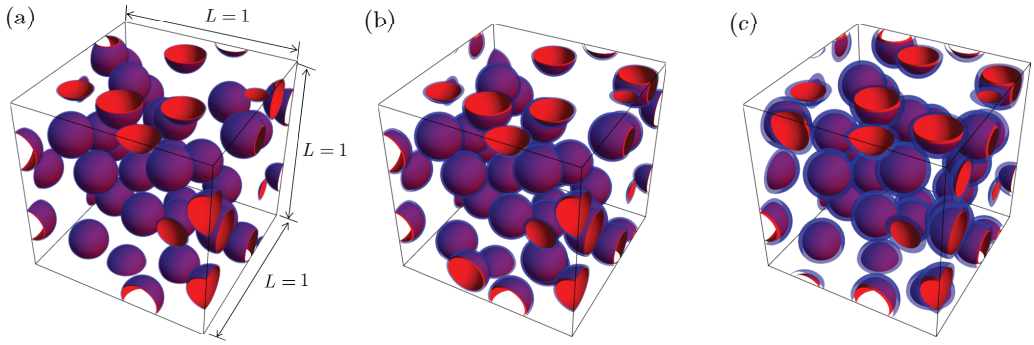

Figure 4.11: Representative unit cells containing a random distribution of $N = 30$ monodisperse spherical particles of radius r at concentration $c_p = 0.15$ that are surrounded by interphases of three different constant thicknesses t: (a) $t = 0.05\,r$, (b) $t = 0.1\,r$, and (c) $t = 0.2\,r$.

- The center-to-center distance between a new particle i and any previously accepted one $j = 1, 2, ..., i-1$ has to exceed the minimum value $s_1 = 2(r + t)(1 + d_1)$, where the offset distance d_1 is fixed here at $d_1 \geq 0.03$. The condition to be checked at each step of the algorithm takes then the form

$$||\mathbf{X}^i - \mathbf{X}^j - \mathbf{h}|| \geq s_1 \tag{4.60}$$

  where $\mathbf{X}^i(\mathbf{X}^j)$ denotes the location of the center of particle $i(j)$ and $\mathbf{h}$ is a vector with entries 0, L, or $-L$ for each of its three Cartesian components with respect to the principal axes of the cubic unit cell.

- The outermost surface of any interphase should be sufficiently distant from the boundaries of the unit cell as enforced by the inequalities

$$|X^i_\alpha - r - t| \geq s_2 \quad \text{and} \quad |X^i_\alpha + r + t - L| \geq s_2 \quad (\alpha = 1, 2, 3), \tag{4.61}$$

  where $s_2 = d_2(r + t)$ with d_2 being fixed here at 0.05.

For this class of monodisperse microstructures, we note that the radius r of the particles and the thickness t of the surrounding interphases are related to the total number of particles N, particle concentration c_p, and interphase concentration c_i via

$$r = L\left(\frac{3c_p}{4\pi N}\right)^{1/3} \qquad \text{and} \qquad \frac{t}{r} = \left(1 + \frac{c_i}{c_p}\right)^{1/3} - 1. \tag{4.62}$$

Previous results based on this approach — for linear (Segurado and Llorca, 2002) as well as for nonlinear (Lopez-Pamies et al., 2013a) problems — have indicated that $N = 30$ particles is, in general, sufficient to approximate isotropic symmetry. Figure 4.11 depicts representative examples of such unit cells with $N = 30$ particles at concentration $c_p = 0.15$ for three different interphase thicknesses t: (a) $t = 0.05\,r$, (b) $t = 0.1\,r$, and (c) $t = 0.2\,r$.

4.4.2 Polydisperse microstructures

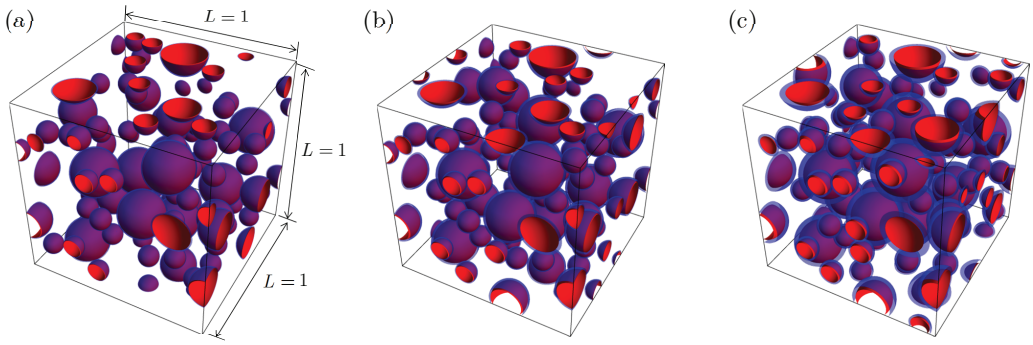

Figure 4.12: Representative unit cells containing a random distribution of $N = 80$ spherical particles of three different radii at concentration $c_p = 0.15$ that are surrounded by interphases with three different constant thickness-to-particle-radius ratios: (a) $t/r = 0.05$, (b) $t/r = 0.1$, and (c) $t/r = 0.2$.

The polydisperse microstructures are constructed by means of a similar constrained adsorption algorithm. The focus is on polydisperse microstructures with three different families of particle sizes such that — consistent with the assumptions made in the derivation of the theoretical results of Section 4.3 — the interphase-thickness-to-particle-radius ratio is the same for all particles. While there is no distinct rule for the creation of such microstructures and the possibilities are many, we consider for definiteness the following procedure:

- Three different families of spherical particles with radii $r^{(I)}$ and respective concentrations $c_p^{(I)}$ $(I = 1, 2, 3)$, surrounded by interphases with thicknesses $t^{(I)}$ and respective concentrations $c_i^{(I)}$ $(I = 1, 2, 3)$, are uti-

lized such that

$$\left\{r^{(1)}, r^{(2)}, r^{(3)}\right\} = \left\{r, \frac{7}{9}r, \frac{4}{9}r\right\} \quad \text{with} \quad r = L\left(\frac{3\,c_p^{(1)}}{4\pi N^{(1)}}\right)^{1/3}, \tag{4.63}$$

$$\left\{c_p^{(1)}, c_p^{(2)}, c_p^{(3)}\right\} = \{0.5\,c_p, 0.25\,c_p, 0.25\,c_p\} \quad \text{with} \quad c_p^{(1)} + c_p^{(2)} + c_p^{(3)} = c_p, \tag{4.64}$$

$$\left\{\frac{t^{(1)}}{r^{(1)}}, \frac{t^{(2)}}{r^{(2)}}, \frac{t^{(3)}}{r^{(3)}}\right\} = \left\{\frac{t}{r}, \frac{t}{r}, \frac{t}{r}\right\} \quad \text{with} \quad \frac{t}{r} = \left(1 + \frac{c_i^{(1)}}{c_p^{(1)}}\right)^{1/3} - 1, \tag{4.65}$$

where $N^{(1)}$ is the number of particles with the largest radius and thickest surrounding interphase, $r^{(1)} = r$ and $t^{(1)} = t$, in the unit cell.

- The microstructures are generated sequentially by first adding the particles with the largest radius $r^{(1)} = r$ and desired thickness $t^{(1)} = t$, until the particle concentration reaches the value $c_p^{(1)} = 0.5c_p$, subsequently adding particles with radius $r^{(2)}$ and surrounding interphases of thickness $t^{(2)} = r^{(2)}t/r$ until $c_p^{(1)} + c_p^{(2)} \approx 0.75c_p$, and finally adding particles with the smallest radius $r^{(3)}$ and smallest interphase thickness $t^{(3)} = r^{(3)}t/r$ until $c_p^{(1)} + c_p^{(2)} + c_p^{(3)} \approx c_p$. In following this construction process, we note that a target concentration c_p (similarly for a target concentration c_i if preferred over a target ratio t/r) can only be achieved approximately up to a small error that depends on the various choices of the parameters. To guarantee adequate spatial discretization, the randomly generated placements of the centers of the particles are enforced to satisfy constraints analogous to those enforced for the case of monodisperse microstructures, cf. inequalities (4.60) and (4.61).

In this chapter we utilize $N^{(1)} = 10$ which results into unit cells containing a total of $N = 80$ particles that prove to be sufficiently isotropic for our purposes. Figure 4.12 depicts representative examples of such unit cells with $N = 80$ particles of three different radii at concentration $c_p = 0.15$ for three different interphase-thickness-to-particle-radius ratios: (a) $t/r = 0.05$, (b) $t/r = 0.1$, and (c) $t/r = 0.2$.

4.4.3 Spatial discretization, particle material behavior, and computation of the overall response

The discretizations of the microstructures are carried out by means of the mesh generator code Netgen (Schöberl, 1997). Hybrid isoparametric 10-node quadratic tetrahedral elements with linearly varying pressure proved to deliver accurate results, and thus were selected to carry out the calculations. Figure 4.13 displays three representative meshes of increasing refinement for a monodisperse microstructure with concentrations of particles $c_p = 0.15$ and interphases $c_i = 0.1$. Mesh sensitivity analyses revealed that meshes containing about 150,000 elements, such as the one shown in Fig. 4.13(c), are refined enough to deliver accurate results for all the cases considered here.

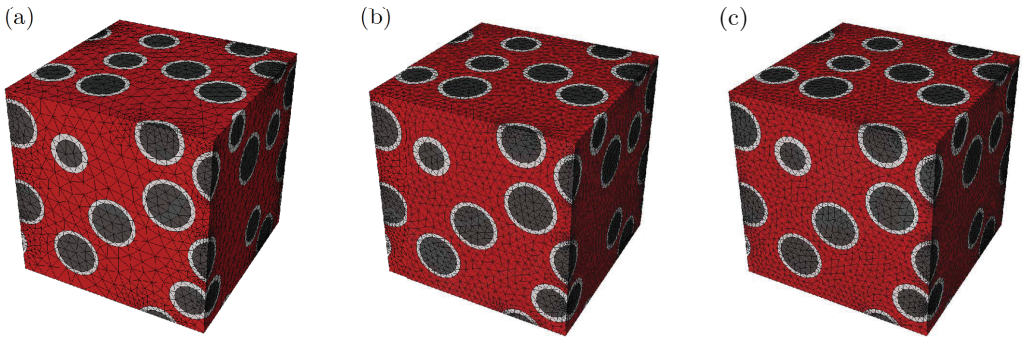

Figure 4.13: Three representative meshes in the undeformed configuration for a distribution of monodisperse particles with concentration $c_p = 0.15$ and interphase concentration $c_i = 0.1$: (a) coarse mesh with about $50,000$ elements, (b) fine mesh with about $100,000$ elements, and (c) very fine mesh with about $150,000$ elements.

Within the utilized formulation, the perfectly rigid behavior (4.2) of the particles can only be modeled approximately by means of a very (but not infinitely) stiff material. Here, for definiteness, we model the particles as a Gaussian elastomer with stored-energy function

$$W_p^{FE}(\mathbf{F}) = \begin{cases} \dfrac{\mu_p^{FE}}{2}\,[I_1 - 3] & \text{if} \quad J = 1 \\ +\infty & \text{otherwise} \end{cases}, \tag{4.66}$$

where the parameter μ_p^{FE} is set to be four orders of magnitude larger than the shear modulus of the underlying matrix material, i.e., $\mu_p^{FE} = 10^4 \times \mu_m$.

By virtue of their periodicity, the computation of the effective stored-energy function (4.7) for any of the above-defined classes of filled elastomers

amounts to subjecting their defining cubic unit cells to the periodic boundary conditions

$$
\begin{aligned}
u_\alpha(0, X_2, X_3) - u_\alpha(L, X_2, X_3) &= (\overline{F}_{\alpha 1} - \delta_{\alpha 1})L, \\
u_\alpha(X_1, 0, X_3) - u_\alpha(X_1, L, X_3) &= (\overline{F}_{\alpha 2} - \delta_{\alpha 2})L, \\
u_\alpha(X_1, X_2, 0) - u_\alpha(X_1, X_2, L) &= (\overline{F}_{\alpha 3} - \delta_{\alpha 3})L
\end{aligned}
\tag{4.67}
$$

($\alpha = 1, 2, 3$) in terms of the displacement field $\mathbf{u} = \mathbf{x} - \mathbf{X}$, and computing the resulting total elastic energy per unit undeformed volume of the unit cell. In expression (4.67), the components u_α and X_α ($\alpha = 1, 2, 3$) refer to a Cartesian frame of reference with origin placed at a corner of the cubic unit cell whose axes $\{\mathbf{e}_\alpha\}$ are aligned with the principal axes of the cubic unit cell (see Fig. 4.13), and $\delta_{\alpha\beta}$ denotes the Kronecker delta.

4.4.4 Assessment of the simulations

Because of the finite number of particles — $N = 30$ for the monodisperse and $N = 80$ for the polydisperse microstructures — included per unit cell, the microstructures simulated here are (not exactly but) only approximately isotropic. In order to assess the isotropy of each realization that is constructed, we examine the co-axiallity between the average Cauchy stress tensor $\overline{\mathbf{T}} \doteq \overline{\mathbf{S}}\,\overline{\mathbf{F}}^T$ and the average left Green-Cauchy strain tensor $\overline{\mathbf{B}} \doteq \overline{\mathbf{F}}\,\overline{\mathbf{F}}^T$ under three types of loading conditions: (*i*) axisymmetric tension where $\overline{\mathbf{F}} = \overline{\lambda}\,\mathbf{e}_1 \otimes \mathbf{e}_1 + \overline{\lambda}^{-1/2}(\mathbf{e}_2 \otimes \mathbf{e}_2 + \mathbf{e}_3 \otimes \mathbf{e}_3)$ with $\overline{\lambda} \geq 1$, (*ii*) axisymmetric compression where $\overline{\mathbf{F}} = \overline{\lambda}\,\mathbf{e}_1 \otimes \mathbf{e}_1 + \overline{\lambda}^{-1/2}(\mathbf{e}_2 \otimes \mathbf{e}_2 + \mathbf{e}_3 \otimes \mathbf{e}_3)$ with $\overline{\lambda} \leq 1$, and (*iii*) simple shear where $\overline{\mathbf{F}} = \mathbf{I} + \overline{\gamma}\,\mathbf{e}_1 \otimes \mathbf{e}_2$ with $\overline{\gamma} \geq 0$. Only microstructures for which the maximum difference between any two corresponding principal axes of $\overline{\mathbf{T}}$ and $\overline{\mathbf{B}}$ is less than 0.05 radians for all three loadings are admitted as approximately isotropic.

All FE results to be presented in the next section correspond to the average of three different realizations, all of which are approximately isotropic in the sense described in the preceding paragraph. The computations are carried out in the commercial code ABAQUS by following an incremental loading path. We utilize the default dual convergence criterion in this code (see Abaqus version 6.11 documentation), namely, the permissible ratio of

the largest solution correction to the largest corresponding incremental solution is set at $|\Delta\mathbf{u}|/|\mathbf{u}_{max}| = 10^{-2}$, while the permissible ratio of the largest residual to the corresponding average force norm is set at $R_{tol} = 5 \times 10^{-3}$. Whenever one of these criteria is not satisfied the computations are stopped. This typically happens whenever the elements in between two adjacent interphases become exceedingly distorted because of the locally large deformations involved.

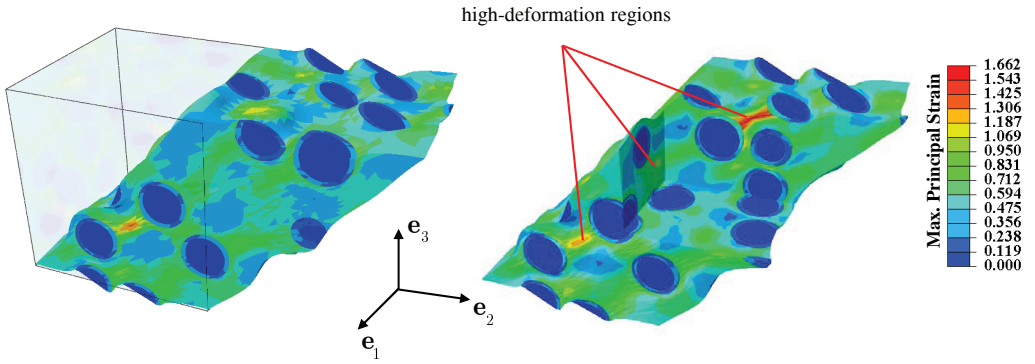

Figure 4.14: Contour plots of the maximum principal logarithmic strain for a monodisperse realization with $c_p = 0.15$, $c_i = 0.05$, Gaussian elastomeric matrix with shear modulus $\mu_m = 1$ MPa, and $\mu_i = 5$ MPa subjected to a macroscopic simple shear strain of $\overline{\gamma} = 0.91$; the undeformed configuration is also depicted for comparison purposes. Part (b) shows an inside view of three pairs of particles/interphases in between which the matrix material is highly deformed.

Figure 4.14 presents an example of large local deformations in between interphases for the case of a monodisperse realization with $c_p = 0.15$, $c_i = 0.05$, Gaussian elastomeric matrix with shear modulus $\mu_m = 1$ MPa, and $\mu_i = 5$ MPa under simple shear. Part (a) shows contour plots of the maximum principal logarithmic strain at an overall shear strain level of $\overline{\gamma} = 0.91$; the initial undeformed geometry is also depicted for comparison purposes. The deformation contours are seen to be highly heterogeneous with principal logarithmic strains as large as 1.66 within regions between interphases. In part (b), an inside view is shown of three regions of strong particle/interphase interaction and high local strains that lead to significant mesh distortion and therefore problems with the numerical convergence of the FE calculations. In principle, re-meshing of these regions should allow to reach further overall deformations, but this is not pursued here.

4.5 Sample results and comparisons with FE simulations

Sample results are now presented that provide quantitative insight into the proposed theoretical result (4.45) and that, at the same time, serve to reveal the importance of the various microscopic quantities (the concentration of the particles c_p, the concentration of the interphases c_i, the nonlinear elastic behavior of the matrix Ψ_m, and the stiffness of the interphases μ_i) on the macroscopic response of filled elastomers. We begin in Section 4.5.1 by presenting results for the linear elastic response of filled elastomers in the small-deformation regime. These are followed in Section 4.5.2 by results for the large-deformation response of filled Gaussian elastomers. Finally, in Section 4.5.3 we present results for a filled elastomer wherein the matrix is characterized by the non-Gaussian stored-energy function

$$\Psi_m(I_1) = \frac{3^{1-\alpha_1}}{2\alpha_1}\mu_1\left[I_1^{\alpha_1} - 3^{\alpha_1}\right] + \frac{3^{1-\alpha_2}}{2\alpha_2}\mu_2\left[I_1^{\alpha_2} - 3^{\alpha_2}\right] \tag{4.68}$$

with $\mu_1 = 0.032$ MPa, $\mu_2 = 0.3$ MPa, $\alpha_1 = 3.837$, $\alpha_2 = 0.559$, corresponding to a model that describes accurately the nonlinear elastic response of a standard silicone rubber over large ranges of deformations (Lopez-Pamies, 2010b).

4.5.1 Linear elastic results

In the limit of small deformations (see remark (i) in Section 4.3.2), the effective stored-energy function (4.45) reduces to (5.29) and hence is completely characterized by the effective shear modulus $\overline{\mu}$ defined by equation (4.52). Figure 4.15 shows results for the normalized effective shear modulus $\overline{\mu}/\mu_m$ for various values of the interphase-thickness-to-particle-radius ratio[4] t/r and interphase stiffness μ_i/μ_m, all as functions of the concentration of particles c_p. Results are also presented for the FE simulations described in Section 4.4 for monodisperse (Figs. 4.15(a) and (c)) and polydisperse (Figs. 4.15(b) and (d)) microstructures.

As expected, an immediate observation from Fig. 4.15 is that the addition

[4]Throughout this section, we shall favor writing the content of interphases in terms of the ratio $t/r = (1 + c_i/c_p)^{1/3} - 1$, instead of directly in terms of their concentration c_i.

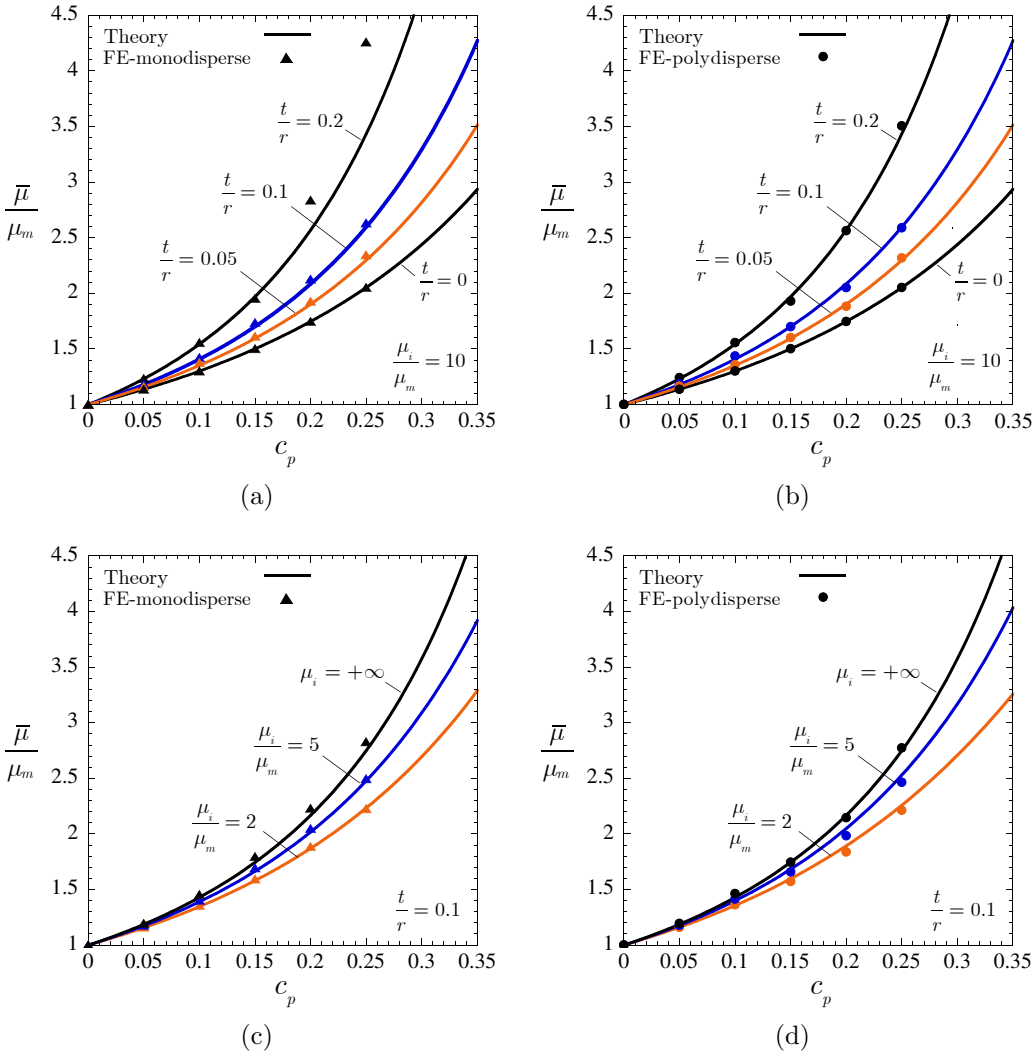

Figure 4.15: The normalized effective shear modulus $\overline{\mu}/\mu_m$ of an isotropic incompressible elastomer, with shear modulus μ_m, filled with an isotropic distribution of rigid spherical particles bonded through isotropic incompressible interphases with various shear moduli μ_i/μ_m and constant thickness-to-particle-radius ratios t/r. Results are shown for the theoretical result (4.52) compared to FE simulations for distributions of (a, c) monodisperse and (b, d) polydisperse particles, all as functions of the concentration of particles c_p.

of rigid particles increases significantly the overall stiffness of elastomers. Remarkably, the presence of interphases (with $\mu_i > \mu_m$) is seen to also have a *comparable* stiffening effect. We note that the stiffening granted by the interphases is highly more sensitive to the value of their thickness t/r than to the value of their stiffness μ_i/μ_m. Indeed, Figs. 4.15(c) and (d) show that interphases that are just 5 times stiffer than the matrix ($\mu_i/\mu_m = 5$) already grant an increase in overall stiffness that is similar to that granted by rigid

interphases ($\mu_i = +\infty$). On the other hand, Figs. 4.15(a) and (b) show that moderate increases in the thickness of the interphases from $t/r = 0.05$, to $t/r = 0.1$, to $t/r = 0.2$, consistently lead to larger enhancements of the overall stiffness. The practical implications of these results are far reaching as they suggest that when dealing with conventional filled elastomers — where interphases are typically in the order of 10 times stiffer than the matrix material (see, e.g., Qu et al., 2011) — their macroscopic response is by and large unaffected by the constitutive complexity of the underlying interphases (in terms of heterogeneity, anisotropy, and non-linearity) and *de facto* simply dependent on their average stiffness and size.

While the effective shear modulus $\overline{\mu}$ defined by equation (4.52) is exact for infinitely polydisperse particles, Figs. 4.15(b) and (d) show it to be in good agreement with the FE results for microstructures with only three families of particle sizes for the entire range of particle concentrations and interphase thicknesses considered, $c_p \in [0, 0.25]$ and $t/r \in [0, 0.2]$. More remarkably, Figs. 4.15(b) and (d) show the theoretical effective shear modulus to also be in good agreement with the FE results for monodisperse particles up to the relatively high particle concentration $c_p = 0.2$ with relatively large interphase thickness $t/r = 0.2$. Consistent with earlier results for suspensions of particles in rubber without interphases (Lopez-Pamies et al., 2013a), these favorable comparisons suggest that polydispersity does *not* play a role in the response of filled elastomers for particle concentrations and interphase thicknesses sufficiently below the percolation limit.

4.5.2 Results for filled Gaussian elastomers

Figure 4.16 presents results for the large-deformation response of a filled Gaussian elastomer with particle concentration $c_p = 0.15$ under: (a) uniaxial compression, (b) uniaxial tension, (c) pure shear, and (d) simple shear. The constitutive stress-deformation relations for these loading conditions read as (see remark (*ii*) in Section 4.3.2)

- *Uniaxial loading* ($\overline{\lambda}_1 = \overline{\lambda}$, $\overline{\lambda}_2 = \overline{\lambda}_3 = \overline{\lambda}^{-1/2}$ with $\overline{\tau}_2 = \overline{\tau}_3 = 0$):

$$\overline{S}_{un} = \overline{\lambda}^{-1}\overline{\tau}_1 = \frac{\mathrm{d}\overline{\Psi}}{\mathrm{d}\overline{\lambda}} = \overline{\mu}\left[\overline{\lambda} - \overline{\lambda}^{-2}\right] \tag{4.69}$$

- *Pure shear* ($\overline{\lambda}_1 = \overline{\lambda}$, $\overline{\lambda}_2 = \overline{\lambda}^{-1}$, $\overline{\lambda}_3 = 1$ with $\overline{\tau}_2 = 0$):

$$\overline{S}_{ps} = \overline{\lambda}^{-1}\overline{\tau}_1 = \frac{\mathrm{d}\overline{\Psi}}{\mathrm{d}\overline{\lambda}} = \overline{\mu}\left[\overline{\lambda} - \overline{\lambda}^{-3}\right] \tag{4.70}$$

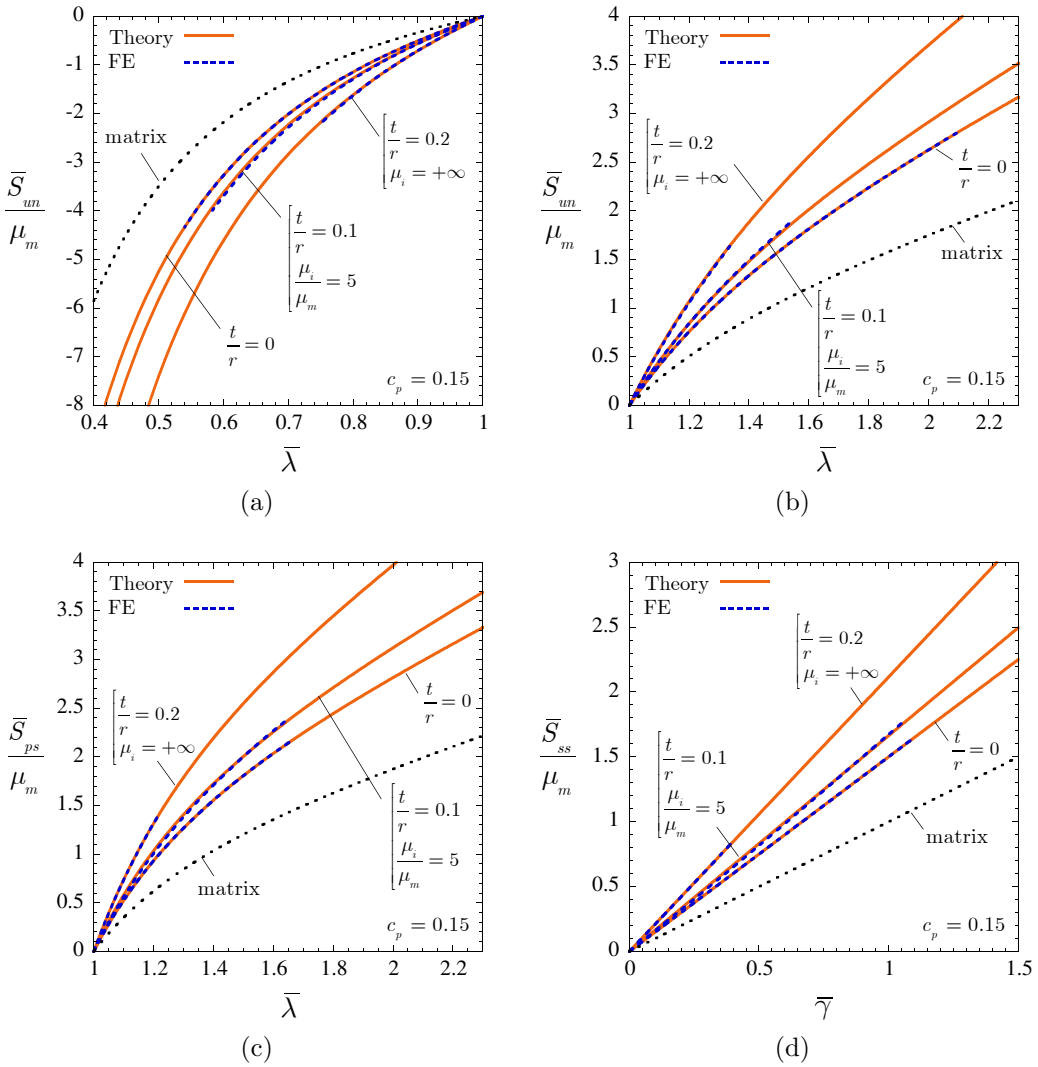

Figure 4.16: Macroscopic response of a filled Gaussian elastomer with particle concentration $c_p = 0.15$ under: (a) uniaxial compressive, (b) uniaxial tensile, (c) pure shear, and (d) simple shear loading conditions, as characterized by the proposed theory, *cf.* expressions (4.69), (4.70), (4.71). Results are shown for three different types of interphases: (*i*) no interphases $t/r = 0$, (*ii*) interphases with moderate shear modulus $\mu_i/\mu_m = 5$ and moderate thickness $t/r = 0.1$, and (*iii*) rigid interphases $\mu_i = +\infty$ with relatively large thickness $t/r = 0.2$. The dashed lines in the plots correspond to results from the FE simulations, while the dotted lines correspond to the response of the unfilled Gaussian elastomer.

- *Simple shear* ($\overline{\lambda}_1 = (\overline{\gamma} + \sqrt{\overline{\gamma}^2 + 4})/2$, $\overline{\lambda}_2 = \overline{\lambda}_1^{-1}$, $\overline{\lambda}_3 = 1$):

$$\overline{S}_{ss} = \frac{\mathrm{d}\overline{\Psi}}{\mathrm{d}\overline{\gamma}} = \overline{\mu}\,\overline{\gamma} \tag{4.71}$$

where $\overline{S}_{un}$, $\overline{S}_{ps}$, $\overline{S}_{ss}$ denote first Piola-Kirchhoff stress measures, $\overline{\tau}_1$, $\overline{\tau}_2$, $\overline{\tau}_3$ have been introduced to denote the macroscopic principal Cauchy stresses, and, again, the effective shear modulus $\overline{\mu}$ is implicitly defined by equation (4.52). Three different types of interphases are considered: (*i*) no interphases $t/r = 0$, (*ii*) interphases with moderate shear modulus $\mu_i/\mu_m = 5$ and moderate thickness $t/r = 0.1$, and (*iii*) rigid interphases $\mu_i = +\infty$ with relatively large thickness $t/r = 0.2$. Corresponding FE results are included in the figure for comparison purposes. No distinction is made of whether the particles are monodisperse or polydisperse since, somewhat remarkably, both classes of simulated microstructures exhibit essentially the same large-deformation response. This is consistent with the linear elastic results of Fig. 4.15, where the monodisperse and polydisperse FE simulations render practically identical effective shear moduli for particle concentrations below $c_p = 0.2$ with interphase-thickness-to-particle-radius ratios below $t/r = 0.2$.

It is plain from Fig. 4.16 that the overall large-deformation response of the Gaussian elastomer is stiffened significantly by the addition of rigid particles for all loading conditions. The figure also makes it plain that the presence of interphases (with $\mu_i > \mu_m$) produces levels of stiffness enhancement that are comparable to those produced by the particles themselves. As it was the case for small deformations, the increase in stiffness generated by the interphases is more dependent on their thickness t/r than on their stiffness μ_i/μ_m. Another important observation from Fig. 4.16 is that the theoretical predictions and FE results are in good qualitative and quantitative agreement for all loading conditions.

To further probe the connections between the proposed theory and the FE simulations, Fig. 4.17 compares their elastic energies $\overline{\Psi}/\mu_m$, normalized by the initial shear modulus μ_m of the underlying Gaussian matrix, as functions of the principal invariants $\overline{I}_1$ and $\overline{I}_2$. Part (a) of the figure shows $\overline{\Psi}/\mu_m$ for fixed values of the second invariant $\overline{I}_2 = 3.32$ for $c_p = 0.15$ and $\overline{I}_2 = 4.40$ for $c_p = 0.05$ as functions of $\overline{I}_1$, while part (b) shows results for fixed values of the first invariant $\overline{I}_1 = 3.40, 3.82$ for $c_p = 0.15$ and $\overline{I}_1 = 4.80, 5.13$ for

$c_p = 0.05$ as functions of $\overline{I}_2$.

The main observation from Fig. 4.17 is that the FE results are approximately linear in the first invariant $\overline{I}_1$ and independent of the second invariant $\overline{I}_2$. This behavior is in accordance with that of the theory, corroborating that both results are very much identical in their functional form. The fact that the macroscopic behavior of filled Gaussian elastomers is functionally the same — i.e., linear in $\overline{I}_1$ and independent of $\overline{I}_2$ — as that of its underlying Gaussian matrix is of note. Indeed, as already mentioned in the discussion of Fig. 4.7, the functional character of the average behavior of nonlinear material systems is in general substantially different from that of its constituents, but that is not the case here.

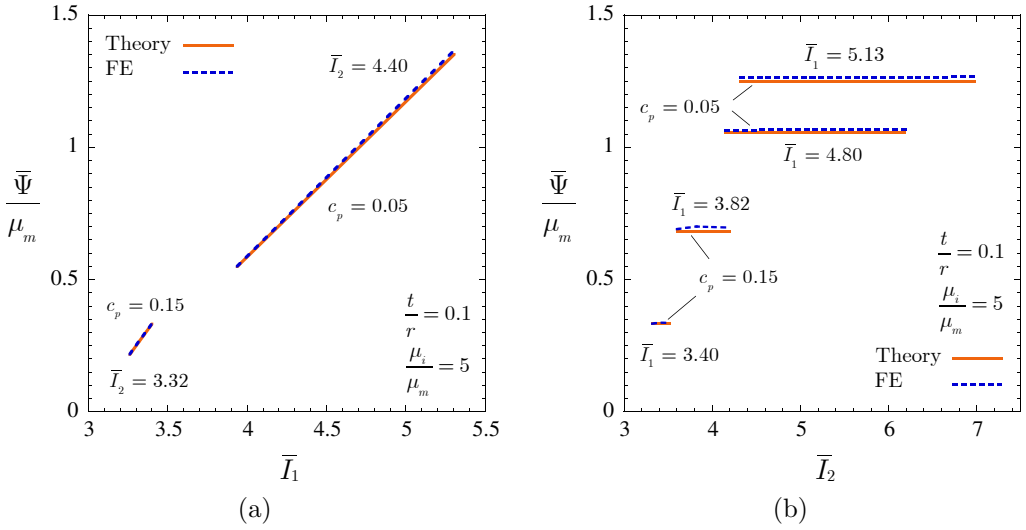

Figure 4.17: Comparison of the effective stored-energy function (4.57) for a filled Gaussian elastomer with corresponding FE simulations. The results are shown in terms of the principal invariants $\overline{I}_1$ and $\overline{I}_2$ for interphase-thickness-to-particle-radius ratio $t/r = 0.1$, interphase shear modulus $\mu_i/\mu_m = 5$, and two values of concentration of particles, $c_p = 0.05$ and 0.15. Part (a) shows results for fixed values of $\overline{I}_2$ as functions of $\overline{I}_1$, while part (b) shows results for fixed values of $\overline{I}_1$ as functions of $\overline{I}_2$.

4.5.3 Results for a filled silicone elastomer

Finally, Fig. 4.18 shows results for the large-deformation response of a filled non-Gaussian elastomer wherein the underlying matrix material is a typical silicone rubber characterized here by the stored-energy function (4.68) with

$\mu_1 = 0.032$ MPa, $\mu_2 = 0.3$ MPa, $\alpha_1 = 3.837$, $\alpha_2 = 0.559$, and thus initial shear modulus $\mu_m = \mu_1 + \mu_2 = 0.332$ MPa. In this case, the proposed

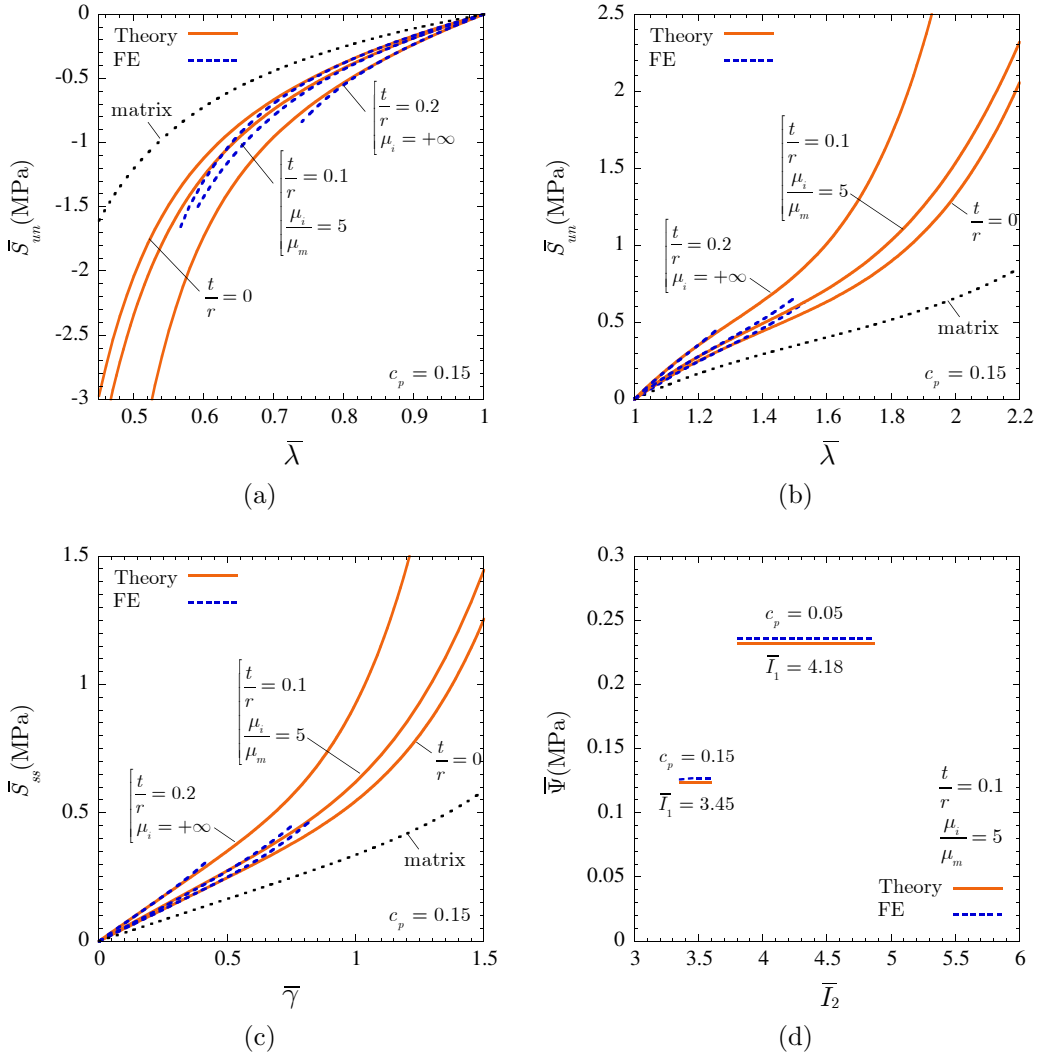

Figure 4.18: Macroscopic response of a filled silicone elastomer under: (a) uniaxial compressive, (b) uniaxial tensile, and (c) simple shear loading conditions. Plots are shown for the theoretical stress-deformation results (4.74), (4.75) with (4.72), and corresponding FE simulations for particle concentration $c_p = 0.15$ and three different types of interphases: (i) no interphases $t/r = 0$, (ii) interphases with moderate shear modulus $\mu_i/\mu_m = 5$ and moderate thickness $t/r = 0.1$, and (iii) rigid interphases $\mu_i = +\infty$ with relatively large thickness $t/r = 0.2$. Part (d) of the figure shows comparisons between the effective stored-energy function (4.72) and corresponding FE results for $t/r = 0.1$, $\mu_i/\mu_m = 5$, $c_p = 0.05, 0.15$ and two fixed values of the first principal invariant $\overline{I}_1$, in terms of the second invariant $\overline{I}_2$.

theoretical effective stored-energy function (4.45) specializes to

$$\overline{\Psi}(\overline{I}_1, \overline{I}_2, c_p, c_i) = (1 - c_p - c_i) \left[\frac{3^{1-\alpha_1}}{2\alpha_1} \mu_1 \left[\mathcal{I}_1^{\alpha_1} - 3^{\alpha_1} \right] + \frac{3^{1-\alpha_2}}{2\alpha_2} \mu_2 \left[\mathcal{I}_1^{\alpha_2} - 3^{\alpha_2} \right] \right] + \frac{\overline{\mu}_0}{2} [\overline{I}_1 - 3] - (1 - c_p - c_i) \frac{\mu_0}{2} \left[\mathcal{I}_1 - 3 \right], \tag{4.72}$$

where $\mathcal{I}_1$ is explicitly given by expression (4.46) in terms of c_p, c_i, $\overline{I}_1$, and the variables $\overline{\mu}_0$, μ_0, which are defined implicitly by the system of two coupled nonlinear algebraic equations

$$\mathcal{F}_1\{\overline{\mu}_0, \mu_0\} = 0, \qquad \mathcal{F}_2\{\overline{\mu}_0, \mu_0\} = \frac{3^{1-\alpha_1}}{2} \mu_1 \mathcal{I}_1^{\alpha_1 - 1} + \frac{3^{1-\alpha_2}}{2} \mu_2 \mathcal{I}_1^{\alpha_2 - 1} - \frac{\mu_0}{2} = 0; \tag{4.73}$$

recall that the function $\mathcal{F}_1$ is defined by expression (4.38).

Parts (a), (b), and (c) of Fig. 4.18 show stress-deformation results for uniaxial compression, uniaxial tension, and simple shear for particle concentration $c_p = 0.15$ and three different types of interphases: (i) no interphases $t/r = 0$, (ii) interphases with moderate shear modulus $\mu_i/\mu_m = 5$ and moderate thickness $t/r = 0.1$, and (iii) rigid interphases $\mu_i = +\infty$ with relatively large thickness $t/r = 0.2$. The constitutive stress-deformation relations for the specified loadings are given by

- *Uniaxial loading* ($\overline{\lambda}_1 = \overline{\lambda}$, $\overline{\lambda}_2 = \overline{\lambda}_3 = \overline{\lambda}^{-1/2}$ with $\overline{\tau}_2 = \overline{\tau}_3 = 0$):

$$\overline{S}_{un} = \overline{\lambda}^{-1} \overline{\tau}_1 = \frac{\mathrm{d}\overline{\Psi}}{\mathrm{d}\overline{\lambda}} = \overline{\mu}_0 \left[\overline{\lambda} - \overline{\lambda}^{-2} \right] \tag{4.74}$$

- *Simple shear* ($\overline{\lambda}_1 = (\overline{\gamma} + \sqrt{\overline{\gamma}^2 + 4})/2$, $\overline{\lambda}_2 = \overline{\lambda}_1^{-1}$, $\overline{\lambda}_3 = 1$):

$$\overline{S}_{ss} = \frac{\mathrm{d}\overline{\Psi}}{\mathrm{d}\overline{\gamma}} = \overline{\mu}_0 \, \overline{\gamma} \tag{4.75}$$

where, as above, $\overline{S}_{un}$, $\overline{S}_{ss}$ denote first Piola-Kirchhoff stress measures, $\overline{\tau}_1$, $\overline{\tau}_2$, $\overline{\tau}_3$ stand for the macroscopic principal Cauchy stresses, and, again, the coefficient $\overline{\mu}_0$ is defined implicitly by the system of equations (4.73). Part (d) of Fig. 4.18 displays results for the effective stored-energy function (4.72) for fixed values of the first principal invariant $\overline{I}_1 = 3.42$ for $c_p = 0.15$ and $\overline{I}_1 = 4.62$ for $c_p = 0.05$, both for interphases with $t/r = 0.1$ and $\mu_i/\mu_m = 5$, in terms of the second invariant $\overline{I}_2$. All four parts of Fig. 4.18 include

corresponding FE results. Akin to the preceding Gaussian case, we make no distinction here of whether the particles are of the same or of different sizes since, again, the simulated monodisperse and polydisperse microstructures turn out to exhibit practically the same response for particle concentrations below $c_p = 0.2$ with interphase-thickness-to-particle-radius ratios below $t/r = 0.2$.

Similar to the foregoing, Figs. 4.18(a) through (c) illustrate that both the addition of particles as well as the presence of interphases have a profound stiffening effect for all deformations. They also show that the theoretical and FE results are in fairly good qualitative and quantitative agreement for all loading conditions, especially for small and moderate deformations. For large enough deformations at which the limiting chain extensibility of the silicone elastomer comes into effect, the analytical results are consistently softer — as expected from their variational construction process (see remark (*ii*) in Section 4.3.2) — than their FE counterparts. Fig. 4.18(d) shows that the FE results for the filled silicone elastomer, much like those for the filled Guassian elastomer, are approximately independent of the second macroscopic invariant $\overline{I}_2$, in functional accord with the proposed theory.

4.6 Comparisons with experimental data and final comments

In the sequel, we deploy the theoretical result (4.45) to scrutinize a series of representative experimental data available in the literature. The objective is to illustrate the use of the proposed theory and to showcase its ability not only to describe the macroscopic response of real filled elastomers but also, and more critically, to unveil how the various microscopic quantities individually contribute to such a macroscopic response.

We begin by considering the experimental data of Mullins and Mullins and Tobin (1965), Omnès et al. (2008) and Smallwood (1944) for the macroscopic response in the small-deformation regime of polyisoprene rubber reinforced with a random and isotropic distribution of carbon black particles. Specifically, Fig. 4.19(a) shows the effective initial shear modulus $\overline{\mu}$, normalized by the shear modulus of the underlying polyisoprene matrix μ_m, as a function of the concentration of carbon black c_p. The discrete symbols (empty circles,

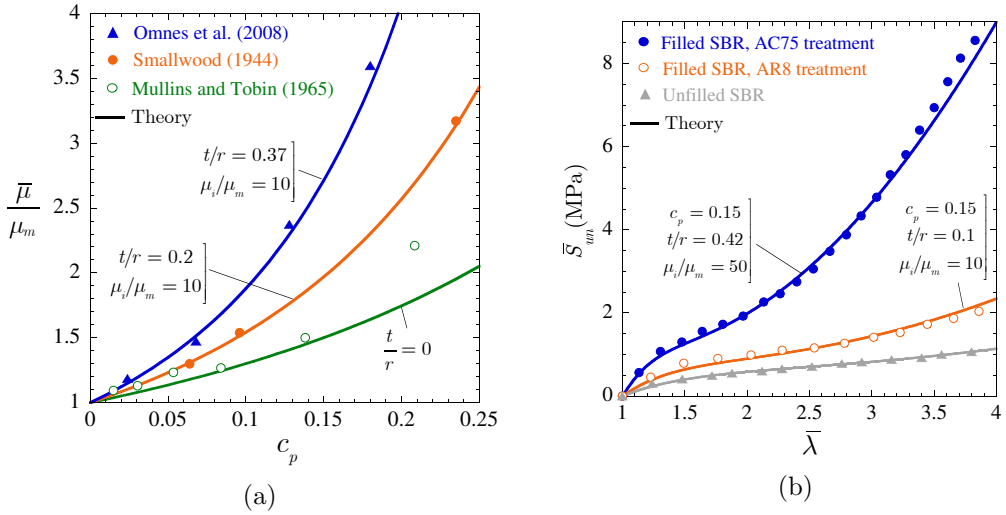

Figure 4.19: Comparisons of the proposed theory with experimental data. Part (a) shows the experimental results of Mullins and Tobin (1965), Omnès et al. (2008) and Smallwood (1944) for the effective initial shear modulus $\overline{\mu}$ of polyisoprene rubber filled with carbon black particles, normalized by the initial shear modulus of the corresponding rubber μ_m, as a function of the concentration of carbon black c_p. Part (b) shows the experimental results of Ramier (2004) for the uniaxial tensile stress-stretch response of SBR rubber filled with silica particles, at concentration $c_p = 0.15$, with two different types of chemical treatments, labeled as AC75 and AR8. In both parts of the figure, the discrete symbols (empty circles, triangles, and solid circles) correspond to the experimental measurements, while the solid lines correspond to the theoretical predictions.

triangles, and solid circles) correspond to the experimental data, while the solid lines stand for the theoretical predictions.

The results of Mullins and Tobin (1965) correspond to specimens with a well-dispersed distribution of roughly spherical aggregates of carbon black that had a relatively large average radius of about 200 nm. By way of swelling experiments, these authors were able to conclude that the elastic properties of the polyisoprene rubber were essentially unmodified by the presence of fillers, but provided no insight into the amount or type of bound rubber surrounding them. Given this partial information, at the level of the theoretical result (4.45), it is reasonable to assume that the shear modulus of the polyisoprene rubber matrix is identical to that of the polyisoprene rubber when synthesized in the absence of carbon black, namely, $\mu_m = 0.44$ MPa. And that the content of interphases is comparatively negligible to that of the relatively large fillers so that $c_i = 0$, or equivalently, $t/r = 0$. Figure 4.19(a) shows that the theoretical predictions based on these inputs are in fairly good agreement

with the experimental measurements of Mullins and Tobin (1965), save for the filled elastomer with the largest particle concentration $c_p = 0.2$.

The specimens studied by Omnès et al. (2008) were also comprised of a well-dispersed distribution of roughly spherical carbon black aggregates but of much smaller size, in the order of 30 nm in average radius. As opposed to Mullins and Tobin (1965), Omnès et al. (2008) did find that the elastic properties of the polyisoprene rubber were somewhat modified by the presence of carbon black. Unfortunately, no concrete measurements of this change were reported nor details about the amount or type of bound rubber surrounding the fillers provided. In view of this partial information, at the level of the theoretical result (4.45), we assume, as a first-order approximation, that the shear modulus of the polyisoprene rubber matrix is identical to that of the polyisoprene rubber when synthesized in the absence of carbon black, which in this case was reported as $\mu_m = 0.53$ MPa. Also, based on the recent experiments of Qu et al. (2011), we take the shear modulus of the interphases to be 10 times stiffer than that of the matrix, namely, $\mu_i = 10 \times \mu_m = 5.3$ MPa. Making use of these values, the thickness of the interphases is selected by fitting the experimentally measured values of the effective shear modulus. As shown in Fig. 4.19(a), it is found that an interphase-thickness-to-particle-radius ratio of $t/r = 0.37$ — corresponding to interphase thicknesses in the order of $t = 0.37 \times 30$ nm $= 11.1$ nm — renders good agreement with the data of Omnès et al. (2008).

Regarding the classical data reported by Smallwood (1944) for carbon black filled rubber, no microscopic information is known other than the concentration of particles c_p. Assuming that the elastic properties of the rubber making up the matrix are unaffected by the presence of carbon black, and that the shear modulus of the interphases is 10 times stiffer than that of the matrix, the theoretical result (4.45) can be seen to describe fairly accurately the measurements of Smallwood (1944) by choosing an interphase-thickness-to-particle-radius ratio of $t/r = 0.2$.

We now turn to examine the experimental data of Ramier (2004) for the large-deformation response under uniaxial tension of SBR rubber filled with a random and isotropic distribution of silica particles. Figure 4.19(b) shows the measured uniaxial (first Piola-Kirchhoff) stress $\overline{S}_{un}$ as a function of the applied stretch $\overline{\lambda}$ for two specimens with the *same* concentration of silica particles, $c_p = 0.15$, which have undergone two different chemical treatments,

labeled as AC75 and AR8. To aid the discussion, Fig. 4.19(b) also shows the uniaxial stress-stretch response for the unfilled SBR rubber. Akin to Fig. 4.19(a), the discrete symbols (empty circles, triangles, and solid circles) correspond to the experimental data, while the solid lines stand for the theoretical predictions.

Irrespectively of the chemical treatment of the particles, the results of Ramier (2004) correspond to specimens with a well-dispersed distribution of roughly spherical aggregates of silica that had an average radius of about 40 nm. It is unclear to what extent the presence of silica with either treatment, AC75 or AR8, affected the elastic properties of the SBR rubber. On the other hand, the AC75 treatment was expected, by design, to promote the formation of thicker and stiffer interphases than the AR8 treatment. The much stiffer response exhibited by the specimen with the AC75-treated silica is consistent with this expectation.

In computing the theoretical predictions for the data of Ramier (2004), given the above-outlined partial information, we assume that the SBR rubber is, to a first approximation, unaffected by the presence of silica. Moreover, we take the SBR rubber to be characterized by the Lopez-Pamies (2010b) stored-energy function

$$\Psi_m(I_1) = \frac{3^{1-\alpha_1}}{2\alpha_1}\mu_1\left[I_1^{\alpha_1} - 3^{\alpha_1}\right] + \frac{3^{1-\alpha_2}}{2\alpha_2}\mu_2\left[I_1^{\alpha_2} - 3^{\alpha_2}\right] \tag{4.76}$$

with material parameters $\mu_1 = 0.3734$ MPa, $\mu_2 = 0.0425$ MPa, $\alpha_1 = 0.3841$, $\alpha_2 = 1.7767$. Fig. 19(b) shows that this model describes accurately the experimentally measured response of the SBR rubber, at least for uniaxial tension. We shall further assume, again, based on the recent experiments due to Qu et al. (2011), that the interphases in the specimen with AR8-treated silica are 10 times stiffer than the matrix, $\mu_i = 10 \times \mu_m = 10 \times (\mu_1 + \mu_2) = 4.16$ MPa, whereas the interphases in the specimen with AC75-treated silica are 50 stiffer, $\mu_i = 50 \times \mu_m = 50 \times (\mu_1 + \mu_2) = 20.80$ MPa. Since there is no experimental evidence available regarding the sizes of the interphases, we select them here by fitting the theory to the experimental stress-stretch responses. As shown by Fig. 19(b), an interphase-thickness-to-particle-radius ratio of $t/r = 0.1$ — corresponding to interphase thicknesses in the order of $t = 0.1 \times 30$ nm $= 3$ nm — leads to a good agreement with the AR8 data. On the other hand, an interphase-thickness-to-particle-radius

ratio of $t/r = 0.4$ — corresponding to interphase thicknesses in the order of $t = 0.4 \times 30$ nm $= 12$ nm — renders good agreement with the AC75 data.

In summary, the above comparisons with experiments indicate that the proposed theory is able to describe and explain the macroscopic response of filled elastomers at finite deformations. In particular, the comparisons indicate that the reinforcement granted by interphases is comparable to that granted by the fillers themselves. These results make it plain that knowledge of the geometry and constitutive properties of the underlying interphases — and not just the fillers — in elastomers is of the essence to be able to predict, and thus also to design from the bottom up, the macroscopic behavior of filled elastomers.

CHAPTER 5

NUMERICAL MODELING OF THE NONLINEAR ELASTIC RESPONSE OF FILLED ELASTOMERS VIA COMPOSITE-SPHERE ASSEMBLAGES

The previous Three chapters have dealt with the development of analytical results to model filled elastomers. In this chapter, we put forward an effective *numerical method* to generate approximate solutions for the overall nonlinear elastic response of filled elastomers subjected to arbitrarily large deformations. The basic idea corresponds essentially to a generalization of the "composite-sphere-assemblage" approach of Hashin (1962) to the nonconvex realm of finite elasticity[1]. More specifically, as elaborated below the strategy is first to idealize the random microstructure of filled elastomers as an assemblage of homothetic composite spheres, And then to generate a variational *statically admissible* solution for the overall nonlinear elastic response of these material systems directly in terms of the response of a single composite sphere subjected to affine stress boundary conditions. While the elastostatics problem of a composite sphere subjected to affine stresses cannot be solved by analytical means; it is a simple matter to perform the relevant calculations numerically with finite elements. Sample applications to various elastomeric materials, concentrations of particles, and loading conditions together with comparisons with corresponding 3D full-field simulations are also provided in this chapter to assess accuracy and numerical efficiency of the method.

[1] An extension of this approach to nonlinear, though convex, problems appears to have been first carried out by Barrett and Talbot (1995) in the context of two-phase dielectrics.

5.1 The problem

Consider a filled elastomer comprising a continuous matrix reinforced by a random distribution of firmly bonded particles that occupies a domain Ω, with boundary $\partial\Omega$, in its undeformed stress-free configuration. The matrix is labeled as phase $r = 1$, while the particles are collectively identified as phase $r = 2$. The domains occupied by each individual phase are denoted by $\Omega^{(r)}$ so that $\Omega = \Omega^{(1)} \cup \Omega^{(2)}$. It is assumed that the characteristic size of the particles is much smaller than the size of Ω, and that their spatial distribution is statistically uniform.

Material points in the solid are identified by their initial position vector $\mathbf{X}$ in Ω. Upon deformation the position vector of a point in the deformed configuration Ω' is specified by $\mathbf{x} = \boldsymbol{\chi}(\mathbf{X})$, where $\boldsymbol{\chi}$ is a continuous and one-to-one mapping from Ω to Ω'. The pointwise deformation gradient tensor is denoted by $\mathbf{F} = \mathrm{Grad}\boldsymbol{\chi}$.

Both the matrix ($r = 1$) and the particles ($r = 2$) are taken to be nonlinear elastic solids characterized by non-negative, objective, and quasiconvex stored-energy functions $W^{(r)}$ of the deformation gradient $\mathbf{F}$, which linearize properly in the limit of small deformations as $\mathbf{F} \to \mathbf{I}$. At each material point $\mathbf{X}$ in the undeformed configuration, the first Piola-Kirchhoff stress $\mathbf{S}$ is thus related to $\mathbf{F}$ via

$$\mathbf{S} = \frac{\partial W}{\partial \mathbf{F}}(\mathbf{X}, \mathbf{F}), \quad W(\mathbf{X}, \mathbf{F}) = (1 - \theta(\mathbf{X}))\ W^{(1)}(\mathbf{F}) + \theta(\mathbf{X})\ W^{(2)}(\mathbf{F}), \quad (5.1)$$

where the indicator function θ is equal to 1 if the position vector $\mathbf{X}$ is inside a particle and zero otherwise. The volume average of θ over Ω corresponds to the initial volume fraction or concentration of particles, which we denote by

$$c \doteq \frac{|\Omega^{(2)}|}{|\Omega|} = \frac{1}{|\Omega|} \int_\Omega \theta(\mathbf{X})\, \mathrm{d}\mathbf{X}. \quad (5.2)$$

Granted the hypotheses of separation of length scales and statistical uniformity of the microstructure together with the constitutive quasiconvexity of W, the overall or macroscopic constitutive response for the above-described reinforced solid is defined as the relation between the volume averages of the first Piola-Kirchhoff stress $\overline{\mathbf{S}} \doteq |\Omega|^{-1} \int_\Omega \mathbf{S}(\mathbf{X})\, \mathrm{d}\mathbf{X}$ and the deformation gradient $\overline{\mathbf{F}} \doteq |\Omega|^{-1} \int_\Omega \mathbf{F}(\mathbf{X})\, \mathrm{d}\mathbf{X}$ when the material is subjected to affine boundary

conditions (Hill, 1972). In the case of affine deformations

$$\mathbf{x} = \overline{\mathbf{F}}\mathbf{X} \quad \text{on} \quad \partial\Omega \tag{5.3}$$

and the derivation of the overall response reduces to finding $\overline{\mathbf{S}}$ for a given $\overline{\mathbf{F}}$. For affine stresses, on the other hand,

$$\mathbf{S}\mathbf{N} = \overline{\mathbf{S}}\,\mathbf{N} \quad \text{on} \quad \partial\Omega \tag{5.4}$$

with $\mathbf{N}$ denoting the outward normal to the boundary, and the derivation reduces to finding $\overline{\mathbf{F}}$ for a given $\overline{\mathbf{S}}$. In either case, the result can be expediently written as (Ogden, 1978)

$$\overline{\mathbf{S}} = \frac{\partial \overline{W}}{\partial \overline{\mathbf{F}}}(\overline{\mathbf{F}}, c), \tag{5.5}$$

where the scalar-valued function

$$\overline{W}(\overline{\mathbf{F}}, c) \doteq \min_{\mathbf{F}\in\mathcal{K}} \frac{1}{|\Omega|} \int_{\Omega} W(\mathbf{X}, \mathbf{F}) \, \mathrm{d}\mathbf{X} \tag{5.6}$$

corresponds physically to the total elastic energy per unit undeformed volume stored in the material; in this last expression, $\mathcal{K}$ denotes a sufficiently large set of kinematically admissible deformation gradient fields with prescribed volume average $\overline{\mathbf{F}}$. An analogous description in terms of a complementary energy is possible, but that route requires the use of multi-valued functions which complicate unnecessarily the analysis (see, e.g.,Lee and Shield, 1980, Khisaeva and Ostoja-Starzewski, 2006; Chapter 5.4 in Ogden, 1997).

The foregoing formulation for the overall finite-deformation response of filled elastomers is valid for any distribution of the underlying reinforcing particles. In the sequel, the focus shall be on the physically relevant case of *isotropic* distributions, but the case of anisotropic distributions is also briefly discussed.

5.2 Approximate solution for isotropic distributions of particles

5.2.1 Idealization of the microstructure as a composite-sphere assemblage

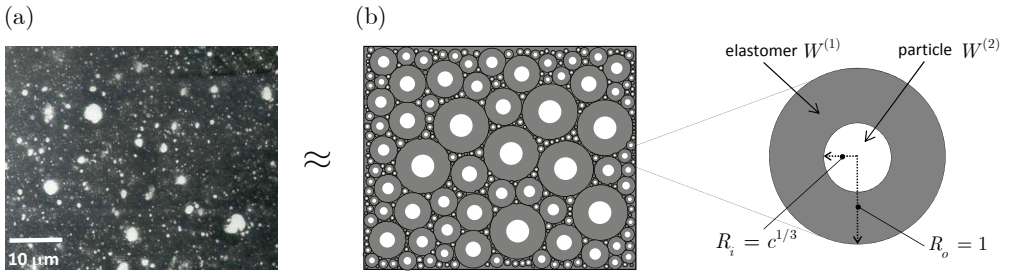

Figure 5.1: (a) Electron micrograph of a styrene-butadiene rubber filled with an isotropic distribution of silica particles (Ramier, 2004) and (b) its idealization as a CSA (composite-sphere assemblage) in the undeformed configuration. All the composite spheres in the assemblage are homothetic in that they have the same ratio of inner-to-outer radius $R_i/R_o = c^{1/3}$.

Figure 5.1(a) shows an electron micrograph of a synthetic rubber filled with an isotropic distribution of silica particles (Ramier, 2004). As is the case with other standard reinforcing fillers, the silica particles are seen to agglomerate into "particles" of roughly spherical shape and many different (i.e., polydisperse) sizes (Leblanc, 2010). Based on this observation, our first step to construct a solution for the overall nonlinear elastic response of isotropic filled elastomers — as characterized by the effective stored-energy function (5.6) — is to idealize their microstructures as a CSA (composite-sphere assemblage). Figure 5.1(b) depicts schematically the polydisperse nature of the CSA, and the fact that the concentration of particle in each composite sphere is equal to the concentration of particles c in the entire assemblage, since all the composite spheres have identical ratios of inner-to-outer radius; the interested reader is referred to Chapter 7 inMilton (2002) for further properties of CSAs.

The exact computation of the overall nonlinear elastic response of a CSA is as difficult as that of any real microstructure. Unlike real microstructures, however, CSAs allow for the construction of variational approximations for their effective stored-energy function (5.6) based on *non-uniform* admissible

trial fields, hence providing the means to account for higher microstructural information beyond merely the concentration of particles.

5.2.2 Variational approximation for the response of a CSA

Having idealized the microstructures of isotropic filled elastomers as a CSA, we now turn to constructing a variational statically admissible[2] approximation for their effective stored-energy function $\overline{W}$ under arbitrarily large deformations. We begin by introducing the Legendre transformation

$$W^*(\mathbf{X}, \mathbf{P}) = \sup_{\mathbf{F}} \{\mathbf{P} \cdot \mathbf{F} - W(\mathbf{X}, \mathbf{F})\}. \tag{5.7}$$

A direct consequence of this definition is that, for any $\mathbf{P}$ and $\mathbf{F}$,

$$W(\mathbf{X}, \mathbf{F}) \geq \mathbf{P} \cdot \mathbf{F} - W^*(\mathbf{X}, \mathbf{P}) \tag{5.8}$$

and hence that

$$\overline{W}(\overline{\mathbf{F}}, c) \geq \min_{\mathbf{F} \in \mathcal{K}(\overline{\mathbf{F}})} \frac{1}{|\Omega|} \int_\Omega \mathbf{P} \cdot \mathbf{F} \mathrm{d}\mathbf{X} - \frac{1}{|\Omega|} \int_\Omega W^*(\mathbf{X}, \mathbf{P}) \mathrm{d}\mathbf{X}. \tag{5.9}$$

For the inequality (5.9) not to be trivial, the field $\mathbf{P}$ needs to be selected divergence-free, in which case it follows from Hill's lemma that

$$\overline{W}(\overline{\mathbf{F}}, c) \geq \overline{\mathbf{P}} \cdot \overline{\mathbf{F}} - \frac{1}{|\Omega|} \int_\Omega W^*(\mathbf{X}, \mathbf{P}) \mathrm{d}\mathbf{X}, \tag{5.10}$$

where the notation

$$\overline{\mathbf{P}} \doteq \frac{1}{|\Omega|} \int_\Omega \mathbf{P}(\mathbf{X}) \, \mathrm{d}\mathbf{X} \tag{5.11}$$

has been introduced for convenience. In view of the definition (5.7), the inequality (5.10) can be written more explicitly as

$$\overline{W}(\overline{\mathbf{F}}, c) \geq \frac{1}{|\Omega|} \int_\Omega W(\mathbf{X}, \mathbf{F}^S) \mathrm{d}\mathbf{X} + \overline{\mathbf{P}} \cdot \overline{\mathbf{F}} - \frac{1}{|\Omega|} \int_\Omega \mathbf{P} \cdot \mathbf{F}^S \mathrm{d}\mathbf{X}, \tag{5.12}$$

[2]The analogous kinematically admissible approximation is discussed in Appendix I.

with the second-order tensor $\mathbf{F}^S$ being implicitly defined in terms of $\mathbf{P}$ as the solution to the algebraic equation

$$\mathbf{P} - \frac{\partial W}{\partial \mathbf{F}}(\mathbf{X}, \mathbf{F}^S) = 0 \tag{5.13}$$

that maximizes the right-hand side of (5.7); note that $\mathbf{F}^S$ does *not* necessarily correspond to the gradient of a deformation field.

The inequality (5.12) is valid for any choice of microstructure (i.e., any indicator function θ) and any choice of divergence-free field $\mathbf{P}$. At this point, we exploit the fact that the microstructure under study here is a CSA and consider divergence-free fields $\mathbf{P}$ that satisfy the affine condition

$$\mathbf{P}\mathbf{N} = \overline{\mathbf{P}}\mathbf{N} \tag{5.14}$$

on the surface of each composite sphere in the assemblage. By virtue of the invariance of the equations of elastostatics under the transformation $(\mathbf{X}, \mathbf{x}) \to (k\mathbf{X}, k\mathbf{x})$, relation (5.12) can then be rewritten as

$$\overline{W}(\overline{\mathbf{F}}, c) \geq \frac{1}{|\mathcal{B}|}\int_{\mathcal{B}} W(\mathbf{X}, \mathbf{F}^S)\mathrm{d}\mathbf{X} + \overline{\mathbf{P}} \cdot \overline{\mathbf{F}} - \frac{1}{|\mathcal{B}|}\int_{\mathcal{B}} \mathbf{P} \cdot \mathbf{F}^S \mathrm{d}\mathbf{X}, \tag{5.15}$$

where now the volume integrals are *not* over the entire domain Ω of the CSA, but only over the domain $\mathcal{B}$ of a *single* composite sphere. While the second-order tensor $\mathbf{F}^S$ does *not* correspond to the gradient of a deformation field over Ω in general, the field $\mathbf{P}$ can be selected so that $\mathbf{F}^S$ does correspond to the gradient of a deformation field over each composite sphere. In that case, by invoking once again Hill's lemma, the inequality (5.15) admits the further simplification

$$\overline{W}(\overline{\mathbf{F}}, c) \geq \frac{1}{|\mathcal{B}|}\int_{\mathcal{B}} W(\mathbf{X}, \mathbf{F}^S)\mathrm{d}\mathbf{X} + \overline{\mathbf{P}} \cdot \overline{\mathbf{F}} - \overline{\mathbf{P}} \cdot \left[\frac{1}{|\mathcal{B}|}\int_{\mathcal{B}} \mathbf{F}^S \,\mathrm{d}\mathbf{X}\right]. \tag{5.16}$$

Now, the right-hand side of inequality (5.16) can be maximized when the constant tensor $\overline{\mathbf{P}}$ is chosen such that

$$\frac{1}{|\mathcal{B}|}\int_{\mathcal{B}} \mathbf{F}^S(\mathbf{X})\mathrm{d}\mathbf{X} = \overline{\mathbf{F}}, \tag{5.17}$$

in which case it reduces finally to

$$\overline{W}(\overline{\mathbf{F}},c) \geq \frac{1}{|\mathcal{B}|}\int_{\mathcal{B}} W(\mathbf{X},\mathbf{F}^S)\mathrm{d}\mathbf{X} \doteq \overline{W}^S(\overline{\mathbf{F}},c). \tag{5.18}$$

In this last expression, again, $\mathcal{B}$ stands for the domain occupied by a single composite sphere with particle concentration c in the undeformed configuration (see Fig. 5.2(b)), $\mathbf{F}^S$ is the deformation gradient tensor defined by the boundary-value problem

$$\mathrm{Div}\left[\frac{\partial W}{\partial \mathbf{F}}(\mathbf{X},\mathbf{F}^S)\right] = 0 \quad \text{in} \quad \mathcal{B} \quad \text{and} \quad \left[\frac{\partial W}{\partial \mathbf{F}}(\mathbf{X},\mathbf{F}^S)\right]\mathbf{N} = \overline{\mathbf{P}}\mathbf{N} \quad \text{on} \quad \partial\mathcal{B}, \tag{5.19}$$

and the constant tensor $\overline{\mathbf{P}}$ is implicitly related to the macroscopic deformation gradient $\overline{\mathbf{F}}$ via

$$\overline{\mathbf{P}} = \frac{1}{|\mathcal{B}|}\int_{\mathcal{B}} \frac{\partial W}{\partial \mathbf{F}}(\mathbf{X},\mathbf{F}^S)\mathrm{d}\mathbf{X} = \frac{\partial \overline{W}^S}{\partial \overline{\mathbf{F}}}(\overline{\mathbf{F}},c), \tag{5.20}$$

the last equality in (5.20) stemming from the divergence theorem.

The macroscopic deformation gradient $\overline{\mathbf{F}}$ and effective stored-energy function $\overline{W}^S$ defined by relations (5.17) and (5.18) with (5.19)–(5.20) constitute the main result of this chapter. They characterize — in the form of a variational approximation — the overall nonlinear elastic response of an elastomer, with arbitrary stored-energy function $W^{(1)}$, filled with an isotropic distribution of particles, with arbitrary stored-energy function $W^{(2)}$, of polydisperse sizes and finite concentration c. The following theoretical and practical remarks are in order:

i. It is plain that the divergence-free field $\mathbf{P}$ devised above is nothing more than a *statically admissible stress field* $\mathbf{S}(\mathbf{X}) = \mathbf{P}(\mathbf{X})$ with prescribed volume average $\overline{\mathbf{S}} = \overline{\mathbf{P}}$ over the entire domain Ω of the CSA. Thus, akin to the classical result in linear elasticity Hashin (1962), $\overline{W}^S$ corresponds physically to the total elastic energy per unit undeformed volume of a CSA associated with a statically admissible stress field. It is emphasized that the derivation of such a solution, depicted schematically in Fig. 5.2, without having had to invoke the cumbersome principle of minimum complementary energy in finite elasticity was made possible by the use of the Legendre transformation (5.7); see Willis (1989) for

relevant comments on this approach.

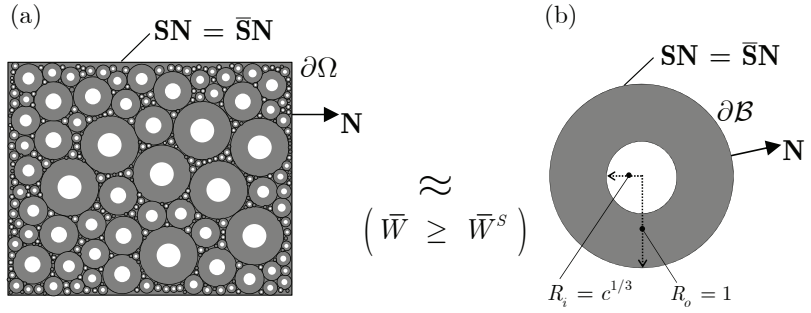

Figure 5.2: Schematic illustrating that the overall response of a CSA subjected to affine stress boundary conditions can be variationally approximated by the overall response of a corresponding single composite sphere subjected to the same affine stress boundary conditions. Specifically, the approximation is such that the total elastic energy $\overline{W}$ of the CSA is bounded from below by the total elastic energy $\overline{W}^S$ of the single composite sphere.

ii. The computation of the overall nonlinear elastic response of filled elastomers, as determined by the above CSA variational approximation, amounts to solving the boundary-value problem (5.19) for the deformation gradient field $\mathbf{F}^S$ over a *single* composite sphere $\mathcal{B}$. And then carrying out the volume integrals (5.17) and (5.18) to finally compute the macroscopic deformation gradient $\overline{\mathbf{F}}$ and effective stored-energy function $\overline{W}^S$ in terms of the applied macroscopic stress $\overline{\mathbf{S}}(= \overline{\mathbf{P}})$. In general, it is not possible to solve equations (5.19) by analytical means, but it is straightforward to solve them numerically. In the next section, we present an effective FE (finite-element) approach to carry out the calculations.

iii. By construction, the effective stored-energy function $\overline{W}^S$ is an exact result (i.e., the equality holds in (5.18)) in the dilute limit of particles as $c \to 0+$. As the concentration of particles increases, $\overline{W}^S$ is expected to progressively deviate from $\overline{W}$ providing increasingly softer approximations for the overall response of filled elastomers. This expectation is supported by comparisons with the 3D full-field simulations presented further below in the applications section.

iv. Owing to the proper linearization of the energies $W^{(1)}$ and $W^{(2)}$ of the matrix and particles, the effective stored-energy function $\overline{W}^S$ linearizes

properly in the limit of small applied stresses as $\overline{\mathbf{S}} \to \mathbf{0}$ reducing to

$$\overline{W}^S(\overline{\mathbf{F}}, c) = \frac{1}{2}\overline{\boldsymbol{\varepsilon}} \cdot \overline{\boldsymbol{\mathcal{L}}}^S \overline{\boldsymbol{\varepsilon}} + O(\overline{\boldsymbol{\varepsilon}}^3), \tag{5.21}$$

where $\overline{\boldsymbol{\varepsilon}} = (\overline{\mathbf{F}} + \overline{\mathbf{F}}^T - 2\mathbf{I})/2$ and $\overline{\boldsymbol{\mathcal{L}}}^S = \overline{\boldsymbol{\mathcal{L}}}^S(c)$ stands for the effective modulus tensor of the filled elastomer in its ground state.

v. For the prominent case when the underlying matrix and particles are constitutively isotropic, it follows that the exact effective stored-energy function $\overline{W}$ is macroscopically isotropic, $\overline{W}(\overline{\mathbf{Q}}\,\overline{\mathbf{F}}\,\overline{\mathbf{Q}}', c) = \overline{W}(\overline{\mathbf{F}}, c)$ for all proper orthogonal second-order tensors $\overline{\mathbf{Q}}$ and $\overline{\mathbf{Q}}'$. In this case, it is not difficult to show that the approximate effective stored-energy function $\overline{W}^S$ has the merit to be functionally exact in that it is identically isotropic; i.e., $\overline{W}^S(\overline{\mathbf{Q}}\,\overline{\mathbf{F}}\,\overline{\mathbf{Q}}', c) = \overline{W}^S(\overline{\mathbf{F}}, c)\ \forall\ \overline{\mathbf{Q}}, \overline{\mathbf{Q}}' \in Orth^+$.

vi. When the underlying matrix and particles are incompressible, the exact macroscopic constraint of incompressibility ensuing from the microscopic constraint $C(\mathbf{X}, \mathbf{F}) = \det\mathbf{F} - 1 = 0\ \forall \mathbf{X} \in \Omega$ is given by $C(\overline{\mathbf{F}}, c) = \det\overline{\mathbf{F}} - 1 = 0$ so that $\overline{W}(\overline{\mathbf{F}}, c) = +\infty$ if $\det\overline{\mathbf{F}} \neq 1$. Owing to the lack of separation of length scales between the particle and the surrounding matrix material in the boundary-value problem[3] (5.19), the resulting approximate macroscopic deformation gradient (5.17) is *not* necessarily such that $\det\overline{\mathbf{F}} = 1$ (even though $\det\mathbf{F}^S = 1$ for all $\mathbf{X} \in \mathcal{B}$). Nevertheless, in the broad range of cases that we have examined numerically, the determinant of the resulting $\overline{\mathbf{F}}$ exhibits little deviation from 1.

5.3 FE solutions for the auxiliary problem of a single composite sphere under affine stresses

In the sequel, we present a FE procedure to construct numerical solutions for the boundary-value problem (5.19) and average quantities (5.17) and (5.18), from which we can then determine the overall response of filled elastomers

[3]In other words, the composite sphere is a composite structure and *not* a composite material.

under general loading conditions. While the above-presented variational approximation applies more generally, for conciseness, attention is restricted here to the physically prominent case of matrix and particles that are *constitutively isotropic*. We begin in Section 5.3.1 by describing the construction of the FE model utilized to carry out the relevant calculations. The description of the numerical method of solution of $\overline{W}^S$ and $\overline{\mathbf{F}}$ for a given $\overline{\mathbf{S}}$ is discussed in Section 5.3.2.

5.3.1 The FE model

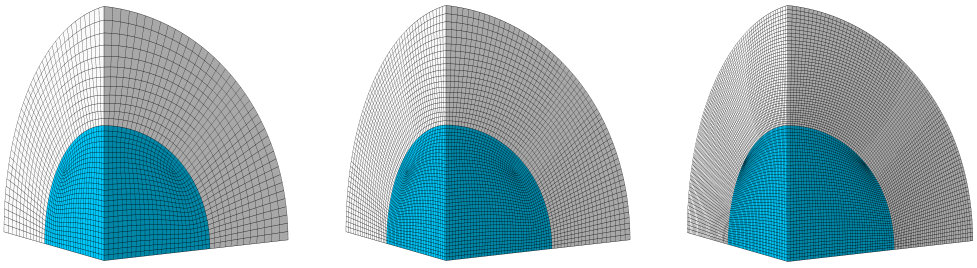

(a) (b) (c)

Figure 5.3: Three representative meshes in the undeformed configuration for a composite sphere with particle concentration $c = 0.15$: (a) coarse mesh with $28,400$ elements, (b) fine mesh with $102,600$ elements, and (c) very fine mesh with $260,800$ elements.

Without loss of generality, we consider the domains occupied by the matrix ($r = 1$) and particle ($r = 2$) in the composite sphere to be such that

$$\mathcal{B}^{(1)} = \{\mathbf{X} : c^{1/3} \leq |\mathbf{X}| \leq 1\} \qquad \text{and} \qquad \mathcal{B}^{(2)} = \{\mathbf{X} : |\mathbf{X}| \leq c^{1/3}\}, \tag{5.22}$$

respectively. That is, the center of the composite sphere is placed at the origin of the laboratory Cartesian axes $\{\mathbf{e}_i\}$, and units of length are chosen so that the outer radius $R_o = 1$ while the particle radius is set at $R_i = c^{1/3}$ in terms of the concentration of particles. The geometric and constitutive symmetries of the problem allow to perform the calculations in just one octant of the composite sphere. The 3D discretization of such a subdomain is performed with help of a mesh generator code in such a way that radial symmetry is preserved. Eight-node hybrid brick elements — where the pressure is treated as a further degree of freedom in order to be able to handle com-

pressible as well as incompressible constitutive behaviors — are utilized for the analysis. Since the computations are carried out using the FE package ABAQUS, we make use in particular of the C3D8H hybrid elements available in this code (Abaqus version 6.11 documentation). Figure 5.3 shows three representative meshes of increasing refinement. Mesh sensitivity studies reveal that meshes with approximately $100,000$ elements (such as the fine mesh shown in Fig. 5.3(b)) produce sufficiently accurate results, irrespectively of the concentration of particle c.

5.3.2 Computation of the overall response

By virtue of the geometric and constitutive isotropy of the problem, the resulting overall elastic response of the composite sphere is isotropic. This implies that the effective stored-energy function $\overline{W}^S$ in this case depends on the macroscopic deformation gradient $\overline{\mathbf{F}}$ only through its singular values $\overline{\lambda}_1, \overline{\lambda}_2, \overline{\lambda}_3$. More explicitly,

$$\overline{W}^S(\overline{\mathbf{F}}, c) = \overline{\Psi}^S(\overline{\lambda}_1, \overline{\lambda}_2, \overline{\lambda}_3, c), \tag{5.23}$$

where $\overline{\Psi}^S(\overline{\lambda}_1, \overline{\lambda}_2, \overline{\lambda}_3, c)$ is a symmetric function with respect to its first three arguments.

A further direct implication of the overall isotropy of the problem is that it suffices to consider affine stress boundary conditions of the diagonal form

$$\mathbf{SN} = \overline{\mathbf{S}}\mathbf{N} \quad \text{on} \quad \partial\mathcal{B} \qquad \text{with} \qquad \overline{\mathbf{S}} = \text{diag}(\overline{s}_1, \overline{s}_2, \overline{s}_3), \tag{5.24}$$

since $\overline{s}_i = \partial\overline{\Psi}^S(\overline{\lambda}_1, \overline{\lambda}_2, \overline{\lambda}_3, c)/\partial\overline{\lambda}_i$ $(i = 1, 2, 3)$ in this case. A convenient way to implement these boundary conditions is to follow radial paths in $(\overline{s}_1, \overline{s}_2, \overline{s}_3)$–stress space. Specifically, we set

$$\overline{s}_1 = s\cos\Theta\sin\Phi, \quad \overline{s}_2 = s\sin\Theta\sin\Phi, \quad \overline{s}_3 = s\cos\Phi, \tag{5.25}$$

where s is the monotonically increasing load parameter of the process, which takes the value of 0 in the undeformed stress-free configuration, and $\Theta \in [0, 2\pi]$ and $\Phi \in [0, \pi]$ are the load path angles. Any desired macroscopic stress state $\overline{\mathbf{S}} = \text{diag}(\overline{s}_1, \overline{s}_2, \overline{s}_3)$ can be accessed by marching along (starting

at $s = 0$) radial paths (5.25) with appropriate fixed values of the angles Θ and Φ.

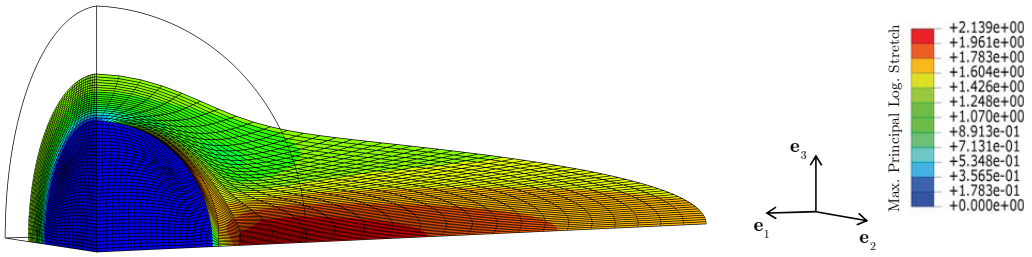

Figure 5.4: Contour plots of the maximum principal logarithmic strain for a composite sphere with $c = 0.15$, Neo-Hookean matrix, and 10^4–times stiffer Neo-Hookean particle subjected to affine uniaxial stress (5.24) with $\overline{\mathbf{S}} = \text{diag}(\overline{s}_1 > 0, 0, 0)$; the undeformed configuration is also depicted for comparison purposes. The overall stretch in the direction of applied stress is $\overline{\lambda}_1 = 3.5$.

For a given radial path (5.25), the FE calculations are carried out by gradually increasing the load parameter s from 0 to the desired final value; for the classes of materials to be studied here, the typical step size in the gradual increase of s is $\Delta s = 10^{-2}$. At each step in such a loading path, the incremental equilibrium equations are solved directly in ABAQUS and the integrals (5.17) and (5.18) defining the macroscopic deformation gradient $\overline{\mathbf{F}}$ and effective stored-energy function $\overline{W}^S$ computed. It is emphasized that the computational cost of these calculations is low and that very large overall deformations can be achieved. For illustrative purposes, Fig. 5.4 shows the deformed mesh of a composite sphere for the case of $c = 0.15$, Neo-Hookean matrix, and 10^4–times stiffer Neo-Hookean particle under affine uniaxial stress (5.24) with $\overline{\mathbf{S}} = \text{diag}(\overline{s}_1 > 0, 0, 0)$. The overall stretch in the direction of applied stress is $\overline{\lambda}_1 = 3.5$. Locally, the deformation is of course even larger (in the matrix) as the contour plots of the maximum principal logarithmic stretch show in the figure.

5.4 Sample applications and discussion

In this section we present a compendium of results for the overall nonlinear elastic response of filled elastomers, as characterized by the CSA formulation described above. Motivated by the properties of typical filled elastomers,

attention is restricted to *isotropic incompressible* matrix materials and (approximately) *rigid* filler particles. Results for the linear elastic response in the small-deformation regime are presented first followed by results for the large-deformation response of filled Gaussian (Neo-Hookean) rubber with matrix stored-energy function

$$W^{(1)}(\mathbf{F}) = \begin{cases} \dfrac{\mu}{2}\left[\mathbf{F}\cdot\mathbf{F}-3\right] & \text{if} \quad \det\mathbf{F}=1 \\ +\infty & \text{otherwise} \end{cases} . \tag{5.26}$$

The third set of results pertains to the response of a filled rubber wherein the underlying elastomeric matrix is characterized by the non-Gaussian stored-energy function

$$W^{(1)}(\mathbf{F}) = \begin{cases} \displaystyle\sum_{i=1}^{2} \frac{3^{1-\alpha_i}}{2\alpha_i}\mu_i\left[(\mathbf{F}\cdot\mathbf{F})^{\alpha_i}-3^{\alpha_i}\right] & \text{if} \quad \det\mathbf{F}=1 \\ +\infty & \text{otherwise} \end{cases} , \tag{5.27}$$

with $\mu_1 = 0.032$ MPa, $\mu_2 = 0.3$ MPa, $\alpha_1 = 3.837$, $\alpha_2 = 0.559$, corresponding to a model that has been shown to accurately describe the nonlinear elastic response of typical silicone rubber over large ranges of deformations (see Section 2.3 in Lopez-Pamies, 2010b). In all the calculations, the comparatively rigid particles are modeled as incompressible Neo-Hookean solids with stored-energy function

$$W^{(2)}(\mathbf{F}) = \begin{cases} \dfrac{\mu_p}{2}\left[\mathbf{F}\cdot\mathbf{F}-3\right] & \text{if} \quad \det\mathbf{F}=1 \\ +\infty & \text{otherwise} \end{cases} , \tag{5.28}$$

where the parameter μ_p is set to be four orders of magnitude larger[4] than the initial shear modulus of the underlying matrix material, namely, $\mu_p = 10^4 \times \mu$ for the case of filled Neo-Hookean rubber and $\mu_p = 10^4 \times (\mu_1 + \mu_2)$ for the case of filled silicone rubber.

The selection of results presented here aims at providing further insight into the proposed CSA approach and at assessing its accuracy and numerical efficiency for a broad range of elastomeric matrix materials, particle concentrations, and loading conditions. To aid in this process, the CSA results are confronted with the recent 3D full-field simulations of Lopez-Pamies et al.

[4]The initial shear moduli of standard reinforcing fillers (e.g., silica) are typically four orders of magnitude larger than those of standard elastomers (e.g., silicone).

(2013a). These are finite-element simulations of the large-deformation response of elastomers reinforced by random isotropic distributions of rigid spherical particles with the same (monodisperse) and with different (polydisperse) sizes. For the values of particle concentration considered here, the dispersion in the size of the particles turns out not to have an effect on the overall response of the simulations (see Section 6 in Lopez-Pamies et al., 2013a). Accordingly, no distinction is made henceforth of whether the presented full-field FE simulations are for monodisperse or for polydisperse microstructures.

5.4.1 Linear elastic results

In the limit of small deformations (see remark *iv* in Section 5.2.2), for the case of isotropic incompressible matrix materials and rigid particles, the CSA stored-energy function (5.18) reduces to

$$\overline{W}^{S}(\overline{\mathbf{F}},c)=\overline{\mu}^{S}\left[\overline{\varepsilon}_1^2+\overline{\varepsilon}_2^2+\overline{\varepsilon}_3^2\right]\qquad\text{with}\qquad\overline{\varepsilon}_1+\overline{\varepsilon}_2+\overline{\varepsilon}_3=0 \tag{5.29}$$

to leading order in the deformation measures $\overline{\varepsilon}_i=\overline{\lambda}_i-1$ $(i=1,2,3)$, where it is recalled that $\overline{\lambda}_i$ denote the singular values of the macroscopic deformation gradient $\overline{\mathbf{F}}$ and $\overline{\mu}^{S}$ stands for the initial effective shear modulus of the filled rubber. Figure 5.5 presents plots for $\overline{\mu}^{S}$, normalized by the initial shear modulus μ of the underlying elastomeric matrix, as a function of the concentration of particles c. Results are also presented for the corresponding full-field FE simulations for isotropic distribution of rigid spherical particles, as well as for the Hashin-Shtrikman and Reuss lower bounds for the effective shear modulus of rigidly reinforced, isotropic, incompressible, linearly elastic materials.

Two plain observations from Fig. 5.5 are that the CSA result stiffens monotonically with increasing values of c, as expected on physical grounds, and that it is in good quantitative agreement with the full-field FE simulations for concentrations up to about $c=0.05$, remaining softer thereafter. This latter behavior is consistent with the fact the CSA result is exact in the dilute limit of particles as $c\to 0+$, but a lower bound for finite values of c (see remark *iii* in Section 5.2.2). More specifically, the CSA result is seen to be consistently stiffer than the Reuss bound, but *softer* than the

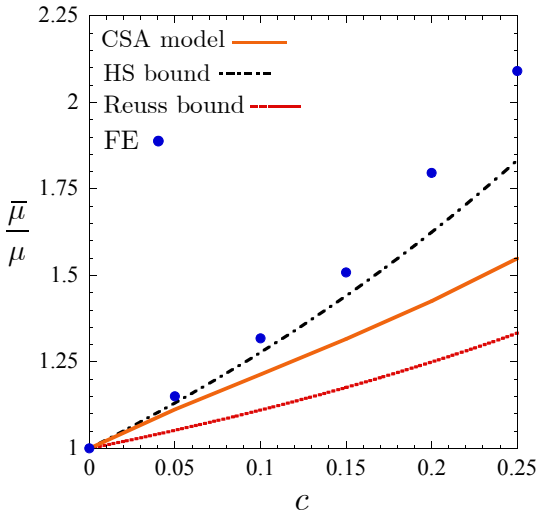

Figure 5.5: The normalized initial effective shear modulus $\overline{\mu}/\mu$ of isotropic incompressible elastomers filled with random isotropic distributions of rigid particles. Plots are shown for: (i) the CSA approximation $\overline{\mu}^S$, (ii) full-field FE simulations, (iii) the Hashin-Shtrikman lower bound $\overline{\mu}^{HS}/\mu = (2+3c)/(2-2c)$, and (iv) the Reuss lower bound $\overline{\mu}^R/\mu = 1/(1-c)$, as functions of the concentration of particles c.

corresponding Hashin-Shtrikman bound beyond $c = 0.05$.

5.4.2 Results for filled Neo-Hookean rubber

Having examined the small-deformation regime, we now turn to consider the response of filled elastomers under arbitrarily large deformations. We begin by considering the basic case of filled Neo-Hookean rubber. Figure 5.6 shows results for the effective stored-energy function of Neo-Hookean rubber reinforced by an isotropic distribution of rigid particles of concentration $c = 0.15$. Part (a) displays the entire energy function in terms of the macroscopic principal stretches $\overline{\lambda}_1$ and $\overline{\lambda}_2$, whereas part (b) displays the cross section of the energy along the axisymmetric deformation plane with $\overline{\lambda}_1 = \overline{\lambda}_2 = \overline{\lambda}$. Results are shown for the CSA approximate energy $\overline{W}^S$ in both parts of the figure, and for the corresponding full-field FE simulations for isotropic distributions of spherical particles in part (b).

A key point to emphasize from Fig. 5.6 is that the construction of the *entire* CSA effective stored-energy function $\overline{W}^S$ over *large ranges* of macroscopic deformations $\overline{\mathbf{F}}$ — which, again, serves to characterize the macroscopic constitutive response of the filled elastomer under general loading conditions

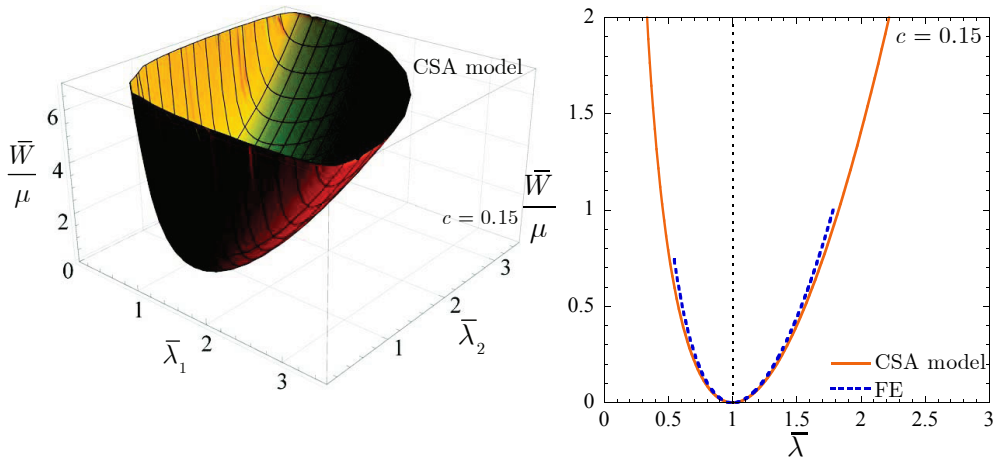

(a) (b)

Figure 5.6: Macroscopic response of Neo-Hookean rubber filled with an isotropic distribution of rigid particles of concentration $c = 0.15$. Part (a) displays the entire effective stored-energy function in terms of the macroscopic principal stretches $\overline{\lambda}_1$ and $\overline{\lambda}_2$, whereas part (b) shows the energy along axisymmetric loading conditions with $\overline{\lambda}_1 = \overline{\lambda}$, $\overline{\lambda}_2 = \overline{\lambda}^{-1/2}$. Results are shown for the CSA approximation $\overline{W}^S$ in both parts, and for corresponding full-field FE simulations for isotropic distributions of spherical particles in part (b).

via (5.20) — is straightforward and computationally inexpensive. Another key point is that the CSA approximation is in good agreement with the full-field FE simulations in the large-deformation regime, even at the relatively high value of particle concentration $c = 0.15$.

To gain more precise insight into the accuracy and range of validity of the CSA approximation, Fig. 5.7 presents results for the large-deformation response of filled Neo-Hookean rubber for particle concentrations of $c = 0.05$ and 0.15 under: (a) uniaxial compression, (b) uniaxial tension, (c) pure shear, and (d) simple shear. The constitutive stress-deformation relations for these loading conditions in terms of the effective stored-energy function $\overline{W}^S$ read explicitly as

- *Uniaxial loading* ($\overline{\lambda}_1 = \overline{\lambda}$, $\overline{\lambda}_2 = \overline{\lambda}_3 = \overline{\lambda}^{-1/2}$ with $\overline{s}_2 = \overline{s}_3 = 0$):

$$\overline{S}_{un} = \frac{\mathrm{d}\overline{W}^S}{\mathrm{d}\overline{\lambda}} \tag{5.30}$$

- *Pure shear* ($\overline{\lambda}_1 = \overline{\lambda}$, $\overline{\lambda}_2 = \overline{\lambda}^{-1}$, $\overline{\lambda}_3 = 1$ with $\overline{s}_2 = 0$):

$$\overline{S}_{ps} = \frac{\mathrm{d}\overline{W}^S}{\mathrm{d}\overline{\lambda}} \tag{5.31}$$

- *Simple shear* ($\overline{\lambda}_1 = (\overline{\gamma} + \sqrt{\overline{\gamma}^2 + 4})/2$, $\overline{\lambda}_2 = \overline{\lambda}_1^{-1}$, $\overline{\lambda}_3 = 1$):

$$\overline{S}_{ss} = \frac{\mathrm{d}\overline{W}^S}{\mathrm{d}\overline{\gamma}} \tag{5.32}$$

where $\overline{S}_{un}$, $\overline{S}_{ps}$, $\overline{S}_{ss}$ denote first Piola-Kirchhoff stress measures. The corresponding full-field FE results for isotropic distributions of spherical particles are also plotted in the figure.

In addition to the monotonic stiffening of the response for increasing values of particle concentration, it is immediate from Fig. 5.7 that the CSA and FE results are in fairly good qualitative and quantitative agreement for all loading conditions. As expected from the variational construction of the CSA formulation (see remark *iii* in Section 5.2.2), the agreement is better for the case of the smaller concentration $c = 0.05$, but remains remarkably good for the relatively high concentration $c = 0.15$, with a maximum difference of about 15% occurring along uniaxial compression. Fig. 5.7 also serves to illustrate the fact that the CSA approach allows to reach much larger overall deformations than those achieved with full-field simulations.

5.4.3 Results for a filled silicone rubber

Figure 5.8 presents various results for the large-deformation response of a filled non-Gaussian rubber, wherein the underlying matrix material is a typical silicone rubber characterized here by the stored-energy function (5.27) with material parameters $\mu_1 = 0.032$ MPa, $\mu_2 = 0.3$ MPa, $\alpha_1 = 3.837$, $\alpha_2 = 0.559$. Parts (a), (b), (c), and (d) of the figure show the macroscopic stress-deformation relation for uniaxial compression, uniaxial tension, pure shear, and simple shear for particle concentrations $c = 0.05$ and 0.15. Results are shown for the CSA approximation and for the corresponding full-field FE simulations.

Akin to all previous results, the overall constitutive response of the filled

elastomer is seen to stiffen for increasing values of particle concentration. Similar to the Neo-Hookean case, here the CSA results also exhibit good qualitative and quantitative agreement with the full-field FE simulations for all loading conditions. The largest discrepancy occurs, again, along uniaxial compressive loading for the largest concentration of particles $c = 0.15$.

In short, the above three sets of sample results indicate that the proposed CSA formulation provides a numerically efficient, functionally sound, and quantitatively fairly accurate approach to compute the overall nonlinear elastic response of isotropic filled elastomers, with small-to-moderate concentration of particles, under arbitrarily large deformations.

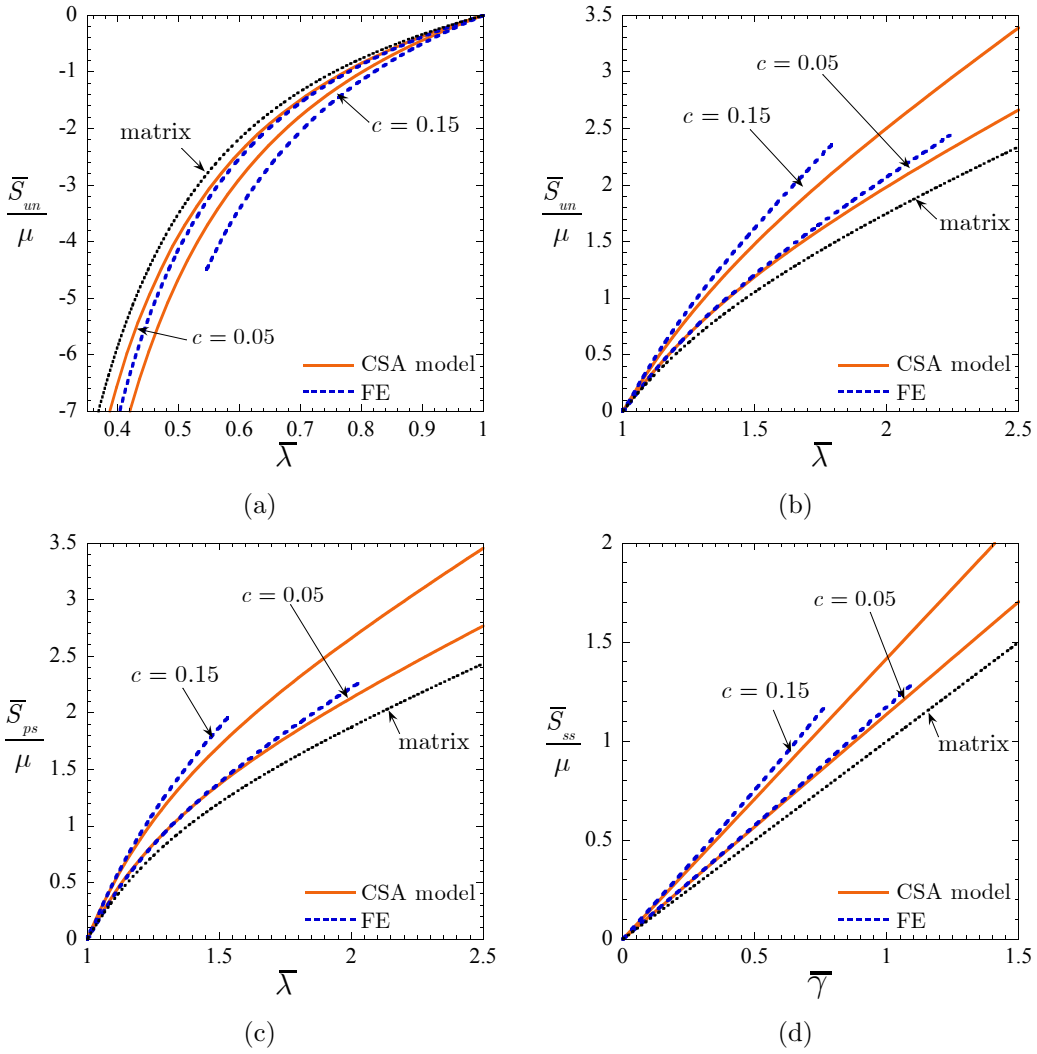

Figure 5.7: Macroscopic response of filled Neo-Hookean rubber with various values of concentration of particles c under: (a) uniaxial compressive, (b) uniaxial tensile, (c) pure shear, and (d) simple shear loading conditions. Plots are shown for the CSA approximation and corresponding full-field FE simulations for isotropic distributions of spherical particles.

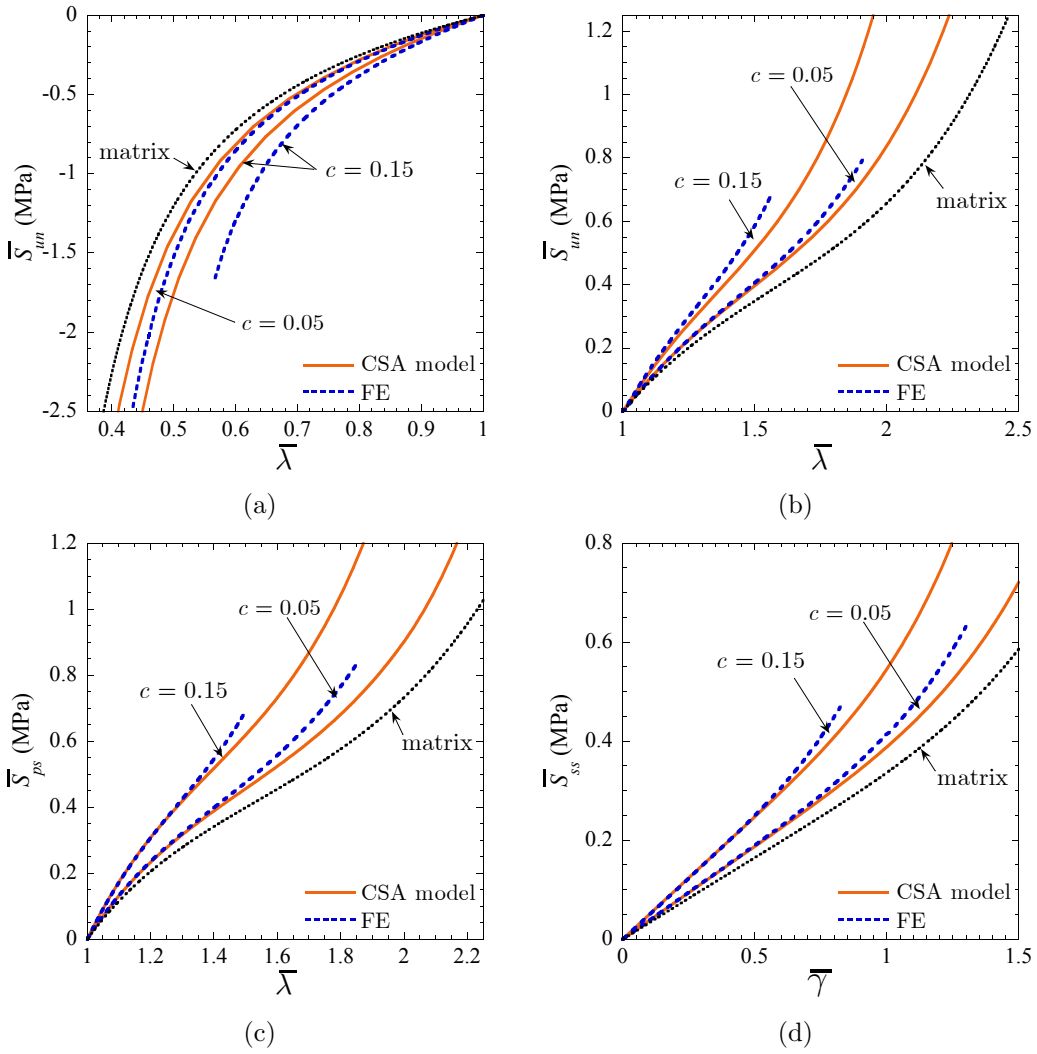

Figure 5.8: Macroscopic response of filled silicone rubber with various values of concentration of particles c under: (a) uniaxial compressive, (b) uniaxial tensile, (c) pure shear, and (d) simple shear loading conditions. Plots are shown for the CSA approximation and corresponding full-field simulations for isotropic distributions of spherical particles.

CHAPTER 6

HOMOGENIZATION OF DIELECTRIC ELASTOMER COMPOSITES WITH INTERPHASIAL CHARGES

In recent years, plenty of experiments (see, e.g., Huang et al., 2004; Nelson and John, 2004; Roy et al., 2005; Huang et al., 2005) have shown that the macroscopic (i.e., homogenized) permittivity of polymers filled with nanoparticles can be drastically different — higher or lower — from that of the same polymers unfilled or filled with microparticles. Motivated by prior work on suspensions of particles in electrolytic solutions by Chew and Sen (1982), and Lewis (2004), in this chapter we show theoretically how such "anomalous" behavior can be described and explained by the presence of interphasial charges. More generally, we show that the manipulation of interphasial charges (possibly via particle surface treatments or coatings) provides a promising path forward for the design of materials with exceptional dielectric properties.

The basic idea rests on a generalization of the "coated-sphere-assemblage" approach pioneered by Hashin (1962) to the realm of particulate composites with interphases that contain *space charges*, or, in homogenization parlance, source terms that oscillate at the microscale[1]. Specifically, the first step is to idealize[2] the random microstructure of filled polymers as assemblages of homothetic multicoated spheres made up of a core (the particle), an inner shell (the interphase), and an outer shell (the matrix), all with different

[1]In this regard, it is important to emphasize that the vast majority of homogenization techniques and results currently available (Milton, 2002) make critical use of the assumption that source terms (such as, for instance, space charges, body forces, and heat sources) oscillate only at the macroscale.

[2]For definiteness, we restrict attention here to the case of *isotropic* microstructures and *isotropic* constitutive properties. However, the arguments apply more generally to particulate composites with anisotropic microstructures and anisotropic constitutive properties (Goudarzi and Lopez-Pamies, 2013).

isotropic permittivities $\varepsilon_p\mathbf{I}$, $\varepsilon_i\mathbf{I}$, and $\varepsilon_m\mathbf{I}$, respectively. Further, the inner shell is taken to contain a distribution of space charges $Q(\mathbf{X})$ — heterogenous but with equal amount of positive and negative charges — per unit volume of the material; see Fig. 6.1 for a schematic depiction. Having idealized the microstructure of filled polymers as such assemblages, their macroscopic permittivity can then be determined *exactly* and in *closed-form* by making use of a neutral-inclusion strategy.

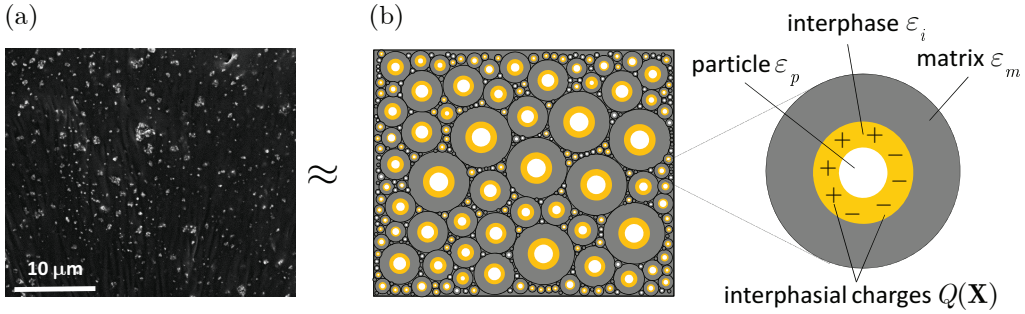

Figure 6.1: (a) Electron micrograph of a PDMS elastomer filled with titania nanoparticles and (b) its idealization as an assemblage of multicoated spheres with interphasial charges. All the multicoated spheres in the assemblage are homothetic in that they are scale-up or scale-down replicas of each other.

6.1 The dielectric response of an assemblage of multicoated spheres with interphasial charges

Consider a homogeneous material with unknown isotropic permittivity $\varepsilon_*\mathbf{I}$ that occupies a domain Ω and is subjected to the electric potential

$$\varphi(\mathbf{X}) = -\overline{\mathbf{E}}\cdot\mathbf{X} \tag{6.1}$$

on its boundary $\partial\Omega$, where $\overline{\mathbf{E}}$ is a prescribed constant vector. We seek to find the permittivity ε_* such that when a multicoated sphere made up of a core (the particle) with permittivity $\varepsilon_p\,\mathbf{I}$, an inner shell (the interphase) with permittivity $\varepsilon_i\,\mathbf{I}$ that contains a distribution of charges $Q(\mathbf{X})$, and an outer shell (the matrix) with permittivity $\varepsilon_m\,\mathbf{I}$ is inserted in Ω, the electric field remains unaltered ($\mathbf{E}(\mathbf{X}) = \overline{\mathbf{E}}$) outside the multicoated sphere. Since the multicoated sphere acts as a *neutral inclusion* in such a medium, the sought-after permittivity ε_* corresponds precisely to the macroscopic permittivity

of a fully dense assemblage of homothetic multicoated spheres that fills the entire domain Ω (see, e.g., the seminal work of Hashin and Shtrikman (1962), Chapter 7 in Milton (2002) and references therein).

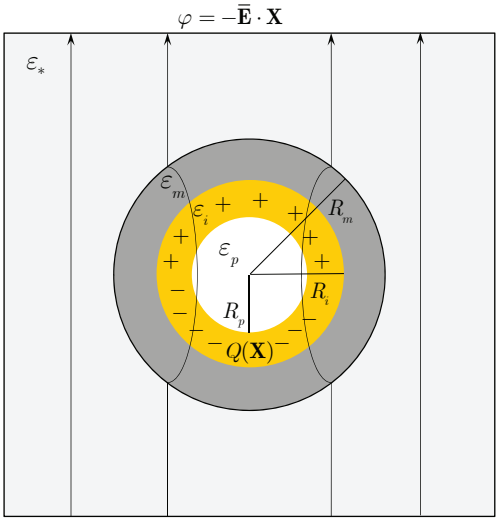

Figure 6.2: Schematic of a multicoated sphere with interphasial charges embedded in the homogeneous material with permittivity $\varepsilon_* \mathbf{I}$ under the affine boundary condition $\varphi(\mathbf{X}) = -\overline{\mathbf{E}} \cdot \mathbf{X}$ on $\partial\Omega$. The multicoated sphere acts as a neutral inclusion in that it does not alter the uniform electric field $\mathbf{E}(\mathbf{X}) = \overline{\mathbf{E}}$ outside of it.

For convenience, we choose the origin of the laboratory axes to coincide with the center of the multicoated sphere and write its heterogeneous permittivity in the compact form

$$\varepsilon(\mathbf{X})\mathbf{I} = [\theta_p(\mathbf{X})\varepsilon_p + \theta_i(\mathbf{X})\varepsilon_i + \theta_m(\mathbf{X})\varepsilon_m]\,\mathbf{I}, \tag{6.2}$$

where $\theta_p(\mathbf{X}) = 1$ if $|\mathbf{X}| \leq R_p$ and zero otherwise, $\theta_i(\mathbf{X}) = 1$ if $R_p \leq |\mathbf{X}| \leq R_i$ and zero otherwise, $\theta_m(\mathbf{X}) = 1$ if $R_i \leq |\mathbf{X}| \leq R_m$ and zero otherwise. Here, R_p, R_i, and R_m stand, respectively, for the radii of the core, the inner shell, and the outer shell; see Fig. 6.2. Similarly, the charge density is conveniently written as

$$Q(\mathbf{X}) = \theta_i(\mathbf{X})\, Q_i(\mathbf{X}). \tag{6.3}$$

In the sequel, for definiteness, we restrict attention to charge densities of the form

$$Q_i(\mathbf{X}) = q_i \, \frac{\overline{\mathbf{E}} \cdot \mathbf{X}}{R_p \, |\mathbf{X}|}, \tag{6.4}$$

where, again, R_p denotes the radius of the filler particle and q_i is any constant of choice (of units F/m) that physically can be viewed as a measure of charge content. The functional form of (6.4) is consistent with the interphasial charge distributions found in suspensions of dielectric spherical particles in electrolytic solutions under an external uniform electric field (Chew and Sen, 1982). It is also consistent with the charge distributions that develop on the surface of conducting spherical particles under the same boundary conditions (Owen, 2003). While sufficiently general for our purposes, the charge distribution (6.4) has the further merit to be simple enough to lead to fully explicit results.

The next step is to solve Gauss equations

$$\mathrm{Div}\,[-\varepsilon(\mathbf{X})\mathrm{Grad}\,\varphi] = Q(\mathbf{X}) \quad \text{for} \quad \mathbf{X} \in \Omega/\Gamma \tag{6.5}$$

and

$$[\![-\varepsilon(\mathbf{X})\mathrm{Grad}\,\varphi]\!] \cdot \mathbf{N} = 0 \quad \text{for} \quad \mathbf{X} \in \Gamma. \tag{6.6}$$

Here, $\mathbf{N} = \mathbf{X}/|\mathbf{X}|$ and $\Gamma = \{\Gamma_p, \Gamma_i, \Gamma_m\}$ has been introduced to denote the set of surfaces of material discontinuity $\Gamma_p = \{\mathbf{X} : |\mathbf{X}| = R_p\}$, $\Gamma_i = \{\mathbf{X} : |\mathbf{X}| = R_i\}$, and $\Gamma_m = \{\mathbf{X} : |\mathbf{X}| = R_m\}$. Making use of spherical coordinates, we look for solutions of the form

$$\varphi(\mathbf{X}) = \begin{cases} a_p R\cos\Phi \quad \text{for } R \le R_p \\ \\ \left[a_i R + \dfrac{b_i}{R^2} - \dfrac{q_i|\overline{\mathbf{E}}|}{4R_p\varepsilon_i}R^2\right]\cos\Phi \text{ for } R_p \le R \le R_i \\ \\ \left[a_m R + \dfrac{b_m}{R^2}\right]\cos\Phi \quad \text{for } R_i \le R \le R_m \\ \\ -|\overline{\mathbf{E}}|R\cos\Phi \quad \text{for } R \ge R_m \end{cases}, \tag{6.7}$$

where $R = |\mathbf{X}|$ and Φ denotes the angle between the applied electric field $\overline{\mathbf{E}}$ and the position vector $\mathbf{X}$. It is straightforward to verify that the electric potential (6.7) satisfies identically the Poisson's equation (6.5). The jump

conditions (6.6) entail that

$$\begin{aligned}
&\varepsilon_p a_p = \varepsilon_i \left[a_i - 2\frac{b_i}{R_p^3} - \frac{q_i|\overline{\mathbf{E}}|}{2\varepsilon_i} \right], \\
&\varepsilon_i \left[a_i - 2\frac{b_i}{R_i^3} - \frac{q_i|\overline{\mathbf{E}}|}{2R_p\varepsilon_i} R_i \right] = \varepsilon_m \left[a_m - 2\frac{b_m}{R_i^3} \right], \\
&\varepsilon_m \left[a_m - 2\frac{b_m}{R_m^3} \right] = -\varepsilon_* |\overline{\mathbf{E}}|,
\end{aligned} \tag{6.8}$$

while the continuity of the electric potential entails further that

$$\begin{aligned}
&a_p R_p = a_i R_p + \frac{b_i}{R_p^2} - \frac{q_i|\overline{\mathbf{E}}|}{4\varepsilon_i} R_p, \\
&a_i R_i + \frac{b_i}{R_i^2} - \frac{q_i|\overline{\mathbf{E}}|}{4R_p\varepsilon_i} R_i^2 = a_m R_i + \frac{b_m}{R_i^2}, \\
&a_m R_m + \frac{b_m}{R_m^2} = -|\overline{\mathbf{E}}| R_m.
\end{aligned} \tag{6.9}$$

Relations (6.8)–(6.9) constitute a system of six linear algebraic equations for the six unknowns a_p, a_i, b_i, a_m, b_m, ε_*, and thus admit a unique solution. After introducing the notation

$$c_p = \frac{R_p^3}{R_m^3} \quad \text{and} \quad c_i = \frac{R_i^3 - R_p^3}{R_m^3} \tag{6.10}$$

for the volume fractions of the particle c_p and the interphase c_i, the solution for the permittivity ε_* can be written explicitly as

$$\begin{aligned}
\varepsilon_* = \varepsilon_m + 3\varepsilon_m(c_i + c_p) &\left[c_i(\varepsilon_i - \varepsilon_m)(2\varepsilon_i + \varepsilon_p) + 3c_p\varepsilon_i(\varepsilon_p - \varepsilon_m) \right] / A \\
&+ 3\varepsilon_m c_p(c_i + c_p) \times \\
&\left[\left(\frac{c_i}{c_p} + 1 \right)^{4/3} (2\varepsilon_i + \varepsilon_p) + 4 \left(\frac{c_i}{c_p} + 1 \right)^{1/3} (\varepsilon_i - \varepsilon_p) + 3(\varepsilon_p - \varepsilon_i) \right] q_i / 4A
\end{aligned} \tag{6.11}$$

where

$$\begin{aligned}
A = \varepsilon_p &[\varepsilon_i(1 - c_i - c_p)(c_i + 3c_p) + c_i\varepsilon_m(c_i + c_p + 2)] \\
&+ \varepsilon_i[\varepsilon_m(c_i + c_p + 2)(2c_i + 3c_p) - 2c_i\varepsilon_i(c_i + c_p - 1)].
\end{aligned} \tag{6.12}$$

The *exact closed-form* solution (6.11) characterizes the macroscopic permittivity of a matrix material with permittivity ε_m, filled with polydisperse spherical particles with permittivity ε_p and volume fraction c_p, that are bonded to the matrix through finite-size interphases with permittivity ε_i and volume fraction c_i containing space charges of the form (6.4). The following theoretical and practical remarks are in order:

i. In the absence of interphases altogether when $c_i = 0$ and $q_i = 0$, the macroscopic permittivity (6.11) reduces to the Maxwell-Garnett formula:

$$\varepsilon_* = \varepsilon_m + \frac{3c_p\varepsilon_m(\varepsilon_p - \varepsilon_m)}{2\varepsilon_m + \varepsilon_p + c_p(\varepsilon_m - \varepsilon_p)}. \tag{6.13}$$

When $\varepsilon_m \geq \varepsilon_p$ ($\varepsilon_m \leq \varepsilon_p$), this result also agrees with the Hashin-Shtrikman (Hashin and Shtrikman, 1962) lower (upper) bound for two-phase dielectrics with arbitrary (not necessarily particulate) isotropic microstructures. While the result (6.13) is unable to describe the permittivities of nanoparticulate composites observed in experiments, it does describe reasonably well the macroscopic permittivity of dielectrics filled with supranano-sized spherical particles over large ranges of volume fractions of particles (Hale, 1976).

ii. In the absence of charges when $q_i = 0$, the macroscopic permittivity (6.11) reduces to the result of Milton (1981):

$$\varepsilon_* = \varepsilon_m + \cfrac{3(c_p + c_i)\varepsilon_m}{1 - c_p - c_i + \cfrac{3\varepsilon_m}{\varepsilon_i - \varepsilon_m + \cfrac{3c_p\varepsilon_i}{c_i + \cfrac{3(c_p + c_i)\varepsilon_i}{\varepsilon_p - \varepsilon_i}}}} \tag{6.14}$$

for an assemblage of homothetic doubly coated spheres. While expression (6.14) accounts for finite-size interphases with homogeneous permittivity ε_i, possibly higher or lower from that of the matrix and particles, it is unable by itself to explain many of the unusually high and low permittivities of nanoparticulate composites observed in experiments. To see this, it suffices to recognize that the result (6.14) is

bounded from above by

$$\varepsilon_* \leq \varepsilon_m + \frac{3(c_p + c_i)}{1 - c_p - c_i}\varepsilon_m, \tag{6.15}$$

and from below by

$$\varepsilon_* \geq \varepsilon_m - \frac{3(c_p + c_i)}{2 + c_p + c_i}\varepsilon_m. \tag{6.16}$$

Thus, even in the limiting cases when $\varepsilon_i/\varepsilon_0 = +\infty$ or $\varepsilon_i/\varepsilon_0 = 1$ (with $\varepsilon_0 \approx 8.85 \times 10^{-12}$ F/m denoting the permittivity of vacuum), the enhancement or reduction in the macroscopic permittivity (6.14) is — away from percolation — only of order $O(\varepsilon_m)$.

iii. The macroscopic permittivity (6.11) is *linear* in q_i, a measure of the amount of charges in the interphases. Accordingly, given that the coefficient multiplying q_i is positive, large positive values of q_i can lead to a great enhancement of the macroscopic permittivity, whereas large negative values of q_i can lead to a great reduction (possibly rendering negative permittivities). Physically, these two behaviors can be understood as follows. Positive values of q_i imply that the interphasial charges form an overall dipole that is aligned in the same direction with the applied electric field $\overline{\mathbf{E}}$ and thus enhances the macroscopic permittivity. On the other hand, negative values of q_i imply that the charges form an overall dipole that is in the opposite direction to $\overline{\mathbf{E}}$ and thus reduces the macroscopic permittivity. In short, the result (6.11) reveals that the presence of interphasial charges can indeed describe and explain both, the enhanced as well as the reduced, dielectric response exhibited by emerging polymer nanoparticulate composites. More generally, it reveals that judicious manipulation of interphasial charges — by means, for instance, of particle surface treatments or coatings — provides a promising path forward for the design of materials with exceptional dielectric properties (and, by the same token (Huang et al., 2004), exceptional electromechanical properties).

6.2 Illustrative results and comparisons with experiments

To gain further physical insight into the properties of the formula (6.11), we now present some illustrative results within the context of comparisons with two representative sets of experiments, one exhibiting enhancement and one exhibiting reduction of the dielectric response.

Figure 6.3 shows results for the relative permittivity $\varepsilon_*/\varepsilon_0$ of a nanocomposite material made up of a P(VDF-TrFE-CTFE) matrix filled with PANI (polyaniline) particles, for a range of small volume fractions of particles c_p. P(VDF-TrFE-CTFE) is a dielectric polymer with permittivity approximately given by $\varepsilon_m/\varepsilon_0 = 52$. On the other hand, PANI is a conductive polymer. The permittivity of PANI particles is therefore modeled here as unbounded, $\varepsilon_p/\varepsilon_0 = +\infty$.

There are four sets of data displayed in Fig. 6.3. The solid line corresponds to the full theoretical result (6.11) for the basic case when the permittivity of the interphases is equal to that of the P(VDF-TrFE-CTFE) matrix, $\varepsilon_i/\varepsilon_0 = \varepsilon_m/\varepsilon_0 = 52$, the thicknesses of the interphases are one-third the size of the radius of the particles that they surround, $t_i/R_p \doteq (R_i - R_p)/R_p = (c_i/c_p + 1)^{1/3} - 1 = 1/3$, and the charge-content parameter is $q_i/\varepsilon_0 = 5200$, two orders of magnitude larger than the matrix permittivity. The triangles correspond to the experiments (measured at room temperature and 1000 Hz) of Huang et al. (2004). The dash line corresponds to the Milton formula (6.14), which, again, accounts for a finite-size interphase between the particles and the matrix but *not* for interphasial charges. In particular, the result displayed in the figure corresponds to interphases of infinite permittivity, $\varepsilon_i/\varepsilon_0 = +\infty$, whose thicknesses are one-third the size of the particles that they surround, $t_i/R_p = 1/3$. Finally, the dotted line corresponds to the Maxwell-Garnett formula (6.13), which does not account for any interphasial phenomena whatsoever.

The main observation from Fig. 6.3 is that the theoretical result (6.11) is able to describe the drastic enhancement exhibited by the experimental data when evaluated at physically sound values of the size of the interphases ($t_i/R_p = 1/3$) and their charge content ($q_i/\varepsilon_0 = 5200$). Another key observation is that interphases with (infinitely) high permittivity but that do not contain space charges can generate a substantial enhancement of the macro-

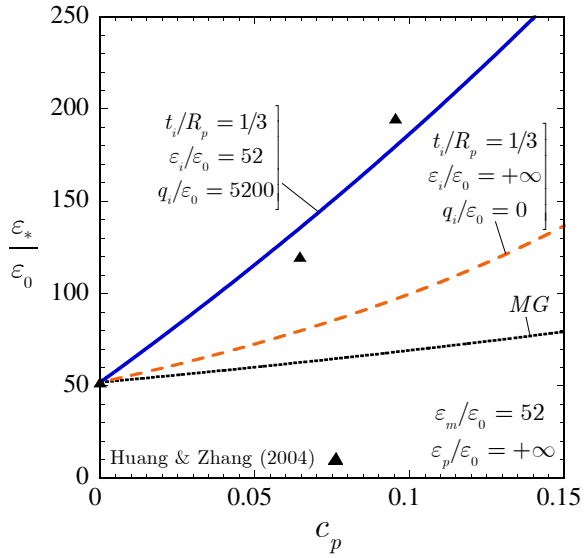

Figure 6.3: Relative permittivity $\varepsilon_*/\varepsilon_0$ of a nanocomposite made up of a P(VDF-TrFE-CTFE) matrix ($\varepsilon_m/\varepsilon_0 = 52$) filled with PANI particles ($\varepsilon_p/\varepsilon_0 = +\infty$), as a function of the volume fraction of particles c_p. The data shown correspond to the theoretical result (6.11) accounting for interphasial charges (solid line), the experiments of Huang et al. (2004) (triangles), the result (6.14) of Milton accounting for interphases with much higher permittivity than that of the matrix (dashed line), and the Maxwell-Garnett formula (dotted line).

scopic dielectric response but not in any way as substantial as that generated by interphases that do contain charges. From the glaring disagreement of the Maxwell-Garnett formula with the other three results, Fig. 6.3 also makes it plain that interphasial phenomena, as expected, dominate the dielectric response of nanocomposites.

Figure 6.4 shows results for the relative permittivity $\varepsilon_*/\varepsilon_0$ of a PDMS (polydimethylsiloxane) elastomer filled with polycrystalline anatase titania particles, for a range of small volume fractions of particles c_p. PDMS is a dielectric elastomer with permittivity approximately given by $\varepsilon_m/\varepsilon_0 = 3.5$. The permittivity of the polycrystalline anatase titania utilized here is much higher, $\varepsilon_p/\varepsilon_0 = 100$.

The triangles and circles in Fig. 6.4 correspond to new[3] experimental data (obtained at room temperature and at 1000 Hz). In particular, the triangles correspond to nanocomposites wherein the titania particles are spheres of radius $R_p = 10$ nm; Fig. 6.1 shows a representative electron micrograph

[3]Full experimental details together with a comprehensive set of electromechanical measurements will be reported elsewhere.

of one of the samples with particle volume fraction $c_p = 0.01$. The circles, on the other hand, correspond to microcomposites wherein the titania particles are only roughly spherical in shape (since they were synthesized in the form of a fine powder) and about 1 μm in average radius. Moreover, the solid line in Fig. 6.4 corresponds to the theoretical result (6.11) for the case when the permittivity of the interphases is equal to that of the PDMS matrix, $\varepsilon_i/\varepsilon_0 = \varepsilon_m/\varepsilon_0 = 3.5$, the interphase-thickness-to-particle-radius ratio is $t_i/R_p = 0.35$, and the charge-content parameter is $q_i/\varepsilon_0 = -350$. The dashed line pertains to the Milton formula (6.14) for the case of interphases with the limiting permittivity of vacuum, $\varepsilon_i/\varepsilon_0 = 1$, whose ratio of thickness to particle radius is $t_i/R_p = 0.35$. The dotted line stands again for the Maxwell-Garnett formula (6.13).

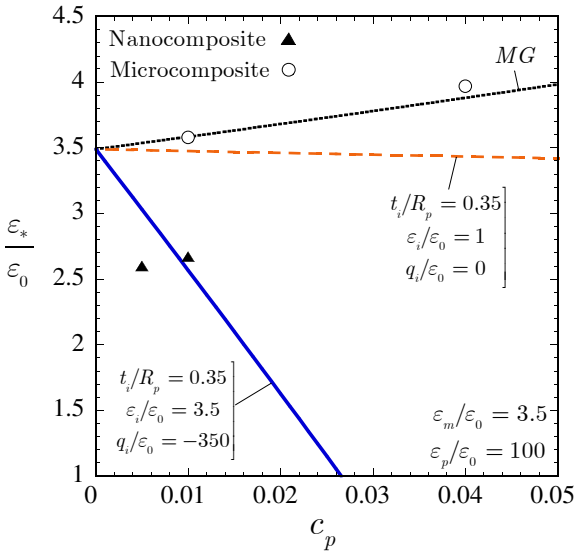

Figure 6.4: Relative permittivity $\varepsilon_*/\varepsilon_0$ of a PDMS elastomer ($\varepsilon_m/\varepsilon_0 = 3.5$) filled with polycrystalline anatase titania particles, as a function of the volume fraction of particles c_p ($\varepsilon_p/\varepsilon_0 = 100$). The data shown correspond to the theoretical result (6.11) accounting for interphasial charges (solid line), experiments wherein the particles are 10 nm (triangles) and 1 μm (circles) in radius, the result (6.14) of Milton accounting for interphases with much lower permittivity than that of the matrix (dashed line), and the Maxwell-Garnett formula (dotted line).

It is plain from Fig. 6.4 that the Maxwell-Garnett formula correlates well with the experimental results for the microcomposite but *not* with those for the nanocomposite, which, consistent with earlier observationsNelson and John (2004), are seen to exhibit a reduction in permittivity with the addi-

tion of titania particles (in spite of the fact that titania has a much higher permittivity than PDMS). The Milton result accounting for interphases of physically plausible size (3.5 nm in thickness, since $t_i = 0.35 \times R_p = 3.5$ nm) with much lower permittivity (that of vacuum in fact, $\varepsilon_i/\varepsilon_0 = 1$) than that of the matrix is seen to lead to slightly lower permittivities with the addition of particles, but not in any way as low as those experimentally displayed by the nanocomposite. By contrast, the theoretical result (6.11) accounting for interphases with the same physically plausible size (3.5 nm in thickness) that contain a small content of charges ($q_i/\varepsilon_0 = -350$) is able to describe the drastic reduction in dielectric response exhibited by the nanocomposite.

CHAPTER 7

CONCLUDING REMARKS

Theoretical and Numerical frameworks has been developed to explain and predict the macroscopic behavior of filled elastomers. The theory provides mathematically sound and quantitatively accurate analytical and approximate solutions to characterize the behavior of non-Gaussian elastomers containing isotropic distribution of rigid spherical particles bounded to the elastomeric matrix through finite size elastomeric interphases. Comparisons with results of numerical simulations as well as experimental results prove the superb ability of the framework in characterizing the behavior of these very important class of composite materials.

7.1 Theoretical framework to account for reinforcing mechanism in filled elastomers

Accounting for the hydrodynamic effect as well as interphasial effects — the major contributors to the overall behavior of filled elastomers — the framework provides a new base for describing the macroscopic behavior of filled elastomers which is of practical interest in design of these materials for advanced applications. Exact and approximate fundamental dilute solutions have been provided throughout this document for the effective behavior of Neo-Hookean matrices containing isotropic distribution of rigid spherical particles firmly bonded to the matrix through interphases. Existence of these fundamental solutions are seminal to tackle the general problem of filler reinforcing mechanisms in filled elastomers through developing a powerful theoretical machinery that can intake any fundamental dilute solution — of the

type derived in this work — and generate solutions for the general problem.

It is noteworthy remarking that in addition to the hydrodynamic and interphasial reinforcement effects, the presence of occluded rubber may also provide additional reinforcement. Occluded rubber refers to the regions of elastomer that are entrapped by the agglomeration of filler particles. To a first approximation, because of its shielding from the rest of the elastomer, its constitutive behavior can be idealized as rigid. In this case, the presence of occluded rubber can be accounted for by the proposed theory by simply reinterpreting c_p as the combined total concentration of fillers and occluded rubber.

The developed framework for non-Convex homogenization, in this work, in its essence, is not limited to the mechanical problems and can be utilized to characterize multi-functional behavior of filled elastomers under coupled fields (e.g., electro/magneto-mechanical behavior) (see, e.g., Lopez-Pamies, 2014). As another problem of interest that can be further perused one can mention particulate composites with interphases which are softer than the matrix (as oppose to what we have considered throughout this work). The existence of soft interphases may allow for debonding and instabilities under some loading conditions.

7.2 Composite-ellipsoid assemblage: A framework for filled elastomers with anisotropic microstructures

Incorporation of composite assemblages in the realm of nonlinear elasticity has been detailed in this document. What has been done so far, is only a debut, and further development is needed. There are possibilities to increase the accuracy of the method by incorporating more sophisticated boundary conditions.

In general, the variational method proposed in Chapter 5 and Goudarzi and Lopez-Pamies (2013) constitutes a powerful platform from which to account for more levels of complexity to model soft solids with anisotropic particulate microstructures. Recent experimental studies have revealed (see, e.g, Chapter 6 in Carpi et al., 2008; Danas et al., 2012) that anisotropic distributions of fillers, such as for instance the chain-like distributions shown in Fig. 7.1(a), may serve to enhance certain multifunctional properties of filled elas-

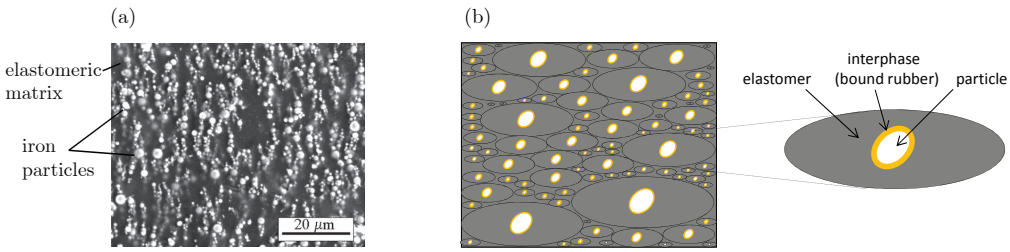

Figure 7.1: (a) Electron micrograph of a magnetorheological elastomer with iron particles distributed anisotropically in chain-like structures (Danas et al., 2012) and (b) its idealization as an ellipsoidal assemblage of possibly non-spherical particles (CEA). All the composite ellipsoids in the assemblage are homothetic in that they are scaled-up or scaled-down versions of each other. Part (b) also illustrates schematically the straightforward incorporation of bound rubber into the CEA idealization.

tomers, including their electro/magnetostriction capabilities. These — and even more complex — microstructures can be idealized as assemblages of composite ellipsoids, wherein the filler particle can be chosen of any required anisotropic shape (not necessarily ellipsoidal). Figure 7.1(b) depicts schematically the case of a composite-ellipsoid assemblage (CEA) of non-spherical particles; all the ellipsoids in the assemblage are scaled-up or scaled-down versions of each other (see, e.g., Chapter 7 in Milton, 2002; Bornert et al., 1996).

It is a simple matter to show that the formulation presented in Section 5.2.2 for CSAs is actually applicable more generally to CEAs — with the domain $\mathcal{B}$ then denoting the single composite ellipsoid of interest. The variational framework (5.17)–(5.20) provides thus a numerically efficient means to bottom-up model the overall nonlinear elastic response of elastomers filled with general classes of anisotropic distributions of particles of anisotropic shapes under arbitrarily large deformations.

7.3 Accounting for space charges in homogenization of dielectric elastomer composites

Accounting for space charges via composite assemblages idea is among the first of its kind dealing with source terms oscillating at microscale. Based on the theoretical solutions provided in Chapter 6, a design guideline for

synthesizing composite metamaterials with dielectric constants far beyond their constituent phases has been proposed.

Interpretation of the existing experimental results for dielectric constant of nanocomposites (as in Lopez-Pamies et al., 2014; Racherla et al., 2010) by considering existence of interphasial charges is a conjecture to be investigated further experimentally, since the amount of the interphasial charges assumed in order to fit the experimental results are orders of magnitude larger than the amount of charges migrating to the surface of metallic particles in presence of an electric potential.

APPENDIX A

THE COEFFICIENTS α_1, α_2, α_3

The coefficients α_1, α_2, α_3 in the pdes (2.22), (2.32), and (2.35) are given by

$$\begin{aligned}
\alpha_1(\overline{\lambda}_1,\overline{\lambda}_2) &= \frac{\overline{\lambda}_1^5\overline{\lambda}_2^3\left(3\overline{\lambda}_1^4\overline{\lambda}_2^2-2\overline{\lambda}_1^2\overline{\lambda}_2^4-1\right)}{3\left(\overline{\lambda}_1^2-\overline{\lambda}_2^2\right)\left(\overline{\lambda}_1^4\overline{\lambda}_2^2-1\right)^2}\Gamma_F \\
&+ \frac{2\overline{\lambda}_1^3\left(2\overline{\lambda}_1^6\overline{\lambda}_2^7-\overline{\lambda}_1^4\overline{\lambda}_2^9-2\overline{\lambda}_1^4\overline{\lambda}_2^3+\overline{\lambda}_2\right)}{3(\overline{\lambda}_1-\overline{\lambda}_2)^2(\overline{\lambda}_1+\overline{\lambda}_2)^2\left(\overline{\lambda}_1^4\overline{\lambda}_2^2-1\right)^2}\Gamma_E \\
&+ \frac{\overline{\lambda}_1^2\overline{\lambda}_2^2-\overline{\lambda}_1^8\overline{\lambda}_2^2-2\overline{\lambda}_1^6\overline{\lambda}_2^4+\overline{\lambda}_1^4\left(\overline{\lambda}_2^6+1\right)}{3\left(\overline{\lambda}_1^2-\overline{\lambda}_2^2\right)^2\left(\overline{\lambda}_1^4\overline{\lambda}_2^2-1\right)}, \\
\alpha_2(\overline{\lambda}_1,\overline{\lambda}_2) &= \frac{\overline{\lambda}_1^3\overline{\lambda}_2^5}{3\left(\overline{\lambda}_1^2-\overline{\lambda}_2^2\right)\left(\overline{\lambda}_1^2\overline{\lambda}_2^4-1\right)}\Gamma_F \\
&- \frac{2\overline{\lambda}_1\overline{\lambda}_2^3\left(\overline{\lambda}_1^4\overline{\lambda}_2^2-2\overline{\lambda}_1^2\overline{\lambda}_2^4+1\right)}{3\left(\overline{\lambda}_1^2-\overline{\lambda}_2^2\right)^2\left(\overline{\lambda}_1^2\overline{\lambda}_2^4-1\right)}\Gamma_E \\
&+ \frac{\left(\overline{\lambda}_1^6+1\right)\overline{\lambda}_2^4-2\overline{\lambda}_1^4\overline{\lambda}_2^6-\overline{\lambda}_1^2\overline{\lambda}_2^8+\overline{\lambda}_1^2\overline{\lambda}_2^2}{3\left(\overline{\lambda}_1^2-\overline{\lambda}_2^2\right)^2\left(\overline{\lambda}_1^2\overline{\lambda}_2^4-1\right)}, \\
\alpha_3(\overline{\lambda}_1,\overline{\lambda}_2) &= -\frac{2\overline{\lambda}_1^4\overline{\lambda}_2^4}{3\left(\overline{\lambda}_1^2-\overline{\lambda}_2^2\right)\left(\overline{\lambda}_1^4\overline{\lambda}_2^2-1\right)}\Gamma_F \\
&- \frac{2\overline{\lambda}_1^2\overline{\lambda}_2^2\left(\overline{\lambda}_1^4\overline{\lambda}_2^2+\overline{\lambda}_1^2\overline{\lambda}_2^4-2\right)}{3\left(\overline{\lambda}_1^2-\overline{\lambda}_2^2\right)^2\left(\overline{\lambda}_1^4\overline{\lambda}_2^2-1\right)}\Gamma_E+\frac{2\overline{\lambda}_1\overline{\lambda}_2\left(\overline{\lambda}_1^2+\overline{\lambda}_2^2\right)}{3\left(\overline{\lambda}_1^2-\overline{\lambda}_2^2\right)^2}
\end{aligned} \tag{A.1}$$

with

$$\Gamma_F = \frac{1}{\sqrt{1-\overline{\lambda}_1^2\overline{\lambda}_2^4}}\mathcal{E}_{\mathcal{F}}\left[\phi_{\mathcal{E}}; \frac{\overline{\lambda}_1^4\overline{\lambda}_2^2-1}{\overline{\lambda}_1^2\overline{\lambda}_2^4-1}\right],$$
$$\Gamma_E = \frac{1}{\sqrt{1-\overline{\lambda}_1^2\overline{\lambda}_2^4}}\mathcal{E}_{\mathcal{E}}\left[\phi_{\mathcal{E}}; \frac{\overline{\lambda}_1^4\overline{\lambda}_2^2-1}{\overline{\lambda}_1^2\overline{\lambda}_2^4-1}\right], \tag{A.2}$$

where

$$\phi_{\mathcal{E}} = \frac{\sqrt{1-\overline{\lambda}_1^2\overline{\lambda}_2^4}}{2\sqrt{\overline{\lambda}_1^2\overline{\lambda}_2^4-1}}\ln\left[2\overline{\lambda}_1\overline{\lambda}_2^2\left(\overline{\lambda}_1\overline{\lambda}_2^2+\sqrt{\overline{\lambda}_1^2\overline{\lambda}_2^4-1}\right)-1\right], \tag{A.3}$$

and the functions $\mathcal{E}_{\mathcal{F}}$ and $\mathcal{E}_{\mathcal{E}}$ stand for, respectively, the elliptic integrals of first and second kind, as defined by

$$\mathcal{E}_{\mathcal{F}}\left[\varphi;t\right] = \int_0^{\varphi}\left[1-t\sin^2\theta\right]^{-1/2}\mathrm{d}\theta \text{ and } \mathcal{E}_{\mathcal{E}}\left[\varphi;t\right] = \int_0^{\varphi}\left[1-t\sin^2\theta\right]^{1/2}\mathrm{d}\theta. \tag{A.4}$$

By direct inspection we remark that

$$\begin{aligned}
&\alpha_1(\overline{\lambda}_1,\overline{\lambda}_2) = \alpha_2(\overline{\lambda}_2,\overline{\lambda}_1),\\
&\alpha_3(\overline{\lambda}_1,\overline{\lambda}_2) = \alpha_3(\overline{\lambda}_2,\overline{\lambda}_1),\\
&\alpha_1(\overline{\lambda}_1,\overline{\lambda}_2) = \alpha_1\left(\overline{\lambda}_1,(\overline{\lambda}_1\overline{\lambda}_2)^{-1}\right),\\
&\alpha_2(\overline{\lambda}_1,\overline{\lambda}_2) = \frac{\alpha_1\left(\overline{\lambda}_1,(\overline{\lambda}_1\overline{\lambda}_2)^{-1}\right)}{\overline{\lambda}_1^4\overline{\lambda}_2^2} + \frac{\alpha_2\left(\overline{\lambda}_1,(\overline{\lambda}_1\overline{\lambda}_2)^{-1}\right)}{\overline{\lambda}_1^2\overline{\lambda}_2^4} + \frac{\alpha_3\left(\overline{\lambda}_1,(\overline{\lambda}_1\overline{\lambda}_2)^{-1}\right)}{\overline{\lambda}_1^3\overline{\lambda}_2^3},\\
&\alpha_3(\overline{\lambda}_1,\overline{\lambda}_2) = -\frac{2\alpha_1\left(\overline{\lambda}_1,(\overline{\lambda}_1\overline{\lambda}_2)^{-1}\right)}{\overline{\lambda}_1^2\overline{\lambda}_2} - \frac{\alpha_3\left(\overline{\lambda}_1,(\overline{\lambda}_1\overline{\lambda}_2)^{-1}\right)}{\overline{\lambda}_1\overline{\lambda}_2^2},\\
&\alpha_1(\overline{\lambda}_1,\overline{\lambda}_2) = \frac{\alpha_1\left((\overline{\lambda}_1\overline{\lambda}_2)^{-1},\overline{\lambda}_2\right)}{\overline{\lambda}_1^4\overline{\lambda}_2^2} + \frac{\alpha_2\left((\overline{\lambda}_1\overline{\lambda}_2)^{-1},\overline{\lambda}_2\right)}{\overline{\lambda}_1^2\overline{\lambda}_2^4} + \frac{\alpha_3\left((\overline{\lambda}_1\overline{\lambda}_2)^{-1},\overline{\lambda}_2\right)}{\overline{\lambda}_1^3\overline{\lambda}_2^3},\\
&\alpha_2(\overline{\lambda}_1,\overline{\lambda}_2) = \alpha_2\left((\overline{\lambda}_1\overline{\lambda}_2)^{-1},\overline{\lambda}_2\right),\\
&\alpha_3(\overline{\lambda}_1,\overline{\lambda}_2) = -\frac{2\alpha_2\left((\overline{\lambda}_1\overline{\lambda}_2)^{-1},\overline{\lambda}_2\right)}{\overline{\lambda}_1\overline{\lambda}_2^2} - \frac{\alpha_3\left((\overline{\lambda}_1\overline{\lambda}_2)^{-1},\overline{\lambda}_2\right)}{\overline{\lambda}_1^2\overline{\lambda}_2},
\end{aligned} \tag{A.5}$$

and

$$\alpha_1(\overline{\lambda},\overline{\lambda}) = \alpha_2(\overline{\lambda},\overline{\lambda}) = \frac{-2+\overline{\lambda}^6-8\overline{\lambda}^{12}}{24(\overline{\lambda}^6-1)^2} + \frac{3\overline{\lambda}^{12}}{8(1-\overline{\lambda}^6)^{5/2}} \ln\left[\frac{1+\sqrt{1-\overline{\lambda}^6}}{\overline{\lambda}^3}\right], \tag{A.6}$$

$$\alpha_3(\overline{\lambda},\overline{\lambda}) = \frac{2-5\overline{\lambda}^6}{12(\overline{\lambda}^6-1)^2} + \frac{\overline{\lambda}^{12}}{4(1-\overline{\lambda}^6)^{5/2}} \ln\left[\frac{1+\sqrt{1-\overline{\lambda}^6}}{\overline{\lambda}^3}\right]. \tag{A.7}$$

We further remark that

$$\begin{aligned} -\frac{1}{3} \le \alpha_1(\overline{\lambda}_1,\overline{\lambda}_2) \le 0, \quad -\frac{1}{3} \le \alpha_2(\overline{\lambda}_1,\overline{\lambda}_2) \le 0, \\ 0 \le \alpha_3(\overline{\lambda}_1,\overline{\lambda}_2) \le \frac{1}{6} \quad \forall\, \overline{\lambda}_1,\overline{\lambda}_2 > 0. \end{aligned} \tag{A.8}$$

APPENDIX B

THE FUNCTION H

In this appendix, we sketch out the main properties of the function $H : \{(a,b) \in \mathbb{R}^2 : a,b > 0\} \to \mathbb{R}$ defined by the Eikonal initial-value problem (2.35)–(2.36) and provide details on its numerical computation. We begin by recognizing from relations (A.5)–(A.7) that equations (2.35)–(2.36) admit solutions such that

$$\begin{aligned} H(\overline{\lambda}_1,\overline{\lambda}_2) = H(\overline{\lambda}_2,\overline{\lambda}_1) = H\left(\overline{\lambda}_1,(\overline{\lambda}_1\overline{\lambda}_2)^{-1}\right) = H\left((\overline{\lambda}_1\overline{\lambda}_2)^{-1},\overline{\lambda}_1\right) \\ = H\left(\overline{\lambda}_2,(\overline{\lambda}_1\overline{\lambda}_2)^{-1}\right) = H\left((\overline{\lambda}_1\overline{\lambda}_2)^{-1},\overline{\lambda}_2\right) \qquad \forall\, \overline{\lambda}_1,\overline{\lambda}_2. \end{aligned} \tag{B.1}$$

as required by the last of the conditions (2.24). A direct implication (see, e.g., Chapter 4 in the monograph by Ogden, 1997) of the symmetry properties (B.1) is that H may be written in the polynomial form

$$H(\overline{\lambda}_1,\overline{\lambda}_2) = \sum_{p,q=0}^{\infty} k_{pq}(\overline{\lambda}_1 - 1)^p(\overline{\lambda}_2 - 1)^q, \tag{B.2}$$

where it is emphasized that the coefficients k_{pq} are not entirely independent but constrained by conditions (B.1). Substituting the representation (B.2) in (2.35)–(2.36) and taking the limit of small deformations as $\overline{\lambda}_1 \to 1$ and $\overline{\lambda}_2 \to 1$ leads to a hierarchy of systems of algebraic equations for the unknown coefficients k_{pq}. These systems are *linear* and hence have a *unique* solution, however, they do not appear to admit a simple recurrence solution and must therefore be solved successively one at a time. For the first four sets of

equations, the solutions read as

$$k_{00} = 0, \qquad k_{10} = k_{01} = 0, \qquad k_{20} = k_{02} = k_{11} = \frac{5}{2},$$
$$k_{30} = k_{03} = -\frac{5}{2},\ k_{21} = k_{12} = -\frac{55}{14}. \tag{B.3}$$

According to the result (B.2) with (B.3), the point $\overline{\lambda}_1 = \overline{\lambda}_2 = 1$ corresponds to a local minimum of H at which $H(1,1) = 0$. Now, from the pde (2.35) it is easy to deduce that the value of the function H evaluated at any critical point (i.e., any point $\overline{\lambda}_1, \overline{\lambda}_2$ at which $\partial H/\partial\overline{\lambda}_1 = \partial H/\partial\overline{\lambda}_2 = 0$) must be necessarily zero. These two results entail then that the point $\overline{\lambda}_1 = \overline{\lambda}_2 = 1$ is the only critical point of the function H defined by (2.35)–(2.36), that this point corresponds to its global minimum, and hence that

$$H(1,1) = 0 \qquad \text{and} \qquad H(\overline{\lambda}_1, \overline{\lambda}_2) > 0 \quad \forall\, \overline{\lambda}_1, \overline{\lambda}_2 \neq 1, \tag{B.4}$$

as required by the first two conditions (2.24).

It also follows from (B.2) with (B.3) that in the limit of small deformations as $\overline{\lambda}_1 \to 1$ and $\overline{\lambda}_2 \to 1$, the function H is indeed given explicitly by relation (2.37) in the main body of the text. In the opposite limit of infinitely large deformations as $\overline{\lambda}_1 \to +\infty$, it is not difficult to recognize that equations (2.35)–(2.36) admit the explicit asymptotic solution

$$H(\overline{\lambda}_1, \overline{\lambda}_2) = \frac{3}{4}\,\overline{\lambda}_1^{\,2} - \frac{9}{16}\left[\ln 4 + 2\ln\overline{\lambda}_2 + 4\ln\overline{\lambda}_1\right]\overline{\lambda}_1^{\,-1} + O(\overline{\lambda}_1^{\,-2}). \tag{B.5}$$

From the symmetry condition $H(\overline{\lambda}_1, \overline{\lambda}_2) = H(\overline{\lambda}_2, \overline{\lambda}_1)$ it follows that

$$H(\overline{\lambda}_1, \overline{\lambda}_2) = \frac{3}{4}\overline{\lambda}_2^{\,2} - \frac{9}{16}\left[\ln 4 + 2\ln\overline{\lambda}_1 + 4\ln\overline{\lambda}_2\right]\overline{\lambda}_2^{\,-1} + O(\overline{\lambda}_2^{\,-2}) \tag{B.6}$$

for $\overline{\lambda}_2 \to +\infty$. Moreover, the asymptotic solution of equations (2.35)–(2.36) for the case when $\overline{\lambda}_1 \to 0$ is given by

$$H(\overline{\lambda}_1, \overline{\lambda}_2) = \frac{3}{4}\,\frac{1}{\overline{\lambda}_1^{\,2}\overline{\lambda}_2^{\,2}} + \frac{3}{4}\overline{\lambda}_2^{\,2} + O\left(\overline{\lambda}_1 \ln\overline{\lambda}_1\right), \tag{B.7}$$

and from the symmetry $H(\overline{\lambda}_1, \overline{\lambda}_2) = H(\overline{\lambda}_2, \overline{\lambda}_1)$ we also then have that

$$H(\overline{\lambda}_1, \overline{\lambda}_2) = \frac{3}{4}\frac{1}{\overline{\lambda}_1^2 \overline{\lambda}_2^2} + \frac{3}{4}\overline{\lambda}_1^2 + O\left(\overline{\lambda}_2 \ln \overline{\lambda}_2\right) \tag{B.8}$$

for infinitely large deformations with $\overline{\lambda}_2 \to 0$. Combining results (B.5)–(B.8) it readily follows that in the limit of infinitely large deformations (as $\overline{\lambda}_1 \to 0, +\infty$ and/or $\overline{\lambda}_2 \to 0, +\infty$) the function H defined by equations (2.35)–(2.36) is given explicitly, to leading order, by relation (2.38) in the main body of the text.

The numerical solution of the initial-value problem (2.35)–(2.36) for H can be generated in a number of different ways using finite differences. We found it more efficient to consider the problem in the alternative set of variables $\overline{L}_1 = \overline{\lambda}_1^2 \overline{\lambda}_2$ and $\overline{L}_2 = \overline{\lambda}_1 / \overline{\lambda}_2$, instead of in terms of the principal stretches $\overline{\lambda}_1$ and $\overline{\lambda}_2$ directly. The advantage of these variables is twofold: *i*) the finite-difference discretization can be performed on a simple Cartesian grid with unilateral boundaries $\overline{L}_1 \geq 1$ and $\overline{L}_2 \geq 1$, and *ii*) the initial condition (2.36) in $\overline{L}_1$–$\overline{L}_2$-space is given at the constant value of $\overline{L}_2 = 1$. The commercial package *Wolfram Mathematica 8.0* was utilized to discretize and solve the equations. In spite of the quadratic nonlinearity of the pde (2.35), we note that the initial-value problem (2.35)–(2.36) admits only one solution that is consistent with the required conditions (B.1) and (B.4).

APPENDIX C

CONDITIONS FOR STRONG ELLIPTICITY AND POLYCONVEXITY OF $\overline{W}$

Explicit necessary and sufficient conditions for an isotropic incompressible stored-energy function to be strongly elliptic have been provided by Zee and Sternberg (1983). When the stored-energy function is written in the form $\overline{W} = \overline{W}(\overline{\lambda}_1, \overline{\lambda}_2)$ with $\overline{\lambda}_3 = \overline{\lambda}_1^{-1}\overline{\lambda}_2^{-1}$, as done in Chapter 1, the conditions read as

$$\begin{aligned}
&\beta_i > 0 \qquad\qquad (i = 1, 2, 3),\\
&w_i + 2\overline{\lambda}_i\beta_i > 0 \qquad (i = 1, 2, 3;\ \text{no summation}),\\
&\left[\overline{\lambda}_2^{-1}\sqrt{w_2 + 2\overline{\lambda}_2\beta_2} + \overline{\lambda}_3^{-1}\sqrt{w_3 + 2\overline{\lambda}_3\beta_3}\right]^2 - \overline{\lambda}_1^{-2}(w_1 - 2\overline{\lambda}_1\beta_1) > 0,\\
&\left[\overline{\lambda}_3^{-1}\sqrt{w_3 + 2\overline{\lambda}_3\beta_3} + \overline{\lambda}_1^{-1}\sqrt{w_1 + 2\overline{\lambda}_1\beta_1}\right]^2 - \overline{\lambda}_2^{-2}(w_2 - 2\overline{\lambda}_2\beta_2) > 0,\\
&\left[\overline{\lambda}_1^{-1}\sqrt{w_1 + 2\overline{\lambda}_1\beta_1} + \overline{\lambda}_2^{-1}\sqrt{w_2 + 2\overline{\lambda}_2\beta_2}\right]^2 - \overline{\lambda}_3^{-2}(w_3 - 2\overline{\lambda}_3\beta_3) > 0.
\end{aligned} \tag{C.1}$$

Here,

$$\beta_1 = \beta\left(\overline{\lambda}_2, (\overline{\lambda}_1\overline{\lambda}_2)^{-1}\right), \quad \beta_2 = \beta\left((\overline{\lambda}_1\overline{\lambda}_2)^{-1}, \overline{\lambda}_1\right), \quad \beta_3 = \beta\left(\overline{\lambda}_1, \overline{\lambda}_2\right), \tag{C.2}$$

$$w_1 = w\left(\overline{\lambda}_2, (\overline{\lambda}_1\overline{\lambda}_2)^{-1}\right), \quad w_2 = w\left((\overline{\lambda}_1\overline{\lambda}_2)^{-1}, \overline{\lambda}_1\right), \quad w_3 = w\left(\overline{\lambda}_1, \overline{\lambda}_2\right), \tag{C.3}$$

with

$$\beta(x, y) = \begin{cases} \dfrac{1}{8}\overline{W}_{11}\left(z, z^{-2}\right) & \text{if} \quad x = y = z \\ -\dfrac{1}{2}y\left(x^2 - y^2\right)^{-1}\overline{W}_1\left(y, (xy)^{-1}\right) & \text{otherwise} \end{cases}, \tag{C.4}$$

$$w(x,y) = \begin{cases} \dfrac{1}{4} z^{-2} \overline{W}_{11}\left(z, z^{-2}\right) & \text{if } x = y = z \\ y^{-1}\left(x^2 - y^2\right)^{-1} \overline{W}_1\left(y, (xy)^{-1}\right) & \\ \qquad + \dfrac{1}{2} x^{-2} \overline{W}_{11}\left(y, (xy)^{-1}\right) & \text{otherwise} \end{cases}, \tag{C.5}$$

and

$$\overline{W}_1(\overline{\lambda}_1, \overline{\lambda}_2) = \frac{\partial \overline{W}}{\partial \overline{\lambda}_1}(\overline{\lambda}_1, \overline{\lambda}_2), \qquad \overline{W}_{11}(\overline{\lambda}_1, \overline{\lambda}_2) = \frac{\partial^2 \overline{W}}{\partial \overline{\lambda}_1 \partial \overline{\lambda}_1}(\overline{\lambda}_1, \overline{\lambda}_2). \tag{C.6}$$

To show that the solution (2.40) for the overall nonlinear elastic response of dilute suspensions of rigid particles in rubber is strongly elliptic, it suffices to show that the function H is strongly elliptic. This follows from the facts that the Neo-Hookean term $\mu/2\left[\overline{\lambda}_1^2 + \overline{\lambda}_2^2 + \overline{\lambda}_1^{-2}\overline{\lambda}_2^{-2} - 3\right]$ in (2.40) is strongly elliptic and that the sum of strongly elliptic functions is strongly elliptic. Now, by making use of the explicit asymptotic expressions (2.37) and (2.38), it is straightforward to show analytically that H satisfies all nine conditions (C.1) for small and large deformations. For arbitrary deformations, it is also straightforward to show — albeit by numerical means — that H satisfies conditions (C.1), and hence that the effective stored-energy function (2.40) is strongly elliptic. By the same token, we note that the approximate solution (2.53) for $\overline{W}$ is strongly elliptic, since the underlying approximation (2.52) for H is strongly elliptic.

An incompressible stored-energy function $\overline{W} = \overline{W}(\overline{\lambda}_1, \overline{\lambda}_2)$ is said to be *polyconvex* if it can be written in the form

$$\overline{W} = \mathcal{W}\left(\overline{\mathbf{F}}, \overline{\mathbf{F}}^{-T}\right) \tag{C.7}$$

with $\mathcal{W}(\cdot,\cdot)$ convex. The constitutive restriction (C.7) of polyconvexity is a stronger constitutive restriction than that of strong ellipticity (C.1) — in fact, polyconvexity implies strongly ellipticity — that was introduced by Ball (1977) to prove existence theorems in finite elasticity. Unlike strong ellipticity (see Geymonat et al., 1993), however, polyconvexity has not yet been given a strict physical interpretation and therefore its enforcement, although mathematically desirable, is still physically arguable.

For the case under study here, it is a trivial matter to deduce from its explicit asymptotic form (2.44) — after recognizing that $\overline{I}_1 = \overline{\mathbf{F}} \cdot \overline{\mathbf{F}}$ and $\overline{I}_2 = \overline{\mathbf{F}}^{-T} \cdot \overline{\mathbf{F}}^{-T}$ — that the effective stored-energy function (2.40) is not

convex in $\overline{\mathbf{F}}^{-T}$ and hence *not* polyconvex.

APPENDIX D

SOLUTION FOR THE SINGLE-PARTICLE PROBLEM IN THE SMALL-DEFORMATION LIMIT

In this appendix, we work out the elasticity solution for the single-particle problem formulated in Section 4.2 from which the effective shear modulus (4.14) is determined.

We find it convenient to begin by considering the boundary-value problem of an isotropic incompressible multicoated sphere occupying the domain $\Omega = \{\mathbf{X} : |\mathbf{X}| \leq r_m\}$, made up of a core (the particle) with initial shear modulus μ_p, an inner shell (the interphase) with initial shear modulus μ_i, and an outer shell (the matrix) with initial shear modulus μ_m, that is subjected to the affine simple shear deformation $\mathbf{x} = \overline{\mathbf{F}}\mathbf{X}$ with $\overline{\mathbf{F}} = \mathbf{I} + \overline{\gamma}\mathbf{e}_1 \otimes \mathbf{e}_2$ on its boundary $\partial\Omega = \{\mathbf{X} : |\mathbf{X}| = r_m\}$. The heterogeneous shear modulus of such a sphere can be written in the compact form

$$\mu(\mathbf{X}) = [1 - \theta_p(\mathbf{X}) - \theta_i(\mathbf{X})]\mu_m + \theta_p(\mathbf{X})\mu_p + \theta_i(\mathbf{X})\mu_i, \tag{D.1}$$

where $\theta_p(\mathbf{X}) = 1$ if $|\mathbf{X}| \leq r$ and zero otherwise, $\theta_i(\mathbf{X}) = 1$ if $r \leq |\mathbf{X}| \leq r + t$ and zero otherwise. Here, r and t stand, respectively, for the initial radius of the core and the thickness of the inner shell. In the limit as the applied amount of shear $\overline{\gamma} \to 0$, the equilibrium displacement field $\mathbf{u} = \mathbf{x} - \mathbf{X}$ that minimizes the total elastic energy $\overline{\Psi}$ (per unit undeformed volume) of the

sphere takes the form $\mathbf{u} = u_1(\mathbf{X})\mathbf{e}_1 + u_2(\mathbf{X})\mathbf{e}_2 + u_3(\mathbf{X})\mathbf{e}_3$ with

$$\begin{aligned}
u_1(\mathbf{X}) &= \overline{\gamma}\left[B^{(1)} + B^{(2)}\frac{r^5}{|\mathbf{X}|^5} + B^{(3)}\frac{|\mathbf{X}|^2}{r^2}\right]X_2 \\
&- \overline{\gamma}\left[5B^{(2)}\frac{r^5}{|\mathbf{X}|^5} + \frac{4}{5}B^{(3)}\frac{|\mathbf{X}|^2}{r^2} - 3B^{(4)}\frac{r^3}{|\mathbf{X}|^3}\right]\frac{X_1^2X_2}{|\mathbf{X}|^2}, \\
u_2(\mathbf{X}) &= \overline{\gamma}\left[B^{(1)} + B^{(2)}\frac{r^5}{|\mathbf{X}|^5} + B^{(3)}\frac{|\mathbf{X}|^2}{r^2}\right]X_1 \\
&- \overline{\gamma}\left[5B^{(2)}\frac{r^5}{|\mathbf{X}|^5} + \frac{4}{5}B^{(3)}\frac{|\mathbf{X}|^2}{r^2} - 3B^{(4)}\frac{r^3}{|\mathbf{X}|^3}\right]\frac{X_1X_2^2}{|\mathbf{X}|^2}, \\
u_3(\mathbf{X}) &= -\overline{\gamma}\left[5B^{(2)}\frac{r^5}{|\mathbf{X}|^5} + \frac{4}{5}B^{(3)}\frac{|\mathbf{X}|^2}{r^2} - 3B^{(4)}\frac{r^3}{|\mathbf{X}|^3}\right]\frac{X_1X_2X_3}{|\mathbf{X}|^2},
\end{aligned} \tag{D.2}$$

and

$$B^{(I)} = [1 - \theta_p(\mathbf{X}) - \theta_i(\mathbf{X})]B_m^{(I)} + \theta_p(\mathbf{X})B_p^{(I)} + \theta_i(\mathbf{X})B_i^{(I)} \qquad (I = 1, 2, 3, 4), \tag{D.3}$$

to $O(1)$ in $\overline{\gamma}$ (see, e.g., Chapter XI in Love, 1906). By the same token, the corresponding traction field takes the form $\mathbf{t} = \mathtt{t}_1(\mathbf{X})\mathbf{e}_1 + \mathtt{t}_2(\mathbf{X})\mathbf{e}_2 + \mathtt{t}_3(\mathbf{X})\mathbf{e}_3$ with

$$\begin{aligned}
\mathtt{t}_1(\mathbf{X}) &= 2\mu(\mathbf{X})\overline{\gamma}\left[B^{(1)} - 4B^{(2)}\frac{r^5}{|\mathbf{X}|^5} + \frac{8}{5}B^{(3)}\frac{|\mathbf{X}|^2}{r^2} + \frac{3}{2}B^{(4)}\frac{r^3}{|\mathbf{X}|^3}\right]\frac{X_2}{|\mathbf{X}|} \\
&+ 2\mu(\mathbf{X})\overline{\gamma}\left[20B^{(2)}\frac{r^5}{|\mathbf{X}|^5} - \frac{19}{5}B^{(3)}\frac{|\mathbf{X}|^2}{r^2} - 12B^{(4)}\frac{r^3}{|\mathbf{X}|^3}\right]\frac{X_1^2X_2}{|\mathbf{X}|^3}, \\
\mathtt{t}_2(\mathbf{X}) &= 2\mu(\mathbf{X})\overline{\gamma}\left[B^{(1)} - 4B^{(2)}\frac{r^5}{|\mathbf{X}|^5} + \frac{8}{5}B^{(3)}\frac{|\mathbf{X}|^2}{r^2} + \frac{3}{2}B^{(4)}\frac{r^3}{|\mathbf{X}|^3}\right]\frac{X_1}{|\mathbf{X}|} \\
&+ 2\mu(\mathbf{X})\overline{\gamma}\left[20B^{(2)}\frac{r^5}{|\mathbf{X}|^5} - \frac{19}{5}B^{(3)}\frac{|\mathbf{X}|^2}{r^2} - 12B^{(4)}\frac{r^3}{|\mathbf{X}|^3}\right]\frac{X_1X_2^2}{|\mathbf{X}|^3}, \\
\mathtt{t}_3(\mathbf{X}) &= 2\mu(\mathbf{X})\overline{\gamma}\left[20B^{(2)}\frac{r^5}{|\mathbf{X}|^5} - \frac{19}{5}B^{(3)}\frac{|\mathbf{X}|^2}{r^2} - 12B^{(4)}\frac{r^3}{|\mathbf{X}|^3}\right]\frac{X_1X_2X_3}{|\mathbf{X}|^3}.
\end{aligned} \tag{D.4}$$

In these expressions, $B_m^{(I)}$, $B_p^{(I)}$, and $B_i^{(I)}$ $(I = 1, 2, 3, 4)$ are constants to be determined from the boundary conditions applied at $\partial\Omega = \{\mathbf{X} : |\mathbf{X}| = r_m\}$ and from the continuity of the displacement and traction fields at the surfaces of material discontinuity $\Gamma_p = \{\mathbf{X} : |\mathbf{X}| = r\}$ and $\Gamma_i = \{\mathbf{X} : |\mathbf{X}| = r + t\}$. Upon recognizing that $B_p^{(2)} = B_p^{(4)} = 0$, these conditions lead to a

system of 10 linear algebraic — and thus readily solvable — equations for the 10 unknowns $B_p^{(1)}, B_p^{(3)}, B_i^{(1)}, B_i^{(2)}, B_i^{(3)}, B_i^{(4)}, B_m^{(1)}, B_m^{(2)}, B_m^{(3)}, B_m^{(4)}$. The explicit expressions for these constants, in terms of the shear moduli μ_p, μ_i, μ_m, and the lengths r, t, r_m, are fairly cumbersome and thus not reported here. Having determined the equilibrium displacement field $\mathbf{u}$ over the entire sphere, its total elastic energy (per unit undeformed volume) is simply given by

$$\overline{\Psi} = \frac{1}{2|\Omega|}\int_{\partial\Omega} \mathbf{t}\cdot\mathbf{u}\,\mathrm{d}S = \left[B_m^{(1)} + \frac{42\,r_m^2}{50\,r^2}B_m^{(3)} - \frac{45\,r^3}{50\,r_m^3}B_m^{(4)}\right]\mu_m\,\overline{\gamma}^2. \tag{D.5}$$

Now, in the limit when the radius of the sphere is taken to be infinitely large and the core is taken to be rigid, as $r_m \to +\infty$ and $\mu_p \to +\infty$, the total elastic energy (D.5) reduces to the effective stored-energy function for the single-particle problem formulated in Section 4.2, in the limit of small deformations and for the specific case of simple shear loading, namely,

$$\overline{\Psi} = \overline{\mu}^{\,\mathrm{dil}}\,\mathrm{tr}\overline{\boldsymbol{\varepsilon}}^{\,2} = \frac{\overline{\mu}^{\,\mathrm{dil}}}{2}\overline{\gamma}^2. \tag{D.6}$$

The solution (4.14) for $\overline{\mu}^{\,\mathrm{dil}}$ provided in the main body of the text follows by comparing (D.5) with (D.6). As also remarked in the main body of the text, the product $\mu_p B_p^{(3)}$ does not vanish in this limit and thus the stress field within the particle — contrary to the classical solution (Eshelby, 1957) without an interphase — is *not* uniform.

APPENDIX E

A KINEMATICALLY ADMISSIBLE APPROXIMATION FOR THE RESPONSE OF A CSA

Following a parallel reasoning to that presented in Section 5.3.2, it is not difficult to deduce that

$$\overline{W}(\overline{\mathbf{F}}, c) \leq \frac{1}{|\mathcal{B}|} \int_{\mathcal{B}} W(\mathbf{X}, \mathbf{F}^K)\, \mathrm{d}\mathbf{X} \doteq \overline{W}^K(\overline{\mathbf{F}}, c), \tag{E.1}$$

where the deformation gradient field $\mathbf{F}^K$ is defined implicitly by the boundary-value problem

$$\mathrm{Div}\left[\frac{\partial W}{\partial \mathbf{F}}(\mathbf{X}, \mathbf{F}^K)\right] = 0 \quad \text{in} \quad \mathcal{B} \qquad \text{and} \qquad \mathbf{x} = \overline{\mathbf{F}}\mathbf{X} \quad \text{on} \quad \partial\mathcal{B}. \tag{E.2}$$

The effective stored-energy function $\overline{W}^K$ corresponds physically to the total elastic energy per unit undeformed volume of a CSA associated with a kinematically admissible field — one in which every composite sphere satisfies the equilibrium equations in its interior and is subjected to the affine deformation $\mathbf{x} = \overline{\mathbf{F}}\mathbf{X}$ on its boundary.

Much like $\overline{W}^S$, the effective stored-energy function $\overline{W}^K$ is by construction an exact result (i.e., the equality holds in (E.1)) in the dilute limit of particles as $c \to 0+$. As c increases, $\overline{W}^K$ is expected to deviate from $\overline{W}$ providing increasingly stiffer approximations for the overall response of filled elastomers. For the case of interest here when the particles are much stiffer than the elastomeric matrix, this deviation is exceedingly drastic leading to overly stiff approximations. Figure E.1 illustrates this behavior for the case of filled Neo-Hookean rubber. Part (a) displays results for the normalized initial effective shear modulus $\overline{\mu}/\mu$ in the small deformation regime as a function of particle concentration c, while part (b) shows results for the stress-

deformation relation for $c = 0.15$ under uniaxial tensile loading conditions.

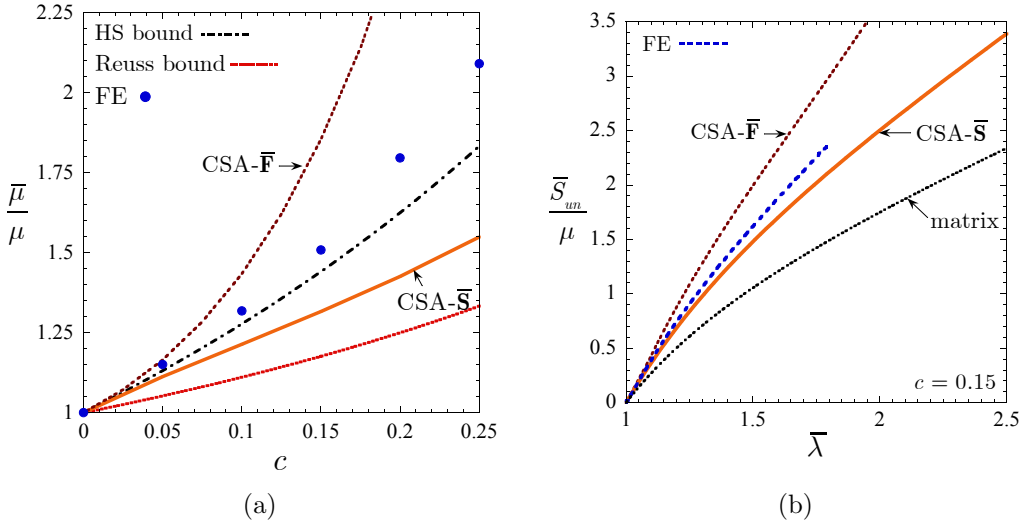

Figure E.1: Comparisons between the kinematically admissible approximation (E.1)–(E.2), denoted as CSA-$\overline{\mathbf{F}}$, and the statically admissible approximation (5.17)–(5.20), denoted as CSA-$\overline{\mathbf{S}}$, for the overall response of filled Neo-Hookean rubber. Part (a) shows results for the normalized initial shear modulus $\overline{\mu}/\mu$ as a function of particle concentration c, while part (b) shows stress-deformation results for $c = 0.15$ under uniaxial tension.

REFERENCES

Abaqus version 6.11 documentation, Dassault Systèmes Simulia Corp., Providence, RI, USA, 2011.

Arruda, E.M., Boyce, M.C., 1993. A three-dimensional constitutive model for the large stretch behavior of rubber elastic materials. Journal of the Mechanics and Physics of Solids 41, 389–412.

Avellaneda, M., 1987. Iterated homogenization, differential effective medium theory and applications. Communications on Pure and Applied Mathematics 40, 527–554.

Ball, J.M., 1977. Convexity conditions and existence theorems in nonlinear elasticity. Archive for Rational Mechanics and Analysis 63, 337–403.

Bar-Cohen, Y., 2004. Electroactive polymer (EAP) actuators as artificial muscles: reality, potential, and challenges. volume 5. SPIE press Bellingham, WA.

Barrett, K.E., Talbot, D.R.S., 1995. Bounds for the effective properties of a nonlinear two-phase composite dielectric, in: Proc. 8th Int. Symp. Continuum Models and Discrete Systems, Varna, Bulgaria.

Batchelor, G.K., Green, J.T., 1972. The hydrodynamic interaction of two small freely-moving spheres in a linear flow field. Jounral of Fluid Mechanics 56, 375–400.

Beatty, A.M., 2003. Open-framework coordination complexes from hydrogen-bonded networks: Toward host/guest complexes. Coordination Chemistry Reviews 246, 131–143.

Bergström, J., Boyce, M., 1999. Mechanical behavior of particle filled elastomers. Rubber chemistry and technology 72, 633–656.

Born, M., Wolf, E., 1999. Principles of optics: electromagnetic theory of propagation, interference and diffraction of light. Cambridge University Press.

Bornert, M., Stolz, C., Zaoui, A., 1996. Morphologically representative pattern-based bounding in elasticity. Journal of the Mechanics and Physics of Solids 44, 307–331.

Braides, A., 1985. Homogenization of some almost periodic coercive functional. Rend. Accad. Naz. Sci. XL 103, 313–322.

Braides, A., Lukkassen, D., 2000. Reiterated homogenization of integral functionals. Mathematical Models and Methods in Applied Sciences 10, 47–71.

Bruggeman, D., 1935. Calculation of various physics constants in heterogenous substances i dielectricity constants and conductivity of mixed bodies from isotropic substances. Annalen der Physik 24, 636–664.

Carpi, F., De Rossi, D., Kornbluh, R., Pelrine, R.E., Sommer-Larsen, P., 2008. Dielectric elastomers as electromechanical transducers. Elsevier.

Chen, H.S., Acrivos, A., 1978. The solution of the equations of linear elasticity for an infinite region containing two spherical inclusions. International Journal of Solids and Structures 14, 331–348.

Chew, W.C., Sen, P.N., 1982. Dielectric enhancement due to electrochemical double layer: Thin double layer approximation. The Journal of Chemical Physics 77, 4683–4693.

Dacorogna, B., 2007. Direct methods in the calculus of variations. volume 78. Springer.

Danas, K., Kankanala, S., Triantafyllidis, N., 2012. Experiments and modeling of iron-particle-filled magnetorheological elastomers. Journal of the Mechanics and Physics of Solids 60, 120–138.

deBotton, G., Shmuel, G., 2010. A new variational estimate for the effective response of hyperelastic composites. Journal of the Mechanics and Physics of Solids 58, 466–483.

Duan, H.L., Jiao, Y., Yi, X., Huang, Z.P., Wang, J., 2006. Solutions of inhomogeneity problems with graded shells and application to core-shell nanoparticles and composites. Journal of the Mechanics and Physics of Solids 54, 1401–1425.

Einstein, A., 1906. Eine neue bestimmung der moleküldimensionen. Annalen der Physik 324, 289–306.

Eshelby, J.D., 1957. The determination of the elastic field of an ellipsoidal inclusion, and related problems. Proceedings of the Royal Society A: Mathematical, Physical and Engineering Sciences 241, 376–396.

Fritzen, F., Forest, S., Böhlke, T., Kondo, D., Kanit, T., 2012. Computational homogenization of elasto-plastic porous metals. International Journal of Plasticity 29, 102–119.

Fukahori, Y., 2007. Generalized concept of the reinforcement of elastomers. part 1: Carbon black reinforcement of rubbers. Rubber chemistry and technology 80, 701–725.

Galli, M., Botsis, J., Janczak-Rusch, J., 2008. An elastoplastic three-dimensional homogenization model for particle reinforced composites. Computational Materials Science 41, 312–321.

Gent, A.N., 1996. A new constitutive relation for rubber. Rubber chemistry and technology 69, 59–61.

Gent, A.N., Park, B., 1984. Failure processes in elastomers at or near a rigid spherical inclusion. Journal of Materials Science 19, 1947–1956.

Gent, A.N., Pulford, C.T.R., 1983. Mechanisms of rubber abrasion. Journal of Applied Polymer Science 28, 943–960.

Geymonat, G., Mller, S., Triantafyllidis, N., 1993. Homogenization of nonlinearly elastic materials, microscopic bifurcation and macroscopic loss of rank-one convexity. Archive for Rational Mechanics and Analysis 122, 231–290.

Goudarzi, T., Lopez-Pamies, O., 2013. Numerical modeling of the nonlinear elastic response of filled elastomers via composite-sphere assemblages. Journal of Applied Mechanics 80, 050906.

Goudarzi, T., Spring, D., Paulino, G., Lopez-Pamies, O., . Filled elastomers: A theory of filler reinforcement based on hydrodynamic and interphasial effects, submitted.

Govindjee, S., 1997. An evaluation of strain amplification concepts via monte carlo simulations of an ideal composite. Rubber chemistry and technology 70, 25.

Govindjee, S., Simo, J., 1991. A micro-mechanically based continuum damage model for carbon black-filled rubbers incorporating mullins' effect. Journal of the Mechanics and Physics of Solids 39, 87–112.

Gusev, A.A., 1997. Representative volume element size for elastic composites: A numerical study. Journal of the Mechanics and Physics of Solids 45, 1449–1459.

Guth, E., 1945. Theory of filler reinforcement. Journal of Applied Physics 16, 20.

Hale, D.K., 1976. The physical properties of composite materials. Journal of Materials Science 11, 2105–2141.

Hashin, Z., 1962. The elastic moduli of heterogeneous materials. Journal of Applied Mechanics 29, 143–150.

Hashin, Z., Shtrikman, S., 1961. Note on a variational approach to the theory of composite elastic materials. Journal of the Franklin Institute 271, 336–341.

Hashin, Z., Shtrikman, S., 1962. A variational approach to the theory of the effective magnetic permeability of multiphase materials. Journal of Applied Physics 33, 3125–3131.

Heinrich, G., Klüppel, M., Vilgis, T.A., 2002. Reinforcement of elastomers. Current Opinion in Solid State and Materials Science 6, 195–203.

Herve, E., Zaoui, A., 1993. n-layered inclusion-based micromechanical modelling. International Journal of Engineering Science 31, 1–10.

Hill, R., 1972. On constitutive macro-variables for heterogeneous solids at finite strain. Proceedings of the Royal Society A: Mathematical, Physical and Engineering Sciences 326, 131–147.

Huang, C., Zhang, Q., Debotton, G., Bhattacharya, K., 2004. All-organic dielectric-percolative three-component composite materials with high electromechanical response. Applied Physics Letters 84, 4391–4393.

Huang, C., Zhang, Q.M., Li, J.Y., Rabeony, M., 2005. Colossal dielectric and electromechanical responses in self-assembled polymeric nanocomposites. Applied Physics Letters 87, 182901.

Idiart, M.I., 2008. Modeling the macroscopic behavior of two-phase nonlinear composites by infinite-rank laminates. Journal of the Mechanics and Physics of Solids 56, 2599–2617.

Lahellec, N., Mazerolle, F., Michel, J.C., 2004. Second-order estimate of the macroscopic behavior of periodic hyperelastic composites: theory and experimental validation. Journal of the Mechanics and Physics of Solids 52, 27–49.

Leblanc, J.L., 2010. Filled polymers: science and industrial applications. CRC Press.

Lewis, T.J., 2004. Interfaces are the dominant feature of dielectrics at the nanometric level. Dielectrics and Electrical Insulation, IEEE Transactions on 11, 739–753.

Lopez-Pamies, O., 2010a. An exact result for the macroscopic response of particle-reinforced neo-hookean solids. Journal of Applied Mechanics 77, 021016.

Lopez-Pamies, O., 2010b. A new i1-based hyperelastic model for rubber elastic materials. Comptes Rendus Mécanique 338, 3–11.

Lopez-Pamies, O., 2014. Elastic dielectric composites: Theory and application to particle-filled ideal dielectrics. Journal of the Mechanics and Physics of Solids 64, 61–82.

Lopez-Pamies, O., Castañeda, P.P., 2006a. On the overall behavior, microstructure evolution, and macroscopic stability in reinforced rubbers at large deformations: I—theory. Journal of the Mechanics and Physics of Solids 54, 807–830.

Lopez-Pamies, O., Castañeda, P.P., 2006b. On the overall behavior, microstructure evolution, and macroscopic stability in reinforced rubbers at large deformations: Ii—application to cylindrical fibers. Journal of the Mechanics and Physics of Solids 54, 831–863.

Lopez-Pamies, O., Garcia, R., Chabert, E., Cavaill, J.Y., Ponte Castañeda, P., 2008. Multiscale modeling of oriented thermoplastic elastomers with lamellar morphology. Journal of the Mechanics and Physics of Solids 56, 3206–3223.

Lopez-Pamies, O., Goudarzi, T., Danas, K., 2013a. The nonlinear elastic response of suspensions of rigid inclusions in rubber: II — a simple explicit approximation for finite-concentration suspensions. Journal of the Mechanics and Physics of Solids 61, 19–37.

Lopez-Pamies, O., Goudarzi, T., Meddeb, A.B., Ounaies, Z., 2014. Extreme enhancement and reduction of the dielectric response of polymer nanoparticulate composites via interphasial charges. Applied Physics Letters 104, 242904.

Lopez-Pamies, O., Goudarzi, T., Nakamura, T., 2013b. The nonlinear elastic response of suspensions of rigid inclusions in rubber: I — an exact result for dilute suspensions. Journal of the Mechanics and Physics of Solids 61, 1–18.

Lopez-Pamies, O., Idiart, M.I., Nakamura, T., 2011a. Cavitation in elastomeric solids: I — a defect-growth theory. Journal of the Mechanics and Physics of Solids 59, 1464–1487.

Lopez-Pamies, O., Nakamura, T., Idiart, M.I., 2011b. Cavitation in elastomeric solids: II — onset-of-cavitation surfaces for neo-hookean materials. Journal of the Mechanics and Physics of Solids 59, 1488–1505.

Love, A., 1906. A treatise on the mathematical theory of elasticity. Cambridge University Press.

Lusti, H.R., Karmilov, I.A., Gusev, A.A., 2002. Effect of particle agglomeration on the elastic properties of filled polymers. Soft Materials 1, 115–120.

Ma, P.X., 2008. Biomimetic materials for tissue engineering. Advanced Drug Delivery Reviews 60, 184–198.

Michel, J.C., Lopez-Pamies, O., Ponte Castañeda, P., Triantafyllidis, N., 2010. Microscopic and macroscopic instabilities in finitely strained fiber-reinforced elastomers. Journal of the Mechanics and Physics of Solids 58, 1776–1803.

Michel, J.C., Moulinec, H., Suquet, P., 1999. Effective properties of composite materials with periodic microstructure: a computational approach. Computer Methods in Applied Mechanics and Engineering 172, 109–143.

Mikata, Y., Taya, M., 1985. Stress field in and around a coated short fiber in an infinite matrix subjected to uniaxial and biaxial loadings. Journal of Applied Mechanics 52, 19–24.

Milton, G.W., 1981. Concerning bounds on the transport and mechanical properties of multicomponent composite materials. Applied Physics A 26, 125–130.

Milton, G.W., 2002. The Theory of Composites. Cambridge University Press.

Moraleda, J., Segurado, J., Llorca, J., 2009. Finite deformation of incompressible fiber-reinforced elastomers: A computational micromechanics approach. Journal of the Mechanics and Physics of Solids 57, 1596–1613.

Müller, S., 1987. Homogenization of nonconvex integral functionals and cellular elastic materials. Archive for Rational Mechanics and Analysis 99, 189–212.

Mullins, L., Tobin, N.R., 1965. Stress softening in rubber vulcanizates. part i. use of a strain amplification factor to describe the elastic behavior of filler-reinforced vulcanized rubber. Journal of Applied Polymer Science 9, 2993–3009.

Nelson, J.K., John, C.F., 2004. Internal charge behaviour of nanocomposites. Nanotechnology 15, 586.

Norris, A.N., 1985. A differential scheme for the effective moduli of composites. Mechanics of Materials 4, 1–16.

Ogden, R., 1978. Extremum principles in non-linear elasticity and their application to composites — I : Theory. International Journal of Solids and Structures 14, 265–282.

Ogden, R., 1997. Non-linear elastic deformations. Dover Publications.

Omnès, B., Thuillier, S., Pilvin, P., Grohens, Y., Gillet, S., 2008. Effective properties of carbon black filled natural rubber: Experiments and modeling. Composites Part A: Applied Science and Manufacturing 39, 1141–1149.

Owen, G.E., 2003. Introduction to Electromagnetic Theory. Courier Dover Publications.

Ponte Castañeda, P., 1989. The overall constitutive behaviour of nonlinearly elastic composites. Proceedings of the Royal Society A: Mathematical, Physical and Engineering Sciences 422, 147–171.

Ponte Castañeda, P., 1991. The effective mechanical properties of nonlinear isotropic composites. Journal of the Mechanics and Physics of Solids 39, 45–71.

Ponte Castañeda, P., Tiberio, E., 2000. A second-order homogenization method in finite elasticity and applications to black-filled elastomers. Journal of the Mechanics and Physics of Solids 48, 1389–1411.

Qiu, Y.P., Weng, G.J., 1991. Elastic moduli of thickly coated particle and fiber-reinforced composites. Journal of Applied Mechanics, Transactions ASME 58, 388–398.

Qu, M., Deng, F., Kalkhoran, S.M., Gouldstone, A., Robisson, A., Van Vliet, K.J., 2011. Nanoscale visualization and multiscale mechanical implications of bound rubber interphases in rubber-carbon black nanocomposites. Soft Matter 7, 1066.

Racherla, V., Lopez-Pamies, O., Ponte Castañeda, P., 2010. Macroscopic response and stability in lamellar nanostructured elastomers with "oriented" and "unoriented" polydomain microstructures. Mechanics of Materials 42, 451–468.

Ramier, J., 2004. Comportement mécanique d'élastomèrs chargés, influence de l'adhésion charge-polymère, influence de la morphologie. Ph.D. thesis.

Roscoe, R., 1973. Isotropic composites with elastic or viscoelastic phases: General bounds for the moduli and solutions for special geometries. Rheologica Acta 12, 404–411.

Roy, M., Nelson, J.K., MacCrone, R.K., Schadler, L.S., Reed, C.W., Keefe, R., 2005. Polymer nanocomposite dielectrics-the role of the interface. Dielectrics and Electrical Insulation, IEEE Transactions on 12, 629–643.

Schöberl, J., 1997. Netgen an advancing front 2d/3d-mesh generator based on abstract rules. Computing and Visualization in Science 1, 41–52.

Segurado, J., Llorca, J., 2002. A numerical approximation to the elastic properties of sphere-reinforced composites. Journal of the Mechanics and Physics of Solids 50, 2107–2121.

Smallwood, H.M., 1944. Limiting law of the reinforcement of rubber. Journal of Applied Physics 15, 758.

Talbot, D., Willis, J., 1985. Variational principles for inhomogeneous nonlinear media. IMA Journal of Applied Mathematics 35, 39–54.

Talbot, D.R.S., Willis, J.R., 1994. Upper and lower bounds for the overall properties of a nonlinear composite dielectric. i. random microgeometry. Proceedings of the Royal Society of London. Series A: Mathematical and Physical Sciences 447, 365–384.

Torquato, S., 2002. Random heterogeneous materials: microstructure and macroscopic properties. volume 16. Springer.

Triantafyllidis, N., Nestorovic, M.D., Schraad, M.W., 2006. Failure surfaces for finitely strained two-phase periodic solids under general in-plane loading. Journal of Applied Mechanics 73, 505–515.

Wallace, G.G., Teasdale, P.R., Spinks, G.M., Kane-Maguire, L.A., 2008. Conductive electroactive polymers: intelligent polymer systems. CRC press.

Walpole, L.J., 1978. A coated inclusion in an elastic medium. Mathematical Proceedings of the Cambridge Philosophical Society 83, 495–506.

Wang, Y., Ameer, G.A., Sheppard, B.J., Langer, R., 2002. A tough biodegradable elastomer. Nature Biotechnology 20, 602–606.

Willis, J.R., 1977. Bounds and self-consistent estimates for the overall properties of anisotropic composites. Journal of the Mechanics and Physics of Solids 25, 185–202.

Willis, J.R., 1983. The overall elastic response of composite materials. Journal of Applied Mechanics 50, 1202–1209.

Willis, J.R., 1989. The structure of overall constitutive relations for a class of nonlinear composites. IMA Journal of Applied Mathematics 43, 231–242.

Willis, J.R., 1991. On methods for bounding the overall properties of nonlinear composites. Journal of the Mechanics and Physics of Solids 39, 73–86.

Willis, J.R., 1994. Upper and lower bounds for non-linear composite behaviour. Materials Science and Engineering: A 175, 7–14.

Zee, L., Sternberg, E., 1983. Ordinary and strong ellipticity in the equilibrium theory of incompressible hyperelastic solids. Archive for Rational Mechanics and Analysis 83, 53–90.

Zhang, Q.M., Li, H., Poh, M., Xia, F., Cheng, Z.Y., Xu, H., Huang, C., 2002. An all-organic composite actuator material with a high dielectric constant. Nature 419, 284–287.